Tracing Wyville Thomson Ridge Overflow Water in the Rockall Trough

Clare Johnson

2012

A thesis presented for the degree of Doctor of Philosophy at the University of Aberdeen

SCOTTISH
ASSOCIATION
for MARINE
SCIENCE

University of the
Highlands and Islands
Oilthigh na Gàidhealtachd
agus nan Eilean

Abstract

Although it has long been known that cold dense waters from the Nordic Seas overflow the Wyville Thomson Ridge, the water masses' subsequent pathways and fate have been uncertain. This study conclusively places Wyville Thomson Ridge Overflow Water (WTOW) as an important water mass in the eastern subpolar North Atlantic for the first time. Using a variety of chemical tracers (chlorofluorocarbons, oxygen, nutrients and aluminium) in conjunction with temperature and salinity, WTOW is traced southwards into the northern and central Rockall Trough as well as into the channels between the western banks. The overflow water has a clear temperature, salinity and chlorofluorocarbon (CFC-11 and CFC-12) signature. Additionally, levels of aluminium are elevated in WTOW suggesting that this element is potentially a useful and novel water mass tracer. The lower oxygen layer complicates the use of dissolved oxygen and nitrate as tracers in the mid water column. However, higher and lower concentrations respectively in the western trough reveal the presence of WTOW in this area. The overflow water does not appear to have a silicate or phosphate signature. Two branches of WTOW exist in the Rockall Trough: a slow-moving indistinct intermediate branch (600-1200 m) found in both the east and west of the basin; and a coherent deep branch (> 1200 m) that flows southward along the western banks of the trough. As well as having a large spatial footprint within the Rockall Trough, intermediate and deep WTOW are temporally persistent being present 65-75 % of the time between 1975 and 2008. The signature of WTOW at intermediate depths is absent from the Ellett Line record in the mid-1980s and early-1990s. As deep WTOW is still observed during these periods flow over the Wyville Thomson Ridge cannot have ceased. Instead, it is proposed that the strength of the Subpolar Gyre is an important driver in the temporal distribution of intermediate WTOW within the Rockall Trough. When the gyre is strong, such as in the mid-1980s and early-1990s, the mid water column is dominated by waters originating from the west which block the southward flow of intermediate WTOW. In contrast, when the gyre is weak, such as in the late-1990s and 2000s, subpolar waters lie further west enabling intermediate waters within the Rockall Trough to be dominated by the southern originating Mediterranean Overflow Water and the northern water mass of WTOW.

“I, Clare Johnson, confirm that all work is my own and that I composed this thesis. It has not been accepted in any previous application for a degree, all sources of information have been specifically acknowledged and any quotations distinguished by quotation marks.”

Signature _____

Date _____

Acknowledgements

A massive thank you to my director of studies, Professor Toby Sherwin, for all his time and thoughtful comments through what has not been the shortest PhD! His open-door policy and support through my ill-health and subsequent return to studying was particularly appreciated. I also thank my supervisors Dr Tracy Shimmield and Dr Denise Smythe-Wright for their help and input over the years and especially for returning chapters quickly when I was approaching submission. Finally, thanks also go to my thesis panel: Professor Axel Miller, Dr Bill Turrell and Professor Mark Inall, again for all their help, support and time.

This thesis uses a large amount of data, both recent and historical. I thank all the scientists and crew involved in its collection; and staff at various data centres (noted within the methods chapter) for provision of the data. Particular thanks to Professor Toby Sherwin and Dr Emily Venables for collecting seawater samples when I was unable to go to sea, allowing later shore-based analysis and for me to pursue the aluminium side of the research. Additionally, the help of Mr Tim Brand and Dr Rich Abell to analyse the final few aluminium samples was greatly appreciated. Finally, it would be amiss not to acknowledge the effort and foresight of the late Dr Dave Ellett in maintaining the Ellett Line timeseries.

I have very much enjoyed my time at SAMS and thank all those who have made me feel so welcome. Particular thanks go to members of the Physics, Sea Ice and Technology Department for many a happy curry and always being available to help with Matlab questions. My fellow PhD students, of which there have been many, have also been a huge support.

This work was predominantly funded by a UHI studentship. However, additional support for my personal stipend was provided by: the Oceans 2025 project, Jane Foster Bursary for Biogeochemistry, Funds for Women Graduates and the Thomas and Margaret Roddan Trust. Grants for attendance at various conferences were provided by UHI, the Royal Scottish Geographical Society and the Challenger Society for Marine Science. I am very grateful to all organisations for their support, which enabled me to complete this thesis and present the findings to the wider scientific community.

Contents

List of figures

List of tables

Chapter 1.
Introduction

1.1. Research rationale

Flow in the eastern subpolar North Atlantic forms an important part of the global thermohaline circulation. Water is exchanged between the Atlantic and Nordic Seas across the Greenland-Scotland Ridge, the submarine barrier that marks the northern boundary of the Atlantic Ocean. Around 50 % of the upper ocean warm inflow to the Nordic Seas passes through the Rockall Trough and over the Wyville Thomson Ridge, and just under 50 % of the cold dense outflow returns through the Faroese Channels (Hansen et al., 2000). Although most of the return flow exits through the Faroe Bank Channel into the Iceland Basin, around 15 % spills over the Wyville Thomson Ridge into the Rockall Trough (Dickson and Brown, 1994). Whilst it is well known that Wyville Thomson Ridge Overflow Water (WTOW) enters the northernmost Rockall Trough, its subsequent pathways through the trough and towards the wider Atlantic are unclear.

Five years of sustained current measurements of overflow across the Wyville Thomson Ridge estimate the mean transport of WTOW as > 0.2 Sv (Sverdrup, 1 x 10^6 m^3 s^{-1}) for water less than 0 °C, and ~ 0.9 Sv when entrained Atlantic Waters are included (Sherwin et al., 2008). Although this flux is fairly small relative to the rest of the flow across the Greenland-Scotland Ridge, it is not inconsequential. Further, the volume transport of WTOW is comparable to other overflow waters, such as that exiting the Mediterranean Sea (0.68 Sv, Bryden et al., 1994) and Red Sea (0.35 Sv, Murray and Johns, 1997), which can be identified considerable distances from their source. The signature of Mediterranean Overflow Water has been traced as far west as 60 °W in the subtropical North Atlantic (Needler and Heath, 1975), and northwards to the southern boundary of the Subpolar Gyre (Bower et al., 2002). Similarly, Red Sea Water has been tracked significant distances into the Arabian Sea (Mecking and Warner, 1999) and southwest Indian Ocean (Beal and Bryden, 1997). As the WTOW flux is of a similar magnitude to these overflow waters, it raises the possibility that WTOW too may have a footprint over a large spatial area. In this thesis we therefore ask what happens to WTOW once it has crossed the Wyville Thomson Ridge and whether it can likewise be traced. Its presence further afield would necessarily

affect circulation at its depth in the region and possibly the stability of the water column within the eastern subpolar North Atlantic. This could have important implications for the depth of winter mixing and therefore ocean-atmosphere heat exchange. Further, the presence of WTOW could explain the distribution of some unexpected cold water biological species recently found in the northern Rockall Trough (K. Howell, personal communication).

Previous work in the northernmost Rockall Trough suggests that WTOW may not have a concise definition in temperature-salinity space (Ellett et al., 1983; Turrell and Sherwin, 2003), as is true for other overflow waters in the Atlantic (e.g. Fogelqvist et al., 2003). Hence several chemical tracers (chlorofluorocarbons, nutrients and oxygen) were employed in addition to temperature and salinity data. Additionally, as aluminium levels are known to be elevated in dense water exiting the Faroe Bank Channel (Hall and Measures, 1998), the effectiveness of this element as a water mass tracer was investigated in the hope that it may provide further evidence into the fate of WTOW.

1.2. Aims and objectives

The overall aim for this work is to establish conclusively the presence or absence of WTOW within the Rockall Trough. Additionally, several more specific objectives were assigned:

1. To use a variety of physical and chemical tracers to better resolve water mass structure within the Rockall Trough.

2. To establish a working procedure for the collection and determination of aluminium in seawater using previously published methods.

3. To evaluate the applicability of aluminium as a water mass tracer, particularly of WTOW.

4. To determine circulation pathways of WTOW after overflow.

5. To calculate mixing of WTOW in the northern and central Rockall Trough using a mixing model.

1.3. Thesis layout

This thesis is composed of a further eight chapters. In the next chapter (Chapter Two) a detailed discussion of the literature is presented, providing background information on the bathymetry, circulation and water masses of the subpolar North Atlantic and Rockall Trough. Additionally, the idea of water mass tracers is introduced. In Chapter Three the cruise campaign and methodologies employed are discussed, before various sources of historical data used within the thesis are detailed. Chapter Four examines the procedures used to analyse seawater samples for aluminium, as well as several experiments carried out to ensure a robust working method. The physical and chemical signatures of WTOW within the Rockall Trough are examined in Chapter Five allowing the temporal and spatial persistence of the water mass to be determined. Chapter Six details the construction of mixing models for use within the Rockall Trough, whilst Chapter Seven reports the results of this mixing analysis. Finally, an overall discussion is provided in Chapter Eight before the main findings of the thesis are summarised in Chapter Nine.

Chapter 2.
Background

This chapter provides a background discussion of the literature. First, the bathymetry and circulation of the subpolar North Atlantic is detailed before the more localised scale of the Rockall Trough is discussed. Water masses in the eastern subpolar North Atlantic including Wyville Thomson Ridge Overflow Water (WTOW) are introduced. Finally, methods of tracing water masses within the ocean are discussed, with a focus on chlorofluorocarbons and the novel use of aluminium in this manner.

2.1. Bathymetry of the subpolar North Atlantic

The subpolar North Atlantic, in the northern reaches of the ocean, stretches from the western European shelf in the east to the North American continental shelf in the west (Fig. 2.1). It consists of several basins in the north: the Labrador Sea, Irminger Sea, Iceland Basin and Rockall Trough, which open out onto deep (> 4000 m) abyssal plains to the south. A significant feature is the Mid Atlantic Ridge running approximately southwest to northeast between the Irminger and Iceland Basins (RR, Fig. 2.1) before outcropping at Iceland. This volcanic feature is dissected by a number of east-west fracture zones; the deepest of which, the Charlie Gibbs Fracture Zone (CGFZ, Fig. 2.1) at ~ 52 °N (> 3500 m), provides an important route for deep waters to pass between the eastern and western basins.

Another important structure is the submarine ridge running from Greenland, over to Iceland, the Faroe Islands, and finally Scotland (Fig. 2.1). This feature, the Greenland-Scotland Ridge, separates the Nordic Seas to the north (comprising of the Greenland Sea, Iceland Sea, Norwegian Sea and Lofoten Basin) from the Atlantic Ocean to the south. As the majority of the ridge rises to within 500 m of the surface (Fig. 2.2) it is a significant barrier to the meridional exchange of intermediate and deep waters. Although depths of approximately 600 m are seen immediately to the west of the Faroe Islands and along the Wyville Thomson Ridge, the main conduits for deep water are the 620 m deep Denmark Strait (DS, Fig. 2.1) to the east of Greenland, and the 840 m deep Faroese Channels

(Hansen and Østerhus, 2000). The latter, positioned between the Faroe Islands and Scotland, comprises of the northeast-southwest orientated Faroe Shetland Channel (FSC, Fig. 2.1), the Wyville Thomson Basin (WTB, Fig. 2.1), and the southeast-northwest lying Faroe Bank Channel (FBC, Fig. 2.1).

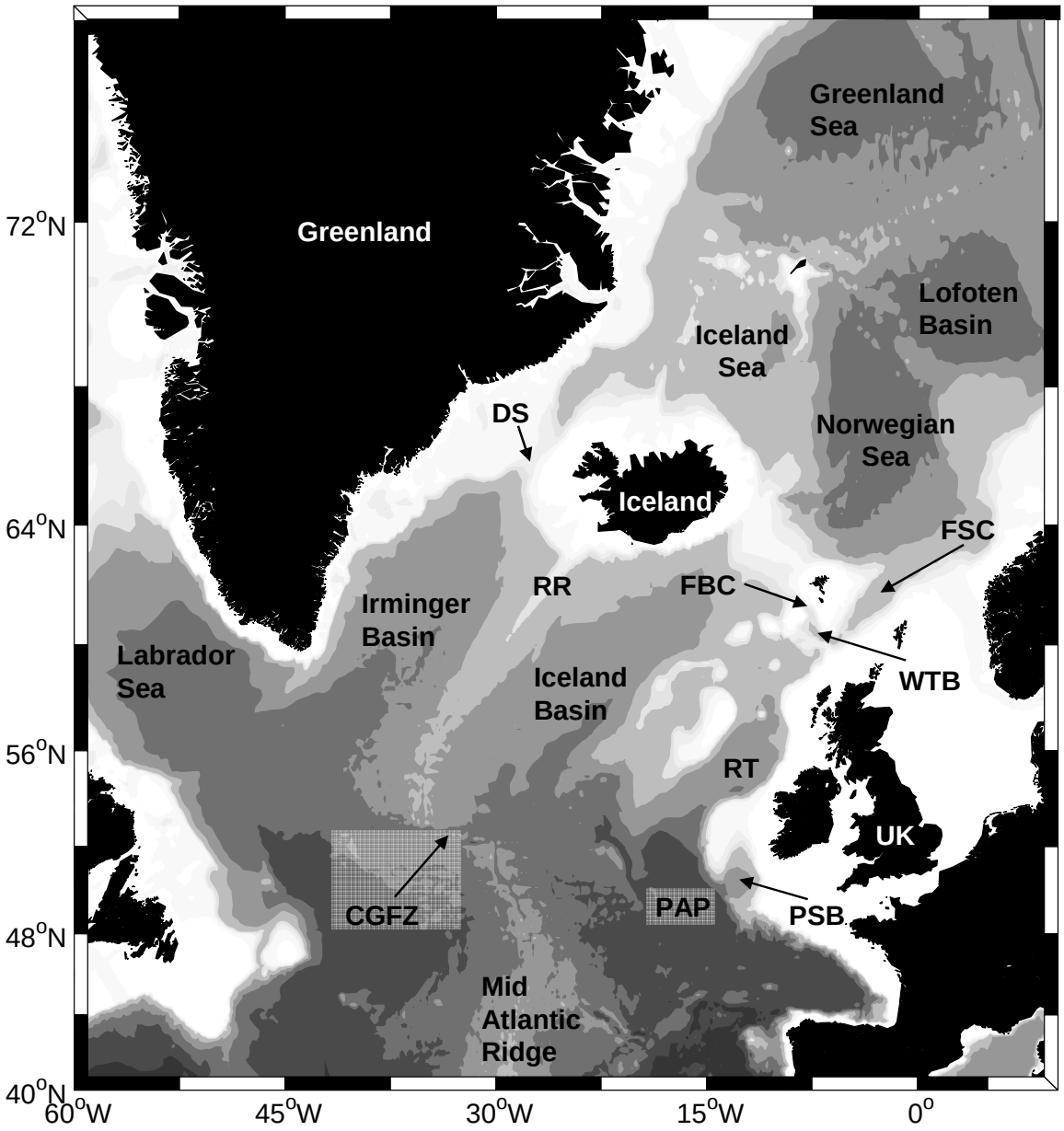

Figure 2.1. Bathymetry of the subpolar North Atlantic. CGFZ: Charlie Gibbs Fracture Zone; DS: Denmark Strait; FBC: Faroe Bank Channel; FSC: Faroe Shetland Channel; PAP: Porcupine Abyssal Plain; PSB: Porcupine Seabight; RR: Reykjanes Ridge; RT: Rockall Trough; WTB: Wyville Thomson Basin. Isobaths: 500m, 1000m, 2000 m, 3000 m and 4000 m. Bathymetry for this and all further figures from GEBCO 1 minute database.

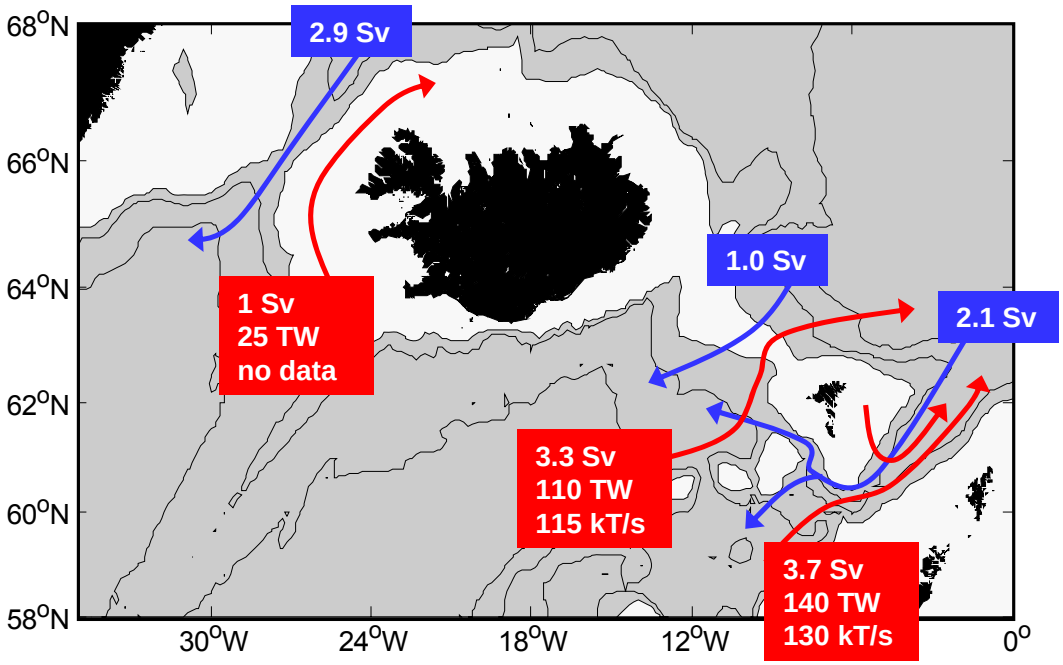

Figure 2.2. Fluxes across the Greenland-Scotland Ridge. Red: volume (Sv), heat (terawatt), and salt (kilotonnes / sec) fluxes in the upper waters (potential density, $\sigma_\theta >$ 27.6 kg m^{-3}) from Hansen and Østerhus (2000); blue: volume fluxes of waters with $\sigma_\theta >$ 27.8 kg m^{-3} from Dickson and Brown (1994). Bathymetry shaded white < 500 m, grey shading > 500 m. Isobaths: 500 m, 1000 m and 2000 m.

2.2. Circulation in the subpolar North Atlantic

Although the subpolar North Atlantic has a cyclonic circulation, an additional, important feature is the north-south exchange of water over the Greenland-Scotland Ridge. In the upper layers (< 600 m) warm and salty water is transported northwards, either in extensions of the North Atlantic Current (NAC; 3, Fig. 2.3) or via a flow along the European Shelf edge (7, Fig. 2.3) (McCartney and Mauritzen, 2001). Although some of the water entering the northern North Atlantic via the NAC recirculates around the subpolar gyre (e.g. in the Irminger Current; 4, Fig. 2.3), around 6.0-7.5 Sv passes over the Greenland-Scotland Ridge and into the Nordic Seas (Hansen and Østerhus, 2000). As this flow is supplemented by the warmer and saltier Shelf Edge Current (7, Fig. 2.3), not only is the volume flux biased towards the east but the heat and salt transports are too (Fig. 2.2). As the upper waters move northwards they are progressively cooled and freshened due to air-sea interactions and deep winter convection (Hansen and Østerhus, 2000). Once in the

Nordic Seas this densification is enhanced by intense winter storms as well as mixing with underlying denser water masses which, due to the Greenland-Scotland Ridge, cannot easily flow southward. Hence, in the Nordic Seas relatively warm and salty upper Atlantic Waters are transformed into cooler, fresher and denser intermediate and deep water masses which eventually move southward towards the Greenland-Scotland Ridge (Fig. 2.4).

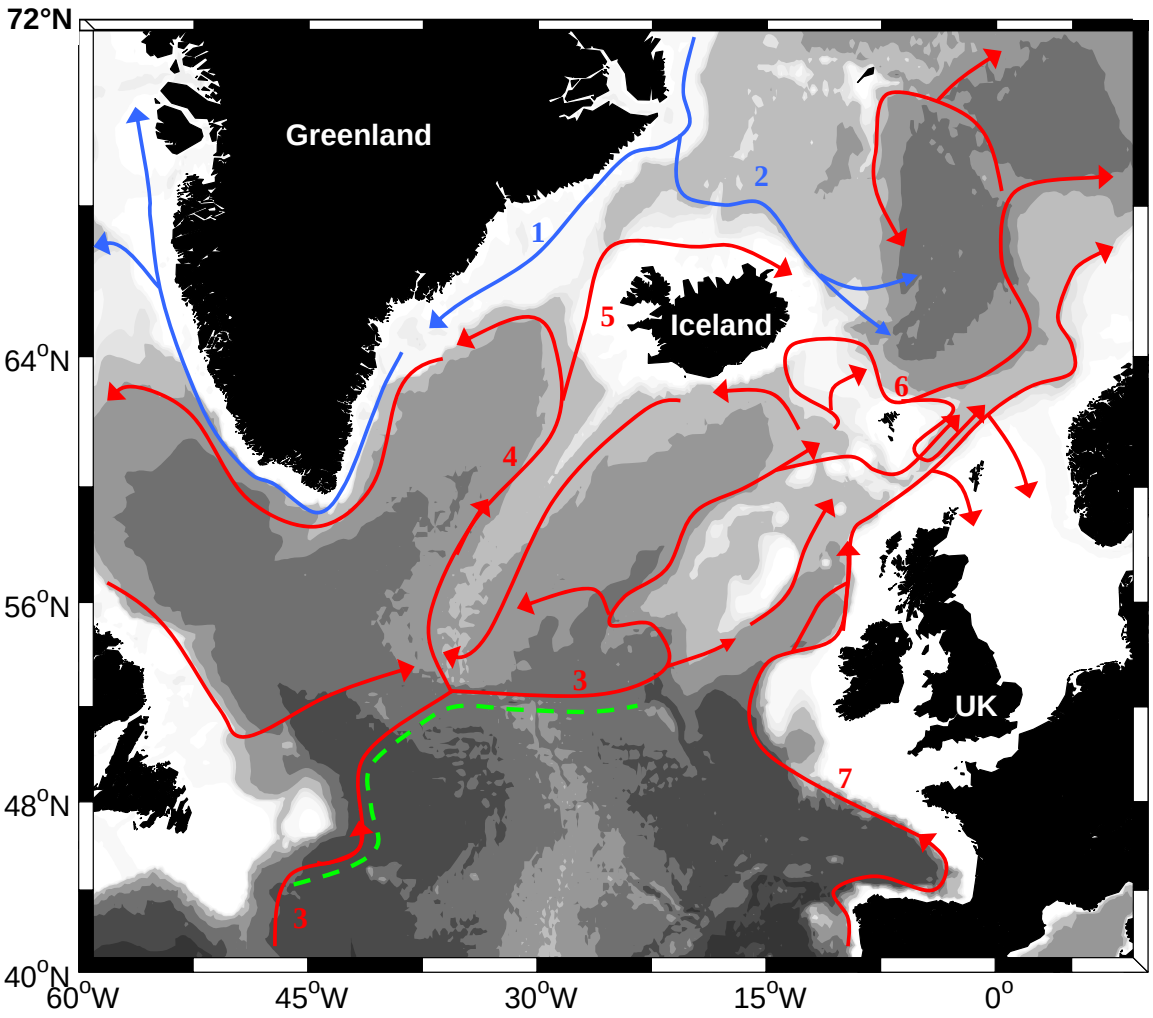

Figure 2.3. Schematic of upper water (< 600 m) circulation within the subpolar North Atlantic. Red lines: warm currents; blue: cold currents; green dashed line: approximate position of the Subpolar Front. 1: East Greenland Current; 2: East Icelandic Current; 3: North Atlantic Current; 4: Irminger Current; 5: North Icelandic Irminger Current; 6: Faroe Current; 7: Shelf Edge Current. Compiled from Blindheim and Rey (2004) ; Bower et al., (2002); Hansen and Østerhus (2000); and Read and Pollard (1992). The Subpolar Gyre refers to the general cyclonic circulation of upper waters south of the Greenland-Scotland Ridge. Isobaths: 500 m, 1000 m, 2000 m, 3000 m and 4000 m.

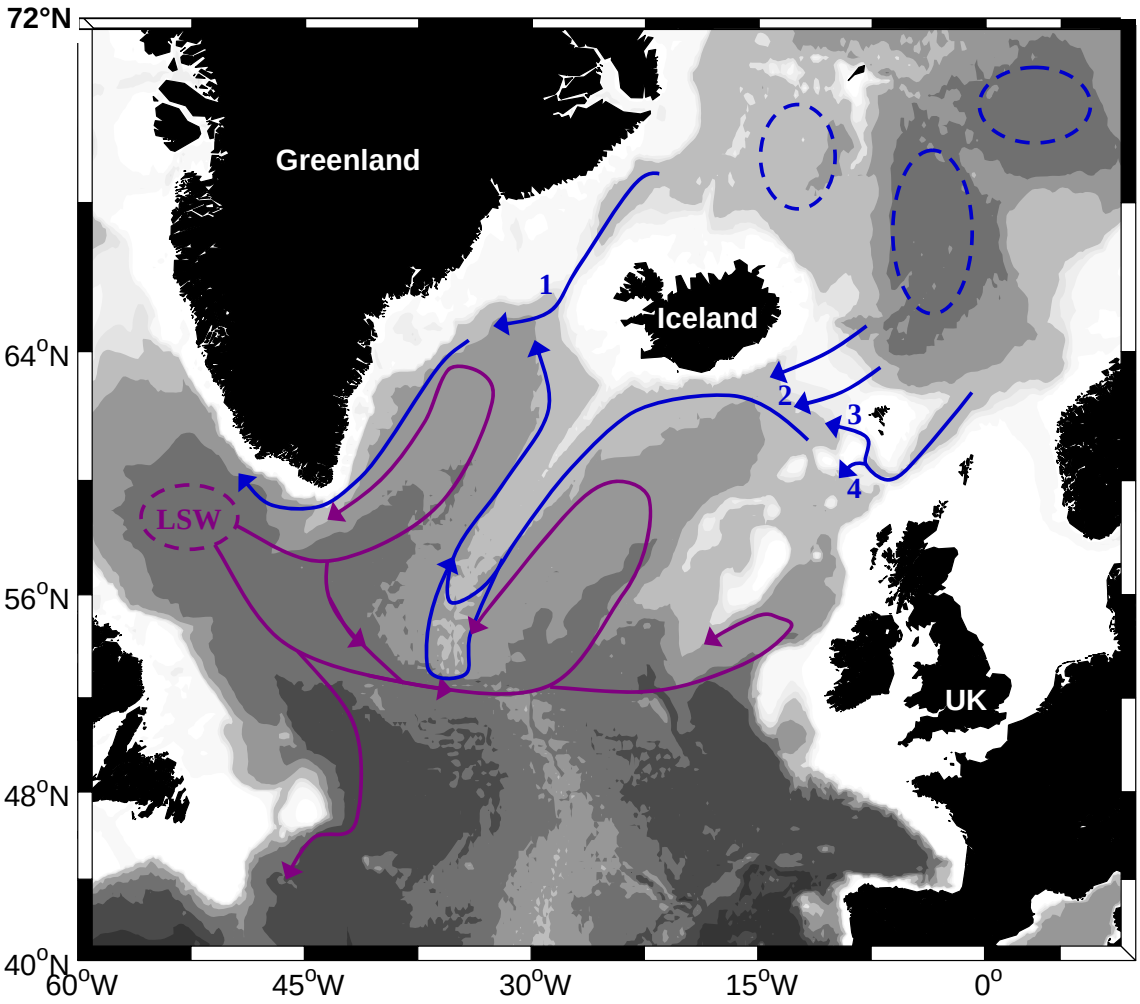

Figure 2.4. Schematic of pathways of overflow waters (blue) and Labrador Sea Water (purple) in the subpolar North Atlantic. Blue dashed lines: areas of deep water formation; purple dashed lines: main area of LSW formation. 1: Denmark Strait Overflow Water (DSOW); 2: Iceland-Faroes Overflow Water; 3: Faroe Bank Channel Overflow Water; 4: Wyville Thomson Ridge Overflow Water; LSW: Labrador Sea Water. Compiled from Hansen and Østerhus (2000) and Lavender et al. (2000). Isobaths: 500 m, 1000 m, 2000 m, 3000 m and 4000 m.

These cold dense waters mainly enter the Atlantic through the Denmark Strait (1, Fig. 2.4) and Faroe Bank Channel (3, Fig. 2.4), although water also spills over the Iceland-Faroe Ridge (2, Fig. 2.4) and Wyville Thomson Ridge (4, Fig. 2.4). Fluxes of water through these pathways with a potential density (σ_θ) > 27.8 kg m^{-3} are estimated at 2.9 Sv, 1.7 Sv, 1 Sv and ~ 0.4 Sv respectively (Dickson and Brown, 1994). As these waters are dense relative to other water masses in the Atlantic, they cascade over the ridge entraining surrounding waters as they sink creating 'overflow waters' (Dickson and Brown, 1994).

As the overflow waters flow cyclonically around the subpolar gyre they are supplemented by an intermediate water mass formed by winter convection in the Labrador Sea (LSW, Fig. 2.4), and Antarctic Bottom Water (AABW) which enters the region from the south. The flux of water with a $\sigma_\theta > 27.8$ kg m^{-3} passing westwards through the Charlie Gibbs Fracture Zone (composing of Iceland-Scotland Overflow Water (2 + 3, Fig. 2.4), LSW and AABW) is estimated at 6.6 Sv (McCartney, 1992). After the addition of Denmark Strait Overflow Water (1, Fig. 2.4), and additional LSW which enters the Irminger Basin by a mid-depth circulation (Lavender et al., 2000; Kase et al., 2001), the flux of water denser than 27.8 kg m^{-3} at the southern tip of Greenland is estimated between 10.7 Sv (McCartney, 1992) and 13.3 Sv (Dickson and Brown, 1994). This water, after circulating the Labrador Sea boundary, continues southward as a deep western boundary current (Talley and McCartney, 1982) eventually crossing the equator.

Circulation patterns in the subpolar North Atlantic are not stationary. Fluxes of the upper waters and overflow waters are known to vary seasonally and inter-annually (e.g. Saunders, 1990; Østerhus et al., 2001) as does LSW production (Rhein et al., 2002). Additionally, the properties of water masses change with time; for example due to changes in the characteristics or importance of component water masses (e.g. Turrell et al., 1999; Fogelqvist et al., 2003), or the depth of winter convection (e.g. Yashayaev, 2007). Another important source of variability, particularly in the eastern subpolar North Atlantic, is changes in the Subpolar Gyre. This is thought to be at least partly related to changes in the atmospheric North Atlantic Oscillation (NAO), a measure of the pressure difference between Iceland and the Azores (Hurrell, 1995), and associated westerly wind strength (e.g. Bersch et al., 1999; Hakkinen and Rhines, 2004). When the NAO index is high the Subpolar Gyre intensifies and expands south-eastwards; conversely when the NAO index decreases (such as occurred in the mid-1990s) the Subpolar Gyre weakens and contracts shifting north-westwards (Johnson and Gruber, 2007). Recent research, however, suggests that the NAO fails to explain the warming of the Subpolar Gyre in the 2000s with the number of blocking atmospheric winter highs instead being the predominant driving factor (Häkkinen et al., 2011b). As westerly winds are blocked by the presence of a winter high over the northern North Atlantic, the greater the number of blocking events the weaker the Subpolar Gyre circulation and the weaker the ocean-atmosphere heat exchange. Hence, the upper ocean is warmer and more saline (Häkkinen et al., 2011a). Whatever the cause of variability in the strength of the Subpolar Gyre, the effects can be observed in positional

changes of the NAC (Bower et al., 2002) which forms the eastern limb of the Subpolar Gyre. For example, the current was located several degrees further west in 1996 than in 1991 (Pollard et al., 2004). As the Subpolar Front (green dashed line, Fig. 2.3), which marks the boundary between subtropical and subpolar waters, is associated with the NAC, changes in the position of this current affects the amount of subtropical waters able to reach the subpolar latitudes (Hätun et al., 2005). This can be observed as positive salinity anomalies, not only in the upper layers of the Rockall Trough but also in the Iceland Basin which cannot be explained by local air-sea interactions (Holliday, 2003; Thierry et al., 2008) and correlate well with the strength of the Subpolar Gyre (Fig. 2.5).

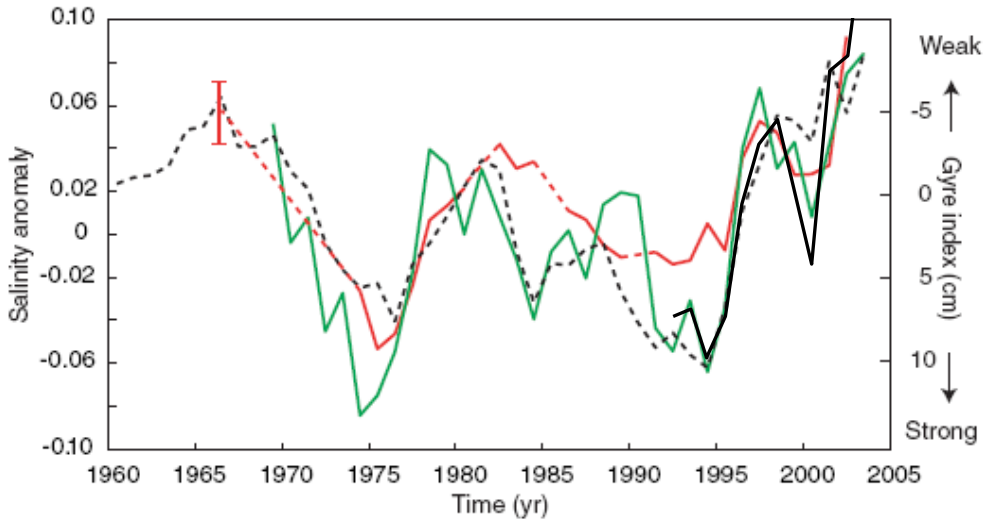

Figure 2.5. Temporal variability of annual observed salinity anomalies in the Iceland Basin (solid green line) and Rockall Trough (solid red line) plotted against the inverted modelled (dashed black line) and observed (solid black line) gyre strength index. The gyre strength index is defined as the principal component associated with the leading North Atlantic sea-surface height mode and observed values are determined from remotely-sensed altimetry records. Salinity anomalies are adjusted for advection lags. Red vertical line indicates range of salinity anomaly in the Rockall Trough in the 1960s. Adapted from Fig. 2, Hätun et al., (2005).

2.3. Lower oxygen layer in the subpolar North Atlantic

Dissolved oxygen and nutrient concentrations in the ocean are not conservative; hence their distributions away from the surface are determined by factors in addition to advection

and mixing. Oxygen concentrations tend to be highest in the surface layer due to inputs from the atmosphere and photosynthesis, and generally decrease with depth due to consumption during the decomposition of organic matter (e.g. Libes, 1992; Chester, 2000). The exception to this is when a relatively young water mass (i.e. one that has not been isolated from the atmosphere for particularly long) such as LSW, is found at depth. Contrastingly, nutrient (nitrate, phosphate and silicate) concentrations tend to be lowest in the mixed layer where they are consumed by phytoplankton, and higher at depth where they are released as organic matter is decomposed. Again this generalisation is interrupted when relatively young water masses and their associated lower nutrient concentrations are found at depth (e.g. Libes, 1992; Chester, 2000).

A prominent feature in the subpolar North Atlantic is a layer of lower oxygen concentrations seen between 700-1500 m in the Rockall Trough and Iceland Basin (Fig. 2.6). At 55-60 ºN values vary from 5.2-5.4 ml l^{-1} (226-235 μmol kg^{-1}) in the Rockall Trough and eastern Iceland Basin, to 5.4-5.6 ml l^{-1} (235-243 μmol kg^{-1}) in the central Iceland Basin, and 5.6-5.8 ml l^{-1} (243-252 μmol kg^{-1}) over the Reykjanes Ridge. The layer is not present in the Irminger Basin with higher concentrations of 6.6-6.8 ml l^{-1} (287-296 μmol kg^{-1}) representing the presence of oxygenated LSW at this depth. Nutrient concentrations in the Rockall Trough and Iceland Basin are elevated in the lower oxygen layer (van Aken and de Boer, 1995). Although the depleted oxygen concentrations in the Rockall Trough have been hypothesised to be related to the presence of MOW (Ellett and Martin, 1973), this water mass has been discounted as the cause in the Iceland Basin (van Aken and Becker, 1996). Instead water observed off the coast of West Africa (Tsuchiya et al., 1992) or Antarctic Intermediate Water (AAIW) (van Aken and Becker, 1996) have been put forward as possible sources. The oxygen depleted water observed off West Africa is thought to be advected northwards as an eastern boundary current (Kawase and Sarmiento, 1986) whilst AAIW is carried northwards in the Gulf Stream and North Atlantic Current (Tsuchiya, 1989; Read, 2001). The northern extent of AAIW is under debate with estimates ranging from 20 ºN to 60 ºN (Mann et al., 1973; Broecker and Takahashi, 1981; Tsuchiya et al., 1992; Read, 2001). Dissolved oxygen concentrations in AAIW observed at 54 ºN (5.6-5.8 ml l^{-1}, 243-253 μmol kg^{-1}) are higher than values in the lower oxygen layer at the same latitude (4.8-5.4 ml l^{-1}; 209-235 μmol kg^{-1}) (Read, 2001). Further, AAIW is observed at a shallower depth (~ 500 dbar) than the lower oxygen layer (van Aken and de Boer, 1995; Read, 2001).

An alternative hypothesis is that the lower oxygen layer does not indicate the presence of an advected water mass, rather that it is formed by *in-situ* remineralisation of sinking organic matter (van Aken and de Boer, 1995; Stoll et al., 1996; de Boer, 1998). Indeed the presence of a layer of depleted oxygen within the permanent pycnocline (at about 1000 m in the Atlantic) is a globally recognised phenomenon (e.g. Wyrtki, 1962; Libes, 1992; Anderson and Sarmiento, 1995; Bearman, 2001). Additional evidence in support of this hypothesis is given in de Boer (1998) who report that it is impossible to produce the characteristics of the lower oxygen layer in the Iceland Basin by mixing Subpolar Mode Water and LSW with either MOW, East African Water or AAIW.

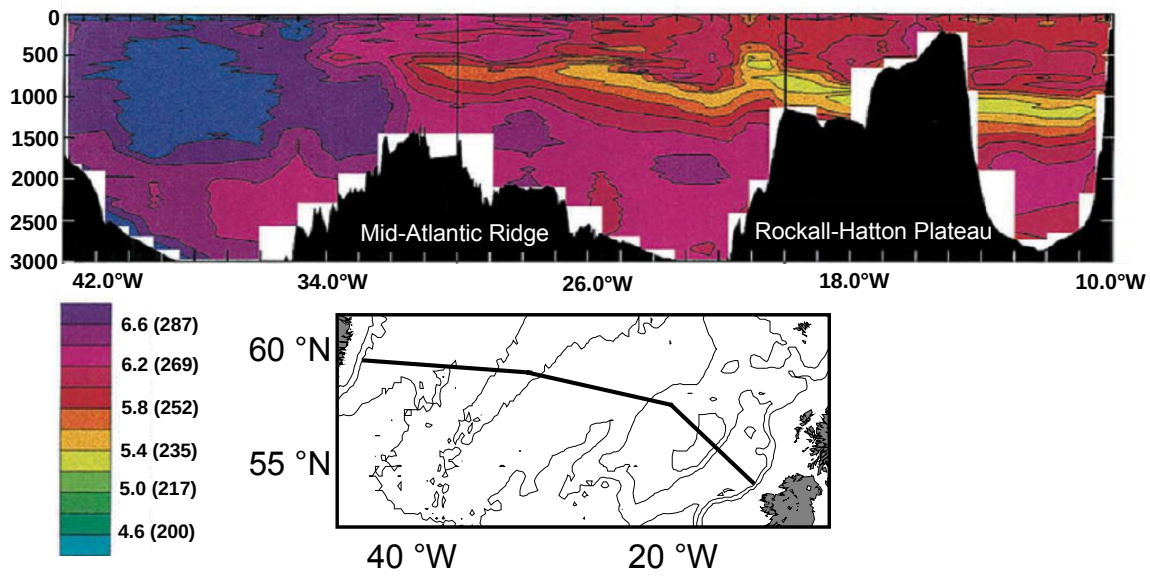

Figure 2.6. Dissolved oxygen concentrations across a zonal section in the subpolar North Atlantic. Concentrations in ml l^{-1} (brackets µmol kg^{-1}). See inset map for section location. From Read (2001).

2.4. Bathymetry of the Rockall Trough and Wyville Thomson Ridge

The Rockall Trough is a relatively small basin in the eastern subpolar North Atlantic (Fig. 2.1). It is bordered to the east by the European continental shelf (< 200 m depth) and to the west by a series of banks that rise to within 200 m of the surface (with the exception of George Bligh Bank (GBB, Fig. 2.7) that is < 500 m). Although these banks separate the Rockall Trough from the Iceland Basin, a number of channels exist providing a link

between the two basins. The deepest of these, between Bill Baileys Bank (BBB, Fig. 2.7) and Lousy Bank (LB, Fig. 2.7), has a depth of ~ 1200 m. A relatively shallow area (1000-1200 m), the Rockall-Hatton Plateau (RHP, Fig. 2.7), lies between Rockall Bank (RB, Fig. 2.7) and Hatton Bank (HB, Fig. 2.7) providing an additional barrier between the Rockall Trough and deeper waters further west. Bathymetry in the Rockall Trough gradually deepens towards the south; depths are typically > 1000 m in the north but > 3000 m at the southern entrance of the trough where it opens onto the Porcupine Abyssal Plain (PAP, Fig. 2.7). The flow of water through the northern part of the trough is interrupted by two seamounts, Rosemary Bank (R, Fig. 2.7) and the Anton Dohrn Seamount (AD, Fig. 2.7), which rise to depths of ~ 500 m. An additional seamount, the Hebrides Terrace Seamount (HT, Fig. 2.7), is situated further south near the continental slope. In the southwest of the trough a depositional feature, the Feni Ridge (FR, Fig. 2.7), runs along the bottom of the eastern flank of the Rockall-Hatton Plateau rising to ~ 2200 m at its crest.

The northern boundary of the trough is defined by the Wyville Thomson Ridge (WTR, Fig. 2.7) which is the easternmost part of the Greenland-Scotland Ridge. The Wyville Thomson Ridge separates the deep Faroese Channels and Wyville Thomson Basin lying to the north, from the northern Rockall Trough to the south. Although most of the ridge has a depth of 500-600 m, the ridge crest shallows towards the east where depths of < 500 m are seen. The deepest point (> 600 m) is a gap located approximately in the centre of the ridge (CG, Fig. 2.8.a). A spur, the Ymir Ridge (YR, Fig. 2.8.a), branches off the Wyville Thomson Ridge to the east of the central gap creating a small 800-950 m deep basin between the two ridges. This basin, called the Ymir Trough (YT, Fig. 2.8.a), has two exits: a > 700 m saddle in the Ymir Ridge crest to the south, and an approximately 5 km wide gulley (the Ellett Gulley, EG Fig. 2.8.b) to the west. This gulley rapidly deepens from 890 m to 1730 m as it enters a second basin, the Cirolana Deep (CD, Fig. 2.8.b). A detailed SWATH survey of the area combined with historical data revealed the presence of a previously unknown canyon (named the Faroe Bank Canyon; FBCa, Fig. 2.8.b) running from the flanks of Faroe Bank into the Ellett Gulley. This canyon has particularly steep eastern sides of about 250 m in height (Sherwin et al., 2008).

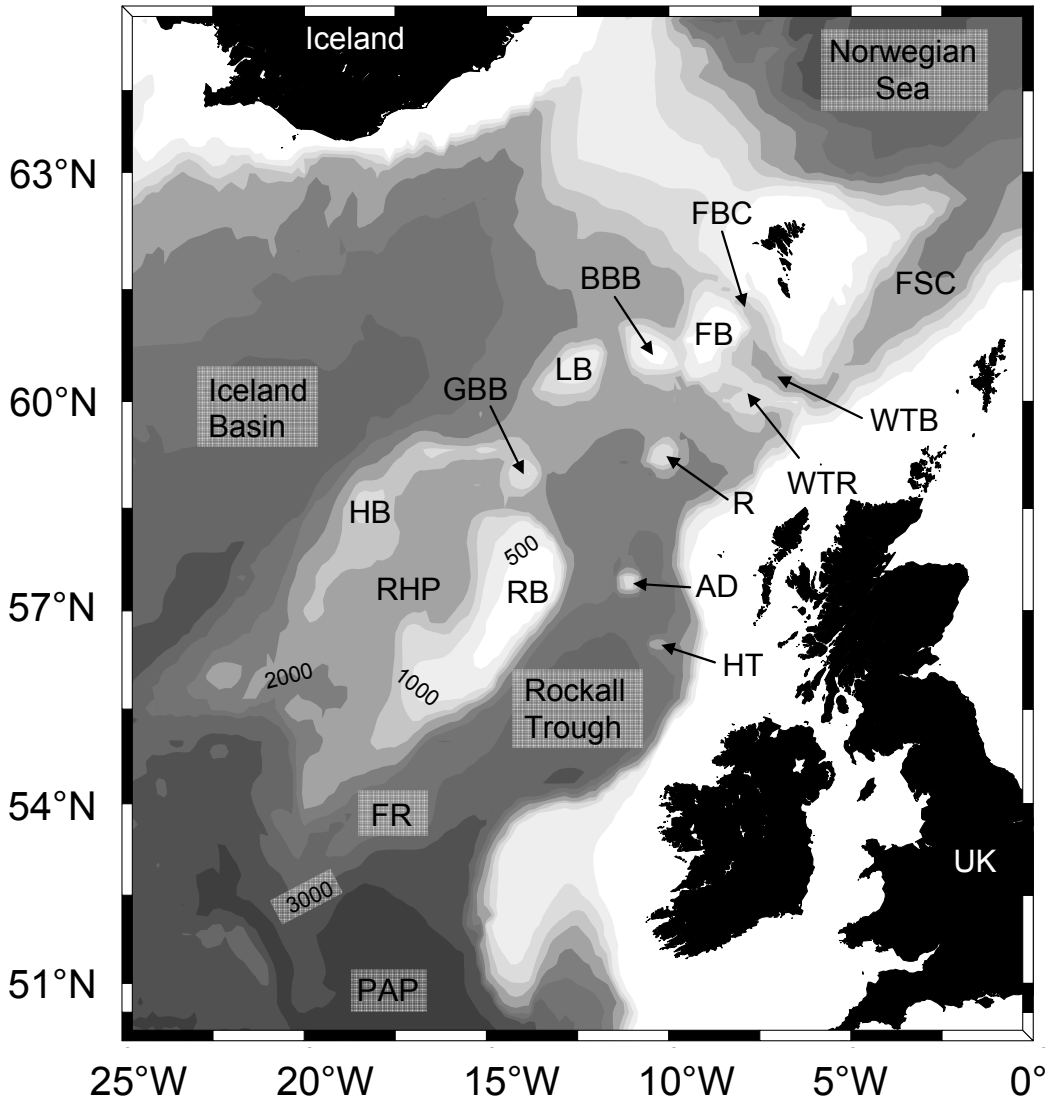

Figure 2.7. Bathymetry of the Rockall Trough. AD: Anton Dohrn Seamount; BBB: Bill Baileys Bank; FB: Faroe Bank; FBC: Faroe Bank Channel; FR: Feni Ridge; FSC: Faroe Shetland Channel; GBB: George Bligh Bank; HB: Hatton Bank; HT: Hebridean Terrace Seamount; LB: Lousy Bank; PAP: Porcupine Abyssal Plain; R: Rosemary Bank; RB: Rockall Bank; RHP: Rockall-Hatton Plateau; WTB: Wyville Thomson Basin; WTR: Wyville Thomson Ridge.

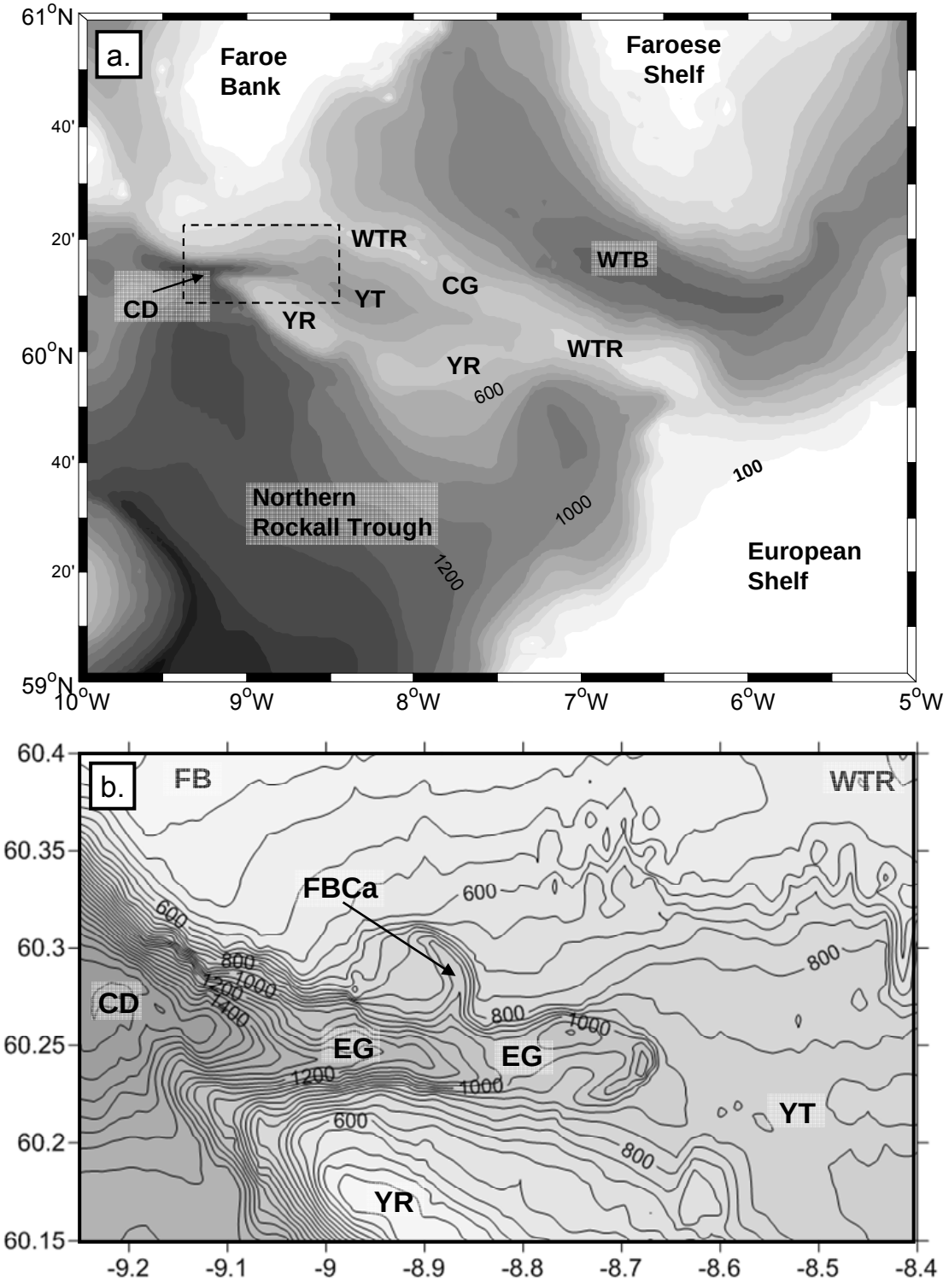

Figure 2.8. Bathymetry of: a. The Wyville Thomson Ridge area and b. detailed bathymetry of the Ellett Gulley (see dashed box in a. for location) adapted from Fig. 1 Sherwin et al. (2008). CD: Cirolana Deep; CG: Central Gap; EG: Ellett Gulley; FB: Faroe Bank; FBCa: Faroe Bank Canyon; WTB: Wyville Thomson Basin; WTR: Wyville Thomson Ridge; YR: Ymir Ridge; YT: Ymir Trough. Contours in a. every 100 m, contours in b. every 50 m.

2.5. Water masses entering the Rockall Trough from the south

2.5.1. Atlantic Waters

Upper waters in the Rockall Trough can be approximately divided into those carried northwards in the Shelf Edge Current, and those entering the area via the North Atlantic Current (Fig. 2.3). Nomenclature for these waters is complex with multiple names in use for a single body of water and the same terms often used for several different water masses. In this thesis we use the term North Atlantic Water (NAW) to describe the water flowing northwards in the Shelf Edge Current, and Eastern North Atlantic Water (ENAW) to define that which is carried in the North Atlantic Current. Water mass characteristics are given in Table 2.1

The slope current extends to 700 dbar (Holliday et al., 2000) and is most clearly seen as a subsurface salinity maximum ($S > 35.36$) at around 200-300 dbar in the vicinity of the continental slope (Hill and Mitchelson-Jacob, 1993). However, at times the current moves further offshore into the Rockall Trough (Burrows and Thorpe, 1999; Holliday et al., 2000). This current is particularly important to the regional salt and heat flux (section 2.2) and keeps Europe warmer than other areas of similar latitudes (Ellett, 1993a).

The upper waters (< 600 dbar) in the remainder of the Rockall Trough are composed of ENAW which, although having a net northward flow, is thought to exhibit an anticyclonic circulation with southward flow observed east of the Anton Dohrn Seamount and northward flow to the west (Ellett et al., 1986; Holliday et al., 2000). A parcel of cooler and fresher water (35.2-35.3, 8.0-8.7 °C, 400-900 dbar), which appears to enter the trough from the west via an anticyclonic circulation, is sometimes observed in the vicinity of Rockall Bank (e.g. Dooley and Henderson, 1980; Booth, 1988; Holliday et al., 2000). The relative importance of upper water originating from the Subpolar Gyre and Subtropical Gyre in the Rockall Trough is known to vary with position of the Subpolar Front (e.g. Holliday, 2003; Hätun et al., 2005).

Water mass	Parameter	Value	Units
Antarctic Bottom Water (AABW)	S	~ 34.95	
measured southern entrance Rockall Trough	θ	~ 2.8	°C
	O_2	230-255	µmol kg^{-1}
Physical data: (Holliday et al., 2000)	NO_3	18.8-22.8	µmol kg^{-1}
Chemical data: this study	PO_4	1.2-1.5	µmol kg^{-1}
Al data: this study	Si	25-45	µmol kg^{-1}
	CFC-11	< 0.9	pmol kg^{-1}
	CFC-12	< 0.4	pmol kg^{-1}
	Al	10-17	nM
Eastern North Atlantic Water (ENAW)	S	~ 35.5	
measured just north of WTR	θ	8-10	°C
	O_2	265-270	µmol kg^{-1}
Physical data: (Fogelqvist et al., 2003)	NO_3	12.5-13.5	µmol kg^{-1}
Chemical data: (Fogelqvist et al., 2003)	PO_4	0.9-1.0	µmol kg^{-1}
Al data: this study	Si	3-6	µmol kg^{-1}
	CFC-11	3.8-4.2	pmol kg^{-1}
S and θ southern entrance to Rockall Trough:	CFC-12	1.2-2.5	pmol kg^{-1}
35.22, 35.53 [a] and 8,10 °C [a] (Harvey, 1982)	Al	3-5	nM
Labrador Sea Water (LSW)	S	34.8-34.9	
measured southern entrance Rockall Trough	θ	3.0-3.5	°C
	O_2	270-280	µmol kg^{-1}
Physical data: (New and Smythe-Wright,	NO_3	16.9-17.4	µmol kg^{-1}
2001)	PO_4	1.0-1.1	µmol kg^{-1}
Chemical data: this study	Si	11-13	µmol kg^{-1}
Al data: this study	CFC-11	~3.4	pmol kg^{-1}
	CFC-12	1.5-1.8	pmol kg^{-1}
	Al	3-7	nM
Mediterranean Overflow Water (MOW)	S	35.5-35.6	
measured southern entrance Rockall Trough	θ	8-10	°C
	O_2	~ 200	µmol kg^{-1}
Physical data: (Reid, 1979)	NO_3	~ 17.6	µmol kg^{-1}
Chemical data: this study	PO_4	~ 1	µmol kg^{-1}
Al data: this study	Si	~ 10	µmol kg^{-1}
	CFC-11	~ 1.9	pmol kg^{-1}
	CFC-12	~ 1.0	pmol kg^{-1}
	Al	~ 19	nM
Modified East Icelandic Water (MEIW)	S	34.70-34.90	
measured southern Faroe Shetland Channel	θ	1.0-3.0	°C
	O_2	305-318	µmol kg^{-1}
Physical data: (Hansen and Østerhus, 2000)	NO_3	11.8-13.0	µmol kg^{-1}
Chemical data: this study	PO_4	0.75-0.95	µmol kg^{-1}
Al data: this study	Si	5.5-7.0	µmol kg^{-1}
	CFC-11	3.9-4.4	pmol kg^{-1}
	CFC-12	1.8-2.1	pmol kg^{-1}
	Al	no data	

North Atlantic Water (NAW)	S	35.45-35.50	
measured eastern Rockall Trough	θ	9.5-10.5	°C
	O_2	255-270	µmol kg^{-1}
Physical data: (Hansen and Østerhus, 2000)	NO_3	9.0-11.5	µmol kg^{-1}
Chemical data: this study	PO_4	0.57-0.67	µmol kg^{-1}
Al data: this study	Si	3-5	µmol kg^{-1}
	CFC-11	2.50-3.25	pmol kg^{-1}
	CFC-12	1.15-1.75	pmol kg^{-1}
	Al	1-3	nM
Norwegian Sea Arctic Intermediate Water (NSAIW)	S	34.87-34.90	
	θ	-0.5-0.5	°C
measured southern Faroe Shetland Channel	O_2	300-307	µmol kg^{-1}
	NO_3	12.5-14	µmol kg^{-1}
Physical data: (Hansen and Østerhus, 2000)	PO_4	0.8-1.0	µmol kg^{-1}
Chemical data: this study	Si	7-10	µmol kg^{-1}
Al data: this study	CFC-11	2.6-3.6	pmol kg^{-1}
	CFC-12	1.2-1.6	pmol kg^{-1}
	Al	16-18	nM
Norwegian Sea Deep Water (NSDW)	S	34.91	
measured southern Faroe Shetland Channel	θ	< -0.5	°C
	O_2	298-300	µmol kg^{-1}
Physical data: (Hansen and Østerhus, 2000)	NO_3	13.5-14.5	µmol kg^{-1}
Chemical data: this study	PO_4	0.9-1.1	µmol kg^{-1}
Al data: this study	Si	10-12.5	µmol kg^{-1}
	CFC-11	1.1-1.3	pmol kg^{-1}
	CFC-12	< 0.6	pmol kg^{-1}
	Al	18-25	nM
Subarctic Intermediate Water (SAIW)	ρ	27.4, 27.6 [a]	kg m^{-3}
measured southern Iceland Basin (physical	S	< 34.90 [a]	
data) and southern entrance Rockall Trough	O_2	210-230	µmol kg^{-1}
(chemical data)	NO_3	18.5-19.0	µmol kg^{-1}
	PO_4	~ 1.2	µmol kg^{-1}
Physical data: (Pollard et al., 2004)	Si	10.6-11.6	µmol kg^{-1}
Chemical data: this study	CFC-11	1.7-3.7	pmol kg^{-1}
Al data: this study	CFC-12	0.8-1.8	pmol kg^{-1}
	Al	~ 2	nM
Wyville Thomson Ridge Overflow Water (WTOW)	S	34.85, 35.25 [a]	
	θ	0.5, 8.0 [a]	°C
measured Rockall Trough	O_2	see table 5.1	
	NO_3	see table 5.1	
Physical data: this study	PO_4	see table 5.1	
Chemical data: this study	Si	see table 5.1	
Al data: this study	CFC-11	0.9, 3.0 [a]	pmol kg^{-1}
	CFC-12	0.4, 1.7 [a]	pmol kg^{-1}
	Al	10, 23 [a]	nM

Table 2.1. Physical and chemical characteristics of water masses found within the Rockall Trough area. [a] *linear definition.*

2.5.2. Subarctic Intermediate Water

At the southern entrance to the Rockall Trough the influence of a cool and fresh water mass (salinity minimum ~ σ_θ 27.3 kg m^{-3}; Harvey and Arhan, 1988), SubArctic Intermediate Water (SAIW), is seen to the west of 18 ºW (Ullgren and White, 2010). This water mass is thought to form at the edges of the Labrador Sea (Ahran, 1990) and is subducted in the vicinity of the Subpolar Front to depths of around 200-400 m (e.g. Ellett et al., 1986; Pollard et al., 1996; Wade et al., 1997). Although the presence of SAIW is clear at the southern entrance of the trough, intense mixing in this area means the signature is quickly lost (Ellett, 1979; Pollard et al., 1996; Ullgren and White, 2010). This process is thought to be enhanced in Winter when convection often mixes the water column to around 600 m (Holliday et al., 2000) and up to 1000 m in severe years (Fuglister, 1960; Ellett et al., 1986). As such there is some evidence that a weak influence of SAIW may be observed in the southern Rockall Trough in the Summer and Autumn (Ellett et al., 1983).

2.5.3. Mediterranean Overflow Water

Mediterranean Overflow Water (MOW) is clearly identifiable as a mid-depth salinity maximum (35.5-35.6, ~1000 m, Table 2.1) in the east of the southern entrance to the Rockall Trough where it interleaves with SAIW (Ellett and Martin, 1973; Ullgren and White, 2010). The presence or absence of MOW in the Rockall Trough, however, is a matter of debate. Reid (1979) presented evidence that MOW not only flows through the trough but also over the Wyville Thomson Ridge and into the Nordic Seas. However, other observations have not found any evidence of MOW further north than around 52-54 ºN (Holliday et al., 2000; New et al., 2001; New and Smythe-Wright, 2001). A comprehensive review of chemical and physical data in the eastern subpolar North Atlantic discounts Reid's hypothesis and again finds no evidence of MOW further north than the Porcupine Seabight (PSB, Fig. 2.1) (McCartney and Mauritzen, 2001). Aspects of the θ-S profile in the central Rockall Trough, along with the lower oxygen layer (section 2.3), have been taken to indicate the presence of MOW (Ellett and Martin, 1973; Ellett et al., 1986), although the θ-S signature is very similar to that of overflow water (Ellett et al., 1983). More recently it has been suggested that the amount of MOW reaching the Rockall Trough is linked to the contraction and expansion of the Subpolar Gyre in response to changes in

the NAO. As the Subpolar Gyre weakens and contracts, a larger volume of MOW reaches the Rockall Trough as indicated by positive salinity anomalies at the density level corresponding to MOW (Lozier and Stewart, 2008). Modelling work supports this finding with the 35.7 isohaline reaching 47 ºN in the eastern North Atlantic during a low NAO index (i.e. weak Subpolar Gyre) compared with 45 ºN in a high NAO period (i.e. stronger Subpolar Gyre) (Bozec et al., 2011).

2.5.4. Labrador Sea Water

At intermediate depths the fairly homogeneous LSW is identified by a marked salinity and potential vorticity minimum between 1600-1900 m (Talley and McCartney, 1982). LSW is known to enter the Rockall Trough from the south and to penetrate to at least 56.6 ºN (Holliday et al., 2000). Since the deepest exit in the northern trough is around 1200 m, LSW must both enter and leave via the southern entrance; a cyclonic recirculation has been observed (Ellett et al., 1986; Holliday et al., 2000; New and Smythe-Wright, 2001). A time series of LSW core salinity at 57.5 ºN from 1975 onwards shows two periods of freshening: the mid 1980s and early 1990s (Ellett, 1993b; Holliday, 2003). One interpretation is that the LSW reservoir in the Rockall Trough is a stagnant pool which gradually erodes with time and is occasionally renewed via periodic inflow. These flushing events are observed as sudden decreases in salinity at the LSW core depth in the trough (Holliday et al., 2000) and uplift of the 35.0 isohaline (Ellett, 1993). An observation of higher CFC-11 concentrations at 56 ºN than at 54 ºN in the basin seems to support this hypothesis (New and Smythe-Wright, 2001). Further, a link between salinity at the LSW density level and NAO index, and therefore associated contraction and expansion of the Subpolar Gyre, has been found with negative salinity anomalies observed during a positive NAO and expanding gyre (Lozier and Stewart, 2008; Bozec et al., 2011). An alternative hypothesis is that the variations of LSW salinity within the Rockall Trough simply reflect annual changes in the Labrador Sea. In this case the two periods of freshening (mid 1980s and early 1990s) could indicate the arrival of a less saline LSW vintage to the area (Yashayaev et al., 2007). However, as magnitudes of freshening observed in the Rockall Trough are larger than those observed in the Labrador Sea this explanation cannot fully explain LSW variability within the trough (Holliday et al., 2000; Lozier and Stewart, 2008).

2.5.5. Deep waters

The densest water mass in the Rockall Trough (> 2000 m; New and Smythe-Wright, 2000) contains the signature of Antarctic Bottom Water (AABW) and although characterised by a relatively low temperature and salinity is most easily identified by elevated silicate levels (Table 2.1). Whilst the deep water within the trough clearly contains an influence of AABW, the water has very different characteristics to AABW found further south. In reality, the water we term AABW within the Rockall Trough, has been heavily modified and is also likely to contain a component of overlying North-East Atlantic Deep Water.

AABW both enters and exits the Rockall Trough via the southern entrance with a cyclonic flow within the basin (McCartney, 1992; New and Smythe-Wright, 2001). Although the water mass is most prevalent in the southern Rockall Trough, a significant component may extend to at least 56 °N over the shallowing bathymetry (New and Smythe-Wright, 2001).

2.6. Historical evidence of water masses entering the Rockall Trough from the north

2.6.1. Water masses north of the Wyville Thomson Ridge

Upper waters (< 400 m) in the Faroese Channels (FBC, FSC, Fig. 2.7) to the north of the Wyville Thomson Ridge enter the area from the subpolar North Atlantic to the south, either via the Shelf Edge Current or extensions of the North Atlantic Current (Fig. 2.3). These waters are cooler and fresher than those in the Rockall Trough and hence often termed Modified North Atlantic Water (Hansen and Østerhus, 2000). Additionally, a proportion of the Faroe Current (6, Fig. 2.3) enters the northern Faroe Shetland Channel via a cyclonic recirculation (Hansen and Østerhus, 2000).

Below ~ 400 m temperatures and salinities decrease rapidly as the intermediate and deep waters that are the precursors to WTOW are encountered (Turrell et al., 1999). Modified Eastern Icelandic Water (MEIW) is identifiable as a mid-depth (400-600 m) salinity minimum (Meincke, 1978) and oxygen maximum (Table 2.1). Although the signature of

MEIW is prominent in the Faroe Shetland Channel it is often less pronounced in the Faroe Bank Channel (Borenas and Lundberg, 1988). Recirculation of the water within the Faroe Shetland Channel (Meincke, 1978; Dooley and Meincke, 1981), or heavy modification due to mixing (Saunders, 1990), or a combination of the two processes (Borenäs and Lundberg, 2004) have been suggested. The distribution of MEIW also varies in a cross-channel direction with a thinner layer in contact with the Wyville Thomson Ridge than the Faroese Continental Shelf (Hansen and Østerhus, 2000). Two particularly cold (< 0.5 °C) and dense water masses form the main body of deep water in the Faroese Channels. Norwegian Sea Arctic Intermediate Water (NSAIW) is predominantly found on the Faroese side of the channels between around 600-800 m and like MEIW is less prevalent near the Scottish Shelf (Turrell et al., 1999) and Wyville Thomson Ridge (Mauritzen et al., 2005). Norwegian Sea Deep Water (NSDW) is the deepest water mass being found between ~ 800 m and the seabed (Turrell et al., 1999). The characteristics of NSAIW and NSDW within the Faroese Channels are known to vary temporally (Turrell et al., 1999) as is the relative importance of the two water masses (Fogelqvist et al., 2003).

2.6.2. Overflow water in the Rockall Trough

Numerous hydrographic surveys and current meter deployments provide unambiguous evidence that cold deep water masses from the Faroese Channels enter the Rockall Trough. Fluxes for water < 0 °C vary between 0.06-0.4 Sv (Table 2.2) with a general consensus around 0.3 Sv (Hansen and Østerhus, 2000). The relative range of volume estimates for overflow water colder than the upper Atlantic waters (< ~ 8 °C) is similar at 0.34-2.1 Sv (Table 2.2). Although part of this variability can be explained by position of the measurement (Sherwin et al., 2008), there is undoubtedly temporal variability in the WTOW flux as seen in the other Greenland-Scotland Ridge overflows (e.g. Saunders, 1990; Østerhus et al., 2001). Despite the clear evidence that WTOW flows out of the Ymir Trough via the Ellett Gulley (Fig. 2.8), joining with any overflow descending the Faroe Bank Canyon (Sherwin et al., 2008), its distribution and circulation pathways within the Rockall Trough are not well established.

Site	Time	Method	Flux	Reference
Ellett Gulley	Aug - Sept 1973	Current meter 12 m above seabed	1.2 Sv < 8.8 ºC 0.33 Sv of -0.5 ºC	(Ellett and Edwards, 1978)
Central gap	Spring 1987	Geostrophic calculation	0.35 Sv < 3 ºC	(Saunders, 1990)
Central gap	Spring 1988	Geostrophic calculation	0.30 Sv < 3 ºC	(Saunders, 1990)
Ridge crest	Various cruises 1983 - 1991	Geostrophic calculation	0.4 Sv < -1.0 ºC	(van Aken and Becker, 1996)
Western WTR crest	Apr 2003	Geostrophic calculation	0.25 Sv < 8.5 ºC 0.16 Sv < 6.0 ºC 0.10 Sv < 0.0 ºC	(Sherwin and Turrell, 2005)
Head of Ellett Gulley	Apr 2003	Geostrophic calculation	2.1 Sv < 8.5 ºC 1.5 Sv < 6.0 ºC 0.7 Sv < 0.0 ºC	(Sherwin and Turrell, 2005)
Ellett Gulley	Apr 2003	Geostrophic calculation	1.4 Sv < 8.5 ºC 0.9 Sv < 6.0 ºC 0.4 Sv < 0.0 ºC	(Sherwin and Turrell, 2005)
Ellett Gulley (exc. Faroe Bank Gulley)	Sept 2003 - Apr 2004	ADCP 10 m above seabed	0.57 Sv < 8.5 ºC 0.11 Sv < 0.0 ºC	(Sherwin et al., 2008)
Ellett Gulley (exc. Faroe Bank Gulley)	Oct 2005 - May 2006	ADCP 10 m above seabed	0.34 Sv < 8.5 ºC 0.06 Sv < 0.0 ºC	(Sherwin et al., 2008)
Ellett Gulley (inc. Faroe Bank Gulley)	May 2006 - Oct 2006	ADCP 10 m above seabed	1.00 Sv < 8.5 ºC 0.30 Sv < 0.0 ºC	(Sherwin et al., 2008)
Ellett Gulley (inc. Faroe Bank Gulley	Oct 2006 - Apr 2007	ADCP 10 m above seabed	0.71 Sv < 8.5 ºC 0.17 Sv < 0.0 ºC	(Sherwin et al., 2008)
Ellett Gulley (inc. Faroe Bank Gulley)	May 2007 - Sept 2007	ADCP 10 m above seabed	0.96 Sv < 8.5 ºC 0.24 Sv < 0.0 °C	(Sherwin et al., 2008)

Table 2.2 Fluxes of Wyville Thomson Ridge Overflow Water obtained from the literature.

It has been suggested that because of its density, WTOW colder than 6 °C must flow southward into the northern and central parts of the Rockall Trough (Sherwin and Turrell, 2005). Geophysical evidence shows that overflow water flows along the southern flanks of both Faroe Bank and Bill Baileys Bank (Boldreel et al., 1998; Kuijpers et al., 1998; Due et

al., 2006), whilst bedforms in the channel between Bill Baileys and Lousy Banks indicate westward flow into the Iceland Basin with the overflow water hugging Bill Baileys Bank (Kuijpers et al., 1998). Further south, scouring of sediments in the western Rockall Trough from George Bligh Bank to at least 57 °N, have been attributed to southward flow of deep water from the Nordic Seas (Howe et al., 2001). It has also been suggested that the sedimentary north-south Feni Ridge (FR, Fig. 2.7), in the deep water to the east of Rockall Bank, has been formed by the southward movement of overflow water (Johnson and Schneider, 1969; Ellett and Roberts, 1973). However, it is unlikely that present day overflow currents are able to mould this feature although there is a possibility that extreme events may help to contribute to the ridge's maintenance (Dickson and Kidd, 1986).

By contrast, hydrographic evidence of WTOW in the Rockall Trough has been less conclusive. In the northern trough water with the characteristics of NSDW has been observed in several surveys near Rosemary Bank. Although this has been attributed to WTOW (Ellett and Martin, 1973; Ellett et al., 1983; Harvey and Theodorou, 1986), the possibility that it overflowed the Faroe Bank Channel and entered the trough from the west has also been raised (Tulloch and Tait, 1959). Further south, water with a similar signature was recorded both at the foot of Rockall Bank and between 1500-2000 m, but was again assumed to have entered the trough from the Iceland Basin rather than over the Wyville Thomson Ridge (Lee and Ellett, 1965). Other observations of this water near Rockall Bank in the central trough has, however, been attributed to WTOW (Ellett et al., 1983; McCartney and Mauritzen, 2001), as was a high CFC-11 signal between 1000-1400 m in a similar location (New and Smythe-Wright, 2001). By contrast, an analysis of a time series of temperature and salinity data between Scotland and Rockall found little evidence of WTOW (Holliday et al., 2000).

One of the most compelling pieces of evidence to date for WTOW in the Rockall Trough comes from the Joint Air-Sea Interaction (JASIN) project which included an intensive CTD (conductivity-temperature-depth) and current meter survey of the north-western trough (Ellett et al., 1983). A cold anticyclonic eddy, that had a length scale of order 100 km and contained significant proportions of NSDW and entrained overlying ENAW, was observed to propagate westwards through the area. The source waters of this eddy were attributed to WTOW.

2.7. Investigating water masses in the ocean

In order to identify water masses (such as WTOW) and investigate their pathways and origins within the ocean, a variety of variables known as tracers can be employed. Although within physical oceanography the most commonly used tracers are potential temperature and salinity, a wealth of extra information can be obtained from the additional use of chemical variables. This is particularly true in a basin (such as the Rockall Trough) with complex oceanography and several water masses at similar density levels which may have overlapping temperature and salinity characteristics (Table 2.1).

Oceanic tracers can be classified as conservative or non-conservative. Conservative tracers are those whose concentrations, once away from their source and the ocean surface, are altered only by mixing and advection. Examples include potential temperature and salinity, as well as the anthropogenic chlorofluorocarbon (CFC) gases which enter the oceans via air-sea exchange. The concentrations of non-conservative tracers, as well as being influenced by mixing and advection, are also affected by one or more biological, chemical or sedimentological process. Examples of non-conservative tracers are nutrients (nitrate, phosphate and silicate) and dissolved oxygen. Although it is more complicated to use these variables to investigate water masses, valuable information can still be obtained.

The field of oceanic tracers is not static, with new water mass tracers being proposed and their applicability investigated. One such novel tracer is aluminium which is discussed in section 2.9. First, however, the use of CFCs as water mass tracers is examined.

2.8. Chlorofluorocarbons as water mass tracers

Chlorofluorocarbons (CFCs) are a group of anthropogenically-produced halogenated hydrocarbons; the two most commonly used as water mass tracers are CFC-11 (CCl_3F) and CFC-12 (CCl_2F_2). Manufacture began in the 1930s with the gases being used as refrigeration coolants, aerosol propellants, foaming agents and in various other applications (Bullister, 1989). As the CFCs were released to the atmosphere, their atmospheric mixing ratios (defined as the number of moles of the gas of interest in 1 mole of dry air) quickly rose from being undetectable prior to ~ 1945 to several hundred parts per trillion (Fig. 2.9).

In the early 1970s the first concerns on the effect of these gases on the atmospheric ozone layer were raised leading to the signing of the Montreal Protocol in 1978 and the gradual phasing out of the compounds (Fine, 2011). However, as the gases are very stable within the atmosphere, mixing ratios remain high although since 1990-2000 levels have begun to decrease (Fig. 2.9).

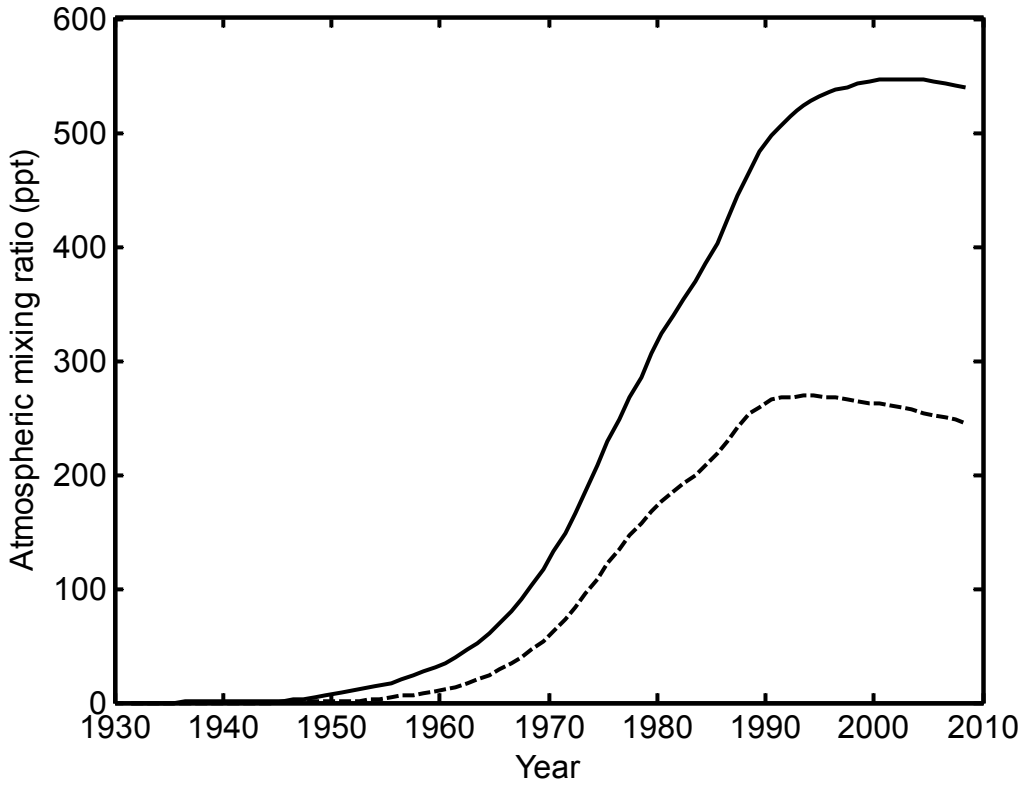

Figure 2.9. Atmospheric mixing ratios (parts per trillion, ppt) for CFC-11 (dashed line) and CFC-12 (solid line) between 1930 and 2008, relative to the SIO-98 calibration scale. Data were downloaded from http://bluemoon.ucsd.edu/pub/cfchist/. Prior to 1979 values are estimated using industrial production and release data (Walker et al., 2000). Errors are around 1-2 %.

CFCs enter the upper ocean via a flux from the atmosphere, mainly in high latitude areas where lower sea surface temperatures enhance the solubility of gases (Fine, 2011) and high wind speeds increase gas transfer rates (Asher and Wanninkhof, 1998). As the solubility of CFC-11 in seawater is much greater than that of CFC-12, the concentration of the former in the ocean is around twice that of CFC-12 despite the latter's higher atmospheric levels (Fine, 2011). Concentrations in the ocean are in the order of pmol kg^{-1} (picomole

kg^{-1}, $1x10^{-12}$ moles kg^{-1}). CFCs pass from surface waters into the ocean interior by convection, mixing and subduction of water masses (Tomczak, 1999). Both CFC-11 and CFC-12 exhibit conservative behaviour except under anoxic conditions (Bullister and Lee, 1995; Shapiro et al., 1997).

Due to the time-varying concentrations in the atmosphere (Fig. 2.9), and therefore also upper ocean, CFC values vary between water masses. Concentrations are generally highest in younger water masses and lowest in water that has been isolated from the atmosphere for considerable periods. Hence, the transient nature of atmospheric concentrations and therefore CFC uptake to the ocean enables its use as a water mass tracer. Since the first CFC profiles from the Pacific were published (Gammon and Wisegarver, 1981) various measurements have been made throughout the world's oceans. Observations were made during the Transient Tracers in the Ocean programme (1980s), World Ocean Circulation Experiment (1990s) and the Climate Variability project (2000s). CFCs have been used to trace LSW and North Atlantic Deep Water within the subpolar North Atlantic (e.g. Sy et al., 1997; Smethie et al., 2000; Rhein et al., 2002; LeBel et al., 2008), and to investigate the composition of water that has overflowed the Greenland-Scotland Ridge (e.g. Fogelqvist et al., 2003; Tanhua et al., 2008). Additionally, the distribution of CFC-11 in the central and southern Rockall Trough has been used to confirm LSW circulation within the basin (New and Smythe-Wright, 2001). CFC-11 concentrations are high (3.8-4.2 pmol kg^{-1}) in NEAW (Fogelqvist et al., 2003) and LSW, although concentrations in this water mass vary between 1.2-2.2 pmol kg^{-1} within the Rockall Trough (New and Smythe-Wright, 2001). In the Faroese Channels MEIW has the highest CFC-11 concentration (5.5-6.7 pmol kg^{-1}) showing that this water mass was last in contact with the atmosphere fairly recently (Fogelqvist et al., 2003). Interestingly NSAIW and NSDW have very different CFC-11 signatures, with concentrations significantly higher in NSAIW (3.5-4.0 pmol kg^{-1}) than in NSDW (0.2-0.5 pmol kg^{-1}) (Fogelqvist et al., 2003).

2.9. Aluminium as a novel water mass tracer

2.9.1. Processes governing aluminium distribution in the ocean

Aluminium has a short residence time (two-five years) in the upper ocean due to its particle-reactive nature (Orians and Bruland, 1986; Obata et al., 2004) although this increases to 150-200 years in the deep ocean (Orians and Bruland, 1986; Moran and Moore, 1991). The main source of aluminium to the surface ocean is the atmosphere (Fig. 2.10), particularly in areas of high atmospheric dust concentrations such as in the Saharan or Asian dust plumes (e.g. Minakawa and Watanabe, 1998; Bowie et al., 2002; Kramer et al., 2004). This dust may enter the ocean via dry deposition or by being washed out of the atmosphere in areas of high rainfall such as the Inter-Tropical Convergence Zone (Measures, 1995). As only around 1.5-10 % of aluminium deposited as dust dissolves in the surface waters (Maring and Duce, 1987), the majority of aluminium in the ocean exists in colloidal or solid phases (Morris et al., 1986) while dissolved concentrations are at the nanomolar (nM, $1x10^{-9}$ moles l^{-1}) level. Other possible sources of aluminium to the surface ocean include advection, exchange with coastal waters, and inputs from ice (Fig. 2.10). The concentrations in rivers are around three orders of magnitude higher than open ocean values, although aluminium is heavily scavenged in estuaries (Hydes and Liss, 1977; Takayanagi and Gobeil, 2000) and coastal zones, particularly in the summer (Kremling and Hydes, 1988; Hydes, 1989). Hence, in the majority of areas, this input is thought to be unimportant relative to the atmospheric loading (e.g. Orians and Bruland, 1986; de Jong et al., 2007). Melting ice has also been shown to be a source of aluminium to surface waters although the effect is thought to be localised (Measures, 1999; Middag et al., 2011).

Removal of aluminium from the surface ocean can occur in a number of ways (Fig. 2.10). Dissolved aluminium may be actively taken up by biology within the surface layer (e.g. Hydes et al., 1988; Chou and Wollast, 1997), or passively scavenged onto particulate matter (e.g. Moore and Millward, 1984; Moran et al., 1992). The relative importance of these two processes is thought to vary between oceanic regions (Orians and Bruland, 1986) with passive adsorption dominant in the North Atlantic (Hydes, 1979; Hydes, 1983). Dissolved and particulate aluminium may be mixed downwards to the intermediate and deep ocean (Hydes et al., 1988; Measures and Edmond, 1988) and particulate aluminium may also enter the interior of the ocean via settlement. It is thought that the majority of

particulate aluminium in the deep ocean (away from the bottom layer) has an atmospheric source (Buat-Menard and Chesselet, 1979).

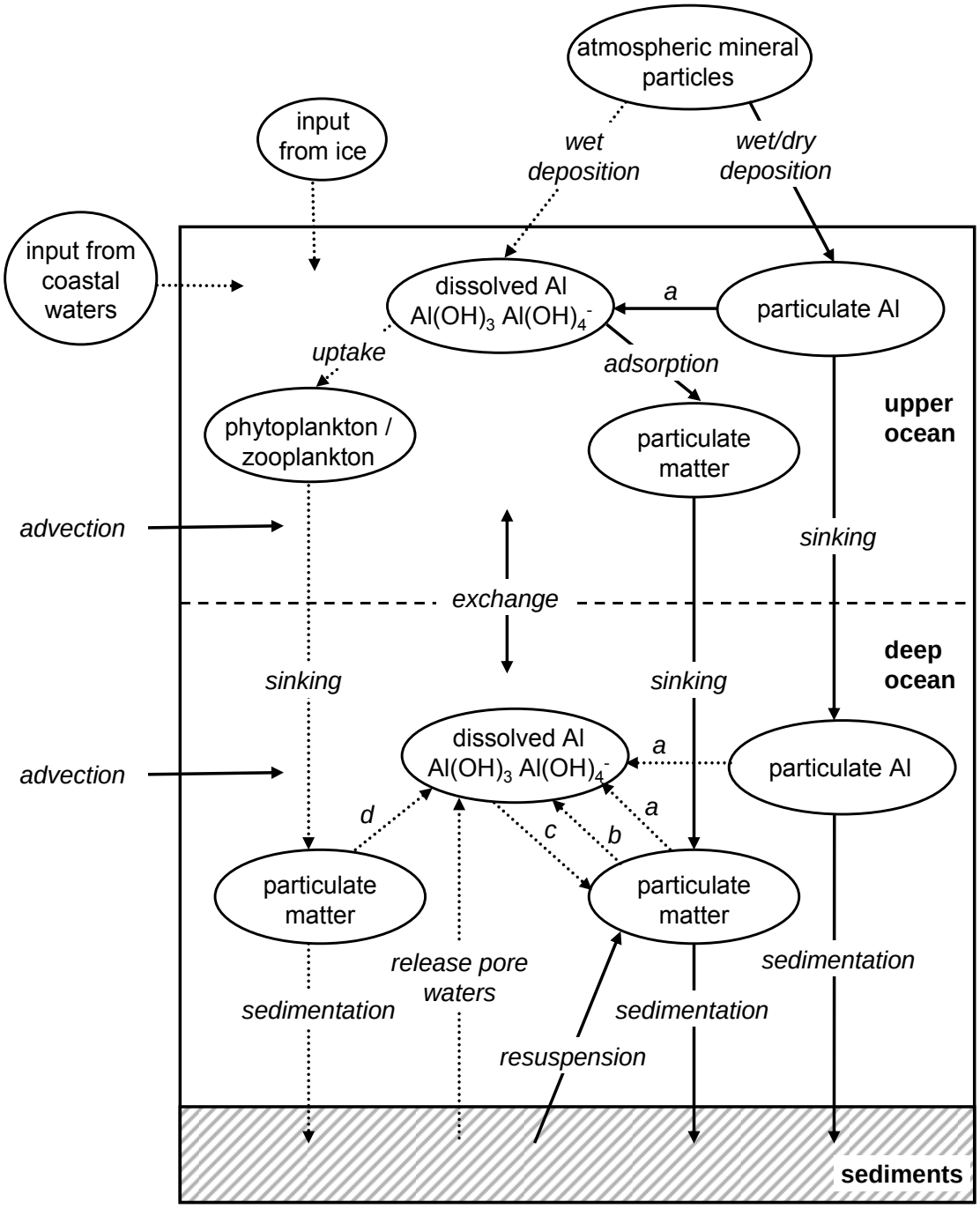

Figure 2.10. Schematic summary of the biological, chemical, sedimentological and physical processes that control aluminium distribution within the ocean. Solid arrows: important processes in the subpolar North Atlantic; dotted arrows: less dominant processes in the subpolar North Atlantic; a: dissolution; b: desorption; c: adsorption; d: decomposition.

Inputs of aluminium into the deep ocean include that exported from the surface layer as well as that which enters the area via horizontal advection. Additionally, several biogeochemical processes are at play (Fig. 2.10). Particulate matter that has entered the deep ocean may be partly dissolved or decomposed releasing aluminium, and any aluminium weakly bound to particle surfaces may desorb and re-enter the aqueous phase (Moore and Millward, 1984). Conversely, dissolved aluminium can adsorb onto particle surfaces. All of these processes, however, have been found to be insignificant in several oceanic areas (e.g. Hydes, 1983; Orians and Bruland, 1986) and deep water aluminium concentrations can be thought of as quasi-conservative (Measures and Edmond, 1990).

The same is not true for bottom waters where concentrations are generally elevated near the seabed indicating a bottom source of aluminium (e.g. Orians and Bruland, 1986; Measures, 1995). Although release of aluminium from pore waters (Measures et al., 1986) and hydrothermal plumes (Lunel et al., 1990) have been found to be important in some areas, the effect is localised. Instead the dominant process is thought to be bottom sediment resuspension, particularly in areas of strong flow such as those influenced by the Deep Western Boundary Current (Lambert et al., 1984; Moran and Moore, 1991) and flow through the Faroe Bank Channel (Hall and Measures, 1998). Indeed well-developed nepheloid layers within the ocean coincide with areas of strong bottom currents (Brewer et al., 1976; Biscaye and Ettreim, 1977). Laboratory experiments have shown that sediment resuspension not only leads to an increase in particulate aluminium levels but also dissolved aluminium concentrations (Hydes, 1977; Mackin and Aller, 1984).

2.9.2. Historical measurements of aluminium in the subpolar North Atlantic and use as a tracer

Published deep water aluminium profiles in the subpolar North Atlantic are predominantly found in two studies: the IOC Baseline Contaminants survey (Hall and Measures, 1998) and a PhD thesis (Lunel, 1990), with some other isolated profiles (Fig. 2.11). After intensive investigation of the literature, it is believed that there are no published aluminium measurements in the Rockall Trough.

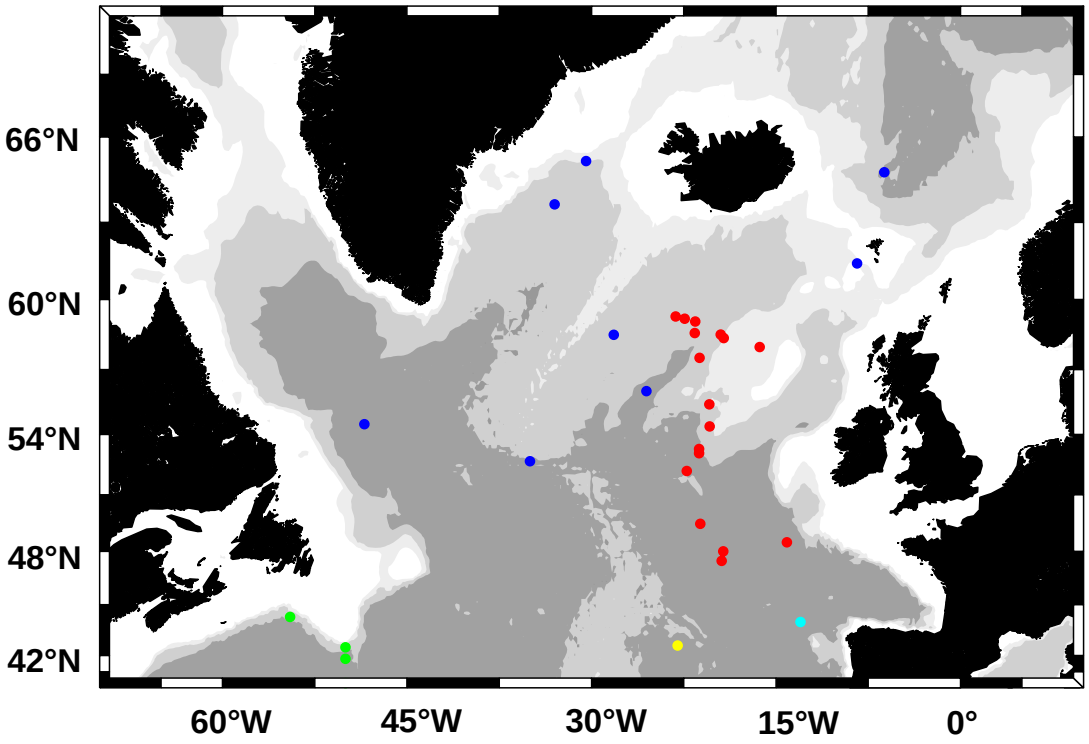

Figure 2.11. Published deep-water aluminium profiles within the subpolar North Atlantic. Cyan: reactive aluminium, Bowie et al. (2002); yellow: dissolved concentrations, de Jong et al. (2007); blue: reactive and dissolved concentrations, Hall and Measures (1998); red: reactive aluminium, Lunel (1990) and green: dissolved concentrations, Moran and Moore (1991). Additionally dissolved measurements in the upper 1000 m along 20 °W are reported by Measures et al. (2008). Contours are at 500 m, 1000 m, 2000 m, 3000 m and 4000 m.

Concentrations in the subpolar North Atlantic vary between water masses with the aluminium distribution predominantly controlled by advective processes (Hall and Measures, 1998). Dissolved levels in the upper waters are generally < 10 nM due to relatively low eolian inputs (~ 0.2 g m^{-2} a^{-1}; Measures et al., 2008) and scavenging (Hall and Measures, 1998). Additionally, the elevated surface layer concentrations observed in the Mediterranean and other areas of high dust input (e.g. Hydes et al., 1988; Kramer et al., 2004) are not present (Lunel, 1990). Dissolved concentrations in LSW are also relatively low with 6.9-7.7 nM being recorded in the Labrador Sea and 4.4 nM in the Iceland Basin (Hall and Measures, 1998). In contrast high reactive aluminium concentrations (defined as dissolved aluminium plus that adsorbed to particles; Hydes and Liss, 1976) of 12.2-13.4 nM are observed in MOW (Lunel, 1990). Interestingly, water exiting the Faroe Bank

Channel has a distinct elevated reactive aluminium signature in the deep waters which is, to a lesser extent, mirrored in the dissolved aluminium levels (Fig. 2.12). As these changes in aluminium concentrations are coincidental with variations in potential temperature and salinity it suggests that this high aluminium signature may be useful in tracing Faroe Bank Channel Overflow Water. It also raises the interesting possibility that WTOW too may have an elevated aluminium signal.

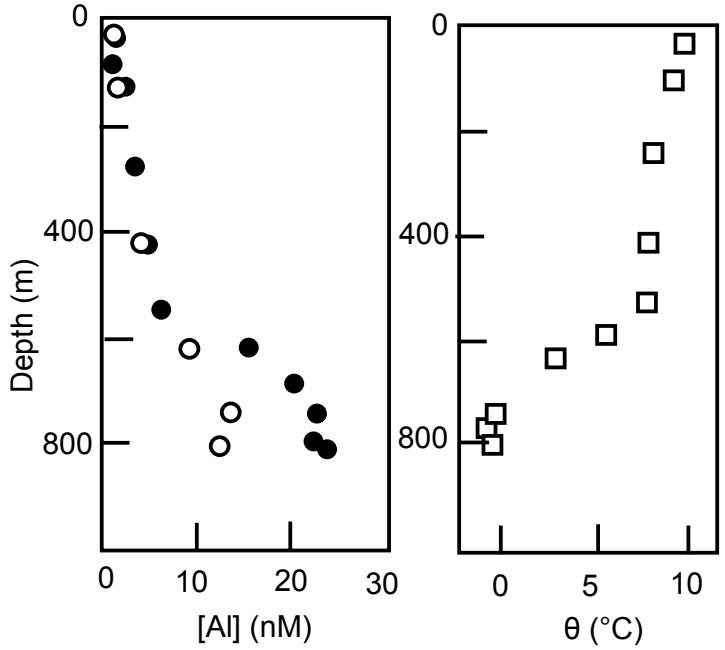

Figure 2.12. Reactive (black circles) and dissolved (white circles) aluminium profiles from the exit of the Faroe Bank Channel along with a potential temperature (white squares) profile. Adapted from Fig. 10, Hall and Measures (1998).

There is clear evidence that aluminium concentrations vary between water masses and that the element can be regarded as quasi-conservative in some oceanic regions (e.g. Measures and Edmond, 1990; Measures and Edmond, 1992), including the subpolar North Atlantic (Hall and Measures, 1998). Additionally, it has been suggested that trace metals (Abdullah, 1985), including aluminium (Hydes, 1983; Burton and Statham, 1988; Lunel et al., 1990), could be valuable water mass tracers. Despite this only one study has used aluminium in this manner, to help determine the composition of MOW (Measures and Edmond, 1988). Hence the investigation into, and use of, aluminium as a water mass tracer is novel.

2.10. Summary

Within this chapter the current knowledge on the circulation and water masses within the wider subpolar North Atlantic as well as the Rockall Trough have been examined. The main objective of this work is to resolve the pathways and fate of WTOW within the subpolar North Atlantic, with a focus on the Rockall Trough. As the Rockall Trough is an area of complex oceanography with the presence of several water masses with overlapping temperature and salinity characteristics, chemical tracers (oxygen, nutrients and CFCs) are employed in addition to these physical variables to address the study objective. In addition to these well established tracers the potential of aluminium as a tracer of WTOW will be investigated.

Chapter 3.
Methodology

This chapter provides information on the collection and analysis of chemical and physical data used within this thesis. First, four cruises to the eastern subpolar North Atlantic and the sampling techniques used during these are detailed. Next, the calibration and processing of sensor data is discussed, before the chemical analyses for the determination of nutrient concentrations in seawater are detailed. Finally, the chapter discusses the historical CTD and CFC data used within this thesis. The methods developed for the collection, storage and analysis of aluminium in seawater are not detailed in this chapter and are instead discussed at length in Chapter 4.

3.1. Cruises and CTD rosette deployment

Temperature, salinity and dissolved oxygen data, along with water samples for nutrient (nitrite, nitrate, phosphate and silicate) and aluminium analysis were collected during four cruises to the eastern subpolar North Atlantic (Table 3.1). Unfortunately, no dissolved oxygen data is available from H44-04-12 as the sensor did not perform well and could not be calibrated.

Cruise	Ship	Dates	Data collected
0804S	*FRV Scotia*	14th – 28th May 2004	T, S, O, N, Al
H44-04-12	*FS Alexander von Humboldt*	7th August – 5th September 2004	T, S, N, Al
CD176	*RRS Charles Darwin*	6th – 28th October 2005	T, S, O, N, Al
D312	*RRS Discovery*	11th – 31st October 2006	T, S, O, N, Al

Table 3.1. Cruises during which temperature (T), salinity (S), dissolved oxygen (O), nutrient (N) and aluminium (Al) data used in this thesis were collected. No oxygen data were collected during H44-04-12.

3.1.1. 0804S, May 2004

A cruise in May 2004 onboard FRV Scotia (0804S), occupied 156 stations in the northern Rockall Trough, in the vicinity of the Wyville Thomson Ridge and in the southern Faroe Shetland Channel (Fig. 3.1). At all stations a *Sea-Bird* rosette fitted with various sensors and 24 20 litre bottles for water sampling (Table 3.2) was lowered from the sea surface to just above the seabed. Although the rosette frame was made of aluminium (Table 3.2) which is less than ideal when collecting water for determinations of this element, the frame was painted to help prevent corrosion. Experience of collecting aluminium measurements over several decades, suggests that if the frame is painted, such as in this case, contamination from the frame is negligible (C. Measures, personal communication). Additionally, it is not thought that the central anodized aluminium pressure housings pose a contamination risk (Measures and Edmond, 1989).

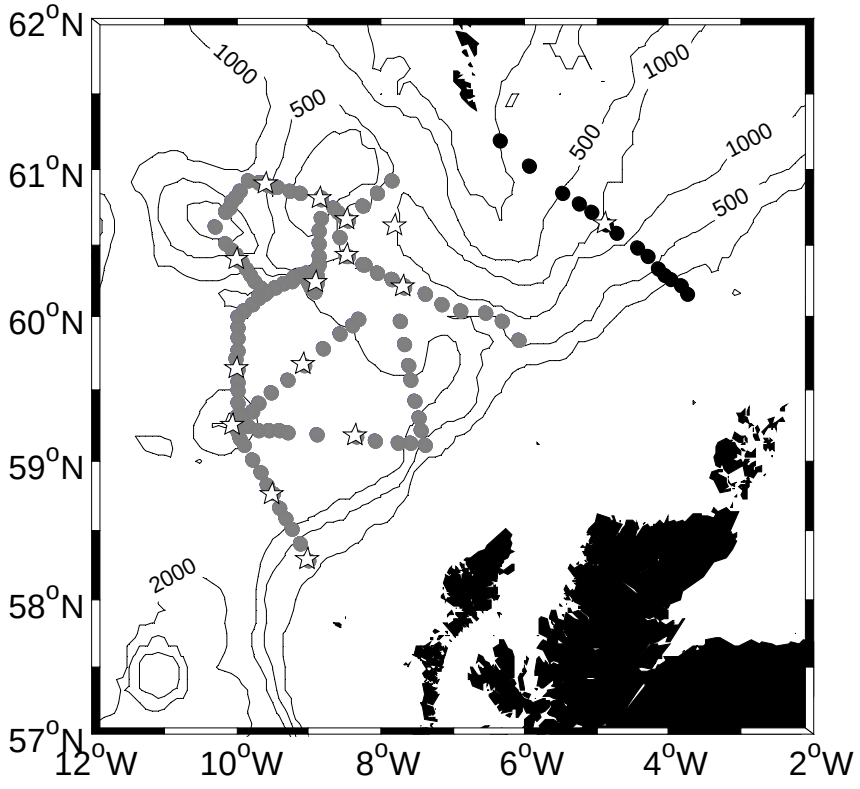

Figure 3.1. Position of stations occupied during 0804S, May 2004. Grey circles: stations where only CTD and dissolved oxygen data were collected; black circles: stations where nutrient values were measured in addition to CTD and oxygen data; white stars: stations where aluminium samples were collected in addition to nutrient, CTD and oxygen data.

	0804S	H44-04-12	CD176	D312
Rosette frame	*Sea-Bird*, painted aluminium and painted stainless steel	*Sea-Bird*, stainless steel wrapped in plastic tape	*Sea-Bird*, stainless steel	*Sea-Bird*, stainless steel
Rosette bottles	24 x 20 l *Sea-Bird*, PVC, internal latex rubber closures	14 x 10 l *Hydro-Bios*, PVC, internal elastic closures	24 x 10 l *Ocean Test Equipment*, PVC, external spring closures	24 x 10 l *Ocean Test Equipment*, PVC, external spring closure
CTD sensor	*Sea-Bird 911plus*	*Sea-Bird 911plus*	*Sea-Bird 911plus*	*Sea-Bird 911plus*
Oxygen sensor	*Sea-Bird 43*	N.A.	*Sea-Bird 43*	*Sea-Bird 43*
CTD sensor position	bottom of rosette frame	side of rosette frame	bottom of rosette frame	primary sensor on side of stabilising fin
Oxygen sensor position	bottom of rosette frame	N.A.	bottom of rosette frame	bottom of rosette frame

Table 3.2. Summary details of the rosette frame and attached bottles and sensors used during the four cruises to the eastern subpolar North Atlantic.

Although it is usual practise to fire the rosette bottles on the upcast after stopping the rosettes ascent to ensure that the bottles are flushed with water from the appropriate depth, during 0804S bottles were fired during the downcast. This is in accordance to Marine Scotland, Science guidelines and allows a more direct comparison between sensor and bottle data. Additionally, it enables sampling of an undisturbed water column which is particularly important in trace metal work where contamination is a major risk. One concern, however, is that increasing external water pressure as the rosette descends may force water into an already fired bottle resulting in spurious contamination of the sample. The excellent agreement between salinity derived from the CTD sensor and that

determined from water collected using the rosette bottles indicates that this was not a problem (Appendix A.i).

Ideally one would sample the rosette bottles for aluminium analysis immediately after its arrival on deck due to the potential risk of contamination from either the walls of the rosette bottle or air which enters the bottle as water is withdrawn. Although this was the case at the majority of stations, the section in the southern Faroe Shetland Channel has been sampled since 1900 (Turrell et al., 1999) and forms part of Marine Scotland, Science's repeat seasonal surveys within the region. Consequently, established sampling procedures needed to be adhered to, and water samples for dissolved oxygen and nutrient analysis were collected prior to those for aluminium determination. At all stations water for calibration of the conductivity probe was drawn last.

3.1.2. H44-04-12, August - September 2004

During the late summer of 2004 a cruise to the southern Iceland Basin and southern entrance to the Rockall Trough (H44-04-12) occupied 29 CTD stations (Fig. 3.2). At each station a CTD rosette system was lowered from the sea surface to just above the seafloor and back at 1 m s^{-1}. In an identical protocol to that used during 0804S, the rosette bottles were fired on the downcast without stopping. Again, the excellent agreement between the conductivity measured by the sensor and that derived from water samples (Appendix A.ii) indicate that contamination due to increasing external water pressure was not a problem.

The rosette system consisted of a stainless steel frame wrapped in plastic tape to reduce corrosion with 14 10 litre rosette bottles (Table 3.2). As several studies have used systems such as this to collect aluminium samples successfully (e.g. Measures and Edmond, 1989; Minakawa and Watanabe, 1998; Obata et al., 2007) no contamination problems are expected. Instead of the CTD sensor being mounted towards the bottom of the frame, it was located at the side of the rosette in a space for an additional rosette bottle.
Water samples for aluminium analysis were drawn first to minimise any potential contamination, before sampling for nutrient determinations and calibration of the conductivity probe.

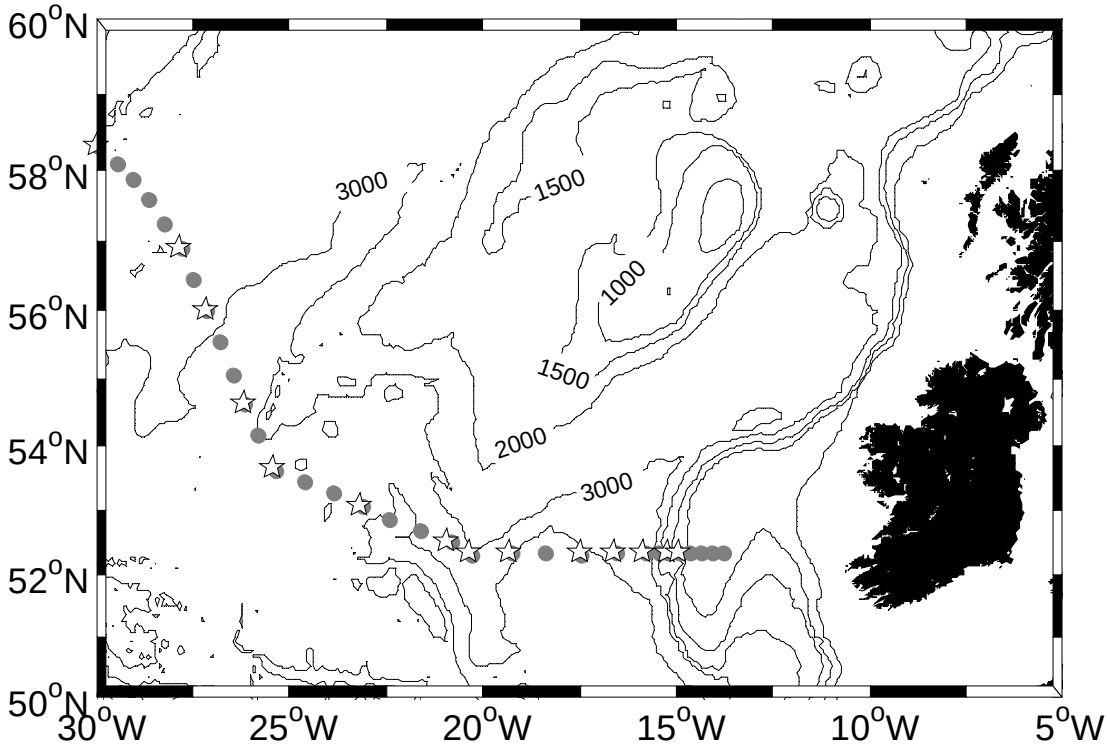

Figure 3.2. Position of stations occupied during H44-04-12, August-September 2004. Grey circles: stations where only CTD data were collected; white stars: stations where aluminium samples were collected in addition to nutrient and CTD data. No dissolved oxygen data exists for H44-04-12.

3.1.3. CD176, October 2005

A cruise onboard RRS Discovery in October 2005 (CD176) occupied the Ellett Line which stretches from the Scottish continental shelf across the Rockall Trough to Rockall. Additional stations on a line eastwards into the trough from George Bligh Bank were also sampled (Fig. 3.3). At all stations a rosette package, consisting of various sensors and bottles attached to a stainless steel frame (Table 3.2), was lowered from the sea surface to just above the seabed and back at 1 m s^{-1}. In contrast to 0804S and H44-04-12, water samples were collected on the upcast after stopping the rosette package for around five minutes to ensure that the rosette bottles were well flushed with the water from the sampling depth.

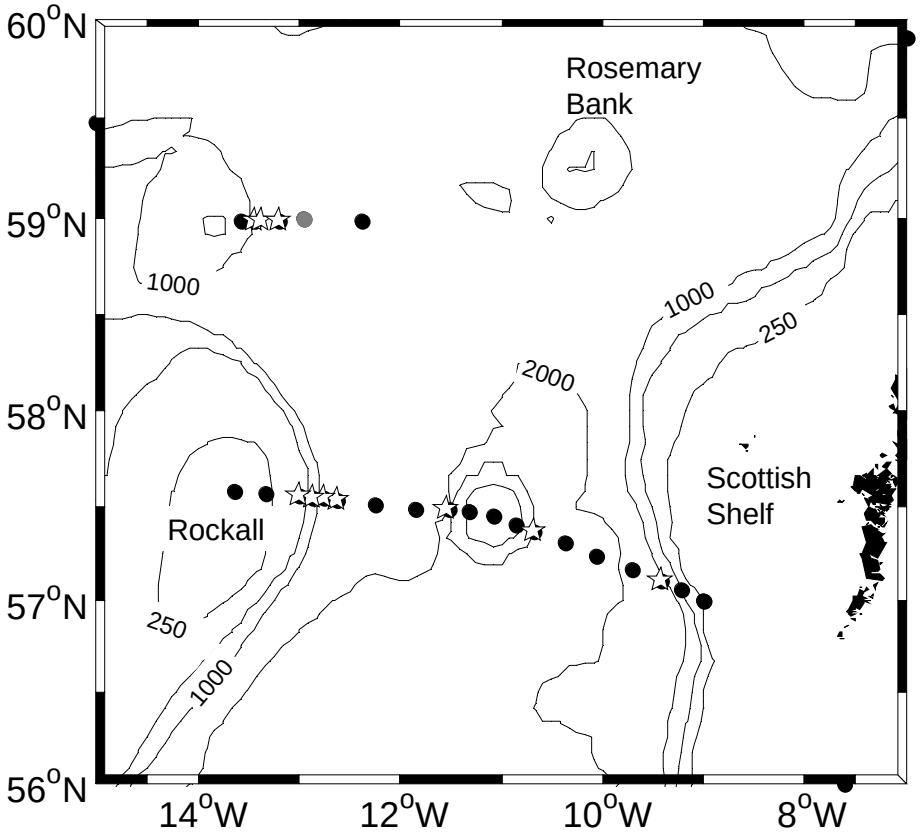

Figure 3.3. Position of stations occupied during CD176, October 2005. Grey circles: stations where only CTD and dissolved oxygen data were collected; black circles: stations where nutrient values were measured in addition to CTD and oxygen data; white stars: stations where aluminium samples were collected in addition to nutrient, CTD and oxygen data.

The first water samples to be removed from the rosette bottles were those for calibration of the oxygen sensor, followed by those for aluminium determination, analysis of nutrient concentrations and finally calibration of the conductivity probe.

3.1.4. D312, October 2006

In October 2006 a cruise onboard RRS Discovery (D312) sampled stations between the Scottish continental Shelf and Rockall along the Ellett Line (Fig. 3.4). At all stations a rosette package was lowered from the sea surface to just above the seabed and back at 1 m s^{-1}. The stainless steel rosette frame had two CTD sensors attached, one positioned towards the bottom of the frame and the other on a stabilising fin protruding from the side

of the rosette (Fig. 3.5). Investigations have shown that in areas of steep temperature and salinity gradients, such as at the bottom of the mixed layer, boluses of water trapped within the rosette frame can cause inaccurate readings from sensors located within the main structure of the package (Brierley, 2003). Additional investigations during D312 suggest that water expelled from the rosette frame as the ship rolls can also affect the accuracy of sensors, not only within the frame but also on the stabilising fin. However, this effect was smaller and less prolonged on the sensor located on the fin (Stinchcombe, 2007). Although changes in temperatures were on the order of hundredths to tenths of a degree Celsius, which will not affect a large scale study such as this, the decision was made to use the CTD probe on the fin as the primary sensor (Fig. 3.5).

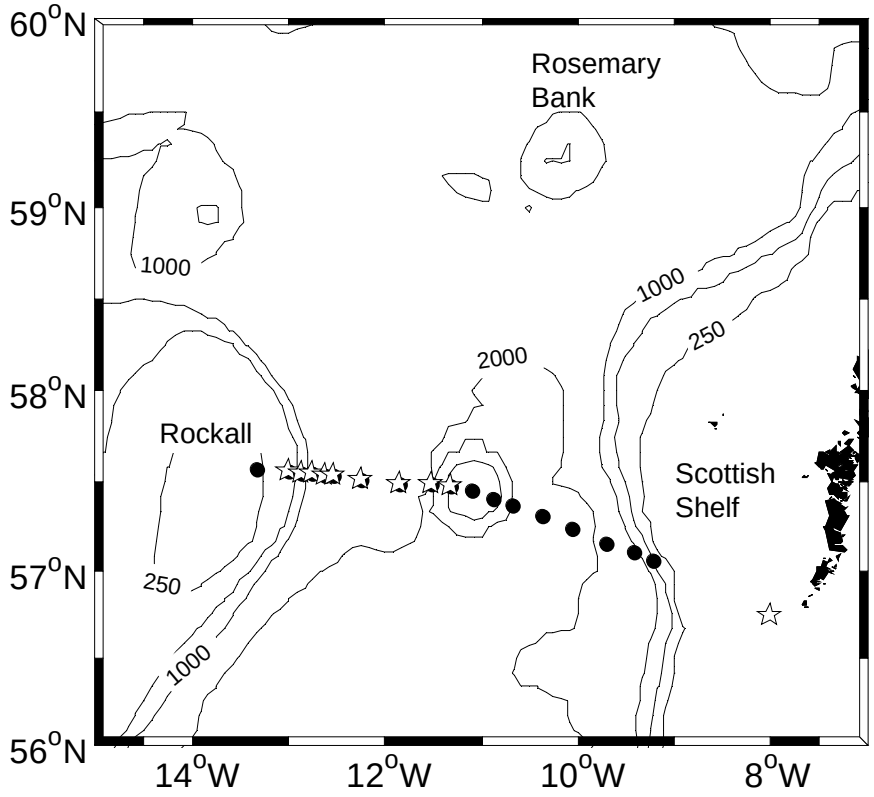

Figure 3.4. Position of stations occupied during D312, October 2006. Black circles: stations where nutrient values were measured in addition to CTD and oxygen data; white stars: stations where aluminium samples were collected in addition to nutrient, CTD and oxygen data.

The first water sample to be removed from the rosette bottles during D312 was for the determination of aluminium. Subsequent samples were collected for calibration of the

oxygen probe, analysis of nutrient concentrations and calibration of the conductivity sensor.

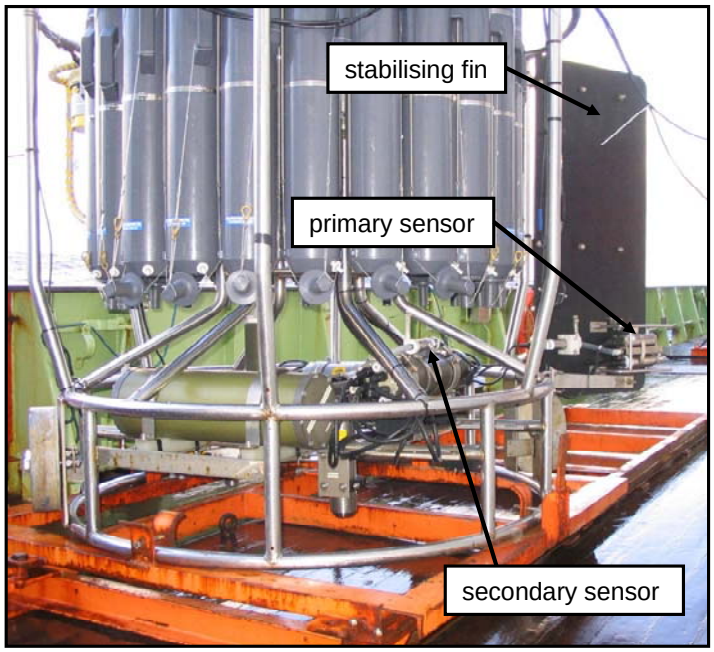

Figure 3.5. Detail of the rosette package used on D312 showing location of primary and secondary CTD sensors. Photograph courtesy of T. Sherwin (SAMS).

3.2. Water sampling

Although water samples were collected for the determination of aluminium concentrations during all four cruises, the methodology involved, including the bottle preparation and storage decisions are complex and therefore discussed in Chapter 4. However, the collection of samples for dissolved oxygen, nutrient and conductivity analyses are detailed below.

3.2.1. Oxygen samples

Water samples to calibrate the dissolved oxygen sensor were taken at a variety of depths, and therefore oxygen concentrations, throughout the duration of the cruises. Samples were

collected via a flexible silicon tube placed over the rosette bottle spigot. The tube was flushed through with the sample before being pinched to reduce the water flow and placed at the bottom of the glass sample bottle. This bottle was immediately inverted ensuring the bottle was completely rinsed by the water without introducing any air bubbles. The silicon tube was next pinched to halt the water flow and the sample bottle righted whilst pressure on the tube was gradually released enabling the bottle to be slowly filled with water. Seawater was allowed to completely fill the sample bottle and overflow for around 30 seconds before the tube was carefully withdrawn. If any bubbles were observed the entire procedure was started again. 1 ml of manganese chloride (60 w/v %) and 1 ml of alkaline iodide solution (32 w/v % sodium hydroxide solution mixed with 60 w/v % sodium iodide solution) were immediately added on deck using automated dispensers. The sample bottle was capped and inverted several times to ensure that the sample and reagents were thoroughly mixed. A white manganese (II) hydroxide forms which oxidises to a toffee-coloured manganese (III) oxy-hydroxide. The sample bottles were stored at room temperature, and again inverted several times after about an hour to ensure that all the dissolved oxygen within the water sample had fully reacted.

3.2.2. Nutrient samples

Water samples for the determination of nutrient (nitrite, nitrate, phosphate and silicate) concentrations within seawater were collected directly from the rosette bottle spigot. Prior to a cruise the plastic sample bottles were pre-cleaned in 2 % HCl before being rinsed in reverse osmosis water. These bottles were then rinsed three times with the seawater before being filled and recapped. Although polyethylene gloves were used for this step during 0804S to ensure that no materials were transferred from the sampler's hands to the seawater sample, no gloves were worn during H44-04-12, CD176 or D312.

Ideally water samples are analysed for nutrient concentrations relatively soon after collection meaning that refrigeration is sufficient to prevent sample degradation. Although during 0804S and D312 samples were analysed within 24 hours, this was not possible during H44-04-12 and CD176. Throughout these two cruises, water samples for nutrient determination were instead filtered and frozen for later shore-based analysis. A 60 ml plastic syringe was washed three times with seawater drawn directly from the rosette bottle

spigot. On the third wash a plastic filter holder containing a 0.7 μm glass microfiber filter was attached to the syringe nozzle and the sample pushed through to rinse the filter paper and its housing. The syringe was refilled with the seawater this time being pressure filtered into a 60 ml plastic sample bottle. The bottle was immediately capped and frozen at -18 °C. Some issues with the quality of silicate data determined from samples that were frozen have been noted. Although silicate concentrations greater than ~ 120 μM are known to lead to problems (Grasshoff et al., 1999), these very high concentrations are not observed in the eastern subpolar North Atlantic. Additionally, the possibility of regeneration of soluble silica that can occur as samples collected in areas of high diatom blooms defrost, can be eradicated by filtering the samples during collection (Diamond, 2001a). As all water samples for nutrient analysis were filtered during H44-04-12 and CD176 no problems associated with the need to freeze the samples are anticipated.

3.2.3. Salinity samples

Water samples to calibrate the conductivity sensors were taken at a variety of depths, temperatures and salinities throughout the cruises. Standard salinity sample bottles, made of glass, were rinsed three times with the seawater sample before being filled up to the shoulder of the bottle. These were then capped with a plastic stopper before the screw-cap was replaced. Samples were stored in crates at room temperature before analysis.

3.3. Sensor calibration and data processing

3.3.1. Calibration of conductivity sensor

Water samples for the calibration of the conductivity sensor were analysed using an *8400B Autosal* salinometer on all cruises. Samples were measured in triplicate and the mean conductivity calculated which was later converted to salinity. The efficiency of the salinometer was checked using *ocean standard seawater* samples of known conductivity.

Water sample salinity was plotted against sensor salinity for the same depth (Appendix A and Stinchcombe, 2007) allowing the relationship between the two to be investigated. The regression coefficient and the correlation equation were calculated (Table 3.3). The regression coefficient (r) is a measure of the strength of the linear relationship between two variables. The correlation equation is the mathematical relationship between two variables *x* and *y* (equation 3.1):

$$y = m\,x + c \qquad (3.1)$$

where *m* is the gradient of the calibration graph and *c* the intercept with the y-axis.

Cruise	**Correlation equation**	**Regression coefficient**	**Residuals (S_{bottle} − corrected S_{sensor})**
0804S	*corrected* $S_{sensor} = \frac{S_{sensor} - 0.091}{0.998}$	1.000	-0.005 to +0.007
H44-04-12	*corrected* $S_{sensor} = S_{sensor} - 0.012$	1.000	-0.020 to +0.022
CD176	*corrected* $S_{sensor} = \frac{S_{sensor} + 0.558}{1.016}$	0.998	-0.010 to +0.014
D312	See Table 3.4.	1.000	-0.003 to +0.002

Table 3.3. Data used in the calibration of salinity derived from CTD conductivity sensors (denoted by S_{sensor}), with salinity determined from bottled samples (S_{bottle}) during 0804S, H44-04-12, CD176 and D312. Calibration graphs for 0804S, H44-04-12 and CD176 are shown in Appendix A. Calibration data for D312 were obtained from Stinchcombe (2007).

All cruises show a very strong linear relationship between salinity derived from bottle samples and the conductivity probe on the CTD with the regression coefficients being, or very close to one. However, a correction (Table 3.3) was applied to the sensor salinity data to obtain the most accurate results. For 0804S, H44-04-12 and CD176 one calibration equation was used for the whole cruise. However, during D312 sudden changes in sensor performance occurred over time meaning that a variety of corrections needed to be applied (Table 3.4).

Station Number	Calibration equation
16149 - 16152	corrected C_{sensor} = 0.99998226 C_{sensor}
16153 - 16162	corrected C_{sensor} = 0.99996807 C_{sensor}
16163 - 16166	corrected C_{sensor} = 1.00004310 C_{sensor}

Table 3.4. Time-dependent calibration equations for the CTD conductivity probe used during D312. Taken from pages 87-88 Stinchcombe (2007).

To further examine the quality of the calibration and establish if there are any biases, corrected sensor salinities were subtracted from bottle derived salinities to calculate residuals (Table 3.3). No trends are seen for 0804S or H44-04-12 when the residuals are plotted against pressure, sample number or sensor salinity (Appendix A). Additionally, the residuals are scattered around zero. However, for CD176 (Appendix A.iii) a slight positive trend is observed with time (gradient 0.001, change ~ 0.008) suggesting a slow drift in either the salinometer or CTD conductivity sensor with time. Due to the use of *ocean standard seawater* to check the salinometers performance, it seems more likely that the drift occurred in the CTD conductivity sensor. It is difficult to determine whether there is additionally, a slight increase in residuals with increasing sensor salinity, and a small negative relationship between pressure and residuals, due to a bias of data points to salinities above ~ 34.9 and lower pressures. Due to the relatively high scatter about the mean the decision was made not to perform any additional calibration to the CD176 salinity data. After the time-dependent calibration equations (Table 3.4) were applied to the D312 salinity sensor data no trends in residuals were observed when plotted against pressure or station number (see pages 87-88 Stinchcombe, 2007).

3.3.2. Calibration of dissolved oxygen sensor

3.3.2.1. Analysis of water samples

All water samples for the calibration of the dissolved oxygen sensors were analysed using the standard colorimetric Winkler Technique. In this method the amount of manganese (III) oxy-hydroxide precipitate, formed when the sample is fixed immediately after

collection, is proportional to the concentration of dissolved oxygen in the sample. During analysis this precipitate is dissolved using excess sulphuric acid, releasing unstable Mn^{3+} ions, which react with the sodium iodide releasing iodine. The amount of iodine formed is therefore proportional to the original concentration of dissolved oxygen in the sample. Hence, when the iodine is titrated with standardised sodium thiosulphate the dissolved oxygen concentration can be determined (Grasshoff et al., 1999).

Analysis of the water samples for dissolved oxygen occurred within two to 24 hours of collection. 1 ml of concentrated sulphuric acid was added and the sample mixed with a magnetic stirrer. Once the manganese (III) oxy-hydroxide was completely dissolved the sample was titrated with ~ 0.3 M sodium thiosulphate using an autotitrator and the volume of thiosulphate required to produce an inflexion point noted.

At the start of each analysis run the sodium thiosulphate was standardised. A sample bottle was filled to the shoulders with tap water and 1 ml of alkaline sodium iodide solution (32 w/v % sodium hydroxide solution mixed with 60 w/v % sodium iodide solution), 5 ml of potassium iodate solution (0.009 M), and 1 ml of concentrated sulphuric acid added. A magnetic stirrer was used to ensure complete mixing before the sample was titrated with ~ 0.3 M sodium thiosulphate using an autotitrator. The volume of thiosulphate required to produce an inflexion point was noted and the procedure repeated until three readings within ± 0.005 ml were obtained. The molarity of the sodium thiosulphate (M_{ss}) was then calculated (equation 3.2):

$$M_{ss} = M_p \, x \, V_p \, x \, E_p \, / \, (V_s \, x \, E_s) \qquad (3.2)$$

where M_p and V_p are the molarity of the potassium iodate solution and volume added to the standardisation sample respectively, and E_p the number of moles of potassium iodide involved in the reaction with the sodium thiosulphate (1). V_s is the mean sodium thiosulphate titre, and E_s the number of moles of sodium thiosulphate required to react with the potassium iodate solution (6).

In order to calculate the concentration of dissolved oxygen in the seawater sample, the molarity of dissolved oxygen in each sample (M_o) was first determined (equation 3.3).

$$M_o = M_{ss} \, x \, V_{ss} \, x \, E_{ss} \, / \, (V_o \, x \, E_o) \quad (3.3)$$

where M_{ss} is the molarity of the standardised thiosulphate calculated from equation 3.2, V_{ss} the titre of sodium thiosulphate added to the water sample, and E_{ss} the number of moles of sodium thiosulphate involved in the reaction with oxygen (4). V_o is the volume of the water sample and E_o the number of moles of oxygen required to react with the sodium thiosulphate (1). Dissolved oxygen concentration in μmol kg^{-1} (C_o) could then be calculated using *in situ* density (ρ, kg l^{-1}) and equation 3.4:

$$C_o \, (\mu mol \, kg^{-1}) = 1x10^3 \, M_o \, / \, \rho \quad (3.4)$$

3.3.2.2. Calibration of sensor

To calibrate the dissolved oxygen sensor, oxygen concentrations derived from the bottled samples were plotted against oxygen concentrations measured by the sensor at the same depths (Appendix B). Regression coefficients and correlation equations were calculated for each cruise (Table 3.5).

Dissolved oxygen measured by the sensors and bottle samples have a strong linear relationship shown by the very high regression coefficients approaching one. However, a correction (Table 3.5) had to be applied to the sensor data due to an offset between sensor derived concentrations and the more accurate oxygen concentrations measured from the bottle samples. The residuals (bottle minus corrected sensor oxygen) are smallest for the data collected during 0804S although this may be related to the sample size (28) being much smaller than for CD176 (312) and D312 (627). No variation in residuals with pressure, sample number or oxygen concentration is seen for 0804S (Appendix B.i) indicating that no additional correction (i.e. beyond that in Table 3.5) needs to be applied to the sensor data. For CD176, a slight negative trend is seen between residuals and sample number (gradient -0.009, change 3 μmol kg^{-1}), and residuals and oxygen concentration (gradient -0.010). However, as no discernible trend is observed between residuals and pressure (Appendix B.ii), and the negative relationships with sample number and oxygen concentration are small, the decision was made not to apply any additional correction to the sensor data. The range of residuals for D312 data (Table 3.5) is larger

than that for 0804S and CD176. Although this may in part be due to the higher number of calibration samples collected, examination of the residual plots (Stinchcombe, 2007, p. 89-90) show the residuals becoming more positive as the cruise progresses (gradient +0.021, change 14 μmol kg^{-1}). The decision was, therefore, made to apply an additional time-dependent correction (Table 3.6). Modified residuals, calculated by subtracting sensor oxygen data after applying the calibration equation (Table 3.5) and additional time-dependent correction (Table 3.6), from bottle samples, show no trend when plotted against sample number or pressure (Stinchcombe, 2007, p. 89-90).

Cruise	**Correlation equation (μmol kg^{-1})**	**Regression coefficient**	**Residuals (O_{bottle} − corrected O_{semsor})**
0804S	*corrected* $O_{sensor} = \frac{O_{sensor} - 29.40}{0.84}$	0.980	-4.2 to +6.1
CD176	*corrected* $O_{sensor} = \frac{O_{sensor} - 12.07}{0.90}$	0.977	-10 to +10
D312	*corrected* $O_{sensor} = \frac{O_{sensor} - 51.6}{0.63}$	0.967	-10 to +14

Table 3.5. Correlation data for calibrations of oxygen sensors used during 0804S, CD176 and D312. Calibration graphs for 0804S and CD176 are shown in Appendix B. Calibration data for D312 were obtained from Stinchcombe (2007). The residuals for D312 are those calculated prior to the additional time-dependent correction (Table 3.6). Final residuals for D312 were -10 to +5 μmol kg^{-1}.

Station Number	Additional correction
16145 – 16149	final O_{sensor} = corrected O_{sensor} – 1.0
16150 – 16154	final O_{sensor} = corrected O_{sensor} – 2.0
16155 – 16159	final O_{sensor} = corrected O_{sensor} – 3.0
16160 – 16164	final O_{sensor} = corrected O_{sensor} – 4.0
16165 – 16169	final O_{sensor} = corrected O_{sensor} – 5.0

Table 3.6. Additional time-dependent correction applied to D312 oxygen sensor data after calibration using the correlation equation (see Table 3.5). From Stinchcombe (2007) pages 89-90.

3.3.3. Processing of sensor data

Initial processing of all sensor data was carried out at sea using *Seasoft* software provided by *Sea-Bird*. Steps included conversion of the raw CTD data to different formats, aligning the CTD and oxygen sensors, removal of spikes and removal of the thermal inertia of the conductivity cells. Additional data processing was carried out using different software programmes depending on the institute doing the bulk of the processing (Table 3.7). Steps included further manual de-spiking, calculation of potential temperature, salinity and density, and application of calibration equations. Data collected during the initial soaking of the rosette, whilst the rosette was held just above the seabed, and during the upcast, were removed before data files were averaged into one or two dBar bins.

3.4. Analysis of nutrient data

The standard method for measuring nutrients in seawater is flow injection analysis using the colorimetric detection of complexes formed after the addition of several reagents (Grasshoff et al., 1999). During 0804S and D312 analysis for nutrient determinations occurred at sea within 24 hours of collection, however, samples collected during H44-04-12 and CD176 were frozen and analysed at SAMS after being defrosted for ~ 18 hours in a refrigerator. Comparable precisions (Table 3.8) and values between these two cruises and

0804S and D312 suggest that no problems occurred as a result of the samples having to be frozen.

	0804S	H44-04-12	CD176	D312
Initial processing	*Sea-Bird Seasoft*	*Sea-Bird Seasoft*	*Sea-Bird Seasoft*	*Sea-Bird Seasoft*
Calculation potential temperature, salinity and density	*Matlab*	*Matlab*	*Matlab*	*PStar*
Removal of soaking and upcast data	*Sea-bird Seasoft*	*Sea-Bird Seasoft*	*Sea-Bird Seasoft*	*PStar*
Initial visual inspection (basic plots)	*Matlab*	*Matlab*	*Matlab*	*PStar*
Application of salinity and oxygen sensor calibrations	*Matlab*	*Matlab*	*Matlab*	*PStar*
Averaging into 1 or 2 dBar files	*Sea-Bird Seasoft*	*Matlab*	*Sea-Bird Seasoft*	*PStar*

Table 3.7. Major processing steps for data from CTD and oxygen sensors and the software used for data collected during 0804S, H44-04-12, CD176 and D312.

Standard limits of detection for the method (three times standard deviation of the blank) are around 0.01 μM, 0.01 μM and 0.02 μM for nitrite and nitrate, phosphate and silicate respectively (Grasshoff et al., 1999). Ideally one would calculate precision, which is a measure of the reproducibility between samples, by measuring each sample in triplicate. However, monetary and time pressures meant that this was not carried out except for CD176. During 0804S a constant precision, calculated by measuring each of six samples chosen at random from throughout the cruise ten times, was applied to all data. A similar method was employed during H44-04-12 except 18 samples from throughout the cruise were analysed in triplicate. Precisions from 0804S, H44-04-12 and CD176 are reported as a relative standard deviation (Table 3.8) calculated by dividing the standard deviation by the mean and multiplying by 100. During D312 around 100 samples were measured in duplicate and precision reported as the percentage difference between the concentrations of the two samples (Table 3.8).

Accuracy of the method (reported as percentage recovery) can be evaluated by measuring a certified reference material and comparing the expected and measured values (Table 3.8). During 0804S seawater nutrient reference materials: *Quasimeme QNU087SW* (N 4.5 µM), *Quasimeme QNU072SW* (P 0.42 µM) and *Quasimeme QNU077SW* (Si 5.0 µM), were analysed randomly throughout the cruise (Webster, 2004a; Webster, 2004b; Webster, 2005). During D312, *Ocean Scientific Instruments standard solutions* (N 10µM, P 1µM, Si 10µM) were run throughout the cruise (Stinchcombe, 2007). Unfortunately, certified reference materials were not run during the analysis of samples collected onboard H44-04-12 or CD176.

Cruise	Variables	Precision (%)	Accuracy (%)	Instrument
0804S	N	1.93	98.2	Bran and Luebbe autoanalyser
	P	3.02	99.4	
	Si	1.43	103.4	
H44-04-12	N	1.31	-	Lachat autoanalyser
	P	2.56	-	
	Si	1.30	-	
CD176	N	0.47	-	Lachat autoanalyser
	P	1.28	-	
	Si	1.54	-	
D312	N	0.7	99.7	Skalar San Plus autoanalyser
	P	1.2	99.0	
	Si	0.6	102.0	

Table 3.8. Nutrients analysed during 0804S, H44-04-12, CD176 and D312, and their respective precision and accuracy. Precision data are reported as relative standard deviations (%) with the exception of D312 data which is the percentage difference between samples measured in duplicate (%). Accuracy is reported as recovery (%) of certified reference materials. This was not carried out for H44-04-12 or CD176 data.

The chemistry of the analysis methods for nitrite and nitrate, phosphate and silicate and the reagents required are discussed in the following sections. Standards were analysed at the start of each run and then approximately after every 25 samples. The data system attached

to the autoanalyser plotted instrument response against the concentration of the standard and calculated the regression equation. Thus, sample absorbance could be converted to nutrient concentrations within the seawater.

3.4.1. Nitrite and Nitrate

The determination of nitrite and nitrate in seawater relies on the reduction of nitrate within the sample to nitrite by a copperised cadmium column. This reduced nitrite, along with any naturally occurring nitrite in the sample, reacts with sulphanilamide under acidic conditions, to form a diazo compound. The coupling of this compound with N-(1-naphthyl)ethylenediamine dihydrochloride leads to the formation of a purple-pink dye with a maximum absorbance at 520 nm (Grasshoff et al., 1999). This absorbance is proportional to original nitrite plus nitrate concentration in the sample. The level of naturally occurring nitrite in the seawater sample can be determined from an additional run that bypasses the cadmium reducing column. By subtracting this value from the nitrite plus nitrate concentration, the amount of nitrate within the sample can be determined. As nitrite concentrations in the eastern subpolar North Atlantic are typically less than 0.2 μM, and nitrate levels one to two orders of magnitude larger, nitrite plus nitrate and nitrate only concentrations can be regarded as being comparable for this study.

Reagents required for the method are: an ammonium chloride buffer solution and a sulphanilamide colour reagent. The ammonium chloride buffer (pH 8.5) is prepared by dissolving 85.0 g of ammonium chloride and 4.0 g of disodium ethylenediamine tetra-acetic acid dihydrate in 1000 ml of deionised water, before adjusting the pH to 8.5 using 13 M sodium hydroxide solution (Diamond, 2001b). An alternative method, used by Marine Scotland, Science, is to simply dissolve 10 g of ammonium chloride in one litre of deionised water (Webster, 2005). The sulphanilamide colour reagent is prepared by dissolving 40.0g of sulphanilamide and 1 g of N-(1-naphthyl)-ethylenediamine dihydrochloride in 100 ml of 85 % phosphoric acid and 900 ml of deionised water. Standards, for calibration, were also required. These were prepared from a 5 mM stock solution formed by dissolving potassium nitrate or sodium nitrate in either a litre of deionised water or low nutrient seawater obtained from *Ocean Scientific Instruments*. Working standards were prepared every few days by diluting the stock solution to various

concentrations between 0.00 – 5.00 μM. If deionised water was used to prepare the standards a salinity correction, obtained from running low nutrient seawater, was applied.

3.4.2. Phosphate

The analysis of phosphate in seawater is based on the reaction of phosphate with various reagents to form a blue phospho-molybdenum complex which absorbs most strongly at 880 nm. Phosphate initially reacts with ammonium molybdate and antimony potassium tartrate, under acidic conditions, to form an antimony-phospho-molybdate complex which is then reduced by ascorbic acid to form the blue phospho-molybdenum complex. The absorbance is proportional to the phosphate concentration in the sample allowing this to be determined (Grasshoff et al., 1999).

Reagents required are: molybdate colour reagent and ascorbic acid reducing solution. The molybdate colour reagent was prepared by mixing together 70.0 ml of concentrated sulphuric acid, 213 ml of 0.03 M ammonium molybdate solution, 72 ml of 0.01 M antimony potassium tartrate solution and 645 ml of deionised water. The ascorbic acid reducing solution was prepared by dissolving 60.0 g granular ascorbic acid in 1 litre of deionised water before the addition of 1.0 g sodium dodecyl sulphate. In addition to the reagents above, a sodium hydroxide – EDTA solution is required to rinse the autoanalyser lines at the end of each day or if the baseline begins to drift. This was prepared by dissolving 65 g of sodium hydroxide and 6 g of tetrasodium ethylenediamine tetraacetic acid (EDTA) in 1 litre of deionised water (Ammerman, 2001). Additionally, a 25 mg P l^{-1} standard stock solution was prepared by dissolving anhydrous potassium phosphate monobasic in either 1 litre of deionised water or 1 litre of low nutrient seawater obtained from *Ocean Scientific Instruments*. A 10 ml of aliquot of this standard was diluted up to 1 litre to form a second stock solution of 250 μg P l^{-1}. Working standards ranging from 0-100 μg P l^{-1} were prepared weekly by diluting the two stock standard solutions. These were used to calibrate the instrument. If deionised water was used to prepare the standards instead of low nutrient seawater an additional salinity correction was applied.

3.4.3. Silicate

Analysis of silicate in seawater is based on the reaction of soluble silica species with molybdate to form a silicamolybdate complex which is then reduced with stannous chloride, in acidic conditions, to form 'molybdenum blue'. This compound has a maximum absorbance at 820 nm with the absorbance being proportional to the concentration of molybdate-reactive silica in the water sample (Grasshoff et al., 1999).

Reagents used were: ammonium molybdate solution, oxalic acid solution (0.8 M) and a hydroxylamine hydrochloride/stannous chloride reducing solution. The ammonium molybdate solution was formed by dissolving 20.0g ammonium molybdate tetrahydrate in 420 ml of deionised water and 8 ml of concentrated sulphuric acid. The hydroxylamine hydrochloride/stannous chloride reducing solution was formed by dissolving 2.0 g of hydroxylamine hydrochloride and 0.30 g stannous chloride, in 22 ml of concentrated sulphuric acid and 978 ml of deionised water (Diamond, 2001a). In addition to the reagents, standards were required for calibration, these were prepared from a 5 mM stock solution of silicofluoride dissolved in either deionised water or *Ocean Scientific Instruments* low nutrient seawater. The stock solution was diluted to form standards covering the range of silicate concentrations expected to be found in the samples, typically from 0 – 100 μM. If deionised water was used an additional salinity correction was applied.

3.5. Historical data

3.5.1. CTD data for spatial analysis

To investigate the spatial extent of WTOW in the eastern subpolar North Atlantic, data from six cruises collected between 1996 and 2001 (Table 3.9 and Fig. 3.6) were used in addition to the four cruises already discussed (section 3.1). Data were obtained from WOCE (World Ocean Circulation Experiment) with the exception of D253 which was downloaded from BODC (British Oceanographical Data Centre). Although all data had

been fully processed, calibrated and checked, the quality was ensured by plotting the data in a variety of ways.

Cruise	Ship	Date	Data Source
D223	*RRS Discovery*	28th September – 19th November 1996	WOCE
K147-2	*RV Knorr*	2nd November – 5th December 1996	WOCE
K151-2	*RV Knorr*	30th May – 5th July 1997	WOCE
D230	*RRS Discovery*	7th August – 17th September 1997	WOCE
D233	*RRS Discovery*	23rd April – 1st June 1998	WOCE
D253	*RRS Discovery*	4th May – 20th June 2001	BODC

Table 3.9. Details of historical CTD data used in this thesis to investigate the spatial extent of WTOW in the eastern subpolar North Atlantic. Data were either obtained from BODC (http://www.bodc.ac.uk) or WOCE (htpp://woce.nodc.noaa.gov).

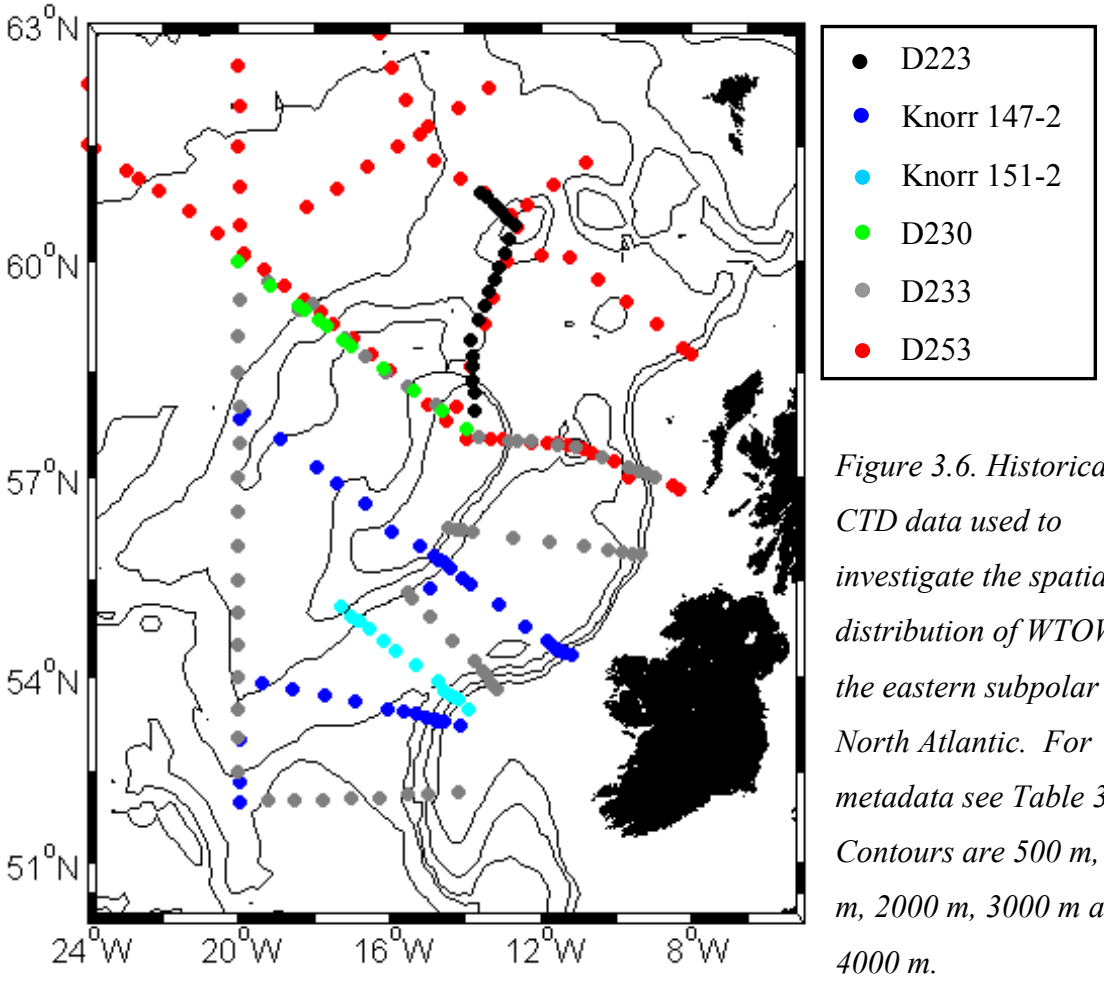

Figure 3.6. Historical CTD data used to investigate the spatial distribution of WTOW in the eastern subpolar North Atlantic. For metadata see Table 3.9. Contours are 500 m, 1000 m, 2000 m, 3000 m and 4000 m.

3.5.2. Ellett Line data

The Ellett Line extends from western Scotland across the Rockall Trough at approximately 57.5 °N. The section was established in 1975 and maintained solely until 1994 by Dave Ellett and other scientists at SAMS. Since 1995 the line has been jointly maintained by SAMS and NOC with occasional occupations by Marine Scotland, Science. In 1996 the section was extended to include the Rockall-Hatton Plateau and Iceland Basin. However, this thesis concentrates on data collected at the 18 stations between the Scottish continental shelf edge and Rockall (Fig. 3.7 and Appendix C.i).

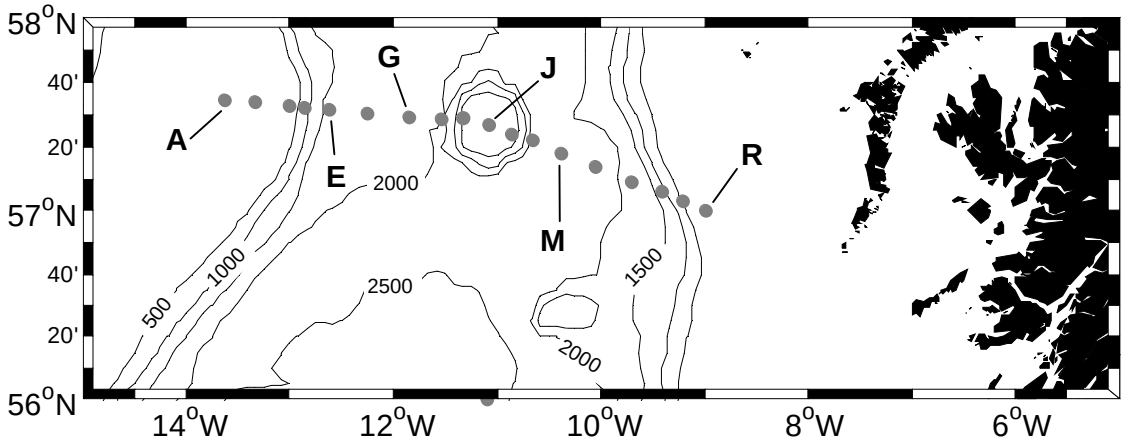

Figure 3.7. Standard Ellett Line stations (A – R) between the Scottish continental shelf edge and Rockall.

Temperature and salinity data have been collected at least annually, with the exception of 1986 and 2002, and were obtained from BODC. Data between 1975 and 1978 were collected with a *Bissett Berman* STD (salinity-temperature-depth probe), between 1978 and 1992 using a *Bissett Berman* CTD, and from 1992 onwards with a *Sea-Bird* CTD (Holliday et al., 2000). All data had been processed, calibrated and quality checked by BODC. A further detailed examination of data quality was carried out by Holliday (2002) who noted that data from some cruises were of a lower standard. These cruises, along with years where less than three stations were occupied because of bad weather or instrumental problems, have not been included in analyses within this thesis (Appendix C.ii).

3.5.3. Chlorofluorocarbon (CFC) data

Water samples for CFC analysis were collected along the Ellett Line and other locations in the vicinity of the Rockall Trough during four cruises: D230, 34AR, M39-5 and D233 (Table 3.10 and Fig. 3.8). Although the majority of water samples were analysed for CCl_4 and CFC-113 (CCl_2F-$CClF_2$) in addition to CFC-11 (CCl_3F) and CFC-12 (CCl_2F_2), the decision was made to concentrate on CFC-11 and CFC-12. This was predominantly because of the non-conservative nature of CCl_4 and CFC-113 under certain conditions such as waters above 5 °C (Huhn et al., 2001; Roether et al., 2001; Waugh et al., 2004). Data were downloaded from the CLIVAR and Carbon Hydrographic Data Office (http://cchdo.ucsd.edu), with the exception of data from 34AR which were downloaded from the International Council for the Exploration of the Sea (http://www.ices.dk/ocean/project/veins). All downloaded data were reported relative to the SIO-93 calibration scale with the exception of D230 data which were reported relative to the SIO-98 scale. CFC-11 and CFC-12 data for this cruise were converted to SIO-93 using equations 3.5 and 3.6 respectively (Bullister and Tanhua, 2010).

$$[\text{CFC-11}]_{\text{SIO-93}} = [\text{CFC-11}]_{\text{SIO-98}} \,/\, 1.0082 \qquad (3.5)$$

$$[\text{CFC-12}]_{\text{SIO-93}} = [\text{CFC-12}]_{\text{SIO-98}} \,/\, 1.0053 \qquad (3.6)$$

Cruise	Ship	Date	Laboratory
D230	*RRS Discovery*	7th August - 17th September 1997	NOCS
34AR	*RV Aranda*	9th August - 29th August 1997	GUMC
M39-5	*RV Meteor*	14th August - 14th September 1997	IfMK
D233	*RRS Discovery*	23rd April - 1st June 1998	NOCS

Table 3.10. Cruises during which CFC-11 and CFC-12 data used in this thesis were collected. GUMC: Dept. of Analytical and Marine Chemistry, Gothenburg University; IfMK: Institut für Meereskunde, Kiel; NOC: National Oceanography Centre (Southampton).

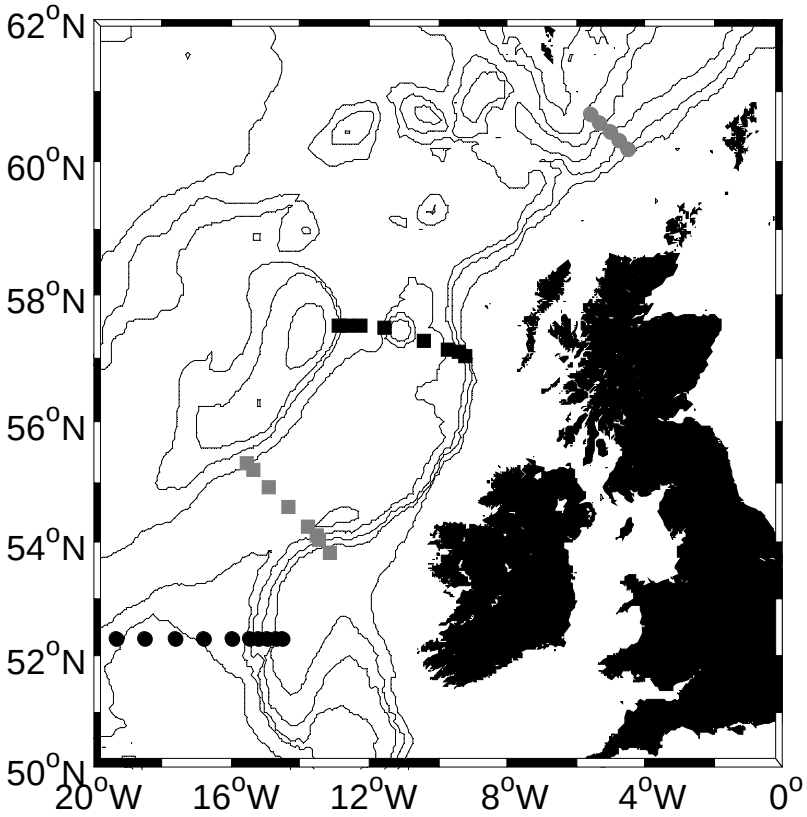

Figure 3.8. Position of stations where CFC-11 and CFC-12 samples were collected in addition to CTD data. Black squares: stations occupied during D230 and D233; grey squares: stations occupied during D233 only; grey circles: stations occupied during 34AR and black circles: stations occupied during M39-5. See Table 3.10 for cruise information. Contours are at 500 m, 1000 m, 2000 m, 3000 m and 4000 m.

Precisions are generally less than 1 % for CFC-11 and CFC-12 and reported to be of a good quality (Gronvall and Launiainen, 1997; Bacon, 1998; Smythe-Wright, 1999). The exception to this is CFC-12 data collected during M39-5, which despite having a high accuracy, has reduced precision as a result of problems during analysis (Schott et al., 1999). All data were plotted in various ways and any data suspected of having quality problems were flagged and treated with caution. Although data from four different cruises are used for this study, all samples were collected within a small timeframe (< 12 months) which is important due to the temporally varying atmospheric, and therefore oceanic, CFC-11 and CFC-12 concentrations (section 2.8).

Water samples for CFC analysis, during all cruises, were collected in 10 litre Niskin bottles that were treated prior to sailing in order to reduce the potential for contamination. All o-

rings, seals and taps were washed in detergent and propan-2-ol before being baked in an oven for 24 hours (Gronvall and Launiainen, 1997; Bacon, 1998; Schott et al., 1999; Smythe-Wright, 1999). Water was drawn directly from the rosette bottle spigot into 100 ml gas-tight glass syringes that were stored under clean running water until analysis within 12 hours. Due to a sample backlog during D230 and D233 some samples were stored for up to 24 hours before analysis, however no sample degradation was reported (Bacon, 1998; Smythe-Wright, 1999).

All water samples were analysed for CFC-11 and CFC-12 using a modified version of the purge and trap method of Bullister and Weiss (1988) in conjunction with Gas Chromatography - Electron Capture Detection (GC-ECD). In general terms the seawater sample is injected into a stripping chamber where it is degassed by an inert carrier gas composed of 5 % methane and 95 % argon. The gas stream, now containing all eluted gasses including CFC-11 and CFC-12, is passed into a metal trap immersed in liquid nitrogen to pre-concentrate the compounds and commence separation. Following approximately a four minute trapping time the trap was heated causing the gases to be re-volatised and released. With the aid of timing and various valves, the gases of interest are passed into the detector whilst the heavier compounds are directed into the waste stream. Once in the GC the gases are separated as they pass along the chromatography column. Thus, the gases enter the ECD differentially enabling peaks to be identified to individual compounds (Boswell and Smythe-Wright, 1996; Grasshoff et al., 1999). Peak areas were corrected for any drift in detector sensitivity before being converted to moles of a gas using calibration curves. As a stable standard in seawater was not available, calibrations were obtained by multiple injections of known volumes of gas standards. During D230 and D233 these standards were obtained from the Climate, Modelling and Diagnostic Laboratory at NOAA (Bacon, 1998; Smythe-Wright, 1999), whilst gas standards from the Pacific Marine Environmental Laboratory, NOAA were used during M39-5 (Schott et al., 1999). Unfortunately there is no information on the origin of the standards used during 34AR.

Chapter 4.
Methodology for the determination of aluminium in seawater

This chapter details the methods used in the collection, storage and determination of aluminium in seawater. First, various analytical methods recorded within the literature are discussed before the method trial, conducted during 0804S, is examined. This trial raised several questions regarding the collection, storage and analysis of samples. Experiments to answer these queries and therefore improve the method and establish a standard procedure, are discussed in the method development section. Finally, the samples used within this thesis are discussed.

4.1. Introduction

Several methods for the determination of aluminium (Al) in seawater at nanomolar (nM) levels have been developed and successfully used. One example is the extraction of a trifluoroacetylacetonate or trifluoropentanedione derivative of Al by solvents before analysis using electron capture gas chromatography (Measures et al., 1984; Measures and Edmond, 1989). This method has a detection limit, defined as three standard deviations (3σ) of a low concentration sample, of 0.6 – 2.0 nM. Although variations of this method had been used on eight oceanographic cruises by 1989 (Measures and Edmond, 1989), the multiple steps required leads to a high risk of contamination and consequently the method is no longer used (Tria et al., 2007). Another method is extraction of Al using 8 hydroxyquinoline before analysis using graphite furnace atomic-absorption-spectrophotometry (Orians and Bruland, 1985). Although this method has a very low detection limit (0.09 nM) and high extraction efficiency (98 ± 6 %), sample preparation again involves multiple steps. Additionally, there can be serious matrix interferences from other ions present in seawater (Orians and Bruland, 1986; Tria et al., 2007). The use of inductively-coupled mass spectrometry has been suggested (Tria et al., 2007). However, the method is not widely used because of serious matrix effects leading to an impractically high limit of detection and relatively high analysis costs.

The final, and most frequently used method is fluorometry (e.g. Hydes et al., 1988; Hall and Measures, 1998; Middag et al., 2011). Although morin [2',3,4',5,7-pentahydroxyflavone] has been used as the fluorometric agent (e.g. Will, 1961; Escriche and Hernandez, 1985), the use of lumogallion [3-(2,4 dihydroxyphenylazo)-2-hydroxy-5-chlorobenzenesulphonic acid] is more common. The method was first proposed in the 1960s (Nishikawa et al., 1967) and later modified for use in natural waters (Shigematsu et al., 1970; Hydes and Liss, 1976). When added to the sample, lumogallion bonds with the Al^{3+} ion present in seawater forming a complex that fluoresces (Brown and Bruland, 2008). As such, the Al concentration can be determined from the intensity of the fluorescence. This method, if run on unfiltered samples, determines reactive Al defined as dissolved Al plus any that is adsorbed to particulate matter (Hydes and Liss, 1976). Detection limits for the method are estimated at ~ 1.9 nM with a precision of ~ 5 % at 37 nM (Hydes and Liss, 1976). More recently, the sensitivity of the lumogallion fluorescence method has been improved by the addition of surfactants, pre-concentration steps and flow injection analysis. When the surfactants of Brij-35 (Kramer et al., 2004) or Triton X-100 (Howard et al., 1986; Ren et al., 2001) are used the limit of detection decreases to ~ 0.7 nM. Pre-concentration reagents used include n-hexanol (Zhang et al., 2000), Toyopearl AF-Chelate 650M (Brown and Bruland, 2008; Middag et al., 2011) and 8-hydroxyquinolene (Resing and Measures, 1994; Hall and Measures, 1998; Kramer et al., 2004). Using pre-concentration alone can decrease the limit of detection to 0.25 nM (Zhang et al., 2000), whilst use in conjunction with surfactants decreases the limit of detection to ~ 0.1 nM (Resing and Measures, 1994; Brown and Bruland, 2008).

For this work the lumogallion fluorometry method was chosen because of its simplicity, low cost, ease of measurement and lack of interferences (Tria et al., 2007). Additionally, if required, a fluorometer can easily be transported and used at sea. As fluorometry is an optical technique there is a possibility that turbidity within the seawater sample may affect the results. However, there is no evidence of this effect within the literature. Although the use of surfactants and/or a pre-concentration step can improve the limit of detection by an order of magnitude, it was decided not to use these additional steps. This was partly because of the increased risk of contamination from the extra reagents and procedures required, but also because sub-nanomolar detection limits are not essential for the relatively high concentrations found in the Atlantic (Orians and Bruland, 1985). This unmodified method has been widely used both in coastal waters and the deep ocean (e.g.

Hydes, 1983; Hydes et al., 1988; Lunel et al., 1990; Upadhyay and Sen Gupta, 1995; Minakawa and Watanabe, 1998; Takayanagi and Gobeil, 2000).

4.2. Method trial, 0804S

4.2.1. Bottle choice and preparation

The container that the seawater sample is stored in is often not mentioned in the literature but is of vital importance. Bottles may contaminate samples by release of: metals adsorbed onto the plastic, metals left over from the production process, or metals inherent to the plastic. Alternatively, the metal of interest maybe lost from the sample because of adsorption onto container walls (Reimann et al., 1999). High [Al] were found in leachates from polypropylene bottles (Moody and Lindstrom, 1977; Hall, 1998; Reimann et al., 1999), and some contamination was reported from high-density polyethylene (HDPE) bottles (Hall, 1998). Lowest [Al] in leachates was reported for Teflon bottles (Moody and Lindstrom, 1977; Reimann et al., 1999) although some evidence suggests Al may be adsorbed onto this plastic (D. Hydes, personal communication) and the cost is prohibitive. As low-density polyethylene (LDPE) containers are recommended for trace metal work (P. Statham, personal communication) and are relatively cheap, it was decided to use this plastic to store all Al samples. Bottles (60 ml LDPE bottles with polypropylene lids) were obtained from *Nalgene* which specialises in containers for trace metal work. Stabilizers, fillers and extenders are excluded from the manufacturing process reducing the likelihood of contamination (Anon, 2009). A narrow-necked design was chosen to minimise exposure to the atmosphere (whilst bottle lids are off) as air-borne particles are the largest contamination source for Al (Skelly and DiStefano, 1988).

Bottles used for trace metal samples are usually rigorously cleaned, first with a detergent and then by soaking in nitric acid and/or hydrochloric acid before rinsing thoroughly in deionised (DI) water (Jones and Laslett, 1994). Acid cleaning causes any metals attached to the bottle surface to be desorbed, although it may introduce contaminants and / or damage the plastic surface causing metals within the plastic to be released. For example HDPE bottles that have been acid-washed have a higher [Al] concentration than those that are factory new (Reimann et al., 1999). Evidence also exists that suggests Al may be

scavenged onto acid-cleaned surfaces (D. Hydes, personal communication). For these reasons sample bottles were not acid-cleaned but instead washed several times using DI water in a clean room as recommended by D. Hydes (personal communication). Cleaned bottles were sealed inside two polyethylene bags and stored in plastic containers until use. Un-powdered gloves were worn at all times whilst handling sample bottles.

4.2.2. Sample collection and storage

During 0804S both unfiltered and filtered samples were collected (see Fig. 3.1 for station locations). Un-powdered gloves were worn at all times and sample bottles were not removed from their plastic bags.

4.2.2.1. Unfiltered samples

Unfiltered samples were collected directly from the rosette bottles into pre-cleaned sample bottles. The polyethylene bag was held tightly around the rosette spigot creating a partially closed system in the aim to reduce contamination from the atmosphere. The sample bottles were rinsed three times with the sample before being filled up to the shoulder. Bottles were immediately capped, resealed within the polyethylene bag and placed within a lidded polyethylene container. This container was stored within a further black polyethylene bag in a cool environment until analysis. Although it is usual to acidify seawater samples when determining trace metal concentrations (e.g. Bruland et al., 1979; Coale et al., 2005) and some laboratories acidify Al samples (e.g. Kramer et al., 2004; de Jong et al., 2007; Obata et al., 2007), this step was not carried out. Addition of acid may cause contamination (Hydes, 1977) or leaching of Al from the polypropylene caps (Brown and Bruland, 2008). Storage experiments have shown that loss of Al from seawater stored in polyethylene bottles at room temperature is less than the precision of the method for up to five days, and around 5% for six days storage (Hydes and Liss, 1977).

4.2.2.2. Filtered samples

Filtered samples were collected by using the water pressure within the rosette bottle to push the seawater through a 0.4 μm polycarbonate filter directly into a pre-cleaned sample

bottle. As such, a polycarbonate filter holder, housing the filter, was connected to the rosette bottle spigot via polyvinyl chloride tubing (Fig. 4.1). Although it is usually not advised to acid-wash plastics that come in contact with water for Al determination (D. Hydes, personal communication), because the filtering system was not factory new a rigorous cleaning procedure was undertaken. The tubing and filter holders were initially soaked in Decon detergent for five days before being rinsed three times in DI water and placed in 10 % AnalaR nitric acid for around three weeks. The equipment was finally rinsed a further three times, again in DI water, and sealed inside polyethylene bags until use. The entire system was flushed with the seawater of interest before ~ 60 ml was collected in the LDPE sample bottle.

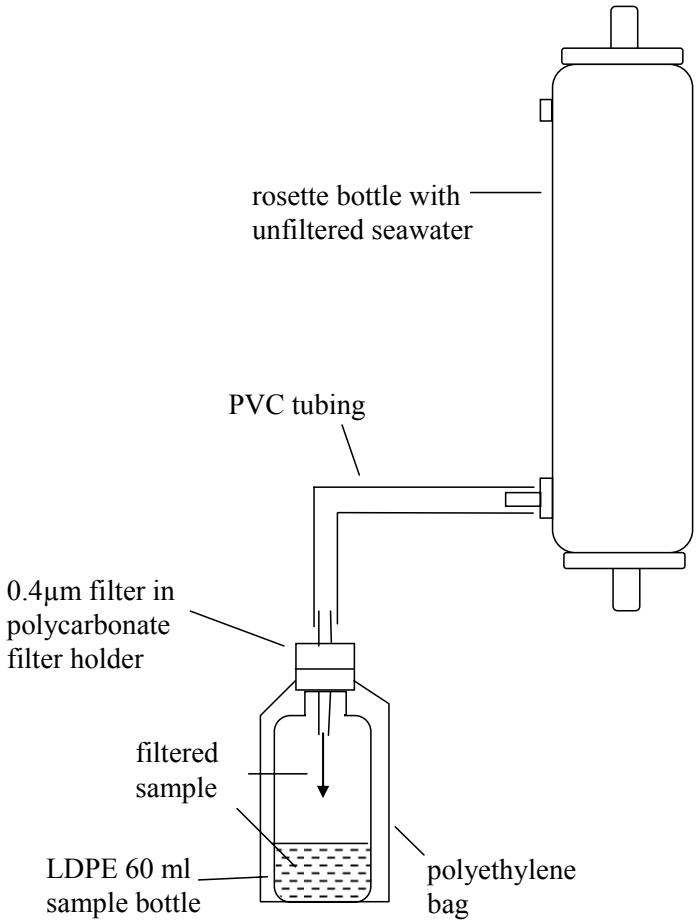

Figure 4.1. Illustration of method used for filtering seawater for later aluminium analysis during 0804S.

4.2.3. Reagent preparation

Three reagents are required: a sodium acetate – acetic acid buffer solution (4 M with respect to sodium acetate, pH 5), a 0.02 w/v % lumogallion solution, and an Al standard for calibration (Hydes and Liss, 1976). All reagents were prepared in a class 100 clean room (unaccredited) prior to the cruise to decrease the risk of contamination particularly from air-borne contaminants. This room is not used for sediment sample preparation and overshoes and un-powdered polyethylene or nitrile gloves were worn at all times. All purchased chemicals were kept inside their original containers and sealed inside zip-locked polyethylene plastic bags. Small aliquots of any liquid chemicals were decanted into LDPE containers when required to ensure that the original chemicals were not contaminated during pipetting. Prepared reagents were kept in LDPE 125 ml Nalgene bottles that had been washed several times in DI water and rinsed in the reagent. Reagents were prepared a week before departure, sealed in zip-lock polyethylene bags and stored inside a lidded plastic container for use at sea. The solutions are stable for at least a month so that during 0804S reagents did not have to be prepared onboard.

The buffer solution was prepared by dissolving 32.81 g of ARISTAR anhydrous acetic acid in 13.16 ml of ARISTAR acetic acid and diluting up to 100 ml with DI water.

The lumogallion solution was prepared by dissolving 0.02 g of lumogallion in 100 ml of DI water. The lumogallion was obtained from *Fluorochem Limited* and imported from Japan.

To prepare the Al standard, 0.1137 g of AnalaR aluminium potassium sulphate 12-hydrate was dissolved in 1000 ml of DI water in a volumetric flask. The flask was inverted for several minutes to ensure complete mixing before 1 ml of the solution was pipetted into another volumetric flask and diluted up to 1000 ml with DI water. This final standard solution was again mixed for several minutes before being sealed in a pre-cleaned LDPE bottle. Adding 1 ml of this standard solution to 50 ml of a calibration sample adds approximately 5 nM of Al enabling a standard addition calibration to be carried out.

4.2.4. Sample preparation

Sample preparation took place at sea in a container specially designed for chemistry although not trace metal analysis. However, the use of a container laboratory meant that no-one other than myself entered the area decreasing the contamination risk. No smoking was allowed near the container entrance, or near the air intake pipe for the container removing this as a potential contamination source. Non-powdered polyethylene or nitrile gloves were worn at all times and lids were not left off sample bottles or reagents longer than required.

Reagents were added to samples within 72 hours of collection with the exception of samples from three stations in the vicinity of the Wyville Thomson Ridge which were prepared within five days of collection. As degradation of a 64 nM sample over six days is < 4 nM (Hydes and Liss, 1977), it is expected that any effects of this delay in the addition of chemicals will be limited. Sample bottles were inverted several times to re-suspend any particulate matter before a 20 ml subsample was removed using a 25 ml *Nalgene* polypropylene measuring cylinder. The measuring cylinder was washed several times in DI water before being rinsed in the sample. Polypropylene has been shown to have high [Al] (Moody and Lindstrom, 1977; Hall, 1998; Reimann et al., 1999). However, as the seawater was not acidified and only in contact with the plastic for less than 30 seconds, it was felt that use of the measuring cylinder did not pose a significant contamination risk. The 20 ml subsample was returned to the original sample bottle (after any remaining sample had been discarded) to avoid confusion, before the addition of 0.2 ml of lumogallion solution, and 0.2 ml of the buffer solution. The sample bottle was immediately recapped, inverted several times to thoroughly mix the reagents and sample, resealed in the polyethylene bag, placed in a polyethylene lidded container and finally placed inside a black polyethylene bag. When the lumogallion method was first proposed (Nishikawa et al., 1967) and adapted for use in natural waters (Shigematsu et al., 1970; Hydes and Liss, 1976), samples were heated to 80 °C for 20 – 90 minutes to allow the Al-lumogallion complex to form. However, later studies showed that leaving prepared samples for at least eight hours at room temperature was sufficient (Kremling and Hydes, 1988). The prepared subsamples were therefore left at room temperature for at least 24 hours to allow the Al-lumogallion complex to form.

4.2.5. Sample analysis

All samples were analysed using a *Perkin Elmer LS-5B* fluorescence spectrometer in the chemistry container where all sample preparation occurred. Samples were measured approximately 24 hours after the addition of reagents. The exception was samples collected at the station in the southern Faroe Shetland Channel which were kept for around 65 hours before analysis because of initial problems with the fluorometer. Later shore-based experiments (detailed in section 4.3.5) suggest little to no degradation of the Al-lumogallion complex should have occurred. However, 65 hours is towards the upper limit of time that samples can be left after the addition of reagents before results become elevated and less precise. The excitation wavelength was set at 465 nm, and the emission wavelength at 555 nm (Hydes and Liss, 1976) with associated slit widths of 15 nm and 2.5 nm respectively.

Samples were gently shaken to resuspend any particulate matter before being carefully decanted, ensuring there were no bubbles, into 5 cm^3 cuvettes. Disposable plastic cuvettes were used because of the lack of a clean DI water supply onboard *FRV Scotia*. Cuvettes were handled by the corners and wiped down to remove any fingerprints or drips before measurement. The fluorescence was allowed to stabilise before being integrated over 10 seconds and noted. Time constraints meant that not all samples could be analysed in triplicate. Instead samples from various depths, and therefore a range of Al concentrations, were analysed eight-ten times to give an idea of the instrumental (intra-bottle) precision.

4.2.6. Preparation of blanks

In any chemical analysis blanks are required to identify and quantify any possible contamination from the procedure or reagents used. These are detailed below along with the measurement of the baseline natural fluorescence of seawater which must also be accounted for.

4.2.6.1. Procedural blank

In order to ensure that no Al is added to or removed from samples during their collection a procedural blank was undertaken. Although the use of seawater of a known Al concentration is preferable, a random rosette bottle was rinsed and filled with DI water. Three samples were taken as this was carried out enabling the baseline [Al] of the water to be determined. The rosette bottle was left for around 40 minutes, the average time between firing of the bottle at depth and sampling on deck. Three samples were then collected using the same procedure as that for unfiltered samples (section 4.2.1). Although no blank was determined for the filtering apparatus, an attempt to quantify the blank associated with the filter papers was made. Six bottles were filled with DI water and a filter paper added to three of these. These bottles were inverted several times and left for around five minutes, the approximate time required to filter a sample, before decanting the seawater into another pre-rinsed bottle to separate the filter paper as required. All procedural blank samples were stored under identical conditions to regular samples (section 4.2.2), and prepared simultaneously to and using the same methods as collected samples (section 4.2.4). The procedural blanks were analysed in triplicate again using the same method as for regular samples (section 4.2.5).

4.2.6.2. Reagent blank

In order to quantify any Al that is added to samples from the chemicals used, a reagent blank was carried out. Six sample bottles were filled with 20 ml of seawater collected from a mid-water column region of constant temperature, salinity and dissolved oxygen. In chemistry it is common for a reagent blank to be determined by measurement of water with an undetectable concentration of the substance of interest (e.g. Miller and Miller, 1989). However, this is difficult within trace metal analysis because of the very low concentrations. As such, three bottles were prepared by adding 0.2 ml of lumogallion solution and 0.2 ml of buffer solution, whilst the remaining three were spiked with 0.4 ml of both reagents (Hydes and Liss, 1976). The reagent blank samples were stored under identical conditions to regular samples (section 4.2.2) and were analysed in triplicate using the same methodology (section 4.2.5). Any difference in fluorescence between the two subsets was attributed to Al added by the reagents.

4.2.6.3. Luminescence blank

Excitation and emission wavelengths used during analysis are chosen to maximise the fluorescence from the Al-lumogallion complex and minimise fluorescence from any other source. However, the natural fluorescence of seawater at pH 5 must be accounted for by the measurement of buffered seawater without the addition of the lumogallion fluorescent agent (Hydes and Liss, 1976). As such, samples from a selection of stations and depths from throughout the cruise were split into two 20 ml subsamples. One subsample was prepared as a regular sample (see section 4.2.4), whilst the second subsample had only 0.2 ml of the buffer solution added. Both samples were stored and analysed as regular samples (sections 4.2.2 and 4.2.5) but in triplicate.

4.2.7. Calibration procedure

In order to convert fluorescence to [Al] a calibration is required. To minimise any matrix effects, standard addition calibrations were carried out using seawater collected from the mid-depth water column in an area of constant temperature, salinity and dissolved oxygen. Water was sampled as for unfiltered samples and stored under identical conditions (section 4.2.2). Subsamples of 50 ml were dispensed into 60 ml LDPE sample bottles. To ensure maximum accuracy, a 10 ml pipette was used with the exception of the first calibration when a 25 ml *Nalgene* measuring cylinder was used. Varying aliquots of Al standard solution (24 nM) were added to samples: three samples had no standard added, three samples 1 ml added, three samples 2 ml added and so on. For the first calibration up to 6 ml was added, however, this was increased to 8 ml for subsequent calibrations to ensure that the calibration graph spanned the entire range of observed [Al]. Finally, 0.5 ml of lumogallion solution and 0.5 ml of the buffer solution were added, and the sample bottle inverted several times before storing as for regular samples (section 4.2.2). Calibration samples were analysed in triplicate using the same method as, and simultaneously to, regular samples (section 4.2.5).

The conversion of sample fluorescence to [Al] is a two step process. Firstly, raw sample fluorescence (F_{RS}) must be adjusted to corrected sample fluorescence (F_{CS}) by the subtraction of blanks (equation 4.1).

$$F_{CS} = F_{RS} - F_{PB} - F_{RB} - F_{LB} \quad (4.1)$$

where F_{PB}, F_{RB} and F_{LB} are the fluorescence associated with the procedural, reagent and luminescence blank respectively. Secondly, the corrected sample fluorescence is converted to [Al] using the regression equation (equation 4.2) obtained from the calibration graph (e.g. Fig. 4.2). The calibration graph was created by plotting [Al] added to the calibration samples (in nM), against mean corrected fluorescence of the calibration samples (in relative fluorescence units (RFU)). The mean corrected fluorescence of calibration samples was calculated by subtracting the mean fluorescence of calibration samples which were not spiked with the Al standard, from the mean fluorescence of calibration samples at any particular concentration.

$$\textit{sample [Al]} = \textit{corrected sample fluorescence } (F_{CS}) \; / \; m \quad (4.2)$$

where m is the gradient of the calibration graph obtained from a least squares method. As the regression line passes through the origin no correction for the y-axis intercept is required.

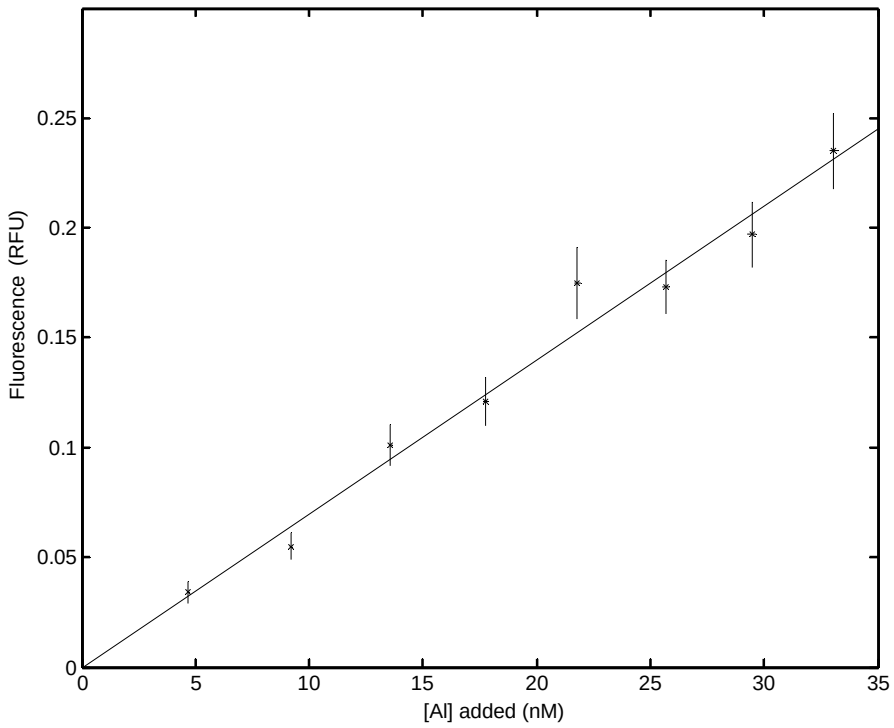

Figure 4.2. Example calibration graph for Al analyses. Fluorescence = 0.007 [Al], r = 0.98. Error bars show total errors. All calibration graphs produced during 0804S had r values greater than 0.98.

4.2.8. Calculation of errors

The analysis of any sample is subject to errors which must be quantified. Each of the multiple steps in the conversion of the measured raw fluorescence to [Al] has its own error.

The standard deviation (SD_{CF}) associated with the conversion of F_{RS} to F_{CS} by the subtraction of the blanks (equation 4.1) can be calculated using equation 4.3.

$$SD_{CF} = (SD_{RF}^{\,2} + SD_{PB}^{\,2} + SD_{RB}^{\,2} + SD_{LB}^{\,2})^{1/2} \quad (4.3)$$

where SD_{RF} is the standard deviation associated with F_{RF}, and SD_{PB}, SD_{RB} and SD_{LB} the standard deviations associated with F_{PB}, F_{RB} and F_{LB} respectively. All standard deviations were obtained from precision measurements.

The conversion of F_{CS} to [Al] occurs via a regression equation (equation 4.2). The error associated with the gradient m (SD_m) can be quantified using a statistical approach (equations 4.4 and 4.5, from Miller and Miller, 1989).

$$S_{y/x} = \left[\frac{\sum_i (y_i - \hat{y}_i)^2}{n-2} \right]^{1/2} \quad (4.4)$$

$$SD_m = \frac{S_{y/x}}{\left[\sum_i (x_i - \bar{x})^2 \right]^{1/2}} \quad (4.5)$$

where y_i is the individual calibration sample fluorescence and $\hat{y}_i$ the predicted sample fluorescence, obtained from the line of best fit (equation 4.2), for the given [Al]. The number of points on the calibration graph is defined by n, whilst x_i is the individual calibration sample [Al] and $\bar{x}$ the mean [Al] of all calibration samples.

The total error associated with each individual [Al] can be calculated by combining SD_{CF} and SD_m (equation 4.6). This final error (RSD_{Al}) is expressed as a proportion of the [Al] of the sample known as a relative standard deviation.

$$RSD_{Al} = \left[\left(100 \frac{SD_m}{m} \right)^2 + \left(100 \frac{SD_{CF}}{F_{CF}} \right)^2 \right]^{1/2} \quad (4.6)$$

4.2.9. Summary

Although the precisions, blanks and errors for Al data from all cruises used within this thesis are collated in section 4.4, the values for 0804S are briefly discussed below.

Both the intra-bottle and inter-bottle precisions during 0804S were around 10 %. Although this is towards the upper end of values within the literature, it compares reasonably favourably with other studies using the fluorometric technique (e.g. Hydes and Liss, 1976 (5 % at 35 nM); Upadhyay and Gupta, 1994 (~ 5 %); Minakawa and Watanabe, 1998 (1.5 - 25 %)). The procedural blank for the rosette bottle is low (0.3 nM) indicating that the use of the unmodified rosette bottles and sampling procedure were sound. However, the blank associated with the filter papers was high and variable (3±2 nM) meaning that it is not possible to correct for this contamination without introducing very large errors. As such the filtered samples collected during 0804S are of a poor quality and are not used within this thesis. One possible explanation for this contamination was that the filter papers and the filter housing were made of polycarbonate which often has a high Al content (Moody and Lindstrom, 1977). Additionally, the filter holders and filter papers were exposed to the atmosphere whilst the filter paper was changed. In an attempt to reduce the contamination associated with the filtering step, the possibility of pressure-filtering samples using a plastic syringe and pre-sealed Sartorius filters was investigated. However, as problems were still prevalent with filtered samples having a higher [Al] than unfiltered samples, the decision was made to concentrate on collecting only unfiltered samples on future cruises.

Total errors for samples collected during 0804S are around 20 %. This is relatively high, in part due to an average luminescence blank being applied to samples instead of the natural luminescence of the seawater being measured for each sample individually.

Although the method for unfiltered samples worked well during 0804S several questions need to be answered in order to create a fully-robust method. These include:

- Can Al samples be collected using unmodified rosette bottles on a regular rosette frame eliminating the need for specialist and expensive equipment?
- How can samples be safely stored if a suitably clean analysis area is not available at sea?
- How long is the Al-lumogallion complex stable for?
- When a commercial reference material is not available how can accuracy of the method be ensured?

These questions were investigated through a series of experiments and are discussed in the next section.

4.3. Method Development

All tests within this section, with the exception of those detailed in 4.3.7, were carried out using a *Perkin-Elmer LS-3B* fluorescence spectrometer with 10 nm slits for both the excitation and emission wavelengths. After failure of this machine a *Turner Trilogy* fluorometer was used. A quartz cuvette was used at all times, being flushed with DI water between samples and rinsed in sample prior to filling. Water used in all experiments was either collected using *RV Calanus* from Scottish coastal waters or obtained from the piped seawater supply at SAMS. Reagents and samples were prepared and analysed as detailed in sections 4.2.3 to 4.2.5, and 4.2.7, unless stated otherwise.

4.3.1. Evaluation of the contamination potential from sample bottles

The decision was made to use LDPE *Nalgene* 60 ml bottles for this work because of their specificity to trace metal work (section 4.1). However, the caps are made from polypropylene which has been shown to contain high levels of Al (Moody and Lindstrom, 1977; Hall, 1998; Reimann et al., 1999). Additionally, significant but variable Al contamination from some polypropylene caps on LDPE bottles has been reported when in contact with acidified seawater (Brown and Bruland, 2008). To investigate whether the caps on the *Nalgene* bottles were a source of contamination 20 sample bottles, picked at random, were filled with 20 ml of seawater. Half were stored upright so the sample had no

contact with the polypropylene cap and the remainder upside down so the sample was continually in contact with the lid. After five days the samples were prepared and analysed. No significant difference was seen between the two treatments with bottles stored upright having a [Al] of 32 ± 3 nM and those stored upside-down having a concentration of 33 ± 3 nM. However, as a precaution all sample bottles used in future analyses were stored upright.

4.3.2. Investigation into the possibility of sample collection using an unmodified rosette

The collection of seawater for trace metal analysis is problematic due to the very low concentrations in seawater and metals inherent to the collection process. Seawater samples are usually collected from plastic bottles mounted on a metal rosette frame with zinc sacrificial electrodes. This system is lowered, from a metal ship, on metal hydrowire which is often greasy and beginning to corrode slightly. Additionally, there are atmospheric contamination possibilities from the ships funnel, rubbish incineration and anybody smoking on deck. To overcome these problems trace metal samples are often collected using specialist or customised equipment. For example, the use of modified bottles mounted on: rosette frames (e.g. Saager et al., 1997), hydrowire (e.g. Yeats et al., 1995) or Kevlar (Nolting et al., 1999); or specially designed samplers (e.g. Flegal and Patterson, 1983). Although this may be necessary for the determination of some trace metals it may not be required to obtain contamination-free seawater for Al analysis. If this is the case it would remove the requirement for expensive equipment which can often limit the ship from which samples can be taken. Although some studies collecting seawater for Al analysis use modified rosette bottles mounted on Kevlar wire (de Jong et al., 2007), plastic rope (Upadhyay and Gupta, 1994) or plastic coated hydrowire (Hall and Measures, 1998); others use regular rosette frames (e.g. Minakawa and Watanabe, 1998; Obata et al., 2007). There is no evidence of contamination when using a stainless steel rosette frame despite the central anodized Al pylon (Measures and Edmond, 1989) or even when using an Al rosette as long as the frame is coated in paint, nylon or epoxy resin (C. Measures, personal communication).

The vast majority of Al work uses rosette bottles modified by coating in Teflon. To investigate whether this is necessary or not to collect contamination-free seawater samples two rosette bottles were filled with seawater. One rosette bottle was a *Sea-Bird* design with a PVC body and external spring; the other was identical except the modification of an internal Teflon coating. Seawater samples were collected during filling of the bottles allowing the baseline [Al] to be determined. Additionally, aliquots were withdrawn from the rosette bottles spigots after approximately 15, 30, 60, 90 and 120 minutes.

Results show that for both rosette bottles although the residual [Al] fluctuates around zero these variations are within the errors of the method (Fig. 4.3). Hence, it appears that modification of the rosette bottle by addition of a Teflon-coating is not required in order to collect contamination-free seawater samples for Al analysis.

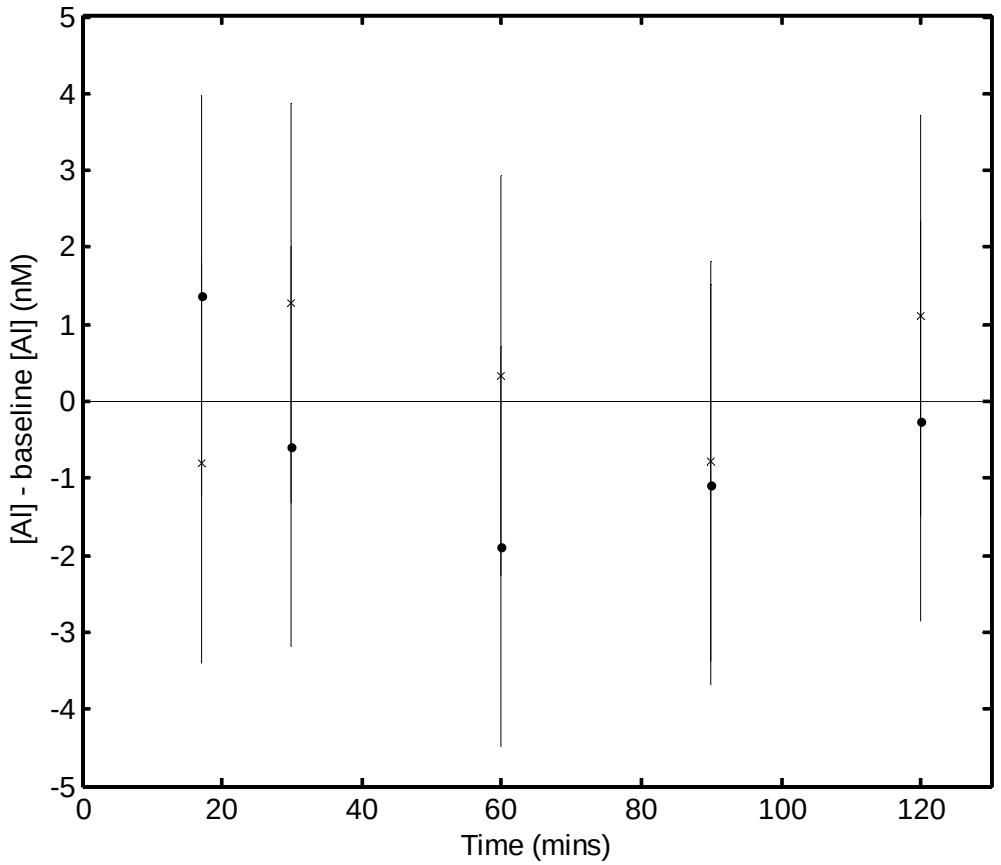

Figure 4.3. Variation of Al concentration with time for seawater in a Sea-Bird PVC rosette bottle (dots) and a Sea-Bird Teflon-coated PVC rosette bottle (crosses). Lines represent spread within replicate samples.

4.3.3. Exploration into storage of samples for later shore-based analysis

During 0804S samples were analysed at sea enabling sampling regimes and protocols to be adapted whilst still in the field. Additionally, any storage artefacts were minimised which is particularly advantageous in trace metal work due to the extremely low concentrations in seawater. However, a container modified for trace metal work is not always available and rough weather can influence the fluorometer performance. As such, it can be advantageous to store the seawater for later analysis in shore-based laboratories. Seawater samples kept at room temperature for six days experience a 5 % loss of Al (Hydes and Liss, 1977) indicating that if samples cannot be prepared within a couple of days of collection an alternative storage method is required. Although some studies acidify samples to prevent degradation, the decision was made not to employ this technique because of the potential for contamination problems (section 4.2.2). Another method that has been used on both filtered and unfiltered samples from estuaries (Takayanagi and Gobeil, 2000) and the deep sea (e.g. Moore, 1981; Moran et al., 1992; Minakawa and Watanabe, 1998), is freezing.

Although several previous studies have investigated whether samples can be frozen without sample degradation, results have been contradictory and sample numbers small. No change in [Al] were reported over a period of 14 days when samples were frozen (Hydes and Liss, 1976; Hydes and Liss, 1977). A comparison of duplicate samples that were either analysed immediately or after freezing showed that although the shape of the profile was unaffected, [Al] in the frozen samples were consistently higher (Caschetto and Wollast, 1979). This was more pronounced at lower concentrations. As chloroform was added to the samples (Caschetto and Wollast, 1979) it is unclear whether the offset is related to the addition of this chemical or the freezing process. Slight scatter was reported in samples that were frozen but again it was uncertain whether this was related to freezing or residual cleaning acid with the sample bottles (Moran and Moore, 1991). Finally, a comparison of 24 duplicate samples analysed either immediately using electron capture gas chromatography or after being frozen for ten days using the lumogallion technique showed a good correlation (Measures et al., 1986). However, the absence of a 1:1 relationship raises the possibility that a correction may need to be applied to [Al] determined from frozen samples. Additionally, the use of different analytical methods for frozen and unfrozen samples introduces an additional variable other than storage into the results. As

the method used to store samples is fundamental to obtaining high quality results a freezing experiment was carried out.

Duplicate samples were collected at eight to twelve depths at five sites in western Scottish coastal waters (Fig. 4.4) in salinities ranging from coastal to deep sea values. Unfiltered samples were collected from *Sea-Bird* PVC rosette bottles mounted on a stainless steel *Sea-Bird* rosette frame coated in epoxy resin (see section 4.2.2. for methodology). Samples were either kept in the dark before analysis within 72 hours of collection, or stored frozen at -18 °C for ten days, thawed at room temperature for 48 hours and analysed.

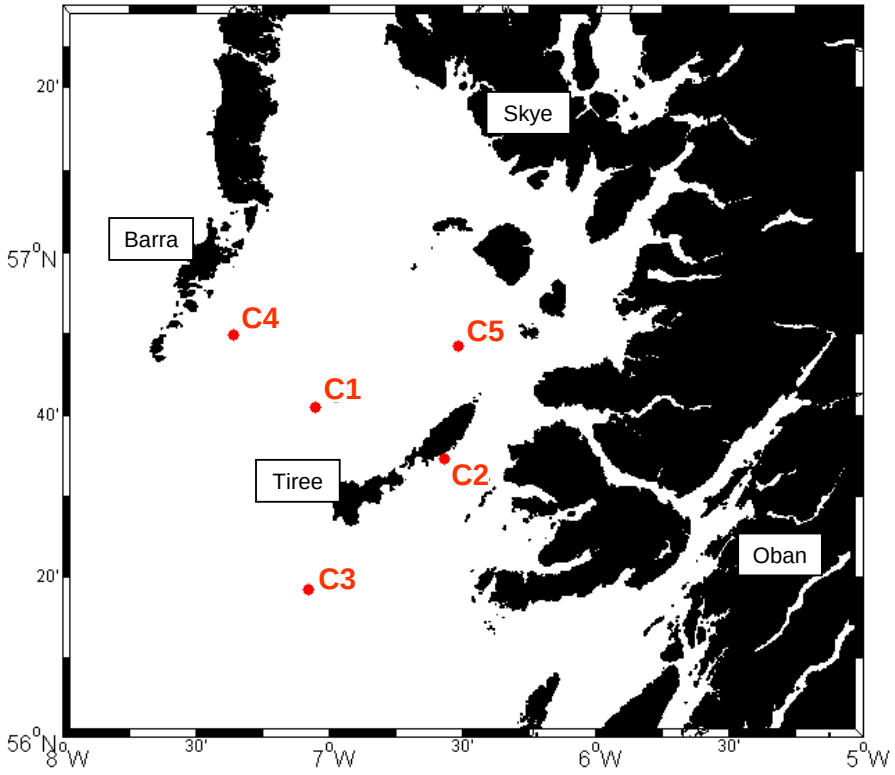

Figure 4.4. Location of stations where water samples were collected for an investigation into effects of freezing on Al concentrations in seawater. Stations were occupied in May 2005 onboard RV Calanus.

Profiles for those samples frozen prior to analysis show a similar shape to those prepared and analysed immediately (Fig. 4.5). Additionally the difference between the values for the two treatments are within the error of the method for nearly all the sample pairs. A good correlation (r 0.90) exists between samples analysed immediately and those frozen

first (Fig. 4.6) with no systematic over- or under-estimation of [Al] in frozen samples. Furthermore, a 1:1 relationship is seen suggesting that no correction needs to be applied.

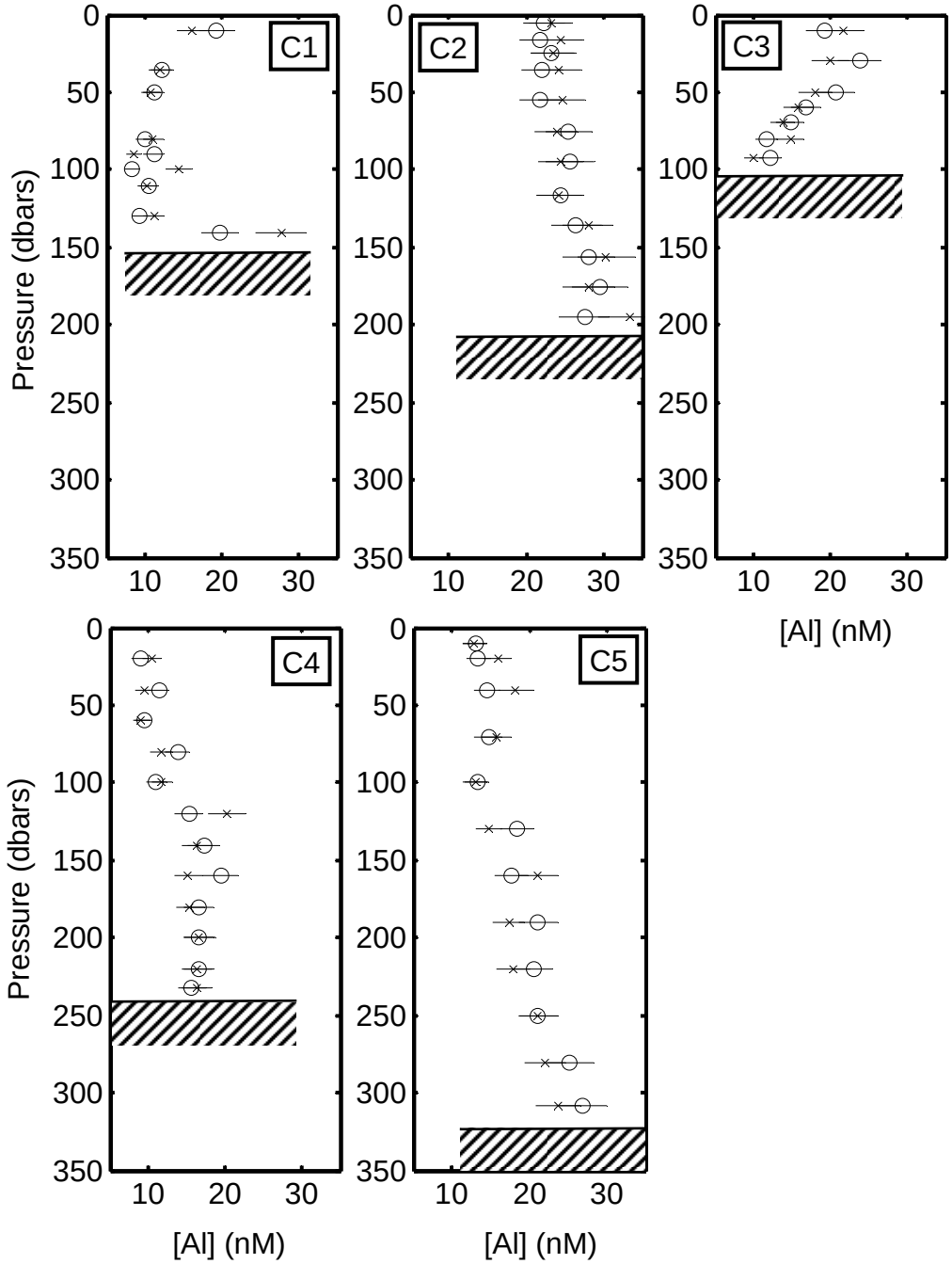

Figure 4.5. Reactive Al profiles collected in Scottish coastal waters (see Fig. 4.5 for locations). Circles: samples analysed within 72 hours of collection; crosses: samples analysed after freezing for 10 days at -18 °C; lines show total errors; hashed area: seabed.

To calculate whether the apparent lack of affect of freezing on the overall [Al] of samples is statistically significant a paired t-test was carried out. The null hypothesis was 'no difference exists between the mean [Al] of the frozen and non-frozen samples'. A paired t-

test assumes that any differences between the duplicate samples are normally distributed, as indicated by a bell-shaped curve on a normal distribution plot and a sigmoid curve on a cumulative frequency graph (Zar, 1984). These requirements are met. The t value (obtained using equation 4.7) was 0.074 (n = 52) with an associated p value of 0.58. As the p value is greater than 0.025 there is insignificant evidence to reject the null hypothesis. Additionally, there is a high probability that any differences in the mean [Al] between samples frozen and analysed immediately is due to sampling error.

$$t = \frac{\overline{d}\sqrt{n}}{SD_d} \tag{4.7}$$

where $\overline{d}$ is the mean of the differences between the duplicate pairs, n the number of samples and SD_d the standard deviation of the differences.

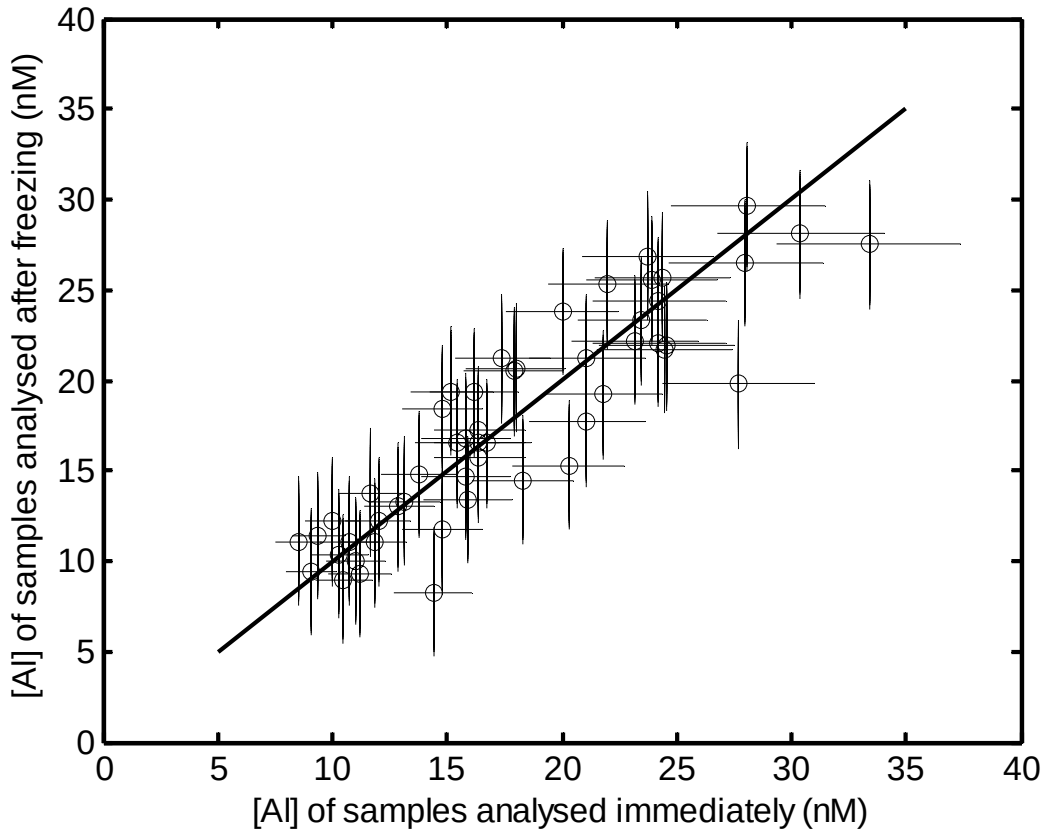

Figure 4.6. Comparison of Al concentrations (nM) in samples analysed within 72 hours of collection with those frozen at -18 °C for 10 days prior to analysis. r = 0.90. Error bars represent total error associated with the method.

A more complicated three-way analysis of variance (ANOVA) test was carried out to determine the significance of freezing on [Al] concentrations relative to the effects of station location and sample depth. Station position and whether samples had been frozen or not were orthogonal variables whilst depth was a nested variable within location. The test was carried out using the general linear model option within *Minitab*, a specialist statistical software package. The F (Fisher) value for the frozen/not-frozen group was 0.22 with a critical value of 5.42 (degrees of freedom $_{group}$ = 1; degrees of freedom $_{error}$ = 47; probability = 0.025). As the observational F value is less than the critical F value there is insignificant evidence to suggest that there is a difference between those samples stored in the freezer and those analysed immediately. Further, there is a one to two order of magnitude difference between the F value for the frozen/not-frozen group, and those obtained for the station position group (F = 146.77) and sample depth group (F = 7.49). This suggests that the effect of freezing samples prior to analysis is also not significant when compared to variations in [Al] caused by sample depth and station.

4.3.4. Evaluation of different calibration standards

At least two possible methods for the preparation of the Al standard solution used to spike calibration samples exist. Aluminium potassium sulphate tri-hydrate can be dissolved (section 4.2.7) as detailed in Hydes and Liss (1976), or alternatively a commercially available reference material can be diluted (e.g. Resing and Measures, 1994; Obata et al., 2007). A comparison of these two methods was made. A single element reference material (1000 ppm Al dissolved in 2 % nitric acid), obtained from the *SPEX Certiprep Group*, was diluted to nanomolar levels by adding 70 µl to a volumetric flask and making up to 1000 ml with DI water. Adding 100 µl of this standard to a 50 ml calibration sample gives approximately a 5 nM increment of Al.

Twenty bottles were filled with 50 ml of seawater: ten were spiked with increments of the aluminium potassium sulphate calibration solution, and the remainder with aliquots of the calibration solution made from the reference material. Both calibrations had a very high regression coefficient ($r > 0.99$) although the gradient for the aluminium potassium sulphate calibration was shallower ($m = 0.016$) than that of the reference material calibration ($m = 0.018$). This means that for a given fluorescence the calculated [Al] will

be higher for the aluminium potassium sulphate calibration than for the reference material calibration. This offset will be larger at higher fluorescences (e.g. a fluorescence of 0.1 RFU gives a difference of 1 nM between the two calibrations whilst a fluorescence of 0.4 RFU produces a disparity of 4 nM). Possible reasons for the discrepancy between the two calibrations include contamination inherent to the aluminium potassium sulphate due to it only being commercially available at the lower purity AnalaR grade, or absorption of moisture by the chemical affecting its mass. Further possibilities are that the calibration solutions may not be completely mixed or that a salinity effect is seen.

To check that the calibration solutions were homogenous, successive aliquots of a calibration solution were analysed. A mean of 44.3 ± 3 nM was obtained which is within the expected precision of the method.

As the seawater calibration samples are spiked with Al standard solutions prepared in DI water a change in salinity is expected. For samples prepared with the aluminium potassium sulphate standard solution, a salinity difference of 5.39 is predicted between a sample not spiked with the standard solution and one to which 8 ml is added. The salinity change associated with the calibration using the standard solution made from dilution of a reference material is 0.69. To investigate the effect of these salinity variations three calibrations were carried out. All the standard solutions were prepared using aluminium potassium sulphate 12-hydrate to ensure that only salinity varied between the different calibrations. The first calibration was prepared as detailed in section 4.2.3 so that when 1 ml of standard solution was added to calibration samples an approximate 5 nM increment of Al was added. The second calibration used an Al standard solution that was an order of magnitude more concentrated, therefore instead of 1 ml aliquots samples were spiked with 0.1 ml increments. The final calibration was prepared so that each sample had the same ratio of seawater to DI water ensuring that no salinity change occurred during the calibration. The shallowest gradient was seen when the largest salinity change occurred (Table 4.1) with the steepest gradient associated with the calibration when salinity was constant. Although this difference equates to no measurable change in [Al] for a low fluorescence, at higher fluorescences a ~ 2 nM difference is observed between the cases when the salinity change was 0.00 and 5.39. As the differences in [Al] between the calibrations with a salinity change of 0.00 and 0.69 are sub-nM, and it is more complex to prepare a calibration ensuring that salinity is constant, it was decided to use a calibration

solution where increments of 0.1 ml of the standard Al solution are required. Additionally, as there is evidence that aluminium potassium sulphate 12-hydrate absorbs moisture making weighing it inaccurate, and the chemical is only manufactured at a low-purity, the commercially available reference material was used to prepare all future calibrations.

Salinity Change	Calibration equation	[Al] for a given fluorescence
0.00	fluorescence = 0.0341 [Al]	0.1 RFU = 3 nM 0.8 RFU = 24 nM
0.69	fluorescence = 0.0335 [Al]	0.1 RFU = 3 nM 0.8 RFU = 24 nM
5.39	fluorescence = 0.0312 [Al]	0.1 RFU = 3 nM 0.8 RFU = 26 nM

Table 4.1. Results from an experiment to investigate the effect of salinity changes in calibration samples on the gradient of the line of best fit and subsequent [Al]. Salinity change is defined as the difference in salinity between a sample spiked with the maximum volume of Al standard solution (0.8 or 8 ml) and the baseline salinity of the seawater.

4.3.5. Investigation into stability of the Al-lumogallion complex

During 0804S the vast majority of samples were analysed within 24 hours of the addition of reagents. However, samples from one station (section 4.2.5) were stored for around 65 hours before analysis. The Al-lumogallion complex is known to be stable for at least 48 hours (Hydes and Liss, 1976) but its stability over longer periods is uncertain. Twenty-seven sample bottles were filled with seawater, prepared and left for various time periods before analysis. Three samples were analysed, in triplicate, after 50 minutes, 20 hours, 24 hours and then every 24 hours up to seven days.

The Al-lumogallion complex forms within 20 hours of the addition of reagents at room temperature (Fig. 4.7) although this is likely to vary with laboratory temperature. The complex is stable for the next 24 hours, however, by the third day after the addition of reagents a small rise in mean [Al] is seen (0.8 nM) with a possible slight increase in

variability. By five days, a large increase in mean [Al] and variability is observed indicating that the Al-lumogallion complex is no longer stable and / or the slightly acidic conditions are causing additional Al to be released from particulate matter within the sample. As such, although the samples from 0804S are analysed just within the acceptable timeframe, all future samples were analysed between 20 and 48 hours after the addition of the reagents.

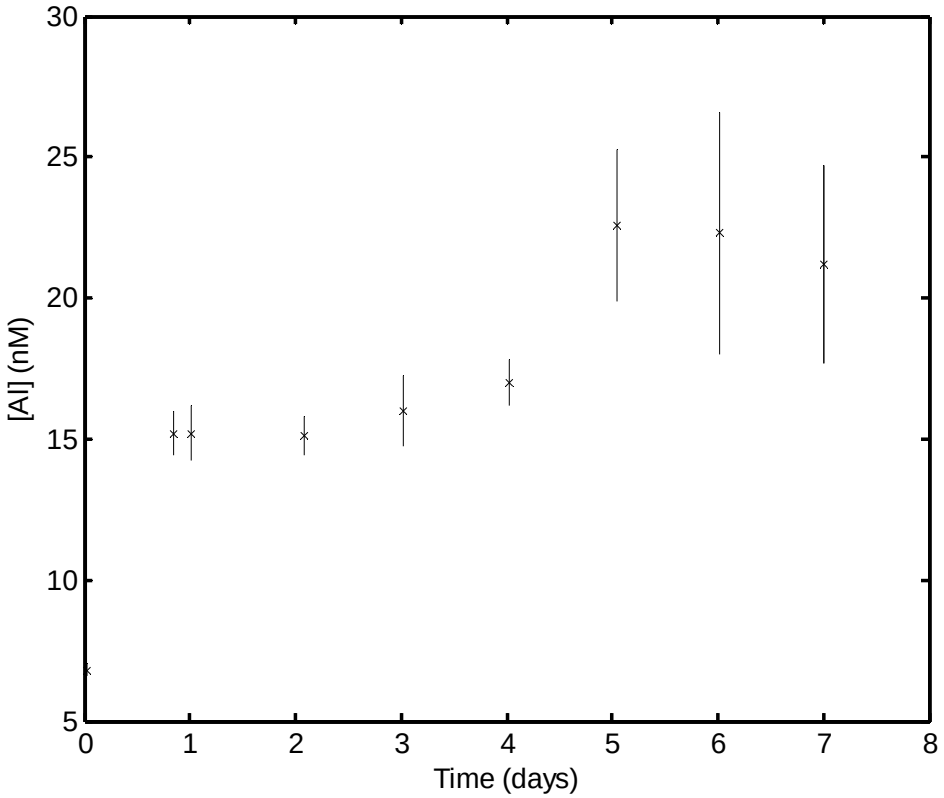

Figure 4.7. Time series of [Al] against time to investigate the stability of the Al-lumogallion complex. Error bars show the range of values between replicate samples.

4.3.6. Establishing excitation and emission wavelengths

The emission and excitation wavelengths are chosen to obtain the largest possible fluorescence for the Al-lumogallion complex whilst minimising fluorescence from any other source. Ideally these are determined empirically for each analysis run. However due to the *Perkin-Elmer LS-3B* fluorescence spectrometer breaking, a custom module for use with a *Turner Trilogy* fluorometer had to be purchased. As this is a fixed-wavelength

instrument a trial to determine the ideal wavelengths was conducted. Samples and luminescence blanks were prepared using seawater collected from a station in Scottish coastal waters (C5, Fig. 4.4) and analysed using a variety of excitation and emission wavelengths. The highest fluorescence signal for the Al-lumogallion complex (~ 0.300 RFU) is seen with an excitation wavelength of 480 nm and an emission wavelength of 570 nm (Fig. 4.8). As at these wavelengths the natural luminescence of seawater is small (< 0.020 RFU) they were used for all future analyses.

4.3.7. Determining accuracy

Accuracy refers to the trueness of a measured value to the actual concentration of the sample. Although the usual method for quantifying this is the analysis of a certified reference material (Miller and Miller, 1989), one is not available for Al at nanomolar concentrations in seawater. However, an interlaboratory comparison study has started using water collected during cruises to the tropical North Pacific (SaFe) and North Atlantic (Geotraces). Water collected from the surface of the SaFe station (S), as well as the surface and ~ 1000 m during Geotraces (GS and GD), were obtained from the University of California, Santa Cruz (UCSC). Since the seawater was acidified to pH 1.7 (Brown and Bruland, 2008), the pH of 20 ml aliquots was first raised by the addition of 720 µl of a concentrated Suprapur sodium carbonate solution. Half of these subsamples were prepared as regular samples (section 4.2.4) and the remainder as luminescence blanks (section 4.2.6.3). Interlaboratory samples were analysed concurrently with samples collected during D312.

Comparison of our values with current consensus values obtained from four trusted laboratories show a good standard of accuracy (Table 4.2). Although the precision is of a lower quality than for the consensus values, this can be explained by the reduced sensitivity of the unmodified lumogallion method chosen for this work. Despite this, the interlaboratory comparison clearly indicates that accurate concentrations are being obtained giving confidence in the methodology and therefore Al concentrations discussed within this thesis.

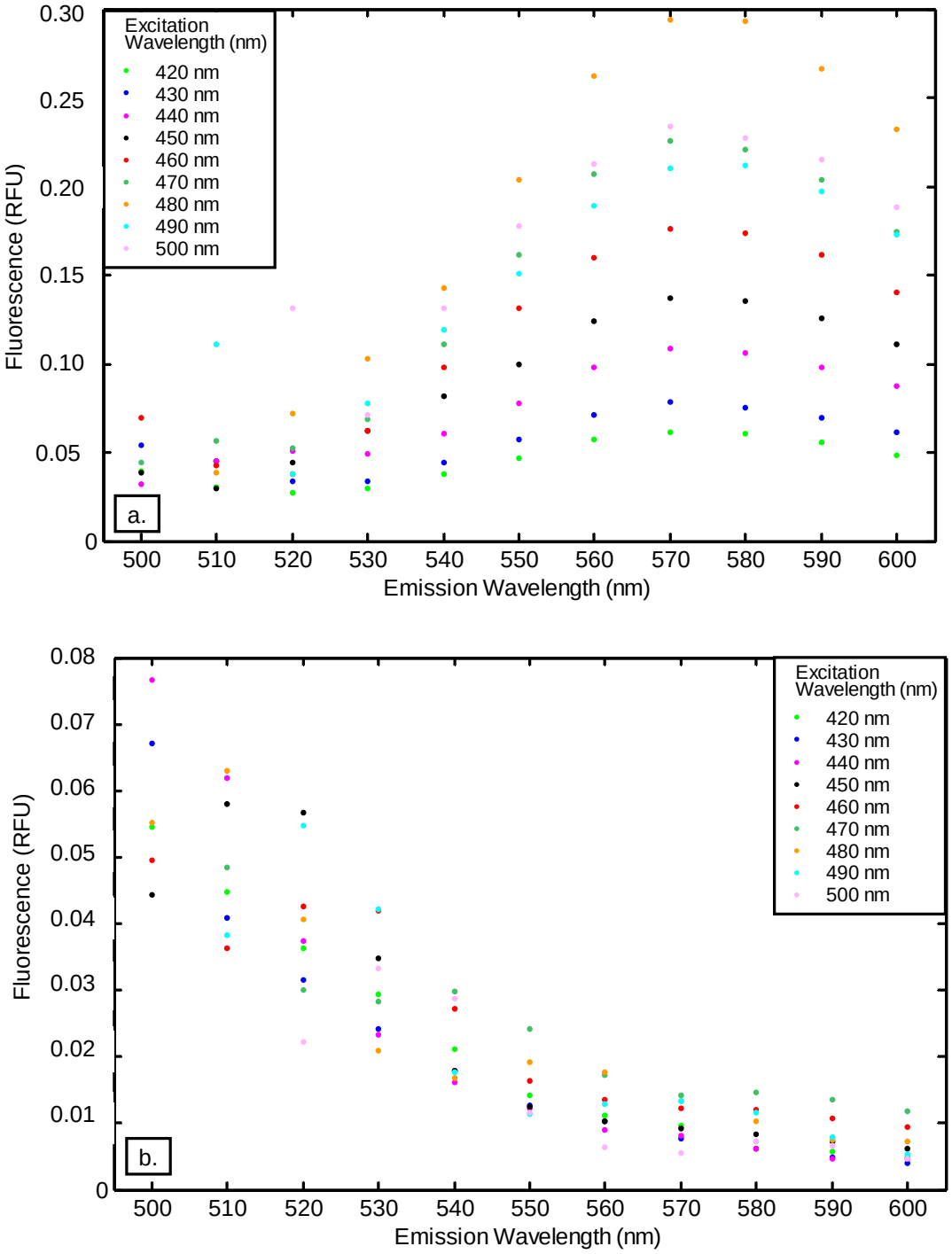

Figure 4.8. Fluorescence with varying emission and excitation wavelengths for a. the Al-lumogallion complex at pH 5; b. the natural luminescence of seawater at pH 5. Please note different scales on the y-axis.

	SaFe surface (S)	Geotraces surface (GS)	Geotraces deep (GD)
This work	2 ± 0.5 (n = 5)	30 ± 1 (n = 12)	18 ± 3 (n = 15)
Consensus values	1.7 ± 0.1	28.3 ± 0.2	18.2 ± 0.1

Table 4.2. Results from an interlaboratory comparison study investigating the accuracy of Al measurements in seawater. Results presented as mean [Al] ± 1 standard deviation (nM). Consensus values obtained from http://www.geotraces.org/science/intercalibration before the addition of data from this study.

4.4. Summary

The knowledge from the various experiments (section 4.3) was combined with the method trial (section 4.2) to create a robust working method for the collection, storage and analysis of seawater for Al determination. This established method was used to analyse unfiltered samples during H44-04-12, CD176 and D312.

All water samples were collected as detailed in section 4.2.2.1, and frozen at -18 °C until later shore-based analysis. Samples were defrosted, in an upright position, for 24 to 48 hours at laboratory temperature before being divided into two 20 ml aliquots. One subsample was prepared as per a sample (section 4.2.4) whilst the other was treated as a luminescence blank (section 4.2.6.3). Fresh reagents were prepared monthly (section 4.2.3). Although some work reports no problems when reagents are stored in glass (Sutheimer and Cabaniss, 1995), we found severe and variable contamination supporting the findings of Hydes and Liss (1977). To eliminate this no glass was used during the preparation or storage of reagents. Instead PMP volumetric flasks and beakers (rinsed in DI water) were used during preparation, and all reagents were stored in *Nalgene* 125 ml LDPE bottles, again washed several times in DI water and rinsed in the reagent.

Calibration samples were spiked using an Al standard solution prepared by the dilution of a commercially available reference material (section 4.3.4). Reagent blanks were regularly prepared (section 4.2.6.2), both prior to the addition of fresh reagents to samples and

during routine analysis. All samples, calibration samples and blanks were analysed between 20 and 48 hours after the addition of reagents (section 4.2.5). Blanks were subtracted from raw sample fluorescence (equation 4.1) before conversion to a final [Al] (equation 4.2) and calculation of total errors (section 4.2.8).

Analytical parameters, such as precision, blanks and limit of detection, vary little between the cruises used in this work and suggest the analytical method was working well (Table 4.3).

Cruise	**0804S**	**H44-04-12**	**CD176**	**D312**
Limit of detection (nM)	2	1	1	1
Intra-bottle precision (%)	10 % at 5 nM (n = 3)	6 % at 37 nM (n = 5)	6 % at 24 nM (n = 4)	6 % at 25 nM (n = 4)
Inter-bottle precision (%)	10 % at 34 nM (n = 2)	5 % at 38 nM (n = 6)	5 % at 43 nM (n = 5)	8 % at 2 nM (n = 5)
Reagent blank (nM)	undetectable	undetectable	undetectable	undetectable
Procedural blank (nM)	0	0	NA	1
Total error (%)	20	10	10	15

Table 4.3. Summary of analytical parameters for reactive Al data used within this thesis. Limit of detection is reported as 3σ of a low concentration sample as common within trace metal work (e.g. Hall and Measures, 1998; Grasshoff et al., 1999). Precisions are reported as relative standard deviations. Procedural blank for 0804S: see section 4.2.6.1 for method; procedural blank for H44-04-12: mean [Al] after 110 minutes minus mean [Al] after rosette on deck; procedural blank for D312: mean [Al] after 60 minutes minus mean [Al] after rosette on deck. No procedural blank was conducted during CD176. Total errors were calculated using method detailed in section 4.2.8.

Data collected during 0804S initially appeared to be of a high quality with changes in Al concentrations concurrent with those of potential temperature, salinity and dissolved oxygen. However, on comparison with other data collected during this thesis, published results (Lunel, 1990; Hall and Measures, 1998), and unpublished data from the Faroe Bank Channel (Fig. 4.9), it became apparent that there was a problem with accuracy. As the offset is more pronounced for higher fluorescences, we believe this problem is likely to be caused by an error in the calibration, probably as a result of an inaccurate Al concentration in the standard solution used to spike the calibration samples. Because calculated Al values during 0804S are higher than other reported values, it suggests that the Al concentration in the standard solution added to the calibration samples was lower than thought. Possible explanations are the contamination inherent to the lower grade AnalaR aluminium potassium sulphate 12-hydrate, absorption of moisture by the chemical, or the affect of changing salinity on the calibration (section 4.3.4). It is worth noting that had a reference material or interlaboratory comparison samples been available during 0804S this problem would have been detected and remedied earlier. During subsequent cruises an Al reference material was used to prepare the calibration standard solutions (section 4.3.4) and no further problems occurred. Although the absolute [Al] of samples collected during 0804S are inaccurate, the fluorescences are of a high quality. As such, data from this cruise are presented as an Al ratio relative to concentrations at 200 m (Fig. 4.9); this is discussed further in section 5.9. Additionally, data from two stations were of a poor quality and consequently were not used within this thesis (Fig. 4.9).

Data collected during H44-04-12 and CD176 appears to be of a reasonable quality with the exception of one station in the Iceland Basin (Fig. 4.9).

Several samples collected during D312 were of a poor quality (Fig. 4.9). Although extensive tests were carried out, we were unable to detect the cause with any certainty but suspect that the solid lumogallion may have degraded due to high laboratory temperatures. These low quality data are not reported within this thesis. However, other data collected during D312 appear to be of a reasonable quality.

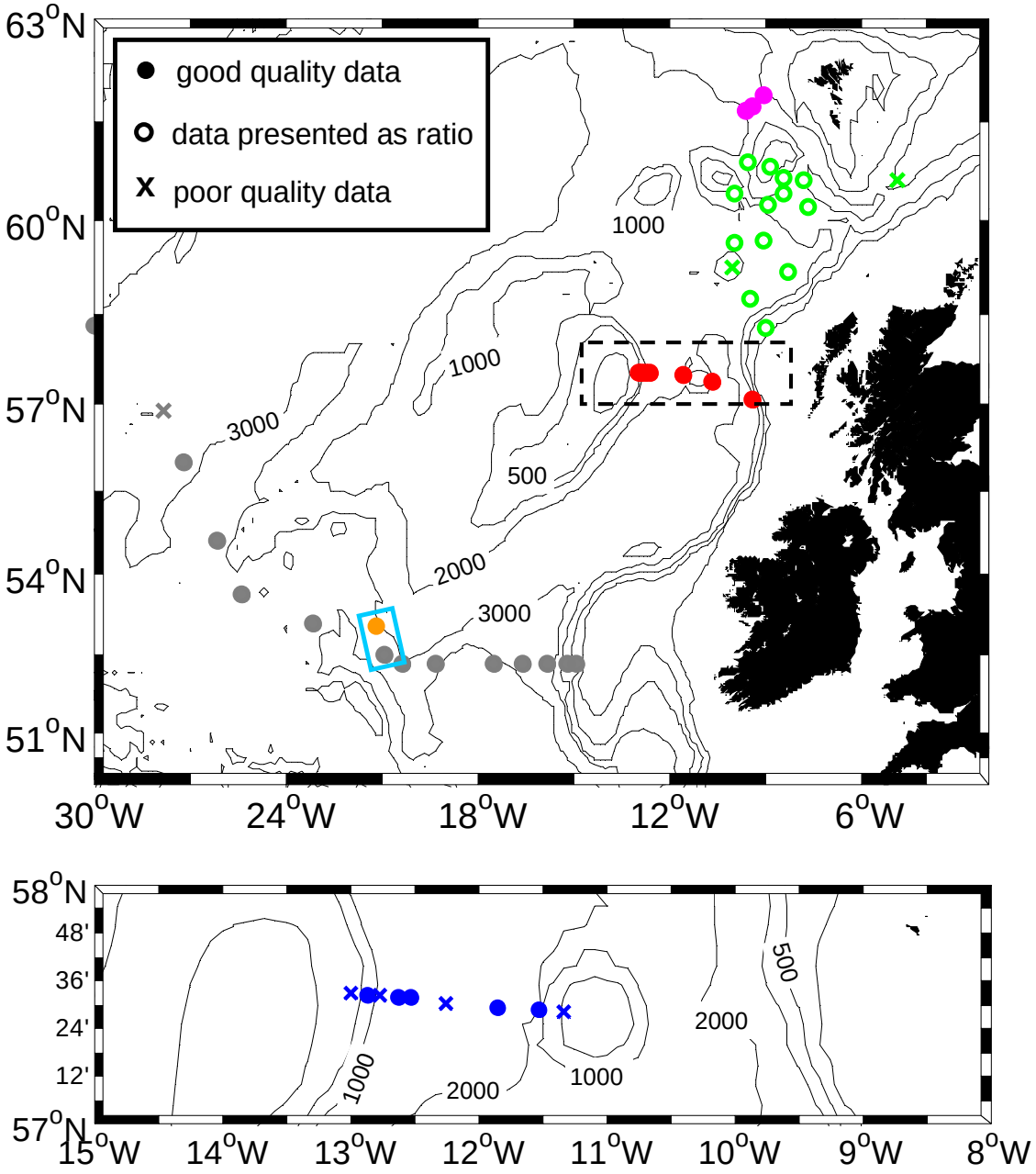

Figure 4.9. Summary of aluminium data used within this thesis collected during: 0804S (green), H44-04-12 (grey), CD176 (red) and D312 (blue). For clarity D312 is show on a separate map (dashed black rectangle shows position within Rockall Trough). Also shown are unpublished data collected by David Hydes (magenta) and a station from Lunel, 1990 (orange) used in a later comparison with data collected during H44-04-12 (cyan rectangle).

Chapter 5.
Physical and chemical signatures of WTOW in the Rockall Trough

This chapter first details the potential temperature (θ) and salinity (S) characteristics of water masses at the northern and southern boundaries of the Rockall Trough, before establishing the physical signature of WTOW in the northern and central areas of the basin. The temporal persistence of WTOW, between 1975 and 2008, in the central trough is evaluated from the Ellett Line time-series and its spatial extent determined using θ-S data from various cruises. This work is published in Johnson et al. (2010). Finally, the chemical signatures (oxygen, nutrient, chlorofluorocarbon and aluminium) of WTOW are discussed.

5.1. Introduction

Potential temperature – salinity (θ-S) diagrams were proposed by Helland-Hansen in 1916. Since then various authors have extended and refined the technique (Tomczak, 1981) establishing θ-S diagrams as an important tool within oceanography. In order to look at θ-S theory, a highly simplified case of three vertically-layered homogeneous bodies of water (X, Y and Z) is examined (Fig. 5.1). When these water bodies are completely unmixed they are represented as three distinct points in θ-S space (Fig. 5.1.a). As waters X and Y, and Y and Z begin to mix; as well as the distinct points X, Y and Z, water also lies along two linear lines X-Y and Y-Z (solid lines, Fig. 5.1.b) known as mixing lines. Waters X and Z are separated in density and physical space by water body Y, hence, θ-S analysis assumes that X and Z cannot mix directly together. As the mixing continues and Y is eroded simultaneously from above and below, eventually no water with the original characteristics of water body Y is left. Hence, although water is still found with θ-S properties of original points X and Z, water lying upon lines X-Y and Y-Z are joined by a curve short of point Y (solid line, Fig. 5.1.c and curve 1, Fig. 5.1.d). As mixing progresses further, θ-S properties begin to lie within mixing triangle X-Y-Z and less and less on mixing lines X-Y and Y-Z (curve 2, Fig. 5.1.d). Eventually, although some unmodified

water at points X and Y remains, no water that is purely a mixture of X and Y, or Y and Z survives and no water lies on lines X-Y or Y-Z (curve 4, Fig. 5.1.d). Finally, water mass theory suggests the water column will mix to such an extent that water body Y is completely eroded and all water lies upon line X-Z (Mamayev, 1975). Thus, use of θ-S diagrams not only allows mixing within the ocean to be qualified but the progress of a water mass to be traced through the ocean until it is lost.

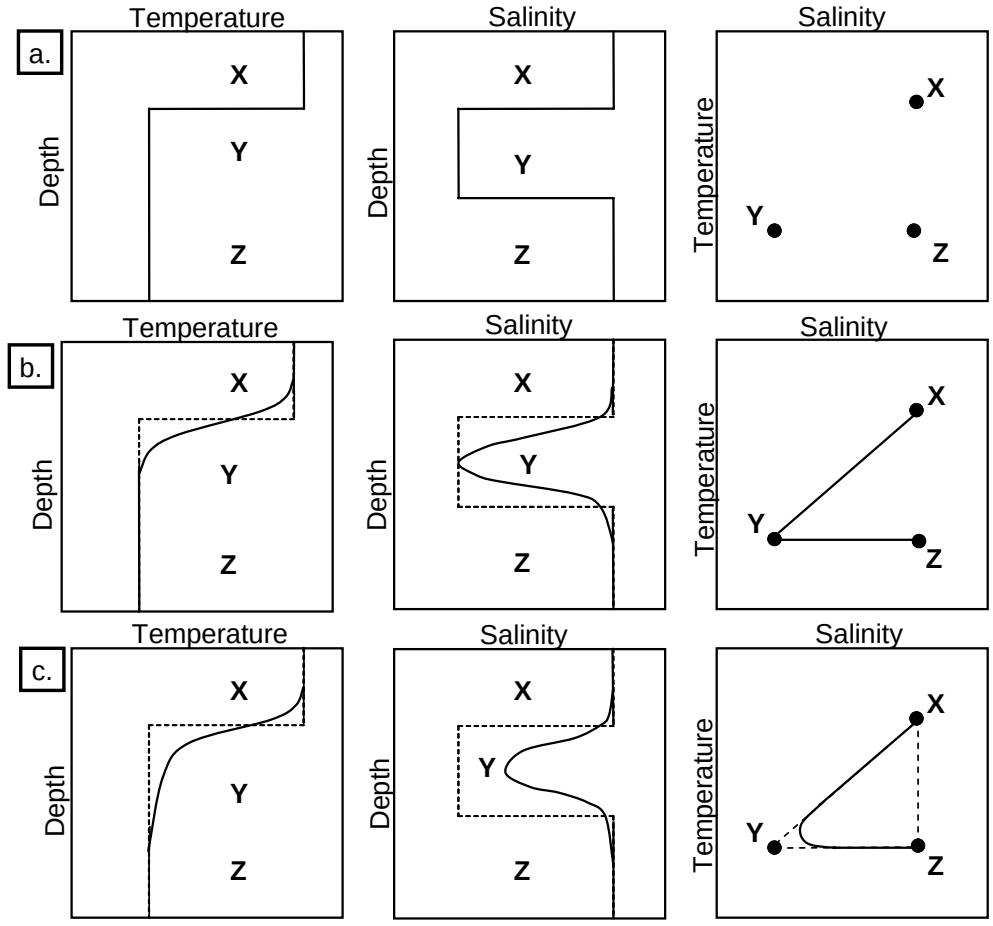

Figure 5.1. Simplified theory of mixing between three water types (X, Y, and X) in θ-S space. a. – c.: from Fig. 5.25, Open University text (2001); d. adapted from Fig. 40, Mamayev (1975). For explanation see text.

In the ocean, bodies of water are usually defined by a range of θ and S characteristics rather than a point in θ-S space; for example, the rectangular definitions of LSW and MOW and linear definitions of ENAW and SAIW (Table 2.1). These classifications allow limited spatial and temporal variability to be accounted for. Despite these wider definitions the theory of mixing lines and mixing triangles still applies.

5.2. Water at the boundaries of the Rockall Trough

5.2.1. Southern boundary

Water at the southern boundary of the Rockall Trough (Line S, Fig. 5.2) contains five water masses that are identifiable in θ-S space (red, Fig. 5.3.a). In the upper ~ 300 m warm and salty water is seen, the saltiest of which is confined to the east indicating NAW carried northwards in the shelf edge current. Over the remainder of the trough the upper waters can be identified as an approximation of the Harvey (1982) definition of ENAW. Below this, to about 1200 m, water falls on one of two distinct curves. Water lying to the east of ~ 16.5 °W trends from upper waters towards MOW which is a particularly salty water mass having a salinity greater than 35.5 in the southern Rockall Trough (Table 2.1). From this intermediate peak in salinity at about 950 m, water properties lie on a linear mixing line towards the cooler and fresher water mass of LSW. The properties of water found in the west of the section, however, trends from the upper waters to the fresher water mass of SAIW. An intermediate salinity minimum is observed at ~ 500 m before water becomes cooler and meets the MOW-LSW mixing line observed in the east, at ~ 900 m (potential density, σ_θ, ~ 27.6 kg m^{-3}). Below this point, water properties in both the east and west of the section trends towards those of LSW and finally AABW.

5.2.2. Northern boundary

Water just to the north of the Wyville-Thomson Ridge crest (line N, Fig. 5.2; black, Fig. 5.3.a), which is the precursor to WTOW, looks very different to that observed at the southern boundary of the Rockall Trough. There is no evidence of MOW, SAIW, LSW or

AABW, with the water column instead being composed of a mixture of the upper waters and the two deep water masses of NSAIW and NSDW. Although MEIW is also transported through the Faroese Channels, it tends to lie north of the central and western ridge (Hansen and Østerhus, 2000) and does not contribute to overflow in this region. An influence of MEIW is observed in the far east of the Wyville Thomson Ridge although overflow in this area is thought to be minimal.

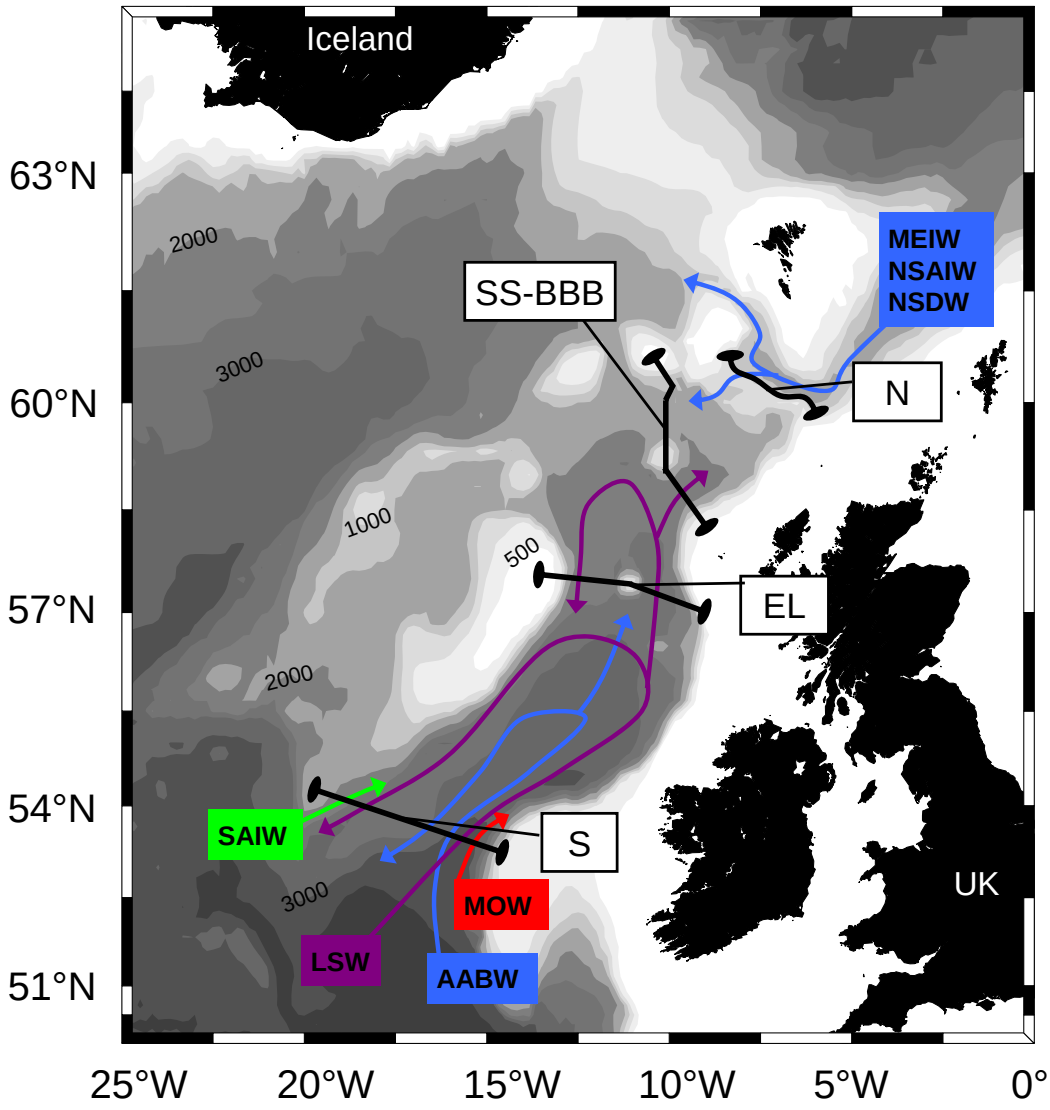

Figure 5.2. Position of CTD lines analysed using θ-S analysis, and intermediate and deep water masses influencing the area. For upper water masses see Fig. 2.3. EL: Ellett Line time-series including D312 occupation; S: southern boundary, K147-2; SS-BBB: Scottish Shelf to Bill Baileys Bank section, 0804S; N: northern boundary, 0804S. See Tables 3.1 and 3.9 for metadata.

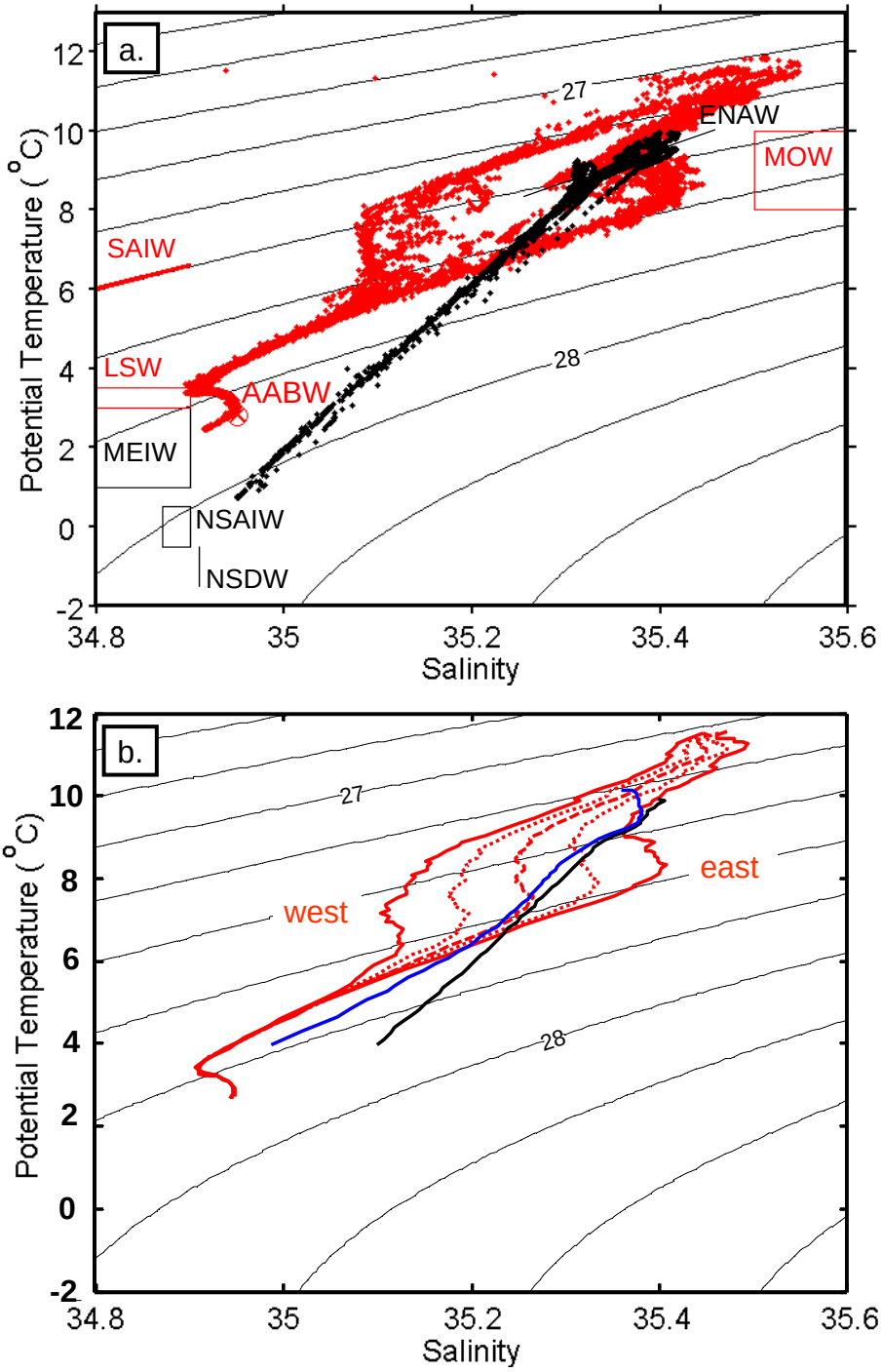

Figure 5.3. θ-S diagram of water: a. from Line S at the southern entrance of the Rockall Trough (red) and Line N on the northern flank of the Wyville Thomson Ridge (black); b. mean profiles from: the east and west of Line S (red solid), entirety of Line N (black solid) and entirety of Line SS-BB (blue solid); and calculated profiles assuming mixing along isopycnals between water from the east and west of Line S (25% east:75% west and 75% east:25% west : red dot; 50% east:50% west : red dash). It is very unlikely that water in the σ_θ = 27.4 – 27.6 kg m^{-3} range along the SS-BB line could be derived from a mixture of the southern water masses. For clarity NAW is not indicated. Isolines show isopycnals, water mass definitions from Table 2.1.

In the following sections, the mixing line between the upper waters, in particular ENAW, and the cold fresh water masses of NSAIW and NSDW is traced southwards into the Rockall Trough. At this point it is important to note that, because of the very similar θ-S signatures of NSAIW and NSDW, it is not possible to establish the individual contributions of these two water masses to WTOW. This is discussed further in section 5.8.

5.3. θ-S signature of WTOW in the northern Rockall Trough

An intensive CTD survey of the northern Rockall Trough conducted during 0804S (see Fig. 3.1 for station locations) provides unambiguous evidence of WTOW in this region. Observations made on a line stretching from the Scottish Shelf over Rosemary Bank to Bill Baileys Bank (SS-BBB, Fig. 5.2) are examined in detail below.

5.3.1. Southeast of Rosemary Bank

In the upper ~ 500 m, warm and saline water approximating to ENAW is observed throughout the section with saltier NAW seen in the slope edge current to the east (black, Fig. 5.4.a). Below this, to around 1150 m, water lies on a very similar mixing line to that found on the northern flank of the Wyville Thomson Ridge (black, Fig. 5.3.b) i.e. that joining ENAW to NSAIW and NSDW. At ~ 1150 m (σ_θ 27.7 kg m^{-3}) a distinct inflexion in θ-S space is observed (black, Fig. 5.4.a). This, and the northern (WTOW) mixing line, are key to recognising WTOW within the intermediate water column as we move further from the ridge. Below the intermediate salinity inflexion water properties move away from the northern mixing line and towards the fresher water mass of LSW. The similarity with the θ-S curve from the southern boundary of the Rockall Trough (red, Fig. 5.3.b) indicates that water at this depth originates from the south. WTOW therefore exists as an intermediate water mass (σ_θ 27.4 – 27.7 kg m^{-3}) sandwiched between water that has entered the trough from the south: ENAW above, and a MOW-LSW mixture and LSW below. Thus, although some previous studies have attributed the intermediate salinity inflexion to MOW

(Ellett and Martin, 1973; Ellett et al., 1986; van Aken and Becker, 1996) it is actually only below the inflexion point that there is any influence of that water mass.

5.3.2. North of Rosemary Bank

To the north of Rosemary Bank, a layer of WTOW can again be seen below the ENAW that fills the upper ~ 500 m (grey, Fig. 5.4.a). Although the intermediate salinity inflexion that indicates the bottom of the intermediate WTOW layer is present, a closer inspection reveals the additional influence of WTOW below this point (Fig. 5.4.b). At stations in the far north of the section (e.g. red, Fig. 5.4.b) water properties lie on the northern mixing line (A, Fig. 5.4.b) between the upper waters and seabed at 1125 m. Hence, the entire water column, below ~ 500 m, is composed of WTOW indicating a coherent body of overflow water hugging the southern flank of Bill Baileys Bank. Further south (e.g. green, Fig. 5.4.b), water properties between 500 m and 1050 m lie on the northern mixing line before bending away at the intermediate inflexion point and starting to trend towards LSW. However, in the deepest 50 m the θ-S deviates away from the southern mixing line (B, Fig. 5.4.b), and back towards the northern mixing line (A, Fig. 5.4.b), indicating the influence of WTOW at the very bottom of the water column. At stations closer to Rosemary Bank (e.g. grey, Fig. 5.4.b), a similar pattern is seen with WTOW again affecting water properties below the intermediate salinity inflexion. Instead of this influence being constrained to the very bottom of the water column, the data is seen to trend from the southern mixing line (B, Fig. 5.4.b) towards that found in the north (A, Fig. 5.4.b) in a series of steps over the deepest 200 m. One possible explanation for this is the influence of a dense component of WTOW that is a residue of a large overflow event across the Wyville Thomson Ridge. Such events can have peak transports of up to 2 Sv that last over several days and draw significant amounts of cold and relatively saline water into the northern Rockall Trough (Sherwin and Turrell, 2005).

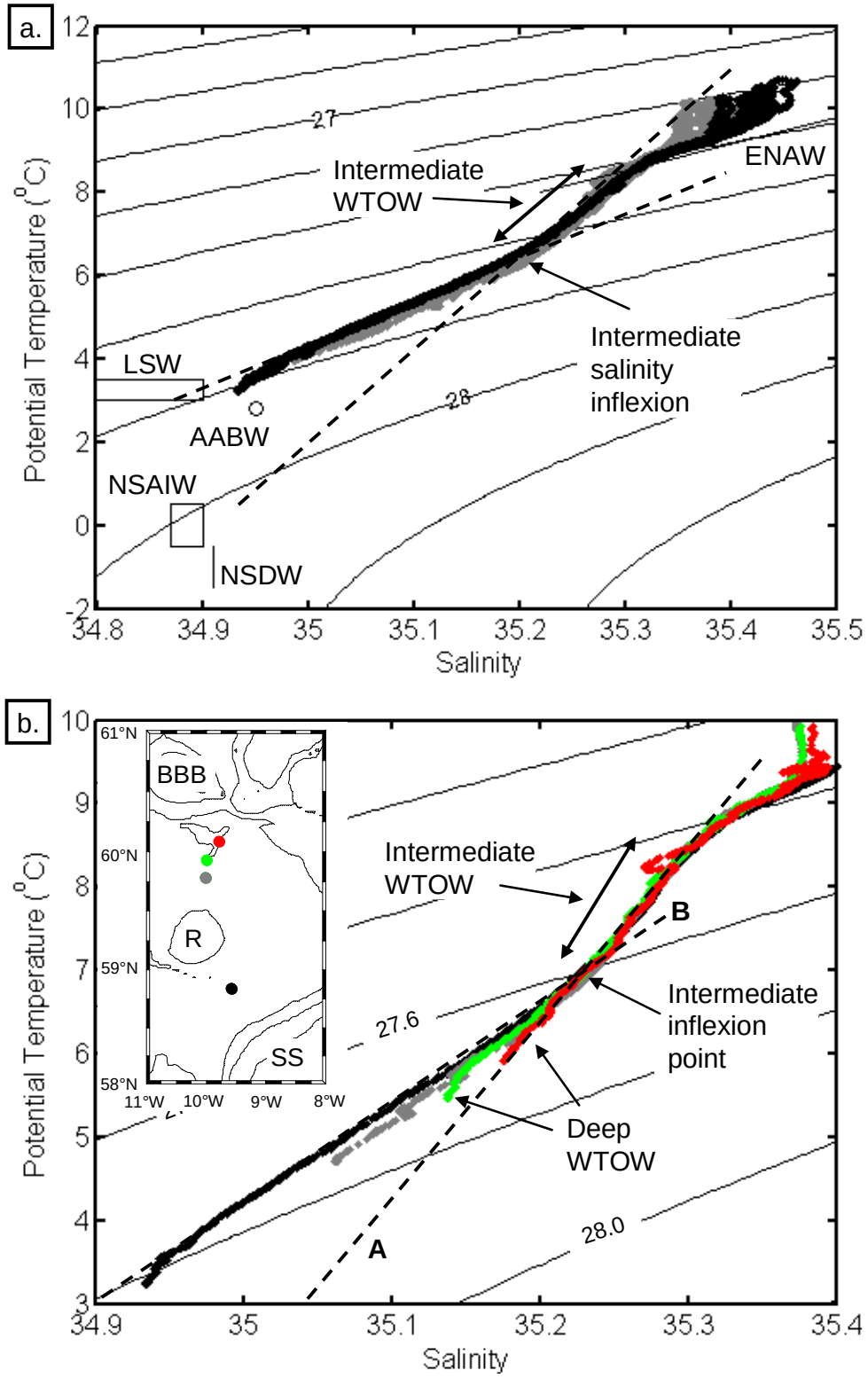

Figure 5.4. θ-S diagrams of water: a. between the Scottish Shelf and Rosemary Bank (black) and Rosemary Bank and Bill Baileys Bank (grey) (Line SS-BBB, Fig. 5.2); b. detail of selected stations between Rosemary Bank and Bill Baileys Bank with a representative station southeast of Rosemary Bank (see insert map for station positions; BBB: Bill Baileys Bank, R: Rosemary Bank, SS: Scottish Shelf). Dashed black lines show the northern (WTOW) mixing line (A) and southern mixing line (B) and were added by hand.

5.3.3. Summary

It is extremely unlikely that water we identify as WTOW, using the northern mixing line, was formed by lateral mixing between the MOW and SAIW seen at the southern entrance to the Rockall Trough. However, as a check mean profiles from the east and west of the section at the southern boundary (Line S, Fig. 5.2) were mixed in fixed proportions along appropriate isopycnals. The resultant θ-S curves (red dotted and dashed lines, Fig. 5.3.b) clearly do not resemble that seen between σ_θ 27.4-27.7 kg m^{-3} in the northern Rockall Trough (blue line, Fig. 5.3.b). For a mixture of MOW and SAIW to form the water we identify as WTOW, they would have to mix in arbitrary proportions along the isopycnal surfaces in order to exactly match the mixing line that is observed to the north of the Wyville Thomson Ridge crest. Such a possibility is so unlikely as to not be credible. It is far more probable that the θ-S plots from the northern Rockall Trough represent water that has entered from the north (i.e. WTOW), sandwiched between water originating from the south, with an additional deeper influence of WTOW in the north of the section.

5.4. θ-S signature of WTOW in the central Rockall Trough

With WTOW clearly established as a water mass in the northern part of the Rockall Trough, we can now investigate whether it reaches as far south as the Anton Dohrn Seamount. This latitude is the location of the Ellett Line time-series (EL, Fig. 5.2; see section 3.3.2) which potentially allows any temporal variability of the WTOW mixing line in this area to be examined. θ-S profiles for all Ellett Line stations showing evidence of WTOW were averaged along isopycnals and standard deviations calculated (Fig. 5.5). The largest variability about the mean is observed between 1975 and 1978 (Fig. 5.5.a) when a *Bissett Berman* STD was in use. A large decrease in the standard deviation is seen post 1992 when a *Sea-Bird* CTD replaced a *Bissett Berman* model used between 1978 and 1992 (Fig. 5.5.b and 5.5.c). In addition to this instrumental variability an element of natural variability is also highly likely to exist. The ratio of NSAIW to NSDW within the Faroese Channels is known to vary as well as the individual characteristics of both water masses

(Turrell et al., 1999; Fogelqvist et al., 2003). Additionally, there are interannual and longer timescale changes within the ENAW (Holliday et al., 2008; Sherwin et al., 2012). Despite these variations the WTOW mixing line and intermediate salinity inflexion remain distinct.

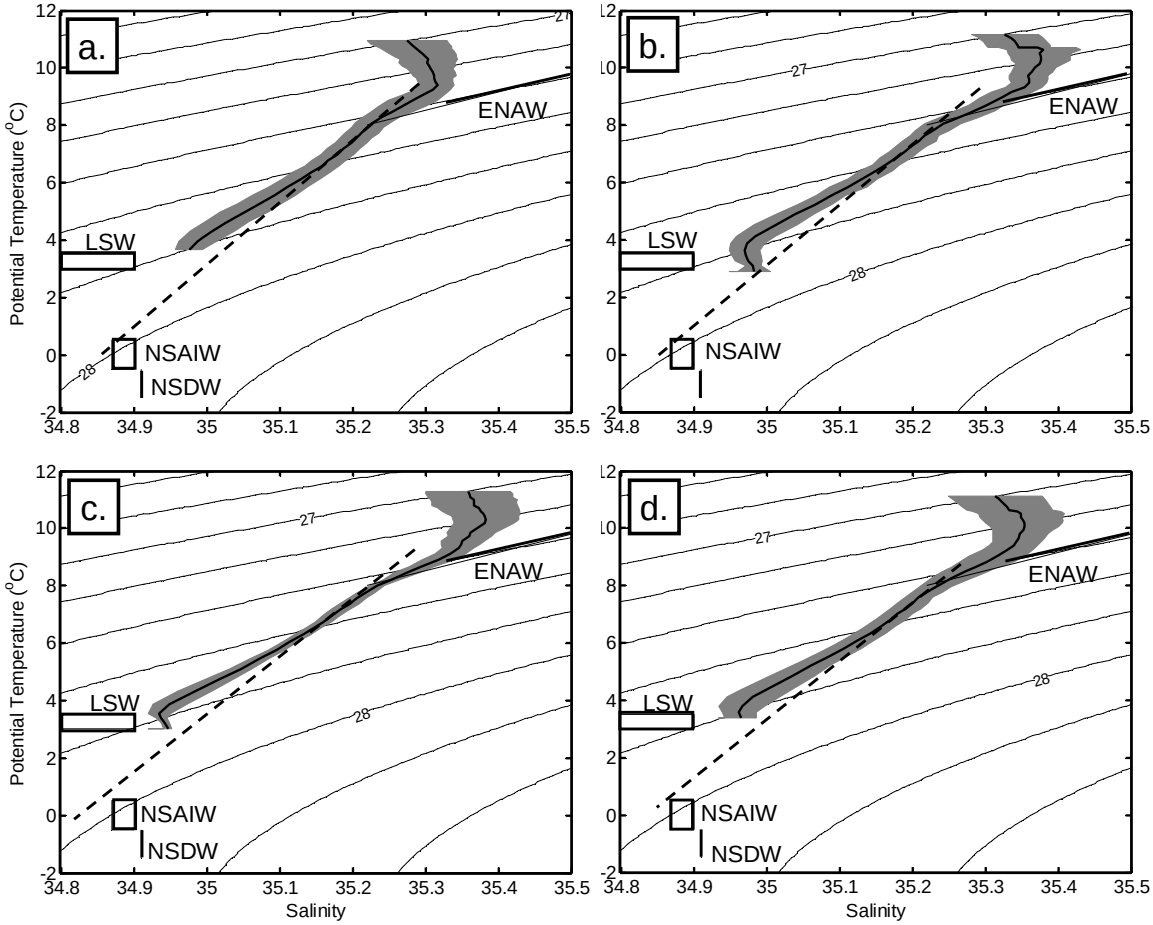

Figure 5.5. Mean θ-S diagram from all Ellett Line (line EL, Fig. 5.2) profiles showing evidence of intermediate WTOW between: a. 1975 and 1978; b. 1978 and 1992; c. 1992 and 2008; d. 1975 and 2008. Grey shading: one standard deviation calculated along isopycnals; dashed line: WTOW mixing line.

In order to carry out a detailed analysis of WTOW in the central Rockall Trough the Ellett Line section occupied in October 2006 (D312) is examined in detail. As well as revealing typical *θ-S* characteristics, the data provides a good illustration of the presence of WTOW in the deep water close to Rockall Bank.

5.4.1. East of Anton Dohrn

In October 2006 there is little spatial variability in water characteristics in the eastern half of the central Rockall Trough (Fig. 5.6.a). In the upper 750 m a warm and salty water mass approximating ENAW is observed. Water between 750 and 1100 m (σ_θ 27.3 – 27.6 kg m^{-3}) once more follows the mixing line first seen on the northern flank of the Wyville Thomson Ridge (black, Fig. 5.3.b) and again in the northern trough (blue, Fig. 5.3.b). Since this water has the characteristic mixture of ENAW, NSAIW and NSDW it is evidently a 400 m thick layer of WTOW. Again there is no direct evidence of MOW or SAIW at this depth. The intermediate salinity inflexion is at a slightly lower density (σ_θ 27.6 kg m^{-3}, 1100 m) than that observed in the northern trough (σ_θ 27.7 kg m^{-3}, 1150 m). Below this point, down to 1800 m, the θ-S profile again trends towards fresher LSW before an influence of AABW is observed. Water denser than the inflexion point again has similar characteristics to those seen at the southern entrance of the trough (red, Fig. 5.3.b) indicating that WTOW is once more sandwiched between water masses entering the trough from the south.

5.4.2. West of Anton Dohrn

By contrast, the θ-S relationship to the west of the Anton Dohrn Seamount is more variable spatially (Fig. 5.6.b). The station immediately to the west of the seamount has comparable features to water in the east, but this similarity decreases towards Rockall Bank.

In general the upper waters (< 700 m) of the western trough are cooler and fresher than those further east which are influenced by NAW and less so by water from the Iceland Basin. Below this, between 700 m and ~ 1150 m, water properties once more lie on the characteristic mixing line seen further north indicating the presence of WTOW. Again an inflexion of the θ-S curve, at the bottom of the intermediate WTOW layer, is observed although this point is slightly denser and deeper (σ_θ 27.7 kg m^{-3}, 1150 m) than that to the east. At the westernmost station (red, Fig. 5.6.b), on the eastern flank of Rockall Bank, there is no evidence of the intermediate salinity inflexion. Instead water below ~ 700 m lies on the WTOW mixing line all the way to the seabed at 1460 m where θ = 4.71 °C, S = 35.09 and σ_θ = 27.8 kg m^{-3}. At the neighbouring station, 6 km to the east (green, Fig.

5.6.b), an intermediate inflexion point is observed at about 1370 m. Water at this point is cooler, fresher and denser than that found in other stations to the east. These observations again suggest a deep coherent body of WTOW hugging the eastern flank of Rockall Bank that is almost certainly flowing southward.

Careful inspection of the *θ-S* profiles also reveals that stations west of the Anton Dohrn Seamount are more saline below the intermediate inflexion point than those in the east of the section (Fig. 5.6.c). Furthermore, the salinity gradually increases towards Rockall Bank. The *θ-S* curve of the station on the western flank of the seamount (blue, Fig. 5.6.c) is almost identical to those seen to the east (black, Fig. 5.6.c), with the exception of water with a higher salinity than AABW in the bottom 100 m (arrows, Fig. 5.6.c). This more saline water is present at other stations in the west (grey curves and arrows, Fig. 5.6.c) and in some other Ellett Line occupations (section 5.5). As was the case north of Rosemary Bank (section 5.3.2), the presence of saline water at depth in the western trough suggests the possible presence of a dense component of WTOW related to a large overflow event.

Figure 5.6 (following page). θ-S diagrams for water along the Ellett Line (57.5 °N) during 2006 (D312): a. east of the Anton Dohrn Seamount; b. west of the Anton Dohrn Seamount (see inset map for station positions; AD: Anton Dohrn, RB: Rockall Bank); c. details of deep water. Black curve in c. is a representative station from a. Dashed black lines show the northern (WTOW) mixing line (A) and southern mixing line (B) and were added by hand.

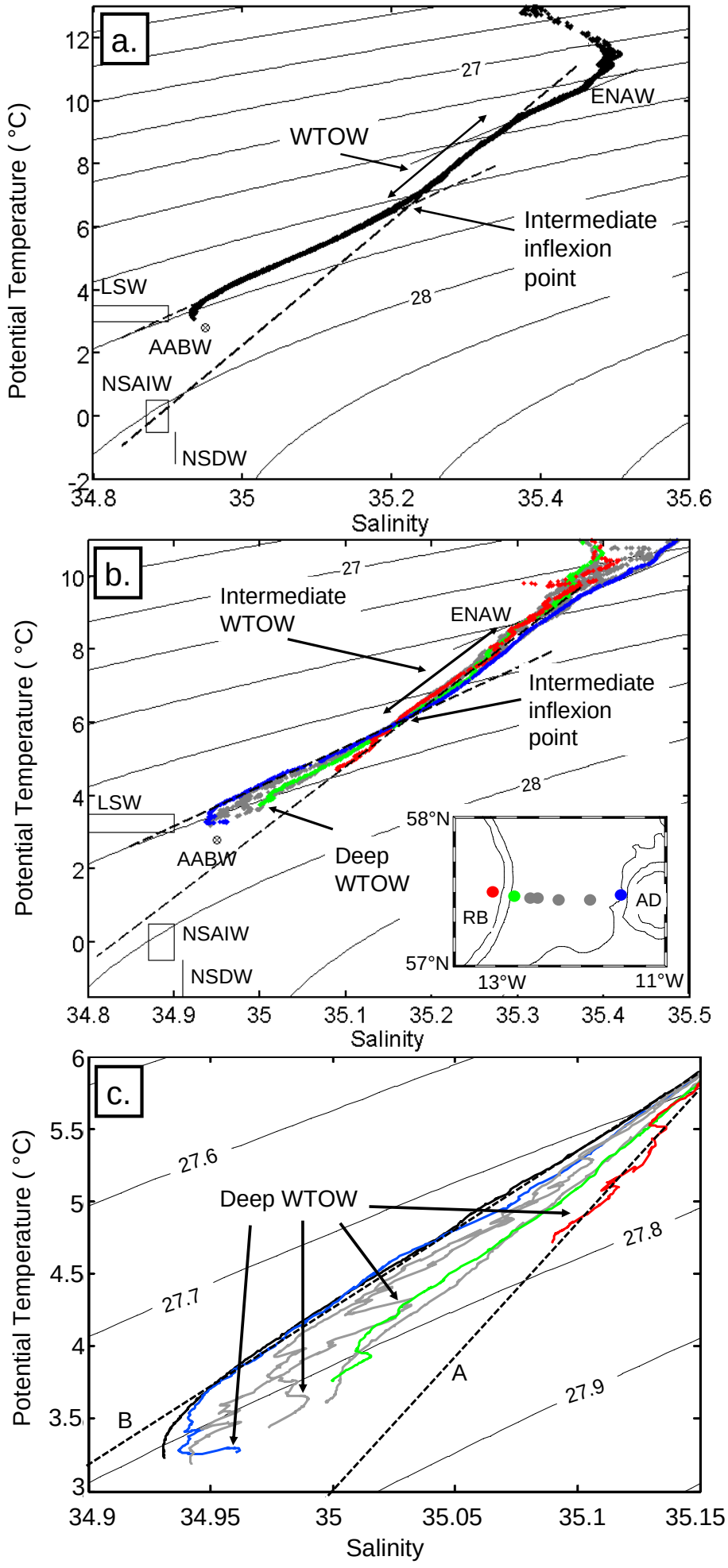
a.
Potential Temperature (°C)
Salinity
27
28
ENAW
WTOW
Intermediate
inflexion
point
LSW
AABW
NSAIW
NSDW
b.
Intermediate
WTOW
ENAW
Intermediate
inflexion
point
Deep
WTOW
58°N
57°N
13°W
11°W
RB
AD
c.
27.6
27.7
27.8
27.9
Deep WTOW
A
B

5.5. Temporal persistence of WTOW determined from *θ-S* data

Before determining the temporal persistence of WTOW using a time-series from the central Rockall Trough, it is useful to estimate the bulk residence time for WTOW in the northern portion of the basin. This calculation provides an indication of the timescale of WTOW flux variability that can be detected in the central Rockall Trough. An approximate residence time (*RT*) can be calculated by dividing the volume of WTOW in the northern Rockall Trough by the flux of WTOW entering the area (equation 5.1).

$$RT = A\,h \,/\, Q \qquad (5.1)$$

where A is the area of the 900 m surface (the average depth of intermediate WTOW) in the Rockall Trough between the ridge and 57.5 °N (1.2×10^{11} m^2); h is the mean thickness of WTOW (400 m); and Q the flux of WTOW over the Wyville Thomson Ridge (0.9 Sv, Sherwin et al., 2008). The estimated RT is ~ 18 months suggesting that most short term (<18 months) variability in overflow rates will go unnoticed at the Ellett Line. Hence the majority of changes in the volume of WTOW observed at intermediate depths at 57.5 °N will be due to events at a longer timescale.

The temporal persistence of WTOW in the central Rockall Trough between 1975 and 2008 (Fig. 5.7) has been determined using data from the Ellett Line time-series (section 3.3.2). For each occupation, separate θ-S diagrams for water east and west of the Anton Dohrn Seamount were produced. Intermediate WTOW was assumed to be present if at least 200 m of water between 600 m and 1200 m lay within a salinity ± 0.02 from the northern mixing line (black, Fig. 5.3.b). Deep WTOW was deemed to occur if saline water, lying between the northern and southern mixing lines (e.g. D312 western Ellett Line, Fig. 5.6.c), was observed below the intermediate inflexion point (σ_θ ~ 27.7 kg m^{-3}) in the western trough only.

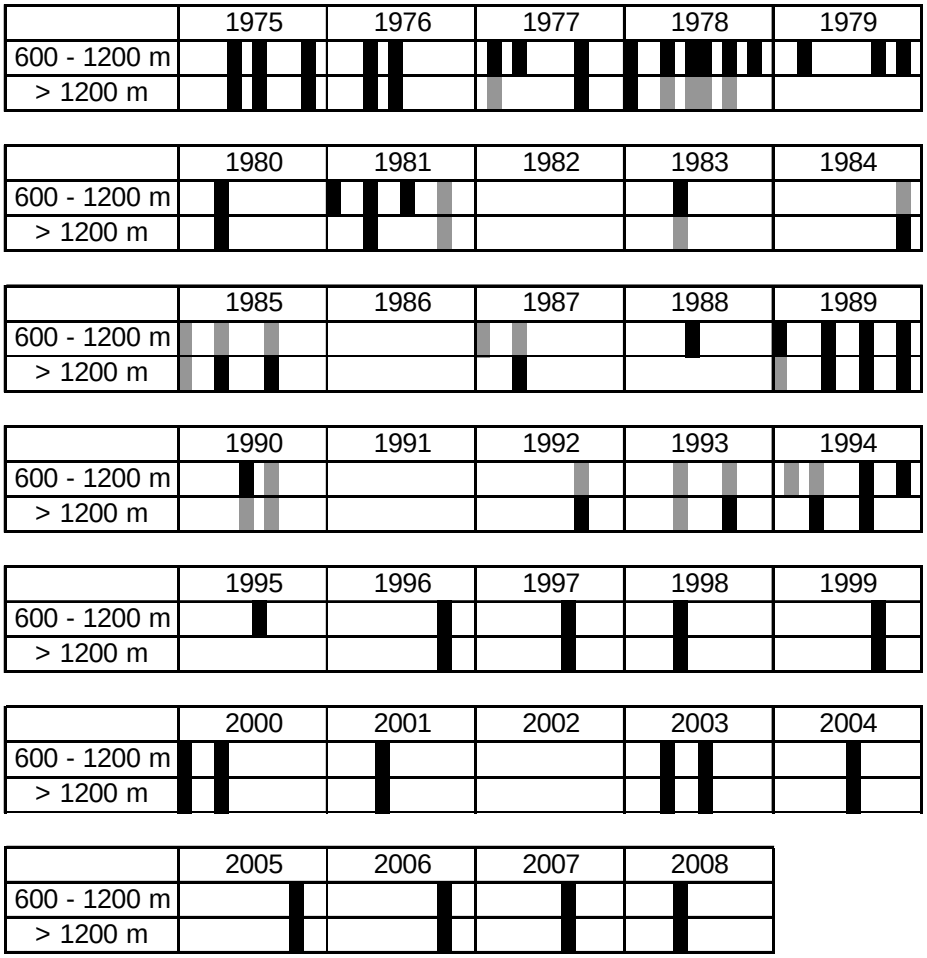

Figure 5.7. Temporal distribution of WTOW (1975 – 2008) at intermediate and deep levels along the Ellett Line (EL, Fig. 5.2) in the Rockall Trough. Grey shading: Ellett Line occupations when no evidence of WTOW at that depth range is observed; black shading: Ellett Line occupations when evidence of WTOW at that particular depth range is seen.

It is clear that at intermediate depths (600 – 1200 m) WTOW is an important water mass in the central Rockall Trough (Fig. 5.7). It is present at a minimum of one occupation per year throughout all but five of the 30 years with usable data, and during 78 % of individual Ellett Line cruises. The signature of intermediate WTOW is absent from the Ellett Line record in the mid 1980s and early 1990s. On these occasions the θ-S curve either lies on a mixing line connecting ENAW directly with LSW (e.g. 1984 to 1987, Fig. 5.8.a), or only a very weak salinity inflexion is present (e.g. mid 1990 – mid 1994, Fig. 5.8.b). An additional feature in the time-series, is the persistence of WTOW at intermediate depths during two periods: between the start of the record and 1981, and after mid 1994 (Fig. 5.7).

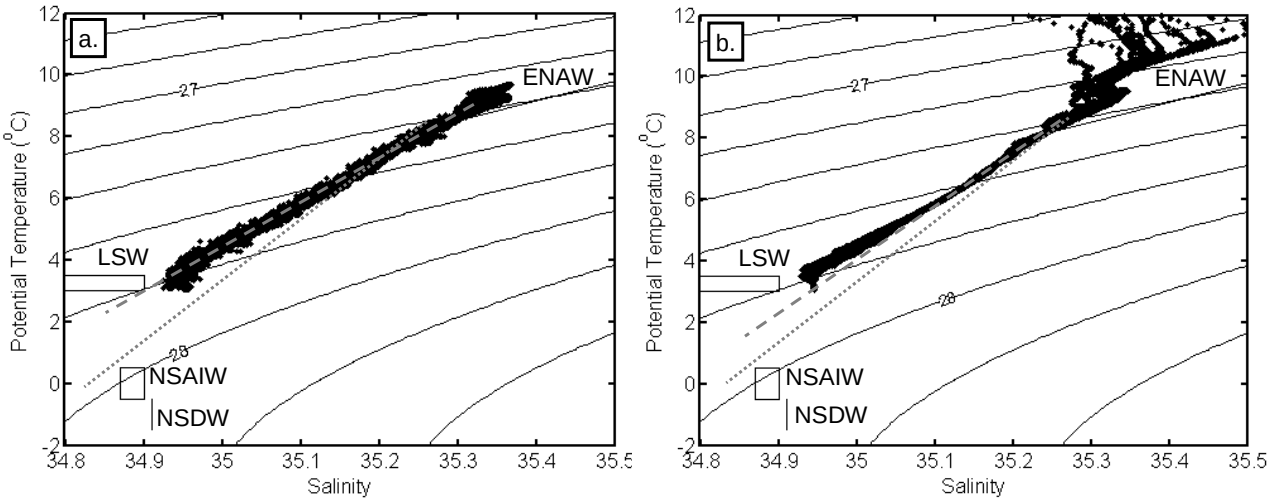

Figure 5.8. Example θ-S profiles from when there is no clear evidence of intermediate WTOW at 57.5 °N in the Rockall Trough. a. C9_87 (January 1987) when water lies on a mixing line linking ENAW with LSW; b. CH105_93 (September 1993) when a weak intermediate salinity inflexion is observed. Grey dashed lines: mixing lines fitted to the data; grey dotted lines: mean WTOW mixing line derived from all Ellett Line sections (see Fig. 5.5.d).

The signature of WTOW below ~ 1200 m appears to have a similar frequency to that of WTOW found at intermediate depths. Deep WTOW is present in a minimum of one cruise per year for all but two out of 27 years with usable data west of the Anton Dohrn Seamount, and in 34 out of 46 cruises (74 %). Especially strong signatures are seen during P300_2 (July 2003) and D312 (October 2006). Two features of particular interest are noted. Firstly, evidence of deep WTOW is observed during the mid 1980s and early 1990s when water properties at intermediate depths do not lie on the northern mixing line or show clear evidence of the intermediate salinity inflexion. This tends to suggest that there may be two separate pathways for WTOW through the Rockall Trough. A non-specific higher branch that results in intermediate water spreading across the section, and a specific lower one, perhaps related to larger overflow events, which allows WTOW to flow against the flanks of the banks that make up the western boundary of the trough. Secondly, at times deep WTOW appears to be consistently present during a number of consecutive cruises, for example during 1975 to 1976. This is particularly true in the later half of the record when the signature of deep WTOW is seen in every Ellett Line occupation after, and including, September 1993 (CH105).

5.6. Spatial distribution of WTOW over a wider area determined from *θ-S* data

Data presented so far suggests that water we identify as WTOW in the northern and central Rockall Trough is extremely unlikely to originate from the south, with *θ-S* evidence consistent with the well documented flow over the Wyville Thomson Ridge. Deep WTOW, below ~ 1200 m, is confined to the western half of the trough (sections 5.3 and 5.4) with no evidence of the water mass observed to the east. As the maximum depth between the northern banks of the Rockall Trough is just below 1200 m, it seems unlikely that much deep WTOW can pass through these channels into the Iceland Basin. Indeed no evidence of this water mass is observed in *θ-S* diagrams from these areas suggesting that the majority of deep WTOW must flow southward through the Rockall Trough. The spatial distribution of intermediate WTOW is more intriguing, with overflow water between 600-1200 m being found in both the east and west of the northern and central Rockall Trough. To investigate the spatial distribution of WTOW at intermediate depths further, around 400 CTD stations from 11 cruises between 1996 and 2007 (Table 3.9 and Fig. 3.6) were compiled. Ideally one would use data collected within a smaller timeframe, although this would limit the spatial extent of the analysis. Additionally, the temporal persistence of intermediate WTOW, particularly after 1994 (Fig. 5.7), and the fact that little variability is observed in the water mass after 1992 (Fig. 5.5.c), suggests that using data compiled from 1996 to 2007 is appropriate.

For each station a *θ-S* diagram was produced and examined for the presence or absence of intermediate WTOW using the same identification criteria as in the northern and central trough (sections 5.3 and 5.4). An additional category for stations that show some, but not clear, evidence of WTOW was added. These stations include those where there are signs of an intermediate inflexion point but the mixing line trends to a point warmer than NSAIW or NSDW (e.g. v, Fig. 5.9.b), and those that show evidence of WTOW but also of MOW and/or SAIW (e.g. ii, Fig. 5.9.b). Water properties at stations where *θ-S* plots show no direct evidence of intermediate WTOW, either lie on a mixing line joining the upper waters with LSW (e.g. vi, Fig. 5.9.b), or show heavy influences of MOW and SAIW (e.g. in the southern Rockall Trough, red, Fig. 5.3.a). A sense of the movement of WTOW away from the ridge can be inferred from the intensity of the inflexion point which is gradually eroded by mixing (see Fig. 5.1.d for theory).

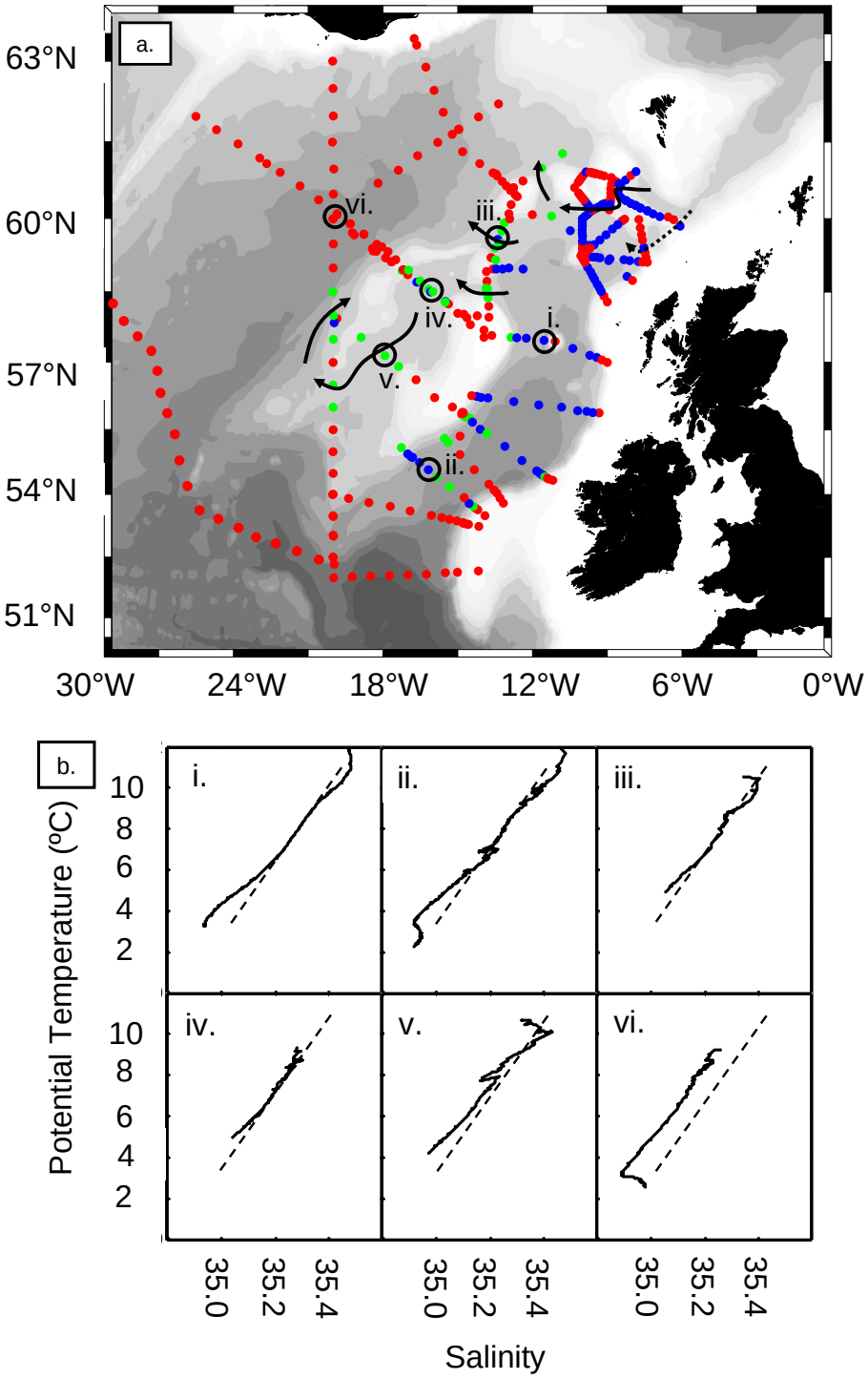

Fig. 5.9. a. Spatial distribution of intermediate WTOW in the Rockall Trough for the years 1996 – 2007. Red dots: no evidence of WTOW (sometimes because of shallow water); blue dots: distinct evidence for the presence of WTOW; green dots: some evidence of WTOW. Arrows show circulation pathways inferred from intensity of the inflexion point. It should be noted that because of possible recirculations these arrows do not necessarily represent a net flux. Black circles and numbers show location of stations in b. b. Selected θ-S diagrams from the study areas. Dashed lines show mean WTOW mixing line (see Fig. 5.5.d).

These observations again indicate that WTOW spreads away from the Wyville Thomson Ridge into the northern, central and southern Rockall Trough, and further, that the Anton Dohrn Seamount is not a significant barrier (Fig. 5.9.a). At intermediate depths there appears to be no difference in distribution between the eastern and western trough. A clear signature of WTOW can be traced southwards to ~ 55 °N in the Rockall Trough and in some years to ~ 54 °N. Intermediate WTOW in the north-western trough flows westward between various banks towards the Iceland Basin, with the exception of the channel between Bill Baileys and Faroe Bank which at < 600 m is too shallow. However, there is insufficient data to say whether this WTOW enters the Iceland Basin proper or recirculates around the bank and re-enters the Rockall Trough. The shallow nature of the channel between Bill Baileys Bank and Faroe Bank, however, suggests that WTOW cannot re-enter the trough via this route. Hence, it appears that at least the WTOW that exits the Rockall Trough between Bill Baileys Bank and Faroe Bank represents a net flux into the Iceland Basin. WTOW at intermediate depths is also observed between George Bligh Bank and Rockall Bank, and on the Rockall-Hatton Plateau. As the intermediate inflexion point is less pronounced in the south of the plateau (v, Fig. 5.9.b) compared to the north (iv, Fig. 5.9.b), it appears that the flow direction is from the trough onto the Rockall-Hatton Plateau. Despite the clear evidence that WTOW moves from the trough towards the west, the θ-S signature can only be traced as far as 20 °W to the west of the Hatton Plateau. It is likely that this disappearance is due to erosion of the WTOW signature through mixing with adjacent water masses that have similar θ-S characteristics.

5.7. Dissolved oxygen and nutrient signature of WTOW

Although oxygen and nutrients are non-conservative tracers valuable information about WTOW in the Rockall Trough can still be gleaned. Data from the D312 (2006) Ellett Line (EL, Fig. 5.2) are again presented. This line allows the common features of intermediate WTOW to be investigated as well as the signature of a particularly strong overflow in the western trough.

A prominent feature in the basin is a layer of water with lower dissolved oxygen levels (range 230 - 235 μmol kg^{-1}) lying between approximately 800 and 1200 m (Fig. 5.10.a).

This layer is not only seen at the Ellett Line latitude but also in the northern and southern Rockall Trough, and Iceland Basin (e.g. Tsuchiya et al., 1992; Read, 2001). It is not, however, observed on the northern flank of the Wyville Thomson Ridge. Although some studies have suggested that the lower oxygen concentrations are the result of the presence of an additional water mass (Tsuchiya et al., 1992; van Aken and Becker, 1996), others have shown that an *in situ* biogeochemical origin is more probable (Stoll et al., 1996; de Boer, 1998). Indeed the presence of a biochemically formed lower oxygen layer at around 1000 m worldwide is a well-documented feature (e.g. Wyrtki, 1962; Libes, 1992; Chester, 2000) (see section 2.3 for more detail). Similarly to the globally-observed phenomenon, the layer in the Rockall Trough is only identifiable by its lower dissolved oxygen concentrations (and to a lesser extent by higher nutrient concentrations) and no signature is observed in the conservative parameters of θ, S, CFC-11 or CFC-12. As such, we also conclude that the layer is formed *in situ* by biochemical processes rather than indicating the presence of an additional, unaccounted for water mass that is advected into the trough.

This lower oxygen layer, whilst likely to mask any dissolved oxygen signature of intermediate WTOW, also suggests the absence of strong circulation and replenishment of water at these depths. The exception to this are the five westernmost stations where the lower oxygen layer is less pronounced and higher concentrations of ~ 240 μmol kg^{-1} are observed (Fig. 5.10.a). Although this difference between the westernmost stations and those further east is close to the error associated with the method (± 8 μmol kg^{-1}; Stinchcombe, 2007; p. 90), the consistency of the enhanced oxygen signature across the five westernmost stations suggests that the signal is not an instrumental artefact. Additionally, the lower oxygen layer is thinnest at the three stations adjacent to Rockall Bank (~ 300 m compared to ~ 500 m further to the east). One possible explanation is the presence of an oxygenated flow of WTOW down the western trough that is eroding the lower oxygen layer in the area. This seems particularly plausible as a strong clear signature of WTOW is also seen in θ-S space during the D312 occupation (section 5.4.2). Unfortunately, the historical record of dissolved oxygen across the Ellett Line is patchy with data either not being readily available or of a poor quality. However, a similar, albeit less pronounced, reduction in the intensity of the lower oxygen layer in the far west of the section, is seen in three out of the five cruises between 1996 and 2009 which have good quality data. As θ-S plots of these cruises suggest a less intense overflow event in the western trough than observed during D312, it is expected that erosion of the lower oxygen

layer will be less marked. Hence, although the majority of intermediate WTOW in the Rockall Trough has no discernible dissolved oxygen signature, it appears, that at times, a flow of WTOW down the western boundary of the trough can be distinguished by erosion of the lower oxygen layer in that area.

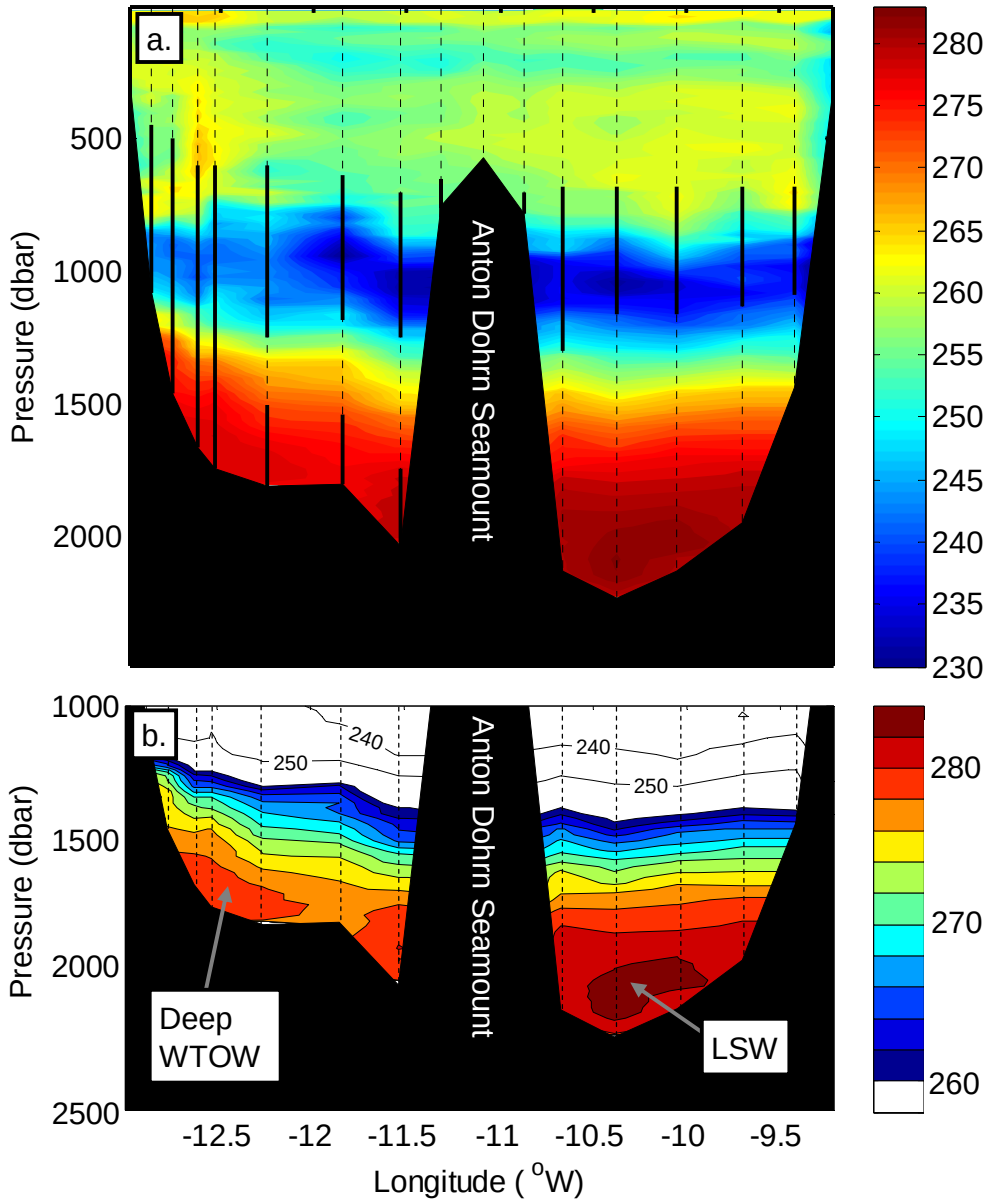

Figure 5.10. Dissolved oxygen distribution (µmol kg^{-1}) in the central Rockall Trough (D312 Ellett Line, see Fig. 5.2 for position). a. Dashed lines: station positions; solid lines: depths showing evidence of WTOW in θ-S plots; b. Detail of water below 1000 m. Please note the different scale and fact that water with an oxygen concentration of < 260 µmol kg^{-1} is uncoloured. Errors associated with the method are around ± 8 µmol kg^{-1} (Stinchcombe, 2007; p. 90).

Below the lower oxygen layer, lines of equal oxygen concentrations slope upwards towards Rockall Bank (Fig. 5.10.b). For example, the 276 μmol kg^{-1} contour rises from ~ 1700 m on the western flank of the Anton Dohrn Seamount to ~ 1400 m on the eastern flank of Rockall Bank. Additionally, water with a higher dissolved oxygen concentration (278-280 μmol kg^{-1}) can clearly be seen hugging the lower flank of Rockall Bank (labelled 'Deep WTOW', Fig. 5.10.b). Therefore, during a pronounced overflow event, such as that seen during the D312 Ellett Line, deep WTOW may be identified by the presence of water with a higher oxygen concentration below ~ 1200 m in the western trough.

The interpretation of nitrate, phosphate and silicate distributions in the Rockall Trough are also, to a lesser extent, complicated by the presence of the lower oxygen layer due to the approximately concurrent increase in nutrient concentrations. As phosphate and silicate levels vary little between different intermediate water masses within the trough (Table 2.1), these two parameters are not good tracers of WTOW. Nitrate concentrations, however, are ~ 3 μmol kg^{-1} lower in ENAW, NSAIW and NSDW than the surrounding water masses of MOW and LSW (Table 2.1), suggesting that this variable may be useful in the identification of WTOW. To investigate this data from the D312 Ellett Line are again presented.

Nitrate concentrations increase from the low values observed in the upper waters to a maximum approximately concomitant with the minimum in dissolved oxygen concentrations (Fig. 5.11). Nitrate levels in the lower oxygen layer are 1.5 – 2.0 μmol kg^{-1} (precision of method ± 0.7 %, section 3.4) higher east of the Anton Dohrn Seamount (red, Fig. 5.11) than in the western trough (blue and green, Fig. 5.11). Hence, although the lower oxygen layer and associated increase in nutrient concentrations mask the nitrate signature of intermediate WTOW, it appears that the influence of a stronger flow of WTOW down the western trough can still be observed. Below the lower oxygen layer, nitrate concentrations at the majority of stations remain nearly constant or decrease slightly as the curve tends towards LSW, before levels again rise in the bottom water due to the presence of AABW. The exception to this is the four stations in the far west of the section (blue, Fig. 5.11). Here, nitrate levels lie on a mixing line (A, Fig. 5.11) between the mid-depth nitrate peak in the lower oxygen layer, and the lower concentrations observed in the cold water masses of NSAIW and NSDW. Water at these depths (1100-1350 m) can therefore again be identified as deep WTOW. It should be noted, that because NSAIW and

NSDW have very similar nitrate concentrations, it is not possible to distinguish the relative contribution of these two water masses to WTOW. At a salinity of ~ 35.1 (~ 1350 m), an inflexion in S-NO_3 space is observed in the four westernmost stations (blue, Fig. 5.11). Here the data trends from the mixing line linking the intermediate NO_3 maximum and the cold northern water masses (A, Fig. 5.11), towards LSW along mixing line B (Fig. 5.11). However, nitrate concentrations from the deepest samples at these stations remain 1-2 μmol kg^{-1} lower than observed in LSW at stations to the east. Although this may be partly explained by the shallower bathymetry near Rockall Bank, the effect is still observed at the deepest station in the far west which has a comparable depth to others west of the Anton Dohrn Seamount. Thus, these lower nitrate concentrations in the far west of the section again suggest the influence of NSDW and / or NSAIW and that water is a mixture of WTOW and LSW. Consequently, it appears that when there is a particularly strong flow of deep WTOW in the western trough, this water may be detected by lower nitrate concentrations than water at a similar depth further east.

5.8. Chlorofluorocarbon signature of WTOW

The chlorofluorocarbons of CFC-11 and CFC-12 are both conservative tracers within the subpolar North Atlantic and are, thus, not affected by biochemical processes (section 2.7). The highest concentrations of both parameters are observed in the upper waters (i, Fig. 5.12) reflecting their atmospheric input. Levels of CFC-11 and CFC-12 are 3.4-3.9 pmol kg^{-1} and 1.7-2.0 pmol kg^{-1} respectively in this layer. Concentrations decrease with depth with the lowest values (CFC-11 < 1.7 pmol kg^{-1}, CFC-12 < 0.8 pmol kg^{-1}) found in AABW (iv, Fig. 5.12) which has been isolated from the atmosphere for a considerable period.

The values of potential temperature, salinity, dissolved oxygen, nitrate, phosphate and silicate are very similar in both NSAIW and NSDW (Table 2.1). Hence, using these parameters alone it is impossible to distinguish the relative importance of these two water masses to WTOW. The concentrations of CFC-11 and CFC-12, however, are much higher in NSAIW than NSDW (Table 2.1). As such, CFC data can be used to differentiate between NSAIW and NSDW and therefore provide important information not available from other sources. Concentrations of both CFC-11 and CFC-12 decrease quickly with

depth within the intermediate WTOW layer (ii, Fig. 5.12). Mixing lines (thick solid lines, Fig. 5.12) show approximate linear mixing between the upper waters and NSDW with no evidence of water properties tending towards the higher CFC concentrations observed in NSAIW. Thus, it appears that WTOW, during D230 (1997) at least, is composed primarily of NSDW and upper waters and that NSAIW is not an important contributor. Data collected during D233 (1998), the only other year with good quality CFC data, reveals identical results.

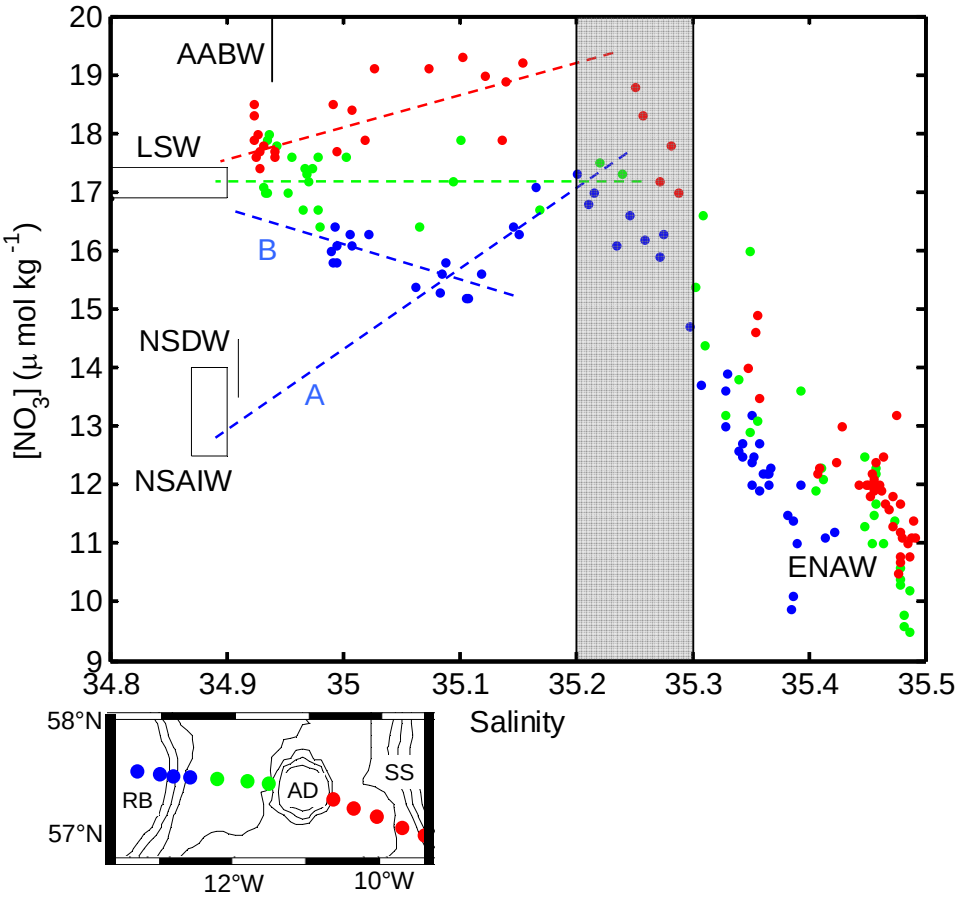

Figure 5.11. Nitrate - salinity diagram for water at all depths along the Ellett Line (EL, Fig. 5.2) during D312. For station locations see insert map; AD: Anton Dohrn Seamount, RB: Rockall Bank, SS: Scottish Shelf. Grey shading: position of minimum dissolved oxygen concentrations. Dashed lines: mixing lines; A: mixing line indicating presence of deep WTOW; and B: mixing line indicating water that is a mixture of deep WTOW and LSW. The instrumental precision associated with NO_3 measurements is ± 0.7 % (section 3.4).

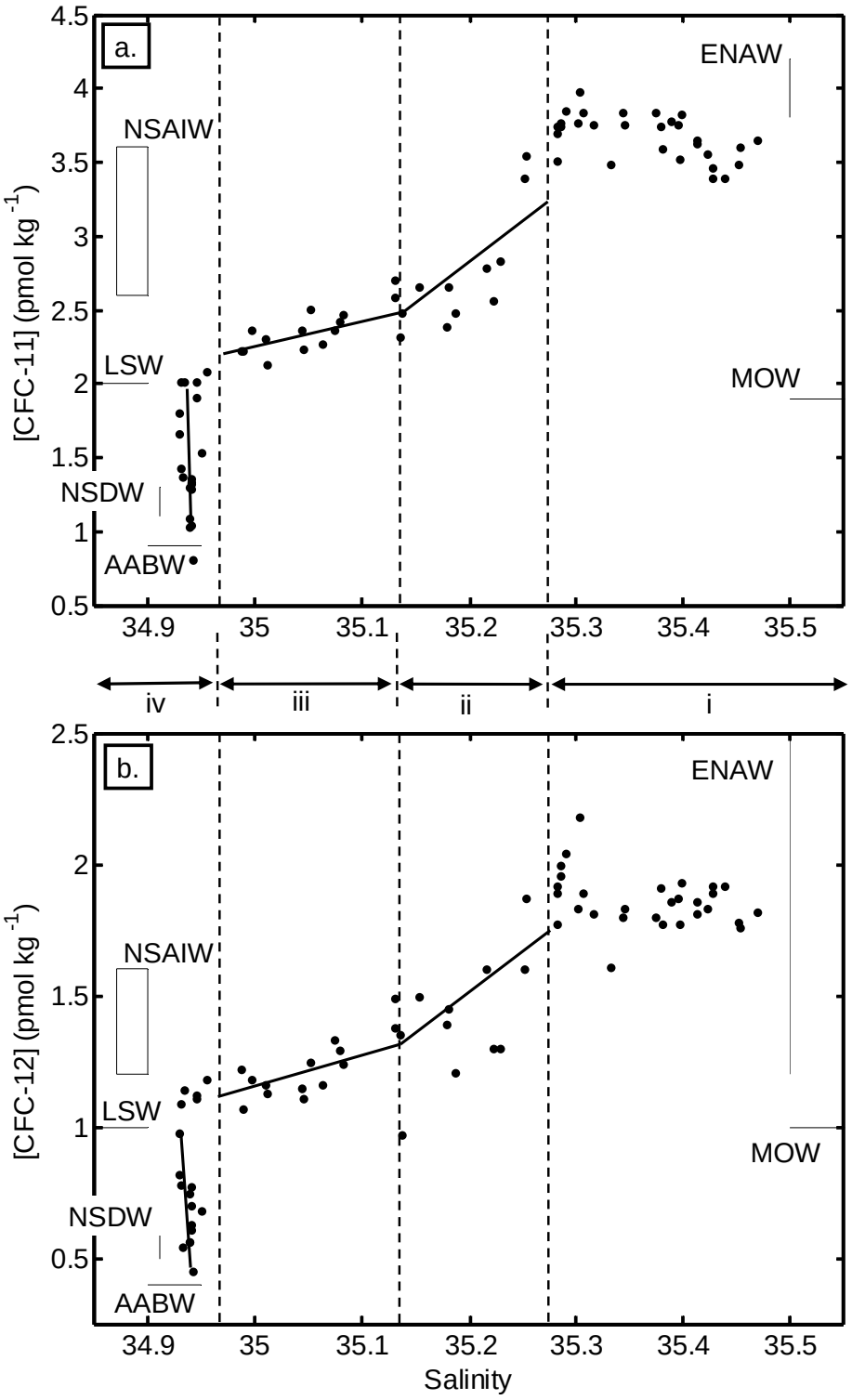

Figure 5.12. CFC – salinity plots from the D230 Ellett Line (EL, Fig. 5.2): a. CFC-11 and b. CFC-12. Dashed lines: boundaries between water masses derived from θ-S diagrams, i: upper waters, ii: intermediate WTOW, iii: water lying on MOW-LSW mixing line, iv: LSW and AABW. Solid lines: mixing lines. Precision of the method is ± 1 % (section 3.3.3).

Below intermediate WTOW, CFC concentrations continue to decrease with depth, although at a slower rate, throughout the MOW-LSW layer (iii, Fig. 5.12). Mixing lines (thick solid lines, Fig. 5.12) show that water properties at these depths are tending towards LSW, where CFC-11 and CFC-12 concentrations of ~ 2.0 pmol kg^{1} and ~ 1.1 pmol kg^{-1} respectively are observed (iv, Fig. 5.12). Below LSW, values decrease rapidly as AABW begins to influence the water column. Although deep WTOW is observed during D230 and D233, there is not a particularly strong signal at this time with the influence of the water mass only seen at one CFC station per cruise. Unfortunately, the data for this station during D233 is of poor quality and during D230 only two samples were collected within the water mass. As such, there is insufficient data to evaluate the CFC signature of deep WTOW at this time.

5.9. Aluminium signature of WTOW

The use of aluminium (Al) as a water mass tracer is relatively novel (section 2.8) and this section reports the first Al measurements made in the Rockall Trough. Al concentrations vary between water masses and the distribution within the water column appears to be predominantly controlled by advection. The exception to this is in the bottom sample at some stations (e.g. black circles, Fig. 5.13.b) where Al values are elevated, possibly as the result of sediment resuspension.

At the southern entrance to the Rockall Trough (see Fig. 3.2 for station locations) low concentrations (3-5 nM) are observed in the upper water mass approximating to ENAW (Fig. 5.13). Below this point at intermediate depths, the Al distribution varies depending on whether SAIW (black, Fig. 5.13) or MOW (red, Fig. 5.13) dominates the water column. Al concentrations in SAIW are again low (~ 2 nM) whilst values in MOW are high (~ 19 nM) producing a large zonal gradient in Al (total errors associated with the method ± 10 %, Table 4.3). Concentrations remain low in LSW (3-7 nM) before increasing to 10-17 nM within the deep water mass of AABW.

Al distributions at the northern boundary to the Rockall Trough (Fig. 5.14; see Fig. 3.1 for station locations) look very different to their southern counterparts as expected due to the

disparity in θ-S space (Fig. 5.3.a). Concentrations are again low in upper waters before increasing, approximately linearly, with depth to a salinity of around 34.90. Unfortunately due to calibration problems during 0804S (section 4.4), data collected from the northern flank of the Wyville-Thomson Ridge during this cruise cannot be expressed as absolute concentrations. To overcome this problem an Al ratio was calculated relative to values measured at 200 m depth. This depth was chosen as it is within the upper waters where Al concentrations appear to remain approximately constant spatially and temporally. Additionally, it is away from atmospheric or sedimentological inputs. If, at a particular station, a sample was not collected at 200 m, an approximate value was obtained using linear interpolation between the nearest measurements above and below this depth. Al ratios from the northern flank of the ridge (red, Fig. 5.14.a) compare well to ratios determined from data collected from the exit of the Faroe Bank Channel (black, Fig. 5.14; D. Hydes, unpublished), which in turn match well with published profiles (Hall and Measures, 1998). As such, it is assumed that the Al concentrations measured in NSAIW and NSDW from the Faroe Bank Channel (black, Fig. 5.14.b) are representative of concentrations found at the northern boundary to the Rockall Trough. Values in NSAIW and NSDW are both high at 16-18 nM and 18-25 nM respectively (total errors ± 10 %).

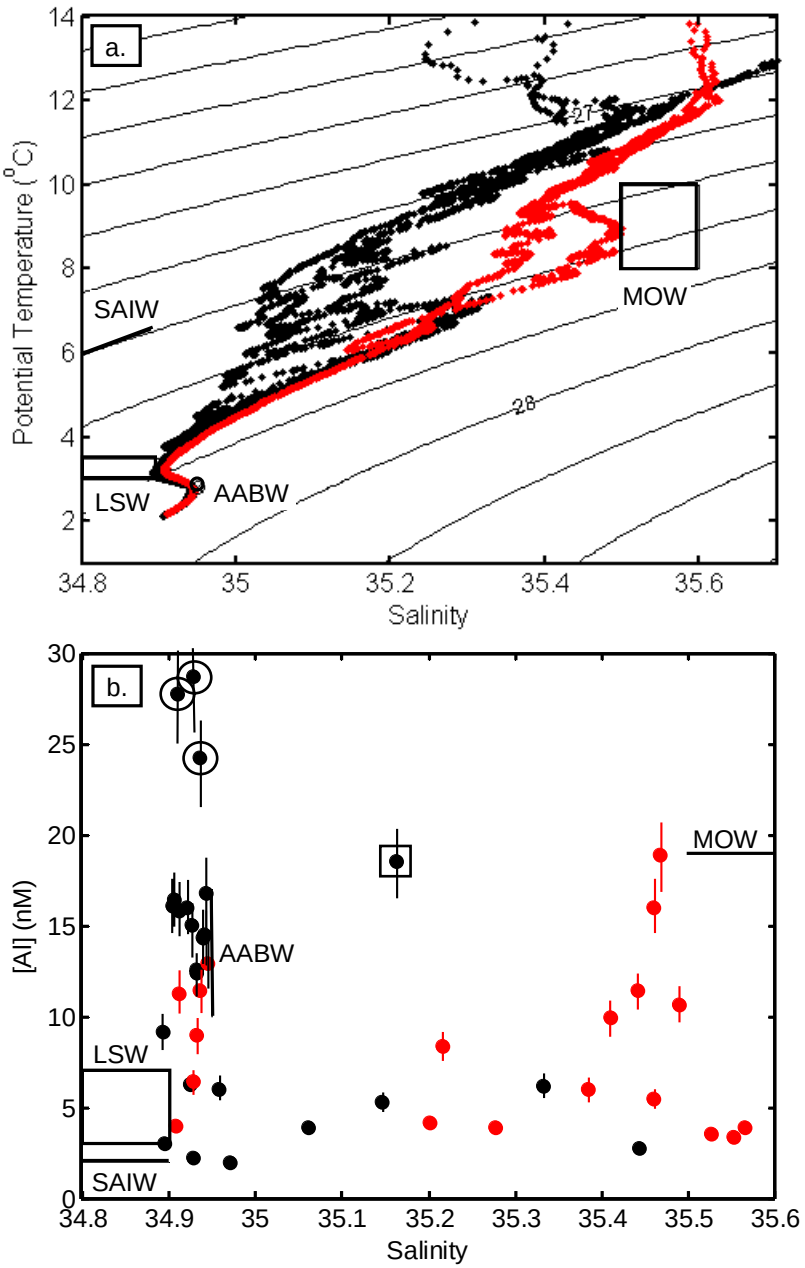

Figure 5.13. a. Potential temperature – salinity diagram, and b. Salinity – aluminium diagram, at the southern entrance to the Rockall Trough (H44-04-12, see Fig. 3.2 for station positions). Black: stations to the west of 18 °W where SAIW dominates; red: stations to the east of 18 °W where MOW dominates; Black circles: samples with elevated [Al] in bottom samples; Black square: sample in the west of the section but influenced by MOW. Error bars show total errors associated with the method (section 4.2.8 and Table 4.3).

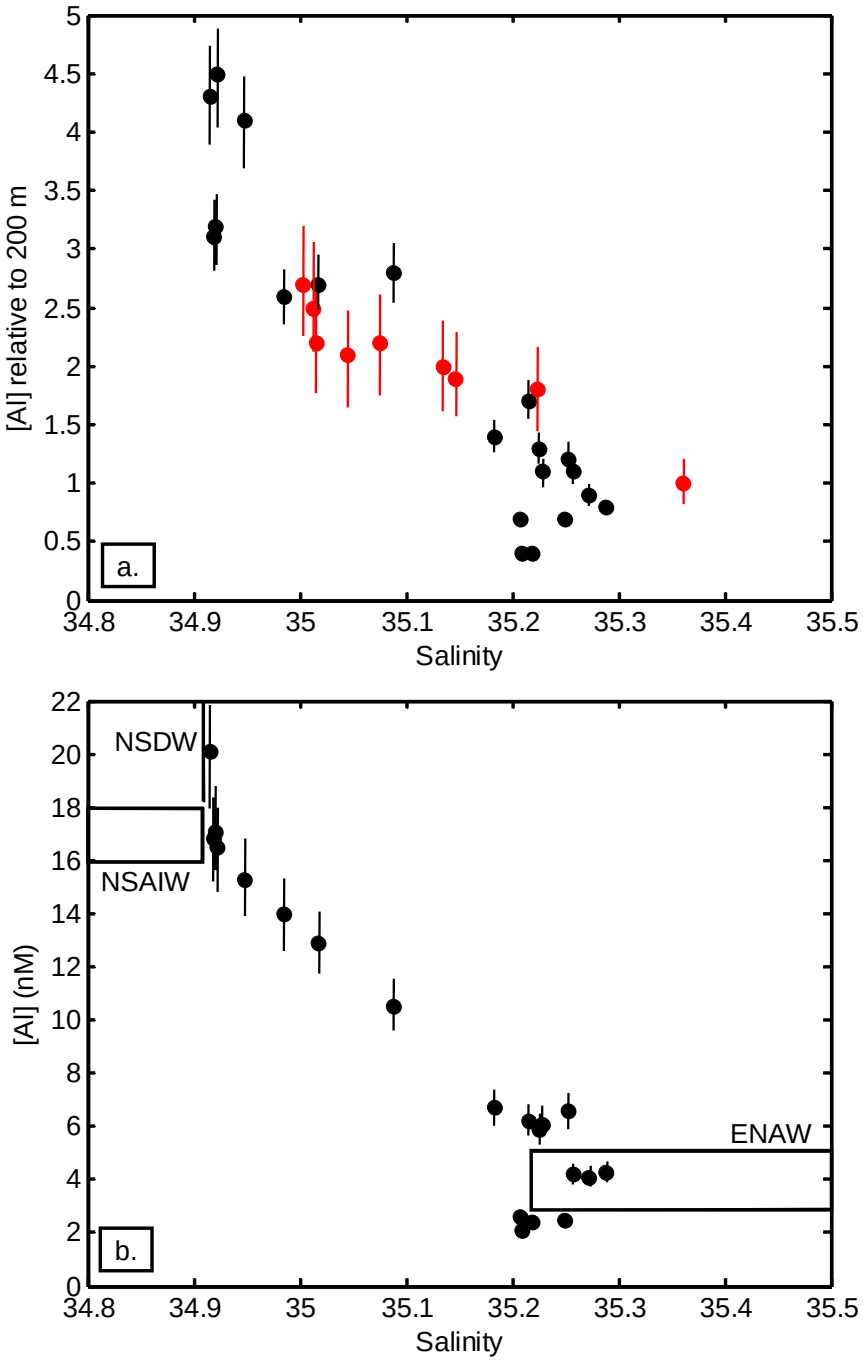

Fig. 5.14. a. [Al] concentration (nM) relative to concentrations at 200 m, against salinity. Black: samples from the exit to the Faroe Bank Channel (D. Hydes, unpublished data; see Fig. 4.9 for station positions); red: samples from the northern flank of the Wyville Thomson Ridge (Sc0804, see Fig. 3.1 for station position). b. Aluminium – salinity plot for data from the exit of the Faroe Bank Channel. Error bars show total errors associated with the method (section 4.2.8 and Table 4.3).

In the central Rockall Trough Al data were collected during the 2005 (CD176) and 2006 (D312) Ellett Lines (see Fig. 4.9 for stations). Al concentrations again vary through the water column with the lowest values being observed in the upper waters and the highest concentrations at depth (Fig. 5.15). At the majority of stations (black, Fig. 5.15) Al levels increase to a peak of ~ 8 nM at around 35.15-35.30, the approximate position of the intermediate salinity inflexion. Transmissometer data suggest that this cannot be explained by a mid-depth nepheloid layer. Additionally, as the properties of water at these depths appear to lie on a mixing line linking the upper waters to NSDW (A, Fig. 5.15), we again identify this water as originating from north of the Wyville-Thomson Ridge (i.e. WTOW). Below the intermediate Al peak (at S = 35.15-35.30), data tends towards the lower Al concentrations of LSW (3-7 nM) on a line approximating to a MOW-LSW mixture (B, Fig. 5.15). Although this mixing line trends to a lower Al concentration than the peak value observed in MOW in the southern Rockall Trough (~ 19 nM), a range of concentrations spanning 10-19 nM within the MOW water mass is seen. Additionally, lower concentrations of around 13 nM were observed near the Porcupine Seabight (Lunel, 1990) suggesting that the identification of this water as a MOW-LSW mixture is still appropriate. In the deepest part of the water column Al concentrations again increase as the curve tends towards AABW (mixing line C, Fig. 5.15).

At stations in the far west of the section deep WTOW is observed (see section 5.4 for more information). Where WTOW clearly fills the entire water column below the upper waters in θ-S plots (e.g. red, Fig. 5.6), water properties at all depths also appear to lie on the WTOW mixing line (A, Fig. 5.15) in *Al*-S space (red, Fig. 5.15). For stations where deep WTOW is only observed at the bottom of the water column (green, Fig. 5.15), water properties above 1100-1200 m lie along the WTOW mixing line (A, Fig. 5.15) towards the mid-depth Al peak. Unfortunately there are no usable data for these stations between salinities of 35.10-35.30. However, it is assumed that concentrations would decrease after the mid-depth Al peak and tend towards LSW along mixing line B. Below a salinity of ~ 35.10, θ-S plots show evidence of deep WTOW. An identical signature is once again seen in the Al data (green, Fig. 5.1.5) with values appearing to drift back towards the WTOW mixing line (A, Fig. 5.15). As points lie between mixing lines A and B, this water, once again, can be identified as a mixture of WTOW and the MOW-LSW water mass.

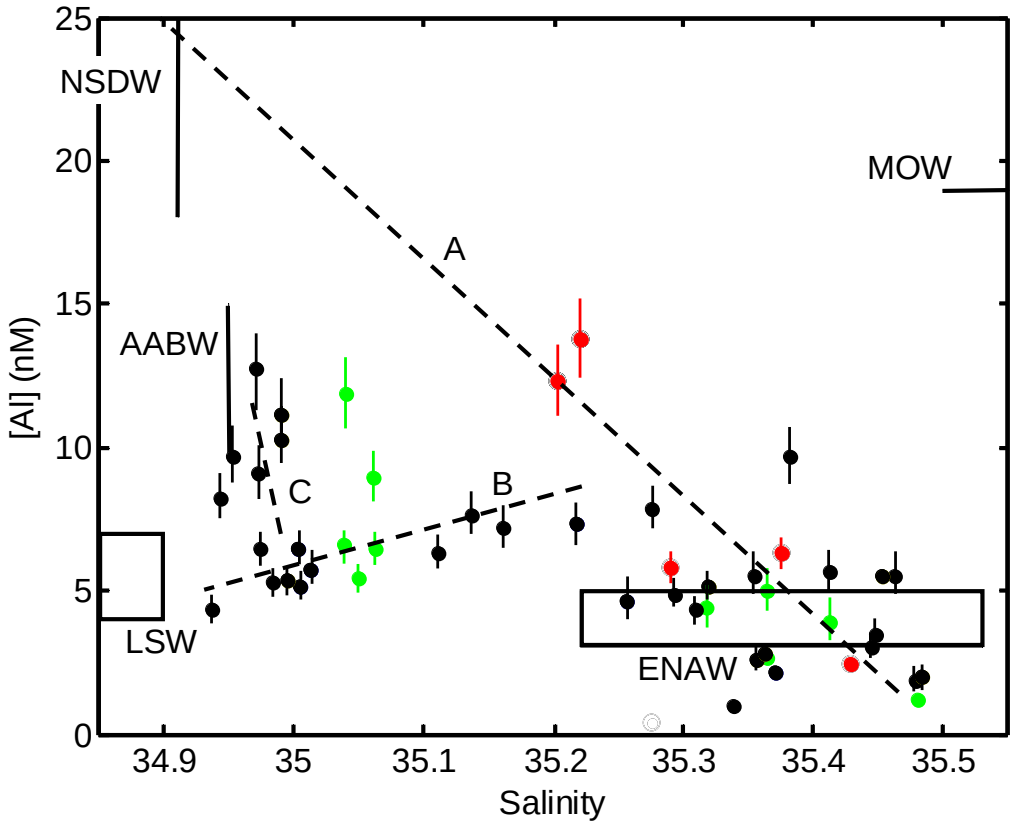

Figure 5.15. Aluminium - salinity plot for the Ellett Line using data collected during CD176 and D312. See Fig. 5.2 for section location. Red: station with WTOW occupying the entire water column below the upper waters; green: stations showing evidence of deep WTOW in water < 35.10; black: stations showing evidence of intermediate WTOW but no evidence of deep WTOW. Dashed lines are mixing lines: A: upper waters to NSDW (i.e. WTOW); B: MOW – LSW mixture; C: LSW to AABW. Error bars show total errors associated with the method (section 4.2.8 and Table 4.3).

5.10. Summary

This chapter has conclusively established WTOW as a significant water mass within the Rockall Trough. It is predominantly found at intermediate depths (600-1200 m), but also as a deeper water mass (>1200 m) in the west of the trough. At both depth ranges WTOW is temporally persistent being present in around three quarters of Ellett Line occupations and during every cruise since the mid 1990s. WTOW not only has a clear signature in θ-S space, but can also be identified using the chemical tracers of oxygen, nitrate, CFC-11, CFC-12 and Al (Table 5.1). The repeated observation that a variety of physical and chemical properties of the water we identify as WTOW lie on a mixing line linking upper

waters and NSDW, or tending towards the mixing line in the case of deep WTOW, heavily suggests that our interpretation is correct. With the presence of WTOW now clearly established within the Rockall Trough, the next two chapters detail the construction and verification of mixing models, and present the results.

Parameter	**Signature of intermediate WTOW (600-1200 m)**	**Signature of deep WTOW (> 1200 m)**
θ and S	At least 200 m of data between 600-1200 m lies on the WTOW mixing line. Presence of intermediate salinity inflexion.	Presence of water lying between MOW-LSW mixing line or LSW, and WTOW. Seen in western trough only.
oxygen	Strong flow seen as erosion of lower oxygen layer in west of trough.	Body of higher oxygen water in west of trough.
nitrate	Strong flow seen as erosion of higher nitrate layer in west of trough.	Lower nitrate concentrations in west of trough. Water properties lie on mixing line between higher nitrate layer and NSDW.
phosphate	No signature.	No signature.
silicate	No signature.	No signature.
CFC-11 and CFC-12	Water properties lie on WTOW mixing line.	No information.
aluminium	Water properties lie on WTOW mixing line. Intermediate Al peak approximately concurrent with intermediate salinity inflexion.	Higher Al concentrations in west of trough. Water properties lie between WTOW and MOW-LSW mixing lines

Table 5.1. Summary of identification features of intermediate (600-1200 m) and deep (> 1200 m) WTOW within the Rockall Trough.

Chapter 6.
Mixing model construction

This chapter details the construction of mixing models used to investigate the constituent water masses within WTOW and its modification along advection pathways. First, a brief description of the theory and methods of water mass analysis is given before the model construction and independent verification using CFC data is discussed. Results from the mixing analyses are discussed in Chapter 7.

6.1. Introduction

Mixing triangles were first used in conjunction with temperature – salinity (θ-S) diagrams to calculate the percentage composition of water in the ocean in 1935 by Thomsen (Mamayev, 1975). The method was extended with the introduction of percentage nomograms that take into account both lateral and vertical mixing by Sverdrup and Fleming in 1941 (Mamayev, 1975). More recently, the graphical method has been defined mathematically (Tomczak, 1981) and expanded to include information from additional variables including non-conservative parameters (e.g. Mackas et al., 1987; Karstensen and Tomczak, 1998; Fogelqvist et al., 2003). This section first discusses the graphical analysis of θ-S diagrams before moving on to the mathematical definition and extension of the method.

6.1.1. Temperature-salinity diagrams

In order to look at θ-S theory a highly simplified case of three vertically-layered homogeneous bodies of water (X,Y and Z) is again examined (Fig. 6.1). These water bodies are represented by a point in θ-S space. As Y has an intermediate density it must lie between water bodies X and Z within the water column (Fig. 5.1), hence waters X and Z are prevented from directly mixing together. As waters X and Y, and Y and Z begin to mix, water also lies along two mixing lines X-Y and Y-Z (Fig. 6.1.a). The proportion of

water body X at any point (*i*) on mixing line X-Y ($P_X{}^i$) can be calculated using equation 6.1 (see Fig. 6.1.a for terms).

$$P_X{}^i = y / (x + y) \quad (6.1)$$

As the mixing continues and water Y is eroded simultaneously from above and below, eventually no water with the original characteristics of water body Y is left. Hence in *θ-S* space water is now said to lie within a mixing triangle, X-Y-Z (Fig. 6.1.b). The proportion of water type X at any point *i* within the mixing triangle can be calculated by drawing a line from point X through point *i* to intersect line Y-Z (equation 6.2; see Fig. 6.1.b for terms).

$$P_X{}^i = x_2 / (x_1 + x_2) \quad (6.2)$$

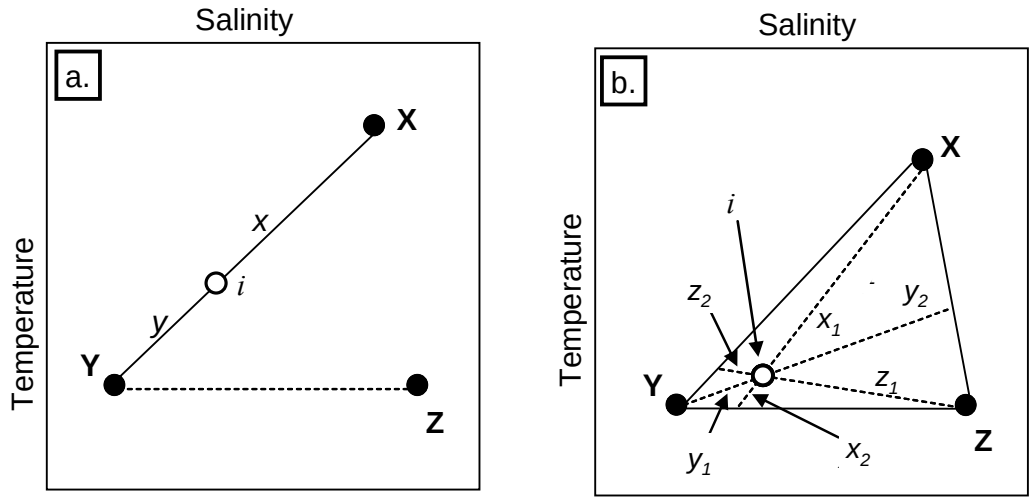

Figure 6.1. Theoretical θ-S diagrams illustrating methods to calculate mixing between a. two water bodies, b. three water bodies. Adapted from Figs. 5.22 and 5.24, Open-University (2001). For more information see section 6.1.1.

In the ocean it is unusual for a body of water to be defined as a point in *θ-S* space with water masses usually defined by a range of temperature and salinity characteristics. For example, the linear definitions of ENAW and WTOW and the rectangular definitions of LSW and MOW (e.g. Fig. 5.3). In mixing analysis a water mass's characteristics are often

simplified to a point in θ-S space, known as a water type, or a series of water types (Tomczak, 1999; Fogelqvist et al., 2003).

Some uses of θ-S diagrams to investigate mixing (such as that illustrated in Fig. 6.1) assume that vertical mixing dominates (i.e. that any modifications to water body Y results from mixing with water bodies X and Z rather than an unknown water mass that may exist at a similar density level to Y along its advection pathways). A detailed knowledge of the oceanography of the region can overcome this assumption by allowing all water masses to be accounted for. Additionally, the combination of a percentage nomogram with a mixing triangle allows both horizontal and vertical mixing to be accounted for (Fig. 6.2). Using mixing triangle X-Y-Z, where two water masses X-Y and Y-Z mix, and the technique illustrated in Fig. 6.1.b, the proportions of water types X, Y and Z at point *i* are 25 %, 50 % and 25 % respectively. The use of a percentage nomogram provides additional information that point *i* is composed of 50 % of water mass X-Y and 50 % of water mass Y-Z which mix together laterally. The proportion of water type X at point *i* ($P_X{}^i$) can also be determined by multiplying the percentage of water mass X-Y at point *i* ($P_{XY}{}^i$) with the percentage of X at point *x* ($P_X{}^x$, equation 6.3). Similarly, the proportion of water type Z at point *i* ($P_Z{}^i$) can be calculated by multiplying the percentage of water mass Y-Z at point *i* ($P_{YZ}{}^i$) with the proportion of Z at point *y* ($P_Z{}^y$, equation 6.4). However, the percentage of water type Y at point *i* ($P_Y{}^i$) is calculated by adding the percentage of Y added to point *i* by water mass X-Y, to the percentage added by water mass Y-Z (equation 6.5).

$$P_X{}^i = P_{XY}{}^i * P_X{}^x \quad (= 0.5 * 0.5 = 0.25) \tag{6.3}$$

$$P_Z{}^i = P_{YZ}{}^i * P_Z{}^y \quad (= 0.5 * 0.5 = 0.25) \tag{6.4}$$

$$P_Y{}^i = P_{XY}{}^i * P_Y{}^x + P_{YZ}{}^i * P_Y{}^y \quad (= 0.5 * 0.5 + 0.5 * 0.5 = 0.50) \tag{6.5}$$

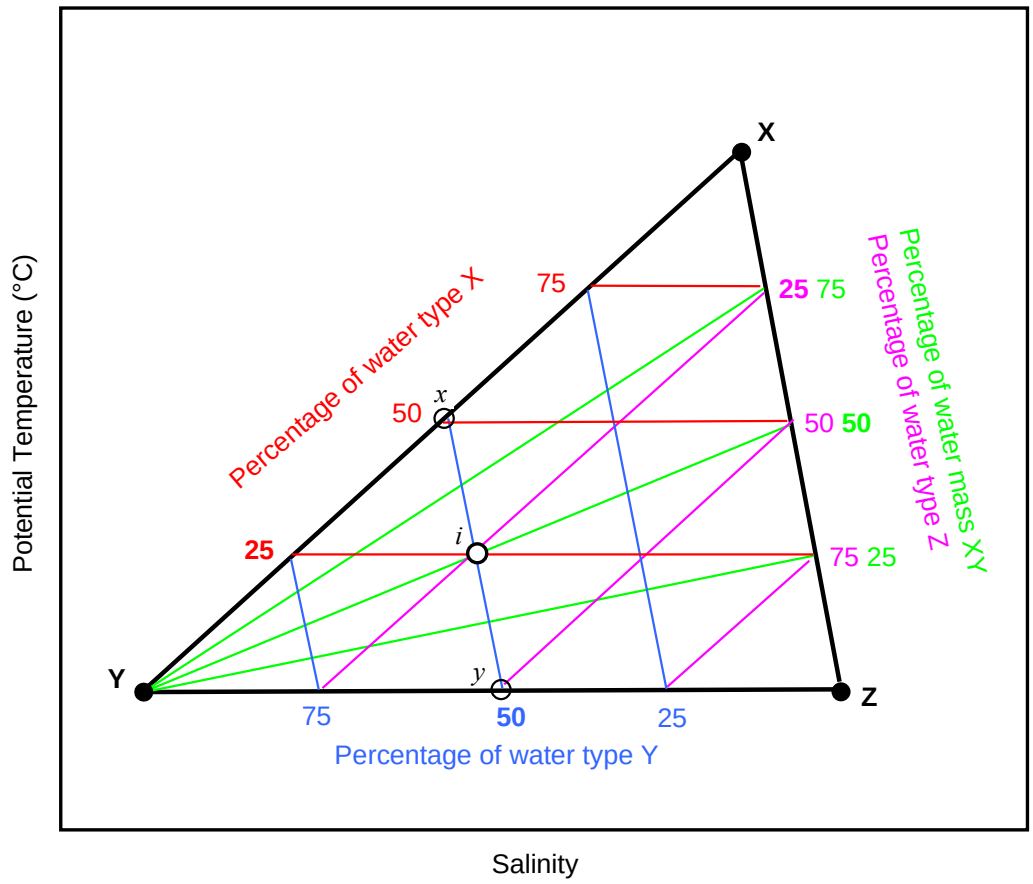

Figure 6.2. Combination of a mixing triangle and percentage nomogram to resolve both horizontal and vertical mixing. For explanation see section 6.1.1. in text. Red: percentage of water type X; blue: percentage of water type Y; magenta: percentage of water type Z; and green: percentage of water mass X-Y. Adapted from Fig. 72, Mamayev (1975).

A limitation of the θ-S diagram is the determination of mixing proportions when four or more water masses mix. Two methods exist to overcome this problem. Firstly the water column can be divided into a series of mixing triangles (e.g. Perez et al., 1993; Castro et al., 1998; Silva et al., 2009) which assumes that at any given point the water is formed from no more than three water types (Mamayev, 1975). Alternatively a quadrangular percentage nomogram can be employed (e.g. Miller, 1950; Tomczak, 1981). This assumes mixing between two water masses (e.g. W-Z and X-Y, Fig. 6.3). Lines of equal proportion of the two water masses (thin solid lines, Fig 6.3) are drawn within the mixing quadrangle allowing the percentage of each water mass at data point i to be determined ($P_{XY}{}^{i}$ = 20 %, $P_{WZ}{}^{i}$ = 80 %). The proportions of water types W and Z at point w ($P_{W}{}^{w}$ and $P_{Z}{}^{w}$) on mixing line W-Z can then be multiplied by $P_{WZ}{}^{i}$ to calculate the input of W and Z to point

i ($P_W{}^i$ and $P_Z{}^i$, equations 6.6 and 6.7). Similarly the proportions of water types X and Y at point x ($P_X{}^x$ and $P_Y{}^x$) on mixing line X-Y can be multiplied by $P_{XY}{}^i$ to determine the importance of X and Y to point *i* ($P_X{}^i$ and $P_Y{}^i$, equations 6.8 and 6.9).

$$P_W{}^i = P_{WZ}{}^i * P_W{}^w \quad (= 0.8 * 0.8 = 0.64) \tag{6.6}$$

$$P_Z{}^i = P_{WZ}{}^i * P_Z{}^w \quad (= 0.8 * 0.2 = 0.16) \tag{6.7}$$

$$P_X{}^i = P_{XY}{}^i * P_X{}^x \quad (= 0.2 * 0.8 = 0.16) \tag{6.8}$$

$$P_Y{}^i = P_{XY}{}^i * P_Y{}^x \quad (= 0.2 * 0.2 = 0.04) \tag{6.9}$$

An adaption of the technique is to assume that the two water masses mix laterally along isopycnals (dashed lines, Fig. 6.4) rather than the lines of percentage contribution (dashed lines, Fig. 6.3).

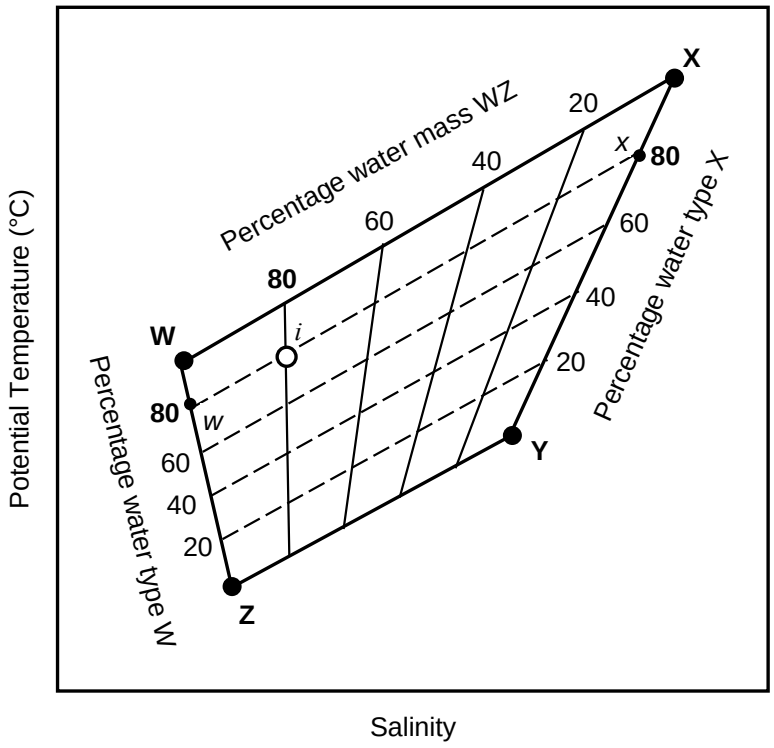

Figure 6.3. A quadrangular nomogram used to investigate both lateral and vertical mixing between four water types. Solid lines: lines of equal proportions of water masses W-Z and X-Y, dashed lines: percentage contribution lines. Adapted from Fig. 78, Mamayev (1975).

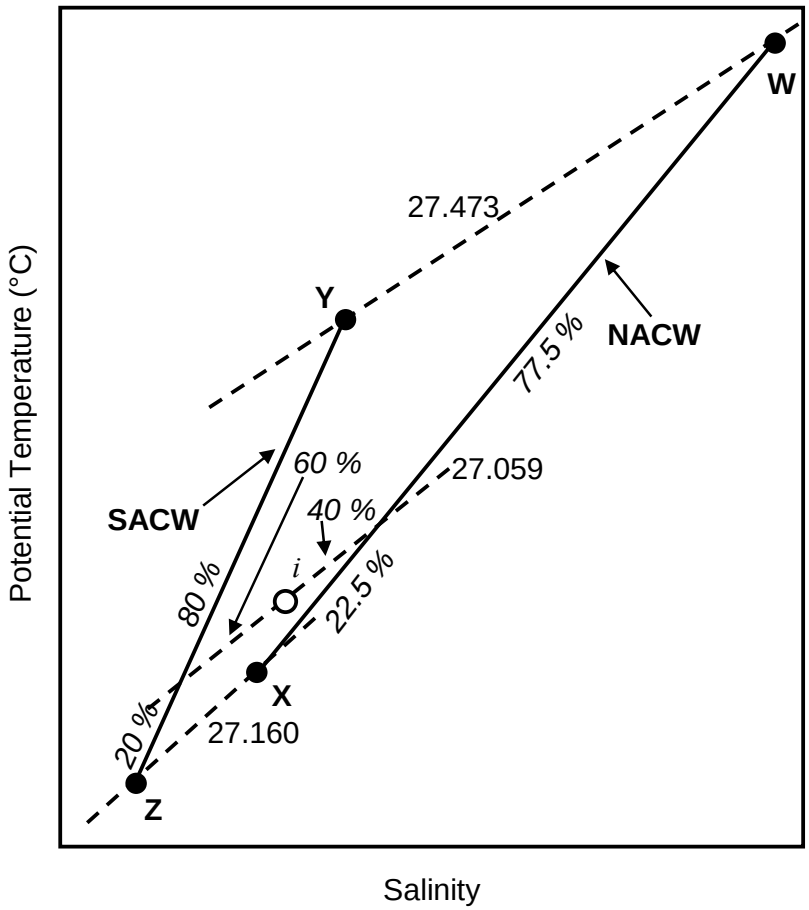

Figure 6.4. A quadrangular nomogram modified to assume lateral mixing occurs along isopycnals. Adapted from Fig. 6, Tomczak (1981). Solid lines: water masses NACW (W-X) and SACW (Y-Z); dashed lines: isopycnals. Data point i is composed of 60 % NACW and 40 % SACW, or 13.5 % W, 46.5 % X, 8 % Y and 32 % Z.

6.1.2. Mathematic extension of temperature-salinity diagrams

A different approach to determine the percentage composition of water at a particular point is to use a series of linear simultaneous equations. This method does not rely on the manual analysis of graphs dramatically increasing the speed and therefore scope of the study. Additionally, the only limitation on the number of water masses that can be investigated within the mixing model is the number of independent parameters that can be used as inputs. For the determination of the mixing between three water masses, two variables such a potential temperature and salinity (equations 6.10 and 6.11) are required with the third equation ensuring the conservation of mass (equation 6.12). As for the

graphical approach it is assumed that the distribution of all parameters used in the model are only affected by mixing, at least within the study area (Tomczak, 1981).

$$S_i = P_X{}^i * S_X + P_Y{}^i * S_Y + P_Z{}^i + S_Z \quad (6.10)$$

$$\theta_i = P_X{}^i * \theta_X + P_Y{}^i * \theta_Y + P_Z{}^i + \theta_Z \quad (6.11)$$

$$1 = P_X{}^i + P_Y{}^i + P_Z{}^i \quad (6.12)$$

where S_i, S_X, S_Y and S_Z are the salinities of point *i* and water types X, Y and Z respectively, and θ_i, θ_X, θ_Y and θ_Z the potential temperatures of point *i* and water types X, Y and Z respectively. The unknown proportions of water types X, Y and Z at point *i* ($P_X{}^i$, $P_Y{}^i$ and $P_Z{}^i$) can be solved using an inverse matrix technique.

To extend the number of water types investigated within the model, and therefore solve the additional unknown mixing proportions, extra input variables are required. In order to determine the mixing between n+1 water types, n variables are required (Tomczak, 1981). The conservative parameters of CFC-11 and CFC-12 have been used in this way (e.g. Fogelqvist et al., 2003; Olsson et al., 2005; Huhn et al., 2008) as has the derived variable of potential vorticity (e.g. You, 2002). Another recent development is the use of non-conservative variables, such as nutrients, as additional model inputs (e.g. Perez et al., 1993; You et al., 2003). As the method assumes conservative behaviour (Tomczak, 1981) the effect of respiration on the nutrient concentrations within the ocean must be accounted for. A term called preformed nitrate (NO) can be calculated from the nitrate (NO_3) and dissolved oxygen concentrations (O_2) using an empirically derived value (equation 6.13).

$$NO = 9\,NO_3 + O_2 \quad (6.13)$$

As for every one mole of oxygen consumed during respiration around one ninth of a mole of nitrogen is released as a NO_3^- ion, NO is approximately conservative (Broecker, 1974). Similarly, preformed phosphate (PO) can be calculated knowing that around 135^{th} of a mole of phosphate (PO_4) is released for each mole of oxygen consumed. However, the empirically derived link between O_2 consumption and NO_3 or PO_4 release is known to vary within the ocean (Broecker, 1974) introducing errors. Further, as water mass analysis

assumes that all input variables must be independent (Tomczak, 1981), a question is raised as to whether only one of NO, PO or O_2 can be used as input variables due to their relationship via the Redfield Ratio.

6.1.3. Errors and limitations of water mass analysis

Errors inherent to water mass analysis include: the water type definition chosen; analytical precision of the parameters used; and assumptions made within the model. Within mixing analysis a point, a water type, is chosen to define a body of water in the ocean such as ENAW or LSW. However, water mass characteristics vary spatially and temporally and are more commonly defined as a rectangle or line in θ-S space. Hence, a water type used within the mixing analysis is just one representation of the total water mass in reality. Several sensitivity studies have investigated the effect of varying water type definitions on outputs from mixing models and found variability in the region of ± 1-5 % (Hinrichsen and Tomczak, 1993; Poole and Tomczak, 1999; Loose et al., 2009). Another source of error within the model is the quality of the parameters used. Whilst temperature and salinity can be measured very precisely, chemical variables often have a higher analytical variability (Tomczak, 1981). An investigation into the effect of these differing precisions on the results of a mixing analysis show that using chemical parameters produces an uncertainty of ± 3-10 % whilst using physical parameters leads to errors of around ± 0.5 % (Hinrichsen and Tomczak, 1993). The errors associated with the chemical variables can be decreased by weighting so they have a lower influence within the mixing model than physical parameters (Mackas et al., 1987). The final limitation is the various assumptions made within the mixing model such as which water bodies come in contact with one another and can therefore mix. The results of the mixing model, however, can be checked for oceanographic consistency and model performance assessed by comparing predicted values of a parameter derived from the mixing model with independent observations (e.g. Castro et al., 1998; Perez et al., 1998; de Brauwere et al., 2007).

6.2. Construction of mixing models

Mixing models for the analysis of waters in the Rockall Trough were mathematically constructed from θ-S diagrams and associated mixing lines, mixing triangles, mixing quadrangles and percentage nomograms. Although the use of mixing line and triangles are well established, few studies use percentage nomograms particularly in the last three decades. Two models were developed; the first for when no θ-S signature of deep WTOW was observed (section 6.2.1), and a second more complex model for when deep WTOW was evident (section 6.2.2). Although chemical data were available, and the possibility of including them in the water mass analysis was considered, it was decided to base the mixing models on just temperature and salinity data. This has several advantages. Firstly temperature and salinity are measured continuously throughout the water column unlike chemical data which are typically determined at a maximum of 24 depths and frequently at far less. Temperature and salinity data are also available from a much larger selection of cruises especially historically. Although nutrient data is available post-1996 from the Ellett Line section (section 3.3), high quality CFC data has only been collected twice in 1997 and 1998 (section 3.4). Hence, by using only temperature and salinity not only can a greater vertical resolution be obtained but temporal variability back to 1975 can also be investigated using the Ellett Line time-series. Secondly, temperature and salinity data tend to have a higher precision than chemical data decreasing the resultant errors of the mixing analysis (Hinrichsen and Tomczak, 1993). This is particularly true for nutrient and oxygen data which must be corrected for non-conservative behaviour (section 6.1.2). Finally, but importantly, by using only temperature and salinity an independent verification of the model performance can be obtained using chemical variables. Temperature and salinity were linearly interpolated onto a 50 m vertical grid before use in the models.

Six water types were defined (Table 6.1). The definitions for AABW, MOW and NSDW were fixed due to the relatively small variability of these water masses within the Rockall Trough. Potential temperatures and salinities were obtained from the literature (Table 2.1) and checked for appropriateness with the data used in this thesis. The definitions for the lower bound of the upper waters (UW(l)) and the upper and lower boundaries of LSW (LSW(u) and LSW(l) respectively) were determined individually for each cruise because of the high temporal and spatial variability. LSW characteristics within the Rockall Trough vary due to changes in the source LSW (Yashayaev, 2007), as well as the

possibility that LSW enters the Rockall Trough in pulses (Holliday et al., 2000; New and Smythe-Wright, 2001). The temperature and salinity of upper waters in the Rockall Trough are known to change on various timescales (Holliday et al., 2008; Sherwin et al., 2012) as well as, in some years, spatially across the Ellett Line due to intrusion of WNAW into the trough (Holliday et al., 2000).

Abbreviation	Water type name	Definition
AABW	Antarctic Bottom Water	34.95, 2.8 °C
LSW(l)	lower bound Labrador Sea Water	approx. bottom of LSW halostad
LSW(u)	upper bound Labrador Sea Water	approx. top of LSW halostad
MOW	Mediterranean Overflow Water	35.5, 9.0 °C
NSDW	Norwegian Sea Deep Water	34.91, -1.0 °C
UW(l)	lower bound upper waters	inflexion in θ-S space away from ENAW mixing line

Table 6.1. Water type definitions used during water mass analysis within the Rockall Trough. LSW(l), LSW(u) and UW(l) are determined for each cruise due to large temporal and spatial variability.

6.2.1. Model when no evidence of deep WTOW

6.2.1.1 Waters less dense than UW(l)

The lower bound of the upper waters, UW(l), was defined as the point where water begins to deviate from an approximation of the ENAW mixing line defined by Harvey (1982). Any water with a potential density (σ_θ) less than that of UW(l) was considered to be composed solely of upper waters (Fig. 6.5.a). Although the upper waters of the Rockall Trough are a combination of ENAW, NAW, subtropical waters, and cooler and fresher WNAW, differentiation between them was not made for this study.

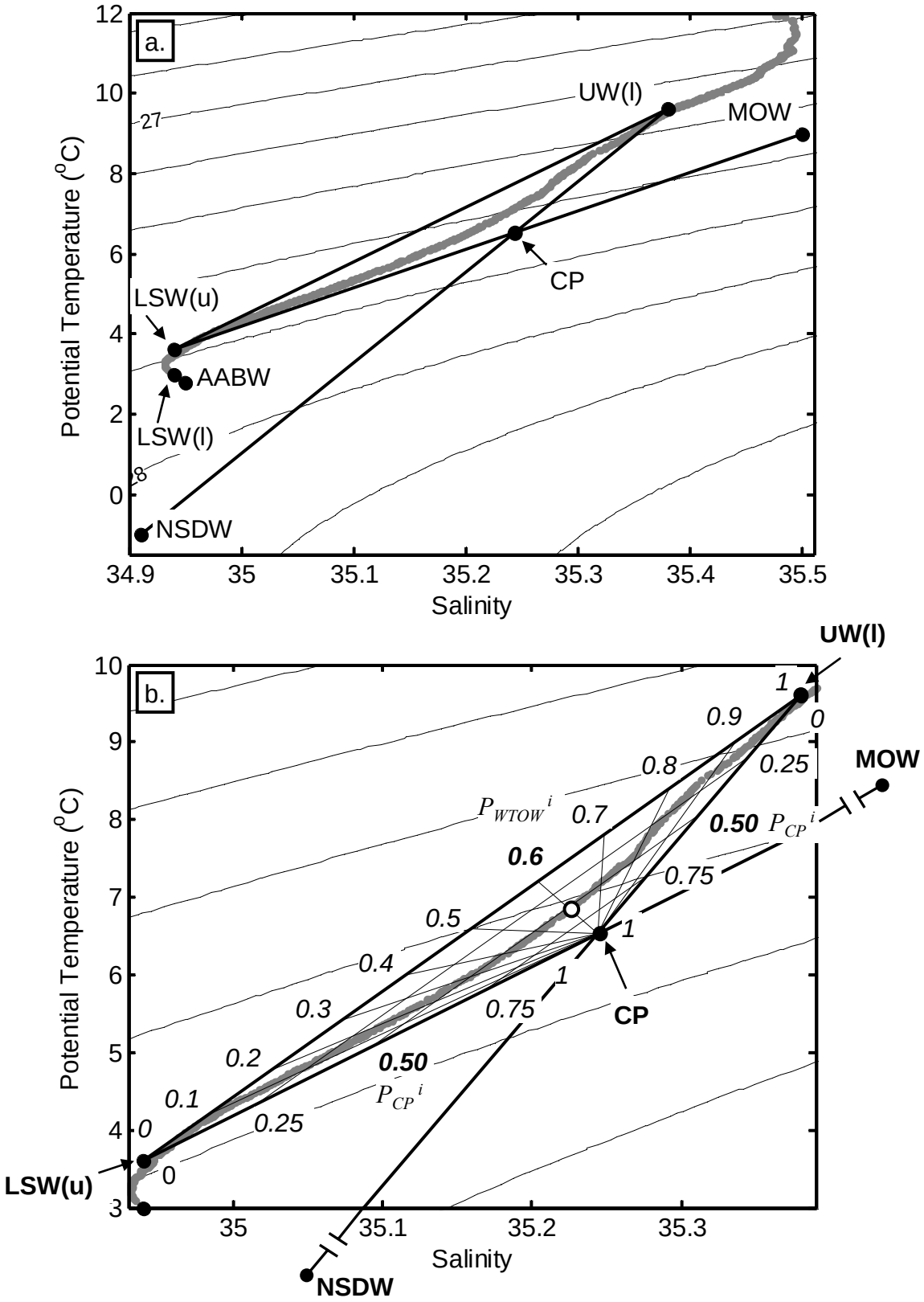

Figure 6.5. Graphical representation of the mixing model used when no signature of deep WTOW was observed, a. water types and mixing lines, b. detail of mixing triangle used to analyse intermediate waters. See section 6.2.1 for more information.

6.2.1.2. Waters with potential densities between UW(l) and LSW(u)

To investigate the mixing of intermediate waters in the Rockall Trough, a mixing triangle was constructed using the UW(l)-NSDW (i.e. WTOW) and MOW-LSW(u) mixing lines (Fig. 6.5.a). The triangle was closed with a line between UW(l) and LSW(u). As these two water bodies are separated in density space by WTOW and MOW-LSW it was assumed that UW and LSW cannot directly mix. Instead any water with intermediate characteristics must result from mixing between mixing lines UW(l)-NSDW and MOW-LSW(u). To calculate the proportion of the water types at any point (*i*) within the mixing triangle several steps were involved.

First, a new water type (CP) was defined as the crossover point of mixing lines UW(l)-NSDW and MOW-LSW(u) (Fig. 6.5.a). This water type is purely a construct in θ-S space and thus is a novel adaption of established technique. It was assumed that a point infinitesimally above CP on the UW(l)-NSDW mixing line was composed entirely of UW(l) and NSDW, whilst a point infinitesimally below CP on the MOW-LSW(u) mixing line was composed entirely of MOW and LSW(u). The composition of these two points ($P_{UW(l)}{}^{CP}$, $P_{NSDW}{}^{CP}$, $P_{MOW}{}^{CP}$ and $P_{LSW(u)}{}^{CP}$) were calculated using two pairs of simultaneous equations (equations 6.14 to 6.17).

$$\theta_{CP} = P_{UW(l)}{}^{CP} * \theta_{UW(l)} + P_{NSDW}{}^{CP} * \theta_{NSDW} \quad (6.14)$$

$$S_{CP} = P_{UW(l)}{}^{CP} * S_{UW(l)} + P_{NSDW}{}^{CP} * S_{NSDW} \quad (6.15)$$

$$\theta_{CP} = P_{MOW}{}^{CP} * \theta_{MOW} + P_{LSW(u)}{}^{CP} * \theta_{LSW(u)} \quad (6.16)$$

$$S_{CP} = P_{MOW}{}^{CP} * S_{MOW} + P_{LSW(u)}{}^{CP} * S_{LSW(u)} \quad (6.17)$$

where θ_{CP}, S_{CP}; $\theta_{UW(l)}$, $S_{UW(l)}$; θ_{NSDW}, S_{NSDW}; θ_{MOW}, S_{MOW}; and $\theta_{LSW(u)}$, $S_{LSW(u)}$ are the potential temperature and salinity of points CP, UW(l), NSDW, MOW and LSW(u) respectively. Equation pair 6.14 and 6.15, and 6.16 and 6.17, as well as all following simultaneous equations, were solved by the inverse matrix technique using the *inv* command in *Matlab*.

Next the proportions of water types UW(l), LSW(u) and CP ($P_{UW(l)}{}^{i}$, $P_{LSW(u)}{}^{i}$ and $P_{CP}{}^{i}$) at a particular data point *i* (S_i, θ_i) were calculated using a mixing triangle approach (Fig. 6.1.b and equations 6.18 to 6.20).

$$\theta_i = P_{UW(l)}{}^{i} * \theta_{UW(l)} + P_{LSW(u)}{}^{i} * \theta_{LSW(u)} + P_{CP}{}^{i} * \theta_{CP} \quad (6.18)$$

$$S_i = P_{UW(l)}{}^{i} * S_{UW(l)} + P_{LSW(u)}{}^{i} * S_{LSW(u)} + P_{CP}{}^{i} * S_{CP} \quad (6.19)$$

$$1 = P_{UW(l)}{}^{i} + P_{LSW(u)}{}^{i} + P_{CP}{}^{i} \quad (6.20)$$

Output of equations 6.18 to 6.20 enabled the proportion of mixing line UW(l)-NSDW (i.e. WTOW) at point *i* ($P_{WTOW}{}^{i}$) to be calculated (see equation 6.21).

$$P_{WTOW}{}^{i} = P_{UW(l)}{}^{i} / (1 - P_{CP}{}^{i}) \quad (6.21)$$

Finally, the proportions of individual water types at point *i* ($P_{UW}{}^{i}$, $P_{MOW}{}^{i}$, $P_{LSW}{}^{i}$ and $P_{NSDW}{}^{i}$), using output from equations 6.14 to 6.21, were calculated (equations 6.22 to 6.25). This step combines vertical mixing within mixing lines UW(l)-NSDW and MOW-LSW(u) with lateral mixing between the two mixing lines (Fig. 6.5.b).

$$P_{UW}{}^{i} = P_{CP}{}^{i} * P_{WTOW}{}^{i} * P_{UW(l)}{}^{CP} + P_{UW(l)}{}^{i} \quad (6.22)$$

$$P_{MOW}{}^{i} = P_{CP}{}^{i} * (1 - P_{WTOW}{}^{i}) * P_{MOW}{}^{CP} \quad (6.23)$$

$$P_{LSW}{}^{i} = P_{CP}{}^{i} * (1 - P_{WTOW}{}^{i}) * P_{LSW(u)}{}^{CP} + P_{LSW(u)}{}^{i} \quad (6.24)$$

$$P_{NSDW}{}^{i} = P_{CP}{}^{i} * P_{WTOW}{}^{i} * P_{NSDW}{}^{CP} \quad (6.25)$$

6.2.1.3. Waters denser than LSW(u)

Any water with a σ_θ between that of LSW(u) and LSW(l) was assumed to be composed entirely of LSW (i.e. $P_{LSW}{}^{i} = 1$). However, it should be noted that the LSW in the Rockall Trough is not the same as the 'pure' LSW found in the Labrador Sea and will contain

proportions of other water masses due to modification along advection pathways. These water masses are not resolved for this study.

Any water denser than LSW(l) was assumed to be a linear mixture of LSW(l) and AABW. The proportions of these two water bodies at any point *i* ($P_{LSW(l)}{}^{i}$ and $P_{AABW}{}^{i}$) were therefore determined from two simultaneous equations (equations 6.26 and 6.27).

$$\theta_i = P_{LSW(l)}{}^{i} * \theta_{LSW(l)} + P_{AABW}{}^{i} * \theta_{AABW} \quad (6.26)$$

$$S_i = P_{LSW(l)}{}^{i} * S_{LSW(l)} + P_{AABW}{}^{i} * S_{AABW} \quad (6.27)$$

where $\theta_{LSW(l)}$, $S_{LSW(l)}$, θ_{AABW} and S_{AABW} are the potential temperature and salinity of water types LSW(l) and AABW. For model output $P_{LSW(l)}{}^{i}$ was considered to be synonymous to $P_{LSW}{}^{i}$.

6.2.2. Model when evidence of deep WTOW

When deep WTOW is observed a more complex mixing model is required to account for its presence throughout nearly the entire water column and therefore mixing with additional water masses. Two mixing triangles (red and blue, Fig. 6.6.a) and two mixing quadrangles (yellow and green, Fig. 6.6.a) were constructed and solved mathematically. These are discussed in descending order through the water column.

6.2.2.1. Waters less dense than UW(l)

The lower bound of the upper waters, UW(l), was defined as for the mixing model when no evidence of deep WTOW is observed (section 6.2.1). Again any water less dense than this point was assumed to be composed entirely of upper waters (i.e. $P_{UW}{}^{i} = 1$) encompassing ENAW, NAW, subtropical waters and WNAW.

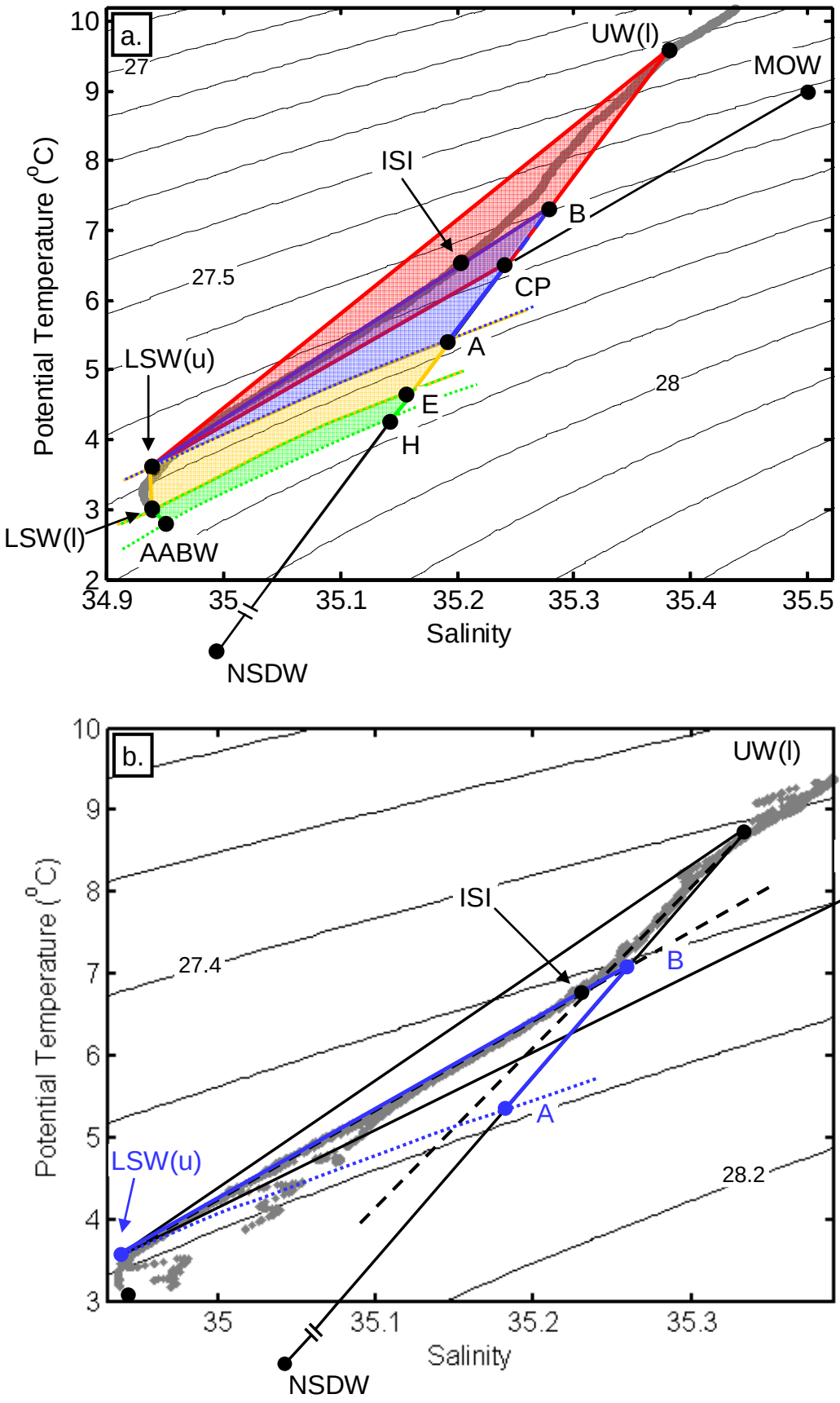
a.
UW(l)
MOW
ISI
B
CP
A
E
H
LSW(u)
LSW(l)
AABW
NSDW
27
27.5
28
Potential Temperature (°C)
Salinity
10
9
8
7
6
5
4
3
2
34.9
35
35.1
35.2
35.3
35.4
35.5
b.
UW(l)
MOW
ISI
B
A
LSW(u)
NSDW
27.4
28.2
Potential Temperature (°C)
Salinity
10
9
8
7
6
5
4
3
35
35.1
35.2
35.3

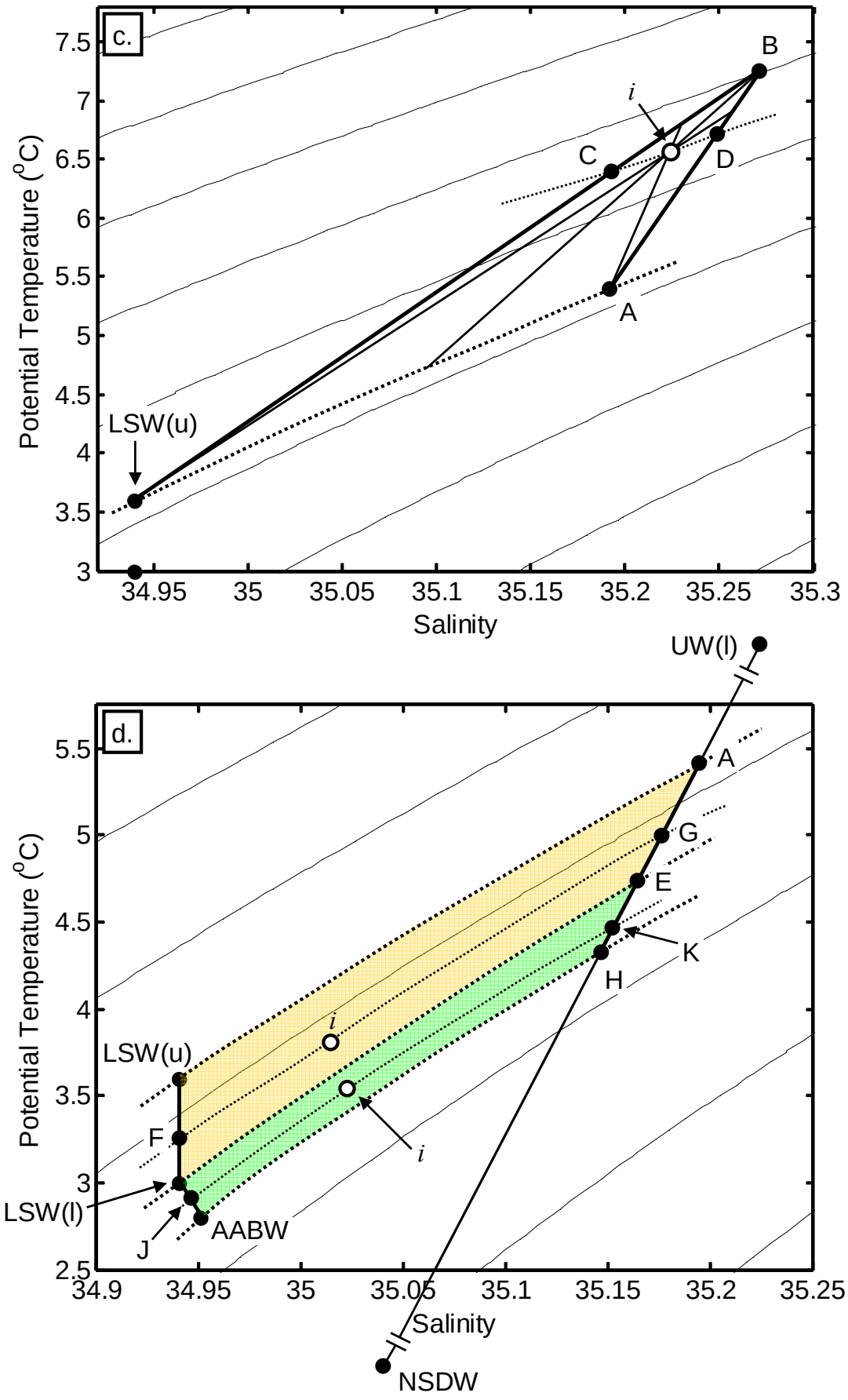
c.
B
i
C
D
A
LSW(u)
Potential Temperature (°C)
Salinity
d.
UW(l)
A
G
E
K
H
i
LSW(u)
F
i
LSW(l)
AABW
J
NSDW
Potential Temperature (°C)
Salinity

Figure 6.6. (previous two pages). Graphical representation of the mixing model used when deep WTOW is observed. Dotted lines indicate lines defined by isopycnals. a. Mixing triangles and quadrangles used within the mixing model; b. Detail of mixing triangle used to analyse water lying between the ISI and LSW(u) showing its construction; c. Mixing triangle from b. showing analysis methods; d. Mixing quadrangles used to analyse water in the σ_θ range of LSW (yellow) and with σ_θ between that of LSW(l) and AABW (green). For more detail see section 6.2.2.

6.2.2.2. Waters with potential densities between UW(l) and LSW(u)

The investigation of the composition of intermediate waters when there is evidence of deeper WTOW requires the potential temperature and salinity of an additional point, the Intermediate Salinity Inflexion (ISI), to be known. This point is defined as the point where the observed WTOW and MOW-LSW mixing lines, fitted to data within the section of interest but when there is no evidence of deep WTOW, intersect (Fig. 6.6.b). The composition of any water less dense than the ISI, but denser than water type UW(l), was calculated using the method employed when no evidence of deep WTOW is observed (red triangle, Fig. 6.6.a and section 6.2.1.2).

Any water with a σ_θ between that of the ISI and LSW(u) was analysed using a new mixing triangle (blue, Fig. 6.6.a) between LSW(u) and two new 'water types' A and B. Again this is an extension of established techniques. A was defined (S_A, θ_A) as the point on mixing line UW(l)-NSDW with the same σ_θ as LSW(u) (Fig. 6.6.b). S_A and θ_A were obtained by comparing σ_θ of LSW(u) to a list of σ_θ calculated from vectors of salinity and potential temperature linearly interpolated onto 100 points between $S_{UW(l)}$ and S_{NSDW}, and $\theta_{UW(l)}$ and θ_{NSDW}. Potential density was calculated using the *Seawater Toolbox* within *Matlab*. B was defined (S_B and θ_B) as the point on mixing line UW(l)-NSDW which was intersected by the observed MOW-LSW(u) mixing line (Fig. 6.6.b). Hence, both A and B contain a mixture of UW(l) and NSDW and are therefore not water types in the pure definition of the term. To resolve the composition of water at any point, *i*, within the mixing triangle several steps were required.

Firstly, a mixing triangle approach was used to calculate the proportion of water types A, B and LSW(u) at point *i* ($P_A{}^i$, $P_B{}^i$ and $P_{LSW(u)}{}^i$) using three simultaneous equations (equations 6.28 to 6.30).

$$\theta_i = P_A{}^i * \theta_A + P_B{}^i * \theta_B + P_{LSW(u)}{}^i * \theta_{LSW(u)} \quad (6.28)$$

$$S_i = P_A{}^i * S_A + P_B{}^i * S_B + P_{LSW(u)}{}^i * S_{LSW(u)} \quad (6.29)$$

$$1 = P_A{}^i + P_B{}^i + P_{LSW(u)}{}^i \quad (6.30)$$

The proportion of water mass A-B at point *i* ($P_{AB}{}^i$) was also calculated (equation 6.31) using output from equations 6.28 to 6.30.

$$P_{AB}{}^i = P_A{}^i / (1 - P_B{}^i) \quad (6.31)$$

The second step assumed that data point *i* results from linear mixing between water from mixing line A-B and mixing line B-LSW(u) and that this mixing occurs along isopycnals. Hence, two new points were defined: C and D (Fig. 6.6.c). The salinity and potential temperature of points C and D ($S_{C\,(i)}$, $\theta_{C\,(i)}$, $S_{D\,(i)}$ and $\theta_{D\,(i)}$) were determined using output from equations 6.28 to 6.30 (equations 6.32 to 6.35).

$$S_{C\,(i)} = (1 - P_B{}^i) * S_{LSW(u)} + P_B{}^i * S_B \quad (6.32)$$

$$\theta_{C\,(i)} = (1 - P_B{}^i) * \theta_{LSW(u)} + P_B{}^i * \theta_B \quad (6.33)$$

$$S_{D\,(i)} = (1 - P_B{}^i) * S_A + P_B{}^i * S_B \quad (6.34)$$

$$\theta_{D\,(i)} = (1 - P_B{}^i) * \theta_A + P_B{}^i * \theta_B \quad (6.35)$$

Next the composition of points C and D were calculated. The composition of point D ($P_{UW(l)}{}^{D(i)}$ and $P_{NSDW}{}^{D(i)}$) could be easily determined using two simultaneous equations (equations 6.36 to 6.37).

$$S_{D\,(i)} = P_{UW(l)}{}^{D\,(i)} * S_{UW(l)} + P_{NSDW}{}^{D\,(i)} * S_{NSDW} \quad (6.36)$$

$$\theta_{D\,(i)} = P_{UW(l)}{}^{D\,(i)} * \theta_{UW(l)} + P_{NSDW}{}^{D\,(i)} * \theta_{NSDW} \quad (6.37)$$

However, as line B-LSW(u) represents non-linear mixing between four water types (UW(l), MOW, LSW(u) and NSDW), the composition at point C ($P_{UW(l)}{}^{C(i)}$, $P_{MOW}{}^{C(i)}$, $P_{LSW(u)}{}^{C(i)}$ and $P_{NSDW}{}^{C(i)}$) was calculated using the method employed for intermediate waters when no deep WTOW is observed (Fig. 6.5 and section 6.2.1.2).

Finally, the proportions of each individual water type, as well as the proportion of water mass WTOW at point *i*, were determined (equations 6.38 to 6.42).

$$P_{UW}{}^{i} = (1 - P_{AB}{}^{i}) * P_{UW(l)}{}^{C\,(i)} + P_{AB}{}^{i} * P_{UW(l)}{}^{D\,(i)} \quad (6.38)$$

$$P_{NSDW}{}^{i} = (1 - P_{AB}{}^{i}) * P_{NSDW}{}^{C\,(i)} + P_{AB}{}^{i} * P_{NSDW}{}^{D\,(i)} \quad (6.39)$$

$$P_{MOW}{}^{i} = (1 - P_{AB}{}^{i}) * P_{MOW}{}^{C\,(i)} \quad (6.40)$$

$$P_{LSW}{}^{i} = (1 - P_{AB}{}^{i}) * P_{LSW(u)}{}^{C\,(i)} \quad (6.41)$$

$$P_{WTOW}{}^{i} = (1 - P_{AB}{}^{i}) * P_{WTOW}{}^{C\,(i)} + P_{AB}{}^{i} * P_{WTOW}{}^{D\,(i)} \quad (6.42)$$

6.2.2.3. Waters with potential densities between LSW(u) and LSW(l)

To determine the composition of waters lying between LSW(u) and LSW(l), a mixing quadrangle was constructed (yellow, Fig. 6.6.a) with points LSW(u), LSW(l), A and E (Fig. 6.6.d). Again this is a novel extension of the standard method. If the salinity at data point *i* was equal to or less than $S_{LSW(u)}$ and $S_{LSW(l)}$ it was assumed to be composed entirely of LSW. If S_i was more saline than $S_{LSW(u)}$ and $S_{LSW(l)}$ its composition was assumed to result from isopycnal linear mixing between a point on line A-E and a point on line LSW(u)-LSW(l). Hence, two new points, F and G were defined (Fig. 6.6.d). F was defined as the point on line LSW(u)-LSW(l) with the same σ_θ as data point *i* and G as the point on line A-E with the same σ_θ as data point *i*. The location of point F in θ-*S* space (S_F

$_{(i)}$ and $\theta_{F\,(i)}$) was determined by comparing the σ_θ of point *i* to a list of σ_θ calculated from vectors of salinity and potential temperature linearly interpolated onto 100 points between $S_{LSW(u)}$ and $S_{LSW(l)}$, and $\theta_{LSW(u)}$ and $\theta_{LSW(l)}$. Similarly, the salinity and potential temperature at point G ($S_{G\,(i)}$ and $\theta_{G\,(i)}$) were obtained from comparing the σ_θ of point *i* to a list of σ_θ calculated from 1x100 vectors of salinity and potential temperature obtained by linear interpolation between S_B and S_{NSDW}, and θ_B and θ_{NSDW}.

The second step was to determine the composition at points F and G. F was assumed to be composed entirely of LSW (i.e. $P_{LSW}{}^{F\,(i)} = 1$). The proportions of water types UW(l) and NSDW at G ($P_{UW(l)}{}^{G\,(i)}$ and $P_{NSDW}{}^{G\,(i)}$ respectively) were calculated using the UW(l) – NSDW mixing line (equations 6.43 to 6.45). WTOW was assumed not to contribute to the water composition at F whilst G was assumed to be composed entirely of WTOW (i.e. $P_{WTOW}{}^{F\,(i)} = 0$ and $P_{WTOW}{}^{G\,(i)} = 1$).

$$S_{G\,(i)} = P_{UW(l)}{}^{G\,(i)} * S_{UW(l)} + P_{NSDW}{}^{G\,(i)} * S_{NSDW} \tag{6.43}$$

$$\theta_{G\,(i)} = P_{UW(l)}{}^{G\,(i)} * \theta_{UW(l)} + P_{NSDW}{}^{G\,(i)} * \theta_{NSDW} \tag{6.44}$$

$$1 = P_{UW(l)}{}^{G(i)} + P_{NSDW}{}^{G\,(i)} \tag{6.45}$$

Finally, the proportion of water mass WTOW at data point *i* was calculated (equation 6.46) enabling the proportions of the individual water types to be determined (equations 6.47 to 6.49).

$$P_{WTOW}{}^{i} = (S_i - S_{F\,(i)}) \,/\, (S_{G\,(i)} - S_{F\,(i)}) \tag{6.46}$$

$$P_{UW}{}^{i} = P_{WTOW}{}^{i} * P_{UW(l)}{}^{G\,(i)} \tag{6.47}$$

$$P_{LSW}{}^{i} = (1 - P_{WTOW}{}^{i}) * P_{LSW}{}^{F\,(i)} \tag{6.48}$$

$$P_{NSDW}{}^{i} = P_{WTOW}{}^{i} * P_{NSDW}{}^{G\,(i)} \tag{6.49}$$

6.2.2.4. Waters denser than LSW(l)

Water denser than LSW(l) was assumed to be a mixture of LSW(l), AABW and WTOW (i.e. NSDW and UW(l)). A mixing quadrangle was again drawn (green, Fig. 6.6.a) with points LSW(l), AABW, E and H (Fig. 6.6.d). Again it was assumed that water at any point (*i*) is formed by linear mixing along an isopycnal between water lying on mixing line LSW(l)-AABW and that lying on mixing line E-H. Hence, two new points, J and K, were defined. J was defined as the point on line LSW(l)-AABW with the same σ_θ as *i*, and K as the point on line E-H with the same σ_θ as *i*. The salinity and potential temperature of J ($S_{J\,(i)}$ and $\theta_{J\,(i)}$) were obtained by comparing the σ_θ of point *i* with a list of σ_θ calculated from 1x100 vectors of salinity and potential temperature linearly interpolated between $S_{LSW(l)}$ and S_{AABW}, and $\theta_{LSW(l)}$ and θ_{AABW}. Similarly, the location of K in θ-S space ($S_{K\,(i)}$ and $\theta_{K\,(i)}$) was determined by comparing the σ_θ of *i* with a vector of σ_θ calculated from two vectors of salinity and potential temperature created by linearly interpolating between point B and NSDW onto 100 levels.

The next step was to calculate the proportions of the constituent water types at points J and K. J was assumed to be composed entirely of LSW(l) and AABW and therefore the composition ($P_{LSW(l)}{}^{J\,(i)}$ and $P_{AABW}{}^{J\,(i)}$) was determined using two simultaneous equations (equations 6.50 and 6.51). K was assumed to be composed of only UW(l) and NSDW, again two simultaneous equations (equations 6.52 and 6.53) were solved to calculate the proportion of these two water types ($P_{UW(l)}{}^{K\,(i)}$ and $P_{NSDW}{}^{K\,(i)}$).

$$S_{J\,(i)} = P_{LSW(l)}{}^{J\,(i)} * S_{LSW(l)} + P_{AABW}{}^{J\,(i)} * S_{AABW} \quad (6.50)$$

$$\theta_{J\,(i)} = P_{LSW(l)}{}^{J\,(i)} * \theta_{LSW(l)} + P_{AABW}{}^{J\,(i)} * \theta_{AABW} \quad (6.51)$$

$$S_{K\,(i)} = P_{UW(l)}{}^{K\,(i)} * S_{UW(l)} + P_{NSDW}{}^{K\,(i)} * S_{NSDW} \quad (6.52)$$

$$\theta_{K\,(i)} = P_{UW(l)}{}^{K\,(i)} * \theta_{UW(l)} + P_{NSDW}{}^{K\,(i)} * \theta_{NSDW} \quad (6.53)$$

Finally, the proportion of water mass WTOW at data point *i* was calculated (equation 6.54) enabling the proportion of individual water types to be determined (equations 6.55 to 6.58).

$$P_{WTOW}{}^{i} = (S_i - S_{J(i)}) / (S_{K(i)} - S_{J(i)}) \quad (6.54)$$

$$P_{UW}{}^{i} = P_{WTOW}{}^{i} * P_{UW(l)}{}^{K(i)} \quad (6.55)$$

$$P_{NSDW}{}^{i} = P_{WTOW}{}^{i} * P_{NSDW}{}^{K(i)} \quad (6.56)$$

$$P_{AABW}{}^{i} = (1 - P_{WTOW}{}^{i}) * P_{AABW}{}^{J(i)} \quad (6.57)$$

$$P_{LSW}{}^{i} = (1 - P_{WTOW}{}^{i}) * P_{LSW}{}^{J}{}_{(i)} \quad (6.58)$$

6.3. Verification of mixing models

In order to independently check how well the mixing models were performing, predicted CFC-11 concentrations were compared with measured CFC-11 concentrations from the Ellett Line. Deepwater profiles from D230 were divided into those showing evidence of deep WTOW and those not using θ-S diagrams. Unfortunately only one station with CFC-11 data showed the presence of deep WTOW. Data from the D233 Ellett Line were examined in the hope of providing additional verification of model performance when deep WTOW is present. However, the CFC-11 data at such stations has a large scatter.

Predicted CFC-11 concentrations ($CFC\text{-}11_{predicted}{}^{i}$) were calculated by combining final water type proportions, derived from the mixing models, with CFC-11 values of the water types (equation 6.59).

$$\begin{aligned} CFC\text{-}11_{predicted}{}^{i} = {} & P_{AABW}{}^{i} * CFC\text{-}11_{AABW} + P_{LSW}{}^{i} * CFC\text{-}11_{LSW} \\ & + P_{MOW}{}^{i} * CFC\text{-}11_{MOW} + P_{NSDW}{}^{i} * CFC\text{-}11_{NSDW} \\ & + P_{UW}{}^{i} * CFC\text{-}11_{UW} \end{aligned} \quad (6.59)$$

where $CFC\text{-}11_{AABW}$, $CFC\text{-}11_{LSW}$, $CFC\text{-}11_{MOW}$, $CFC\text{-}11_{NSDW}$ and $CFC\text{-}11_{UW}$ are the measured CFC-11 concentrations of water types AABW, LSW, MOW, NSDW and UW respectively. With the exception of LSW, all water type CFC-11 values were measured at the boundaries of the Rockall Trough (Table 6.2). This ensures that the predicted CFC-11

concentrations are independent from the measured CFC-11 values used in the model verification. The CFC-11 concentration of LSW varies considerably between the entrance to the Rockall Trough (~3.4 pmol kg^{-1}) and 57.5 °N in the trough (~2 pmol kg^{-1}) possibly as a result of LSW entering the basin in pulses (Holliday et al., 2000; New and Smythe-Wright, 2001). Therefore, the CFC-11 concentration of this water type had to be defined in the central Rockall Trough.

Water type	**[CFC-11] (pmol kg^{-1})**	**Source**
AABW	0.5	D233, southern entrance Rockall Trough
LSW	2.0	D230, Ellett Line
MOW	1.9	M39-5, southern entrance Rockall Trough
NSDW	1.2	34AR, southern Faroe Shetland Channel
UW	3.8	Fogelqvist et al., 2003, Wyville Thomson Basin

Table 6.2. CFC-11 concentrations of water types used in conjunction with output from the mixing models to predict CFC-11 concentrations within the water column. For station positions see Fig. 3.8.

Predicted and observed CFC-11 profiles have a good agreement both when deep WTOW is and is not present (Fig. 6.7). Magnitudes of CFC-11 concentrations and overall patterns of distribution are reproduced well. For the case where deep WTOW is absent (Fig. 6.7.a), both observed and predicted CFC-11 concentrations are near constant in the upper ~ 900 m with the exception of the lower measured values in the upper ~ 100 m which the model is not designed to detect. At around 900 m observed values begin to decrease at a rate of approximately 0.5 pmol kg^{-1} per 100 m to a second inflexion point at around 1200 m. Although the upper and lower inflexions are slightly lower in the water column for the predicted curves (~ 1000 m and ~ 1300 m respectively) the rate of change of CFC-11 concentrations with depth is very similar to that of the observed data. Below ~ 1200 m observed CFC-11 concentrations slowly decrease to around 1750 m where concentrations start to rapidly fall as AABW begins to influence the water. The inflexion points for the calculated profile are again slightly lower in the water column (~ 1300 m and ~ 1900 m respectively) than for the measured data. However, the rate of change of CFC-11 concentrations between the two inflexions, and between the lower inflexion and seabed,

are again very similar to that seen in the measured data. Predicted concentrations at the seabed are 0.2-0.5 pmol kg^{-1} higher than those measured suggesting that the model does not fully resolve the deepest components of AABW. Despite some caveats, the comparison indicates that the model is reproducing mixing within the central Rockall Trough well throughout nearly the entire water column. Unfortunately, only one good quality CFC-11 profile is available in water influenced by deep WTOW (Fig. 6.7.b). Although the fit of the predicted and observed concentrations is less good than for the case when deep WTOW is absent the general trends and magnitudes are similar. Thus, it appears that the mixing model is not only applicable to when deep WTOW is absent but also when this water mass is present. These models are therefore applied to several sections in the northern and central Rockall Trough in the next chapter.

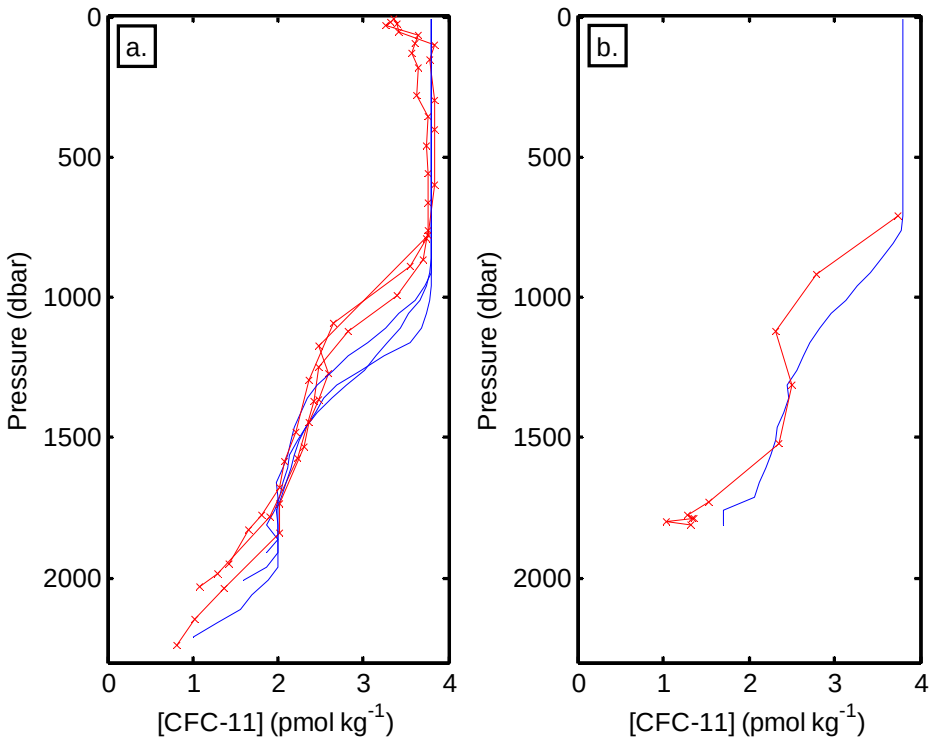

Fig. 6.7. Predicted CFC-11 concentrations (blue) and observed CFC-11 concentrations (red) for D230, a. profiles with no evidence of deep WTOW, b. profile with evidence of deep WTOW. Precision for observed CFC-11 values are ± 1 % (section 3.3.3).

Chapter 7.
Water mass analysis in the Rockall Trough

This chapter details the results from mixing models used to investigate the constituent water masses within WTOW and its modification along advection pathways. Outputs from mixing analyses carried out in the northern and central Rockall Trough, as well as in the channels between the northern banks, are shown. Finally, analyses of Ellett Line stations G and M between 1975 and 2008 are presented.

7.1. Water mass analysis in the northern Rockall Trough

Analysis of a CTD section in the northern Rockall Trough, between the Scottish Shelf and Bill Baileys Bank (SS-BBB, fig. 7.1), shows that WTOW is an important water mass especially to the north of Rosemary Bank. Following the historical notation, the boundary of a water mass is defined as the 50 % contour of its percentage content (Mamayev, 1975). As such, the results of a mixing model can be used to divide the water column into its constituent water masses (Fig. 7.2.a). To the southeast of Rosemary Bank WTOW forms a layer 350 – 500 m thick at intermediate depths, lying below the upper waters and above the mixture of MOW and LSW. In the bottom 150 m of the water column LSW is seen. To the north of Rosemary Bank WTOW is the dominant water mass lying between 150 m and 1250 m and touching the seabed at a number of stations. Thickness of the WTOW layer to the north of Rosemary Bank varies between 450 m and 900 m. Hence, a greater volume of WTOW is seen in the north of the section compared to southeast of Rosemary Bank.

To further investigate WTOW in the Rockall Trough the proportion of NSDW in the water column was determined (Fig. 7.2.b). The results do not necessarily mean that water with the same characteristics as Faroese Channel NSDW is seen in the Rockall Trough; in fact this is only the case if the proportion of NSDW at any point is 100 %. Rather, the results represent the proportion of NSDW involved in the formation of water at that depth. The higher the percentage of NSDW, the larger the input of the water mass and the more like

Faroese Channel NSDW are the water's characteristics. Again a pronounced difference is seen in water lying to the north of Rosemary Bank compared to that lying to the southeast. Water lying between the Scottish Shelf and Rosemary Bank contains a maximum of 8-9 % NSDW whilst water between Rosemary Bank and Bill Baileys Bank contains a maximum of 12-15 %. Again, the layer containing greater than 5 % NSDW is thinner to the southeast (250 - 300 m) compared to the north (~ 500 m), with NSDW influenced waters being in contact with the seabed in this area. Two peaks of NSDW appear north of Rosemary Bank, one hugging the eastern flank of Bill Baileys Bank and the other at around the same depth but closer to Rosemary Bank.

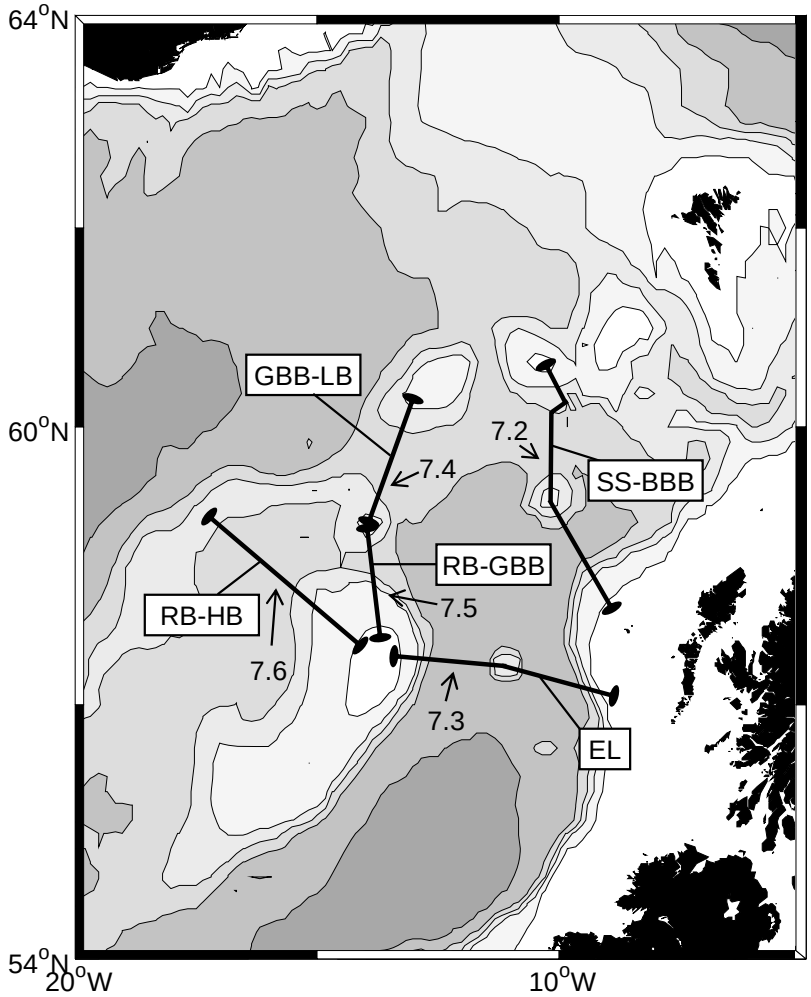

Figure 7.1. Location of sections analysed using mixing models. EL: Ellett Line (D312), GBB-LB: George Bligh Bank to Lousy Bank (D223), RB-GBB: Rockall Bank to George Bligh Bank (D230), RB-HB: Rockall Bank to Hatton Bank (D230) and SS-BBB: Scottish Shelf to Bill Baileys Bank (Sc0704). Arrows show the viewer's orientation for figures 7.2, 7.3, 7.4, 7.5 and 7.6. Contours are 200 m, 400 m, 750 m, 1500 m and 2000 m.

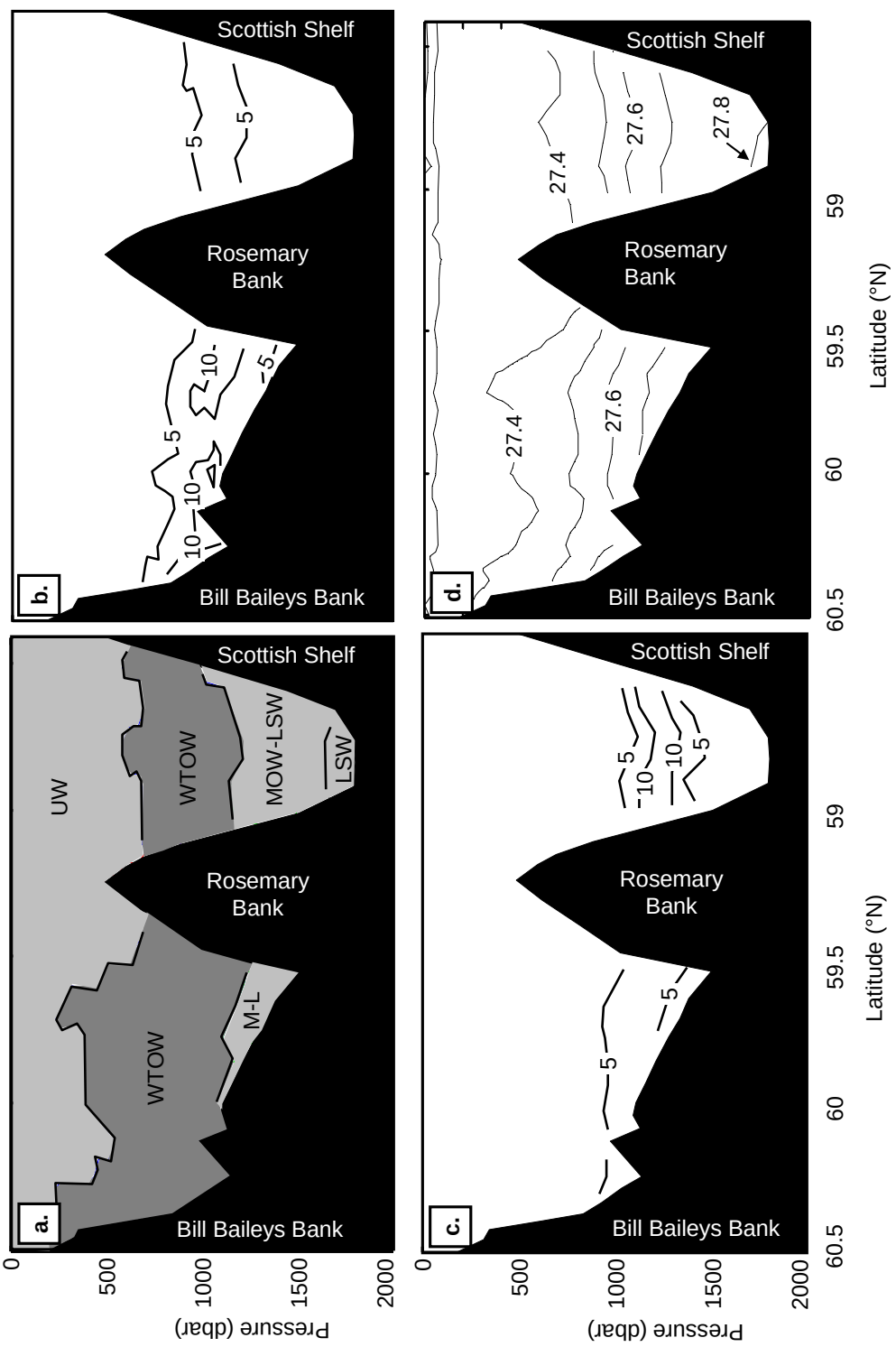

Figure 7.2. Water mass analysis for a section in the northern Rockall Trough (line SS-BBB, Fig. 7.1). a. Water masses entering the Rockall Trough from the south (light grey) and from the north (dark grey). Black lines mark the 50 % contour for each water mass. M-L: MOW-LSW mixture. b. Percentage of NSDW in the water column. c. Percentage of MOW in the water column. d. Contours of potential density (kg m^{-3}).

Examination of the distribution of potential density (Fig. 7.2.d) in the north of the section shows sloping isopycnals indicating the presence of shear within the water column. As the isopycnals rise northwards, hence towards Bill Baileys Bank, this suggests waters lying above the 27.4 kg m^{-3} isopycnal, i.e. upper waters, are flowing towards the east. The directionality of flow of WTOW, and therefore waters containing NSDW, depends on the position of the level of no motion within the water column. Measurements from two historical moorings in the northern Rockall Trough suggest that zero flow exists at some depth between approximately 600 m and 1000 m (Table 7.1). Assuming this to be true, at least some of the WTOW and water containing NSDW between Rosemary Bank and Bill Baileys Bank is flowing westward into the north-western Rockall Trough. Additional evidence for westward flow of WTOW is that overflows in the Northern Hemisphere have a tendency to keep bathymetric slopes to their right (e.g. Killworth, 2001). In comparison, isopycnals at intermediate depths to the southeast of Rosemary Bank are relatively horizontal indicating low shear within the water column and weak baroclinic flow of the WTOW layer.

Mooring i.d.	**Latitude (°N)**	**Longitude (°W)**	**Water depth (m)**	**Instrument depth (m)**	**Mean flow direction (°)**
I1	59.987	12.152	1117	660	65
				1066	288
I2	60.195	9.257	1394	161	19
				565	13
				972	200

Table 7.1. Vector average direction, weighted by speed; and metadata for two historical moorings in the northern Rockall Trough. Moorings were deployed in July 1978 with measurement durations of 40 and 54 days respectively. Data were obtained from BODC and were not de-tided.

For completion the distribution of MOW between the Scottish Shelf and Bill Baileys Bank was calculated (Fig. 7.2.c). In contrast to the distribution of WTOW and NSDW, MOW is more pronounced to the southeast of Rosemary Bank (maximum 12-14 %) relative to the

north of the section (maximum 9 %). Similarly, the thickness of the water layer containing more than 5 % MOW is greater in the south of the section (~ 400 m) compared to north of Rosemary Bank (~ 300 m).

7.2. Water mass analysis in the central Rockall Trough

Analysis of the Ellett Line section from 2006 (EL, figure 7.1) shows that WTOW is also an important intermediate water mass in the central Rockall Trough (Fig. 7.3.a). Again, using the 50 % contour as the boundary of a water mass (Mamayev, 1975), WTOW is present as a 400-500 m thick layer lying between about 700 and 1200 m both in the eastern and western Rockall Trough. However, unlike in the northern Rockall Trough, at intermediate depths there appears to be little difference between WTOW east and west of the Anton Dohrn Seamount. Below ~ 1200 m the water mass of deep WTOW is seen hugging the eastern flank of Rockall Bank with two areas having greater than 50 % WTOW (dark grey, Fig. 7.3.a). Using the 45 % contour (thin solid line Fig. 7.3.a.) or 40 % contour (thin dotted line, Fig. 7.3.a) as the water mass boundary shows deep WTOW clearly.

The distribution of percentage content of NSDW in the Rockall Trough (Fig. 7.3.b) shows a clear difference between the eastern and western basin both above and below ~ 1200 m. At intermediate depths east of the Anton Dohrn seamount, the layer containing greater than 5 % NSDW is around 250 m thick with a maximum contribution to the water at any level of 8 %. In the western Rockall Trough, the thickness of the layer with more than 5 % NSDW is ~ 800 m at intermediate depths with the maximum contribution of ~ 17 %. Below 1200 m no evidence of NSDW is seen in the eastern trough, whilst west of the seamount an extensive influence of NSDW is seen with a maximum contribution of 20 – 25 %. The highest proportion of NSDW is seen hugging the eastern flank of Rockall Bank between 1250 m and 1700 m, with a second maximum seen at the bottom of the water column at station G (see Fig. 3.7 for location). A comparison of NSDW and WTOW distribution at stations E and M (see Fig. 3.7 for station locations) also clearly reveals the influence of the overflow water hugging Rockall Bank (Fig. 7.4).

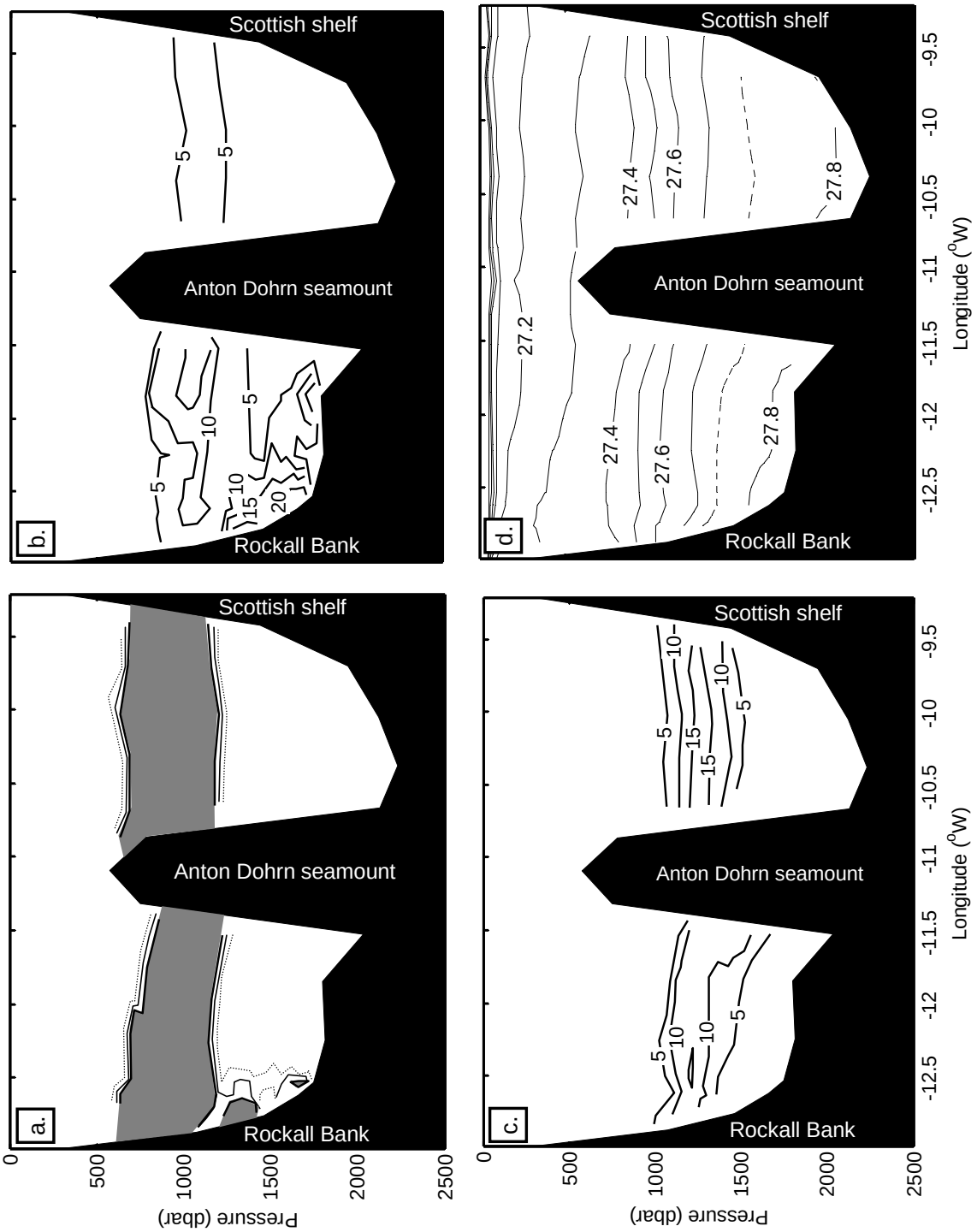

Figure 7.3. Water mass analysis for a section in the central Rockall Trough (EL, Fig. 7.1). a. Percentage of WTOW. Dark grey shading: greater than 50 % WTOW, thin black line: 45 % contour, thin black dotted line: 40 % contour. b. Percentage of NSDW. c. Percentage of MOW. d. Section plot of potential density (kg m^{-3}). Dashed line: 27.75 kg m^{-3} isopycnal.

As to the southeast of Rosemary Bank in the northern Rockall Trough, isopycnals at intermediate depths are relatively horizontal suggesting little baroclinic flow at this depth (Fig. 7.3.d). However, below about 900 m isopycnals in the far west of the section are raised indicating shear within this area. Again, according to geostrophy, this indicates flow towards the north above the 27.5 kg m^{-3} isopycnal. Investigation of the level of no motion using historical moorings at stations F and M along the Ellett Line section (see Fig. 3.7 for positions) shows flow reversal occurs between approximately 1100 m and 1800 m (Holliday et al., 2000). Additional examination of net transport rates and topography suggests the level of no motion to be around 1200 m (Holliday et al., 2000). Assuming this to be true, deep WTOW and the associated NSDW are flowing southward along the eastern flank of Rockall Bank. Again this is in agreement with the propensity of overflows in the Northern Hemisphere to flow with topography on their right (e.g. Killworth, 2001).

The percentage distribution of MOW in the central Rockall Trough shows a difference east and west of the Anton Dohrn Seamount with MOW again being more dominant in the east (Fig. 7.3.c). However, this difference is less pronounced than that seen in the northern Rockall Trough (Fig. 7.2.c). The thickness of the MOW layer, defined as water containing more than 5 % MOW, is similar throughout the section (~ 400 m) with the exception of stations closest to Rockall Bank where the layer thins to around 250 m. The percentage contribution of MOW is higher to the east of Anton Dohrn (maximum 16 - 17 %) compared to a maximum contribution of 14 - 15 % in the west.

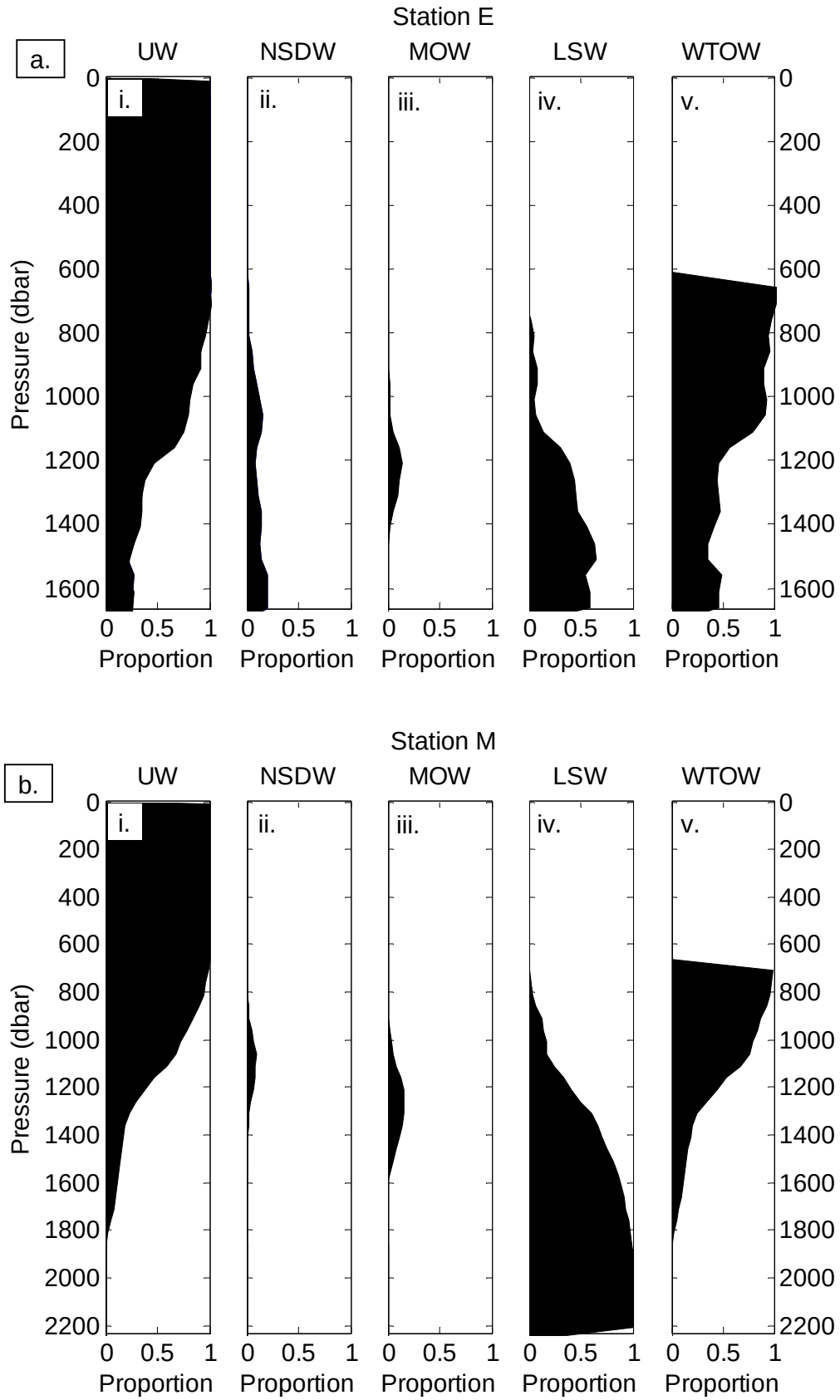

Figure 7.4. Distributions of water types UW (i.), NSDW (ii.), MOW (iii.) and LSW (iv.), and water mass WTOW (v.) with depth for stations E (a.) and M (b.) in the central Rockall Trough. See Fig. 3.7 for station locations.

7.3. Water mass analysis at the northern exits to the Rockall Trough

7.3.1. George Bligh Bank to Lousy Bank

Water in the channel between George Bligh Bank and Lousy Bank (GBB-LB, Fig. 7.1) again shows the presence of WTOW. Using the 50 % contribution contour as the boundary of a water mass (Mamayev, 1975), the water column is composed almost entirely of UW and WTOW with a very thin layer (~ 50 m thick) of the MOW-LSW mixture at the bottom of the channel in the south (Fig. 7.5.a). It should be noted that, due to the vertical interpolation of temperature and salinity on to a regular 50 m vertical grid, the presence of the MOW-LSW layer cannot be established with a large degree of certainty. The UW fills the upper 450 - 700 m of the water column with a layer of WTOW (maximum thickness of ~ 500 m) underlying it. WTOW is piled up both against Lousy Bank to the north and George Bligh Bank to the south creating a layer that is 200 m and 50-100 m higher within the water column respectively.

Comparison with potential density (Fig. 7.5.c.) reveals a similar patter in the 27.4 kg m^{-3} isopycnal. According to geostrophy, water above the 27.4 kg m^{-3} isopycnal flows north-westward on the flank of Lousy Bank and south-eastward on the flank of George Bligh Bank. Assuming a level of no motion at some depth between 600 m and 1000 m, as revealed by historical moorings in the northern Rockall Trough (Table 7.1), flow in at least some of the WTOW is in the opposite direction. Hence, WTOW in the north of the channel flows north-westward towards the Iceland Basin on the flank of Lousy Bank, whilst WTOW in the south of the channel flows south-eastward towards the Rockall Trough. This suggests either a cyclonic circulation within the channel or alternatively an anti-cyclonic circulation around George Bligh Bank to the south. Unfortunately with the current dataset it is not possible to determine which of these two processes dominates.

The 27.5 and 27.6 kg m^{-3} isopycnals (Fig. 7.5.c) do not show the domed shape seen in the 27.4 kg m^{-3} isopycnal, instead only rising in the vicinity of Lousy Bank. Hence, denser WTOW, whilst flowing north-westward in the north of the channel may not exhibit a

return south-eastward flow on the flank of George Bligh Bank suggesting that within the channel a net flux towards the Iceland Basin may occur.

Analysis of NSDW in the channel shows that water with a greater than 5 % contribution of this water mass is limited to the bottom 150 – 200 m (Fig. 7.5.b). The highest contribution of ~ 20 % is observed at the deepest point of the channel. This is similar to the maximum NSDW contribution observed in the central Rockall Trough (Fig. 7.3) but around 5 % higher than the maximum seen in the northern Rockall Trough (Fig. 7.2). The NSDW percentage contribution contours slope slightly towards Lousy Bank to the north. As discussed above it is probable that water denser than 27.5 kg m^{-3}, including that which contains greater than 5 % NSDW, is flowing north-west along the flank of Lousy Bank. As at this density no return south-eastern flow is seen in the south of the channel, water containing greater than 5 % NSDW (the densest WTOW within the channel) is likely to be exiting the Rockall Trough and entering the Iceland Basin. However, there is a possibility that some/all of this water may re-enter the Rockall Trough between Lousy Bank and Bill Baileys Bank if an anticyclonic recirculation exists around Lousy Bank. Again, with the current dataset, it is not possible to tell whether such a circulation does or does not exist.

7.3.2. Rockall Bank to George Bligh Bank

Analysis of a section running between Rockall Bank and George Bligh Bank (RB-GBB, Fig. 7.1) again shows WTOW to be an important water mass. At intermediate depths WTOW forms a layer ~ 700 m thick lying below UW, and at the deepest station above a thin layer of the MOW-LSW mixture (Fig. 7.6.a). The WTOW layer is around 200 m thicker than observed in the central Rockall Trough or in the channel between George Bligh and Lousy Banks (sections 7.2 and 7.3.1 respectively). However, the thickness is comparable to that observed between Rosemary Bank and Bill Baileys Bank in the northern Rockall Trough (section 7.1).

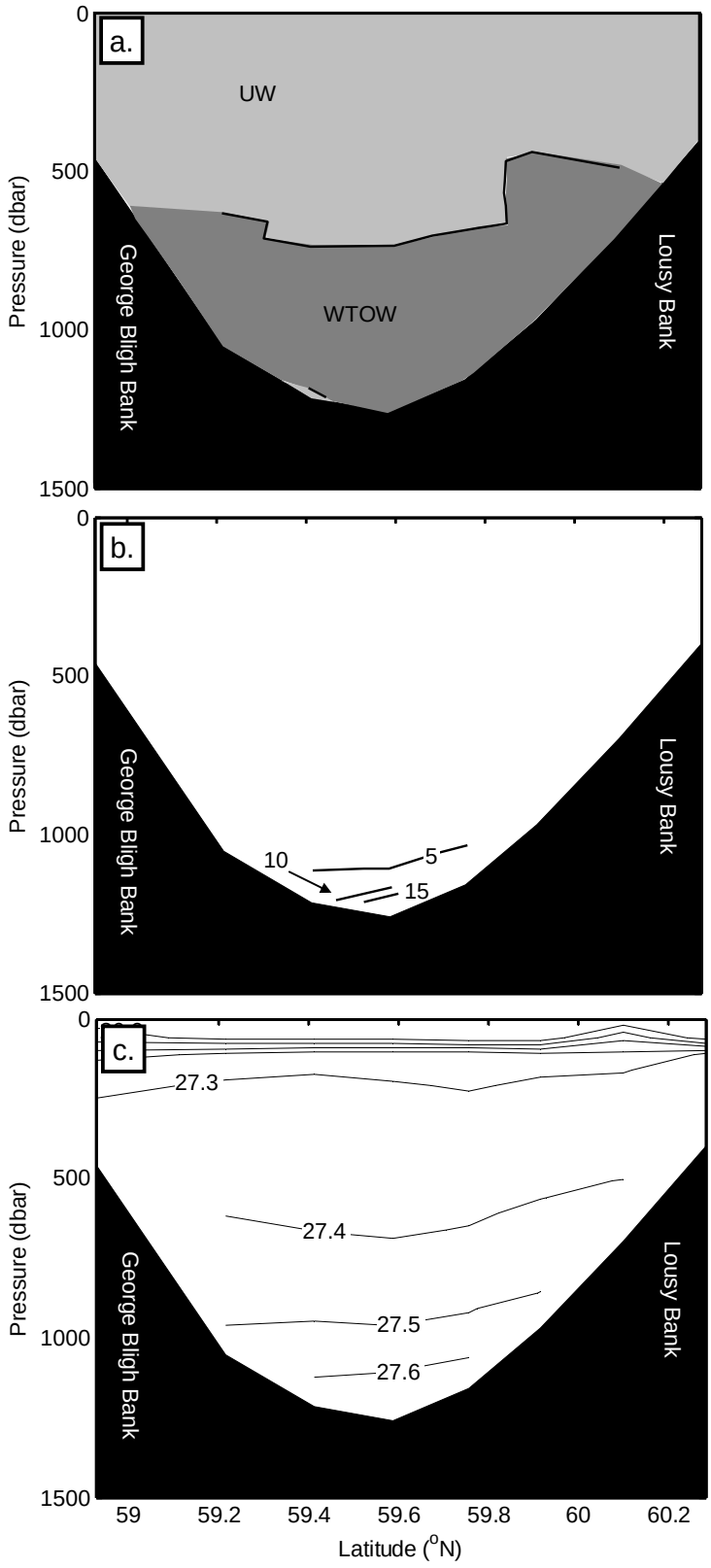

Figure 7.5. Results of water mass analysis on a section between George Bligh Bank and Lousy Bank (GBB-LB, Fig. 7.1). a. Water masses in the channel. Contours: 50 % content; dark grey shading: WTOW; light grey shading: other water masses. b. Percentage contribution of NSDW. c. Potential density section (kg m^{-3}).

The MOW-LSW layer is only observed at the deepest station and is around 100 m thick. It is underlain by another deeper layer of WTOW, this time also with a thickness of about 100 m. To investigate this further, and at a higher vertical resolution, the original potential temperature and salinity data from the deepest station were interpolated onto a 10 m regular vertical grid instead of the usual 50 m spacing. The newly interpolated data were entered into the appropriate mixing model. Outputs show that the separation of the two layers of WTOW by an approximately 100 m thick layer of MOW-LSW is a real phenomenon and not an artefact of interpolation. Below about 900 m the proportion of WTOW (blue line, Fig. 7.6.b) begins to decrease to a minimum of ~ 30 % at around 1150 m. Conversely, the contribution of MOW-LSW (green line, Fig. 7.6.b) increases at the same rate to a maximum of ~ 70 % at 1150 m. Below the minima/maxima at ~ 1150 m WTOW contributions increase to ~ 65 % at the seabed whilst MOW-LSW proportions decrease to ~ 35 % at the same depth. Hence, with the water mass boundary definition set as the 50 % contribution contour (black dashed line, Fig. 7.6.b), the water column between just below 1100 m and just below 1200 m is occupied by the water mass of MOW-LSW rather than WTOW. Below around 1200 m, to the sea bed, however, is composed of a layer of deep WTOW. Water containing greater than 5 % NSDW is confined to the deepest station below ~ 900 m and is predominantly coincidental with the layer of deep WTOW. The maximum contribution of NSDW to the water column of ~ 20 % is just above the seabed.

A section plot of potential density (not shown), shows isopycnals in the channel are mostly horizontal although the 27.4 kg m^{-3} isopycnal (~ 600 m depth) and the 27.6 kg m^{-3} isopycnal (~ 1100 m) rise slightly towards the southern flank of George Bligh Bank. However, this isopycnal slope is less pronounced than observed between George Bligh Bank and Lousy Bank and there is no evidence of eastward flow on the flank of Rockall Bank.

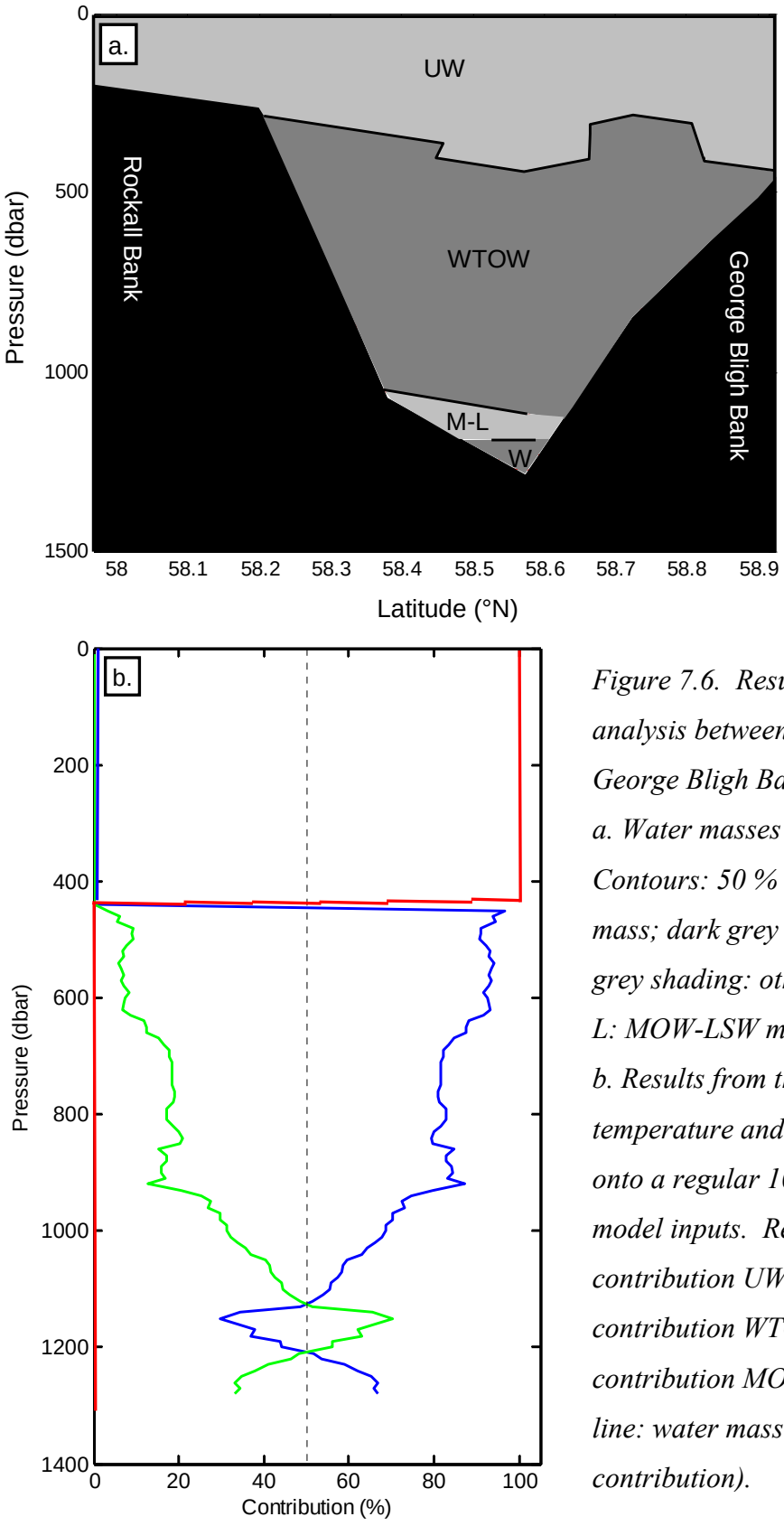

Figure 7.6. Results from water mass analysis between Rockall Bank and George Bligh Bank (RB-GBB, Fig. 7.1). a. Water masses within the channel. Contours: 50 % contribution of water mass; dark grey shading: WTOW; light grey shading: other water masses; M-L: MOW-LSW mixture; W: WTOW. b. Results from the deepest station with temperature and salinity interpolated onto a regular 10 m vertical grid as model inputs. Red: percentage contribution UW, blue: percentage contribution WTOW; green: percentage contribution MOW-LSW; dashed black line: water mass boundary (50 % contribution).

7.3.3. Rockall-Hatton Plateau

Analysis of a section between Rockall Bank and Hatton Bank across the Rockall-Hatton Plateau (RB-HB, Fig. 7.1) again reveals the presence of WTOW (Fig. 7.7.a). The layer containing more than 50 % of this water mass is thinner than observed between Rockall Bank and George Bligh Bank (~ 700 m, Fig. 7.6) but is comparable to that observed in the central Rockall Trough (400 – 500 m, Fig. 7.3). The WTOW layer is approximately 100 m higher in the water column in the west of the section than in the east. Once again WTOW is overlain by UW and underlain by a ~ 100 m thick layer of the MOW-LSW mixture.

The maximum proportion of NSDW observed on the Rockall-Hatton Plateau is 8 % (Fig. 7.7.b) which is around 10 % lower than that observed in the central or northern Rockall Trough or between the northern banks. Water containing greater than 5 % NSDW, rather than forming a layer across the plateau, is present as a parcel of water hugging the south-eastern flank of Hatton Bank.

Examination of the potential density distribution (Fig. 7.7.c) reveals the 27.4 and 27.5 kg m^{-3} isopycnals are domed upwards in the west of the section. This suggests the presence of a cold core cyclonic eddy with the pocket of water containing greater than 5 % NSDW at its centre.

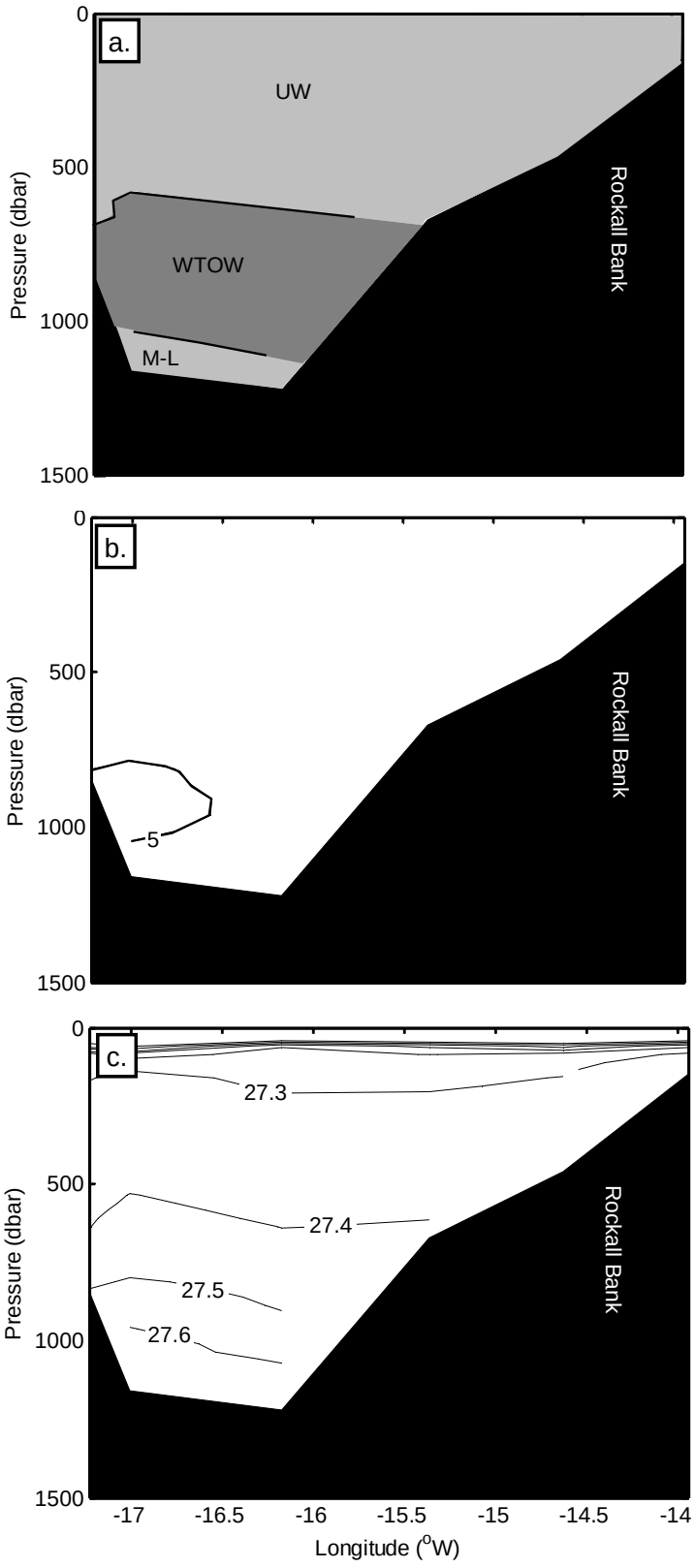

Figure 7.7. Results of water mass analysis between Rockall Bank and Hatton Bank on the Rockall Hatton Plateau (RB-HB, Fig. 7.1). a. Water masses on the plateau. Contours: 50 % content; dark grey shading: WTOW; light grey shading: other water masses. M-L: MOW – LSW mixture. b. Percentage contribution of NSDW. c. Potential density section (kg m^{-3}).

7.4. Water mass analysis using the Ellett Line time-series

To investigate variability of WTOW in the Rockall Trough, water mass analysis was carried out on data from two stations along the Ellett Line: station G to the west of the Anton Dohrn Seamount; and station M to the east (see Fig. 3.7 for station locations). This enabled any differences between the eastern and western trough to be examined in addition to temporal variability. Station G has a depth of ~ 1800 m whilst station M lies in deeper water of ~ 2300 m. Although water at station G is sometimes influenced by deep WTOW, such as the extreme example of 2006 (Fig. 7.3), this is relatively infrequent and usually limited to the bottom 200 m of the water column. The decision was therefore made to exclude deep WTOW from the analysis. Hence, below the intermediate salinity inflexion (ISI, Fig. 6.6; mean depth ~ 1200 m) the proportions of WTOW and NSDW at station G can be considered as the lower bound whilst the proportion of MOW is the maximum possible contribution.

Water containing greater than 50 % WTOW (all shading, Fig. 7.8) is present at both stations G and M throughout the Ellett Line record. The water mass occupies intermediate depths, centred upon approximately 1000 ± 100 m, and with a mean thickness of about 350 m. Water with over 75 % WTOW (mid and dark grey, Fig. 7.8) is present throughout the majority of the time-series in both the eastern and western trough. At station G, water with a minimum contribution of 75 % WTOW is present continually between the start of the record and 1985, during the late 1980s, and between 1995 and 2008. Between 1990 and 1995 the layer is present but not continuous (Fig. 7.8.a). In the eastern trough, at station M, water containing more than 75 % WTOW forms a continual layer for nearly the entire record with the exception of 1980-1982 and 1986 (Fig. 7.8.b). The highest percentage contribution of WTOW (> 95 %, dark grey, Fig. 7.8) is seen at the start of the record, especially at station G, and from around 2000 to 2005 in both sides of the trough. It is important to note that water with a large percentage contribution of WTOW will not necessarily have an identifiable intermediate salinity inflexion in θ-S space. For example, data lying close to line UW(l) – LSW(u) within the intermediate water mixing triangle (Fig. 6.5.b) will contain between 0 and 100 % WTOW ($P_{WTOW}{}^{i}$ = 0 – 1, Fig. 6.5.b). The mixing model assumes that UW and LSW cannot mix directly due to the presence of WTOW and the MOW-LSW mixture separating the two water masses vertically.

However, WTOW and MOW-LSW may mix together. For water to lie upon line UW(l) – LSW(u), the intervening WTOW and MOW-LSW layers must have mixed to such an extent that the crossover point has been completely eroded. Hence, although no intermediate salinity inflexion will be observed, water still contains the influence of both WTOW and the MOW-LSW mixture.

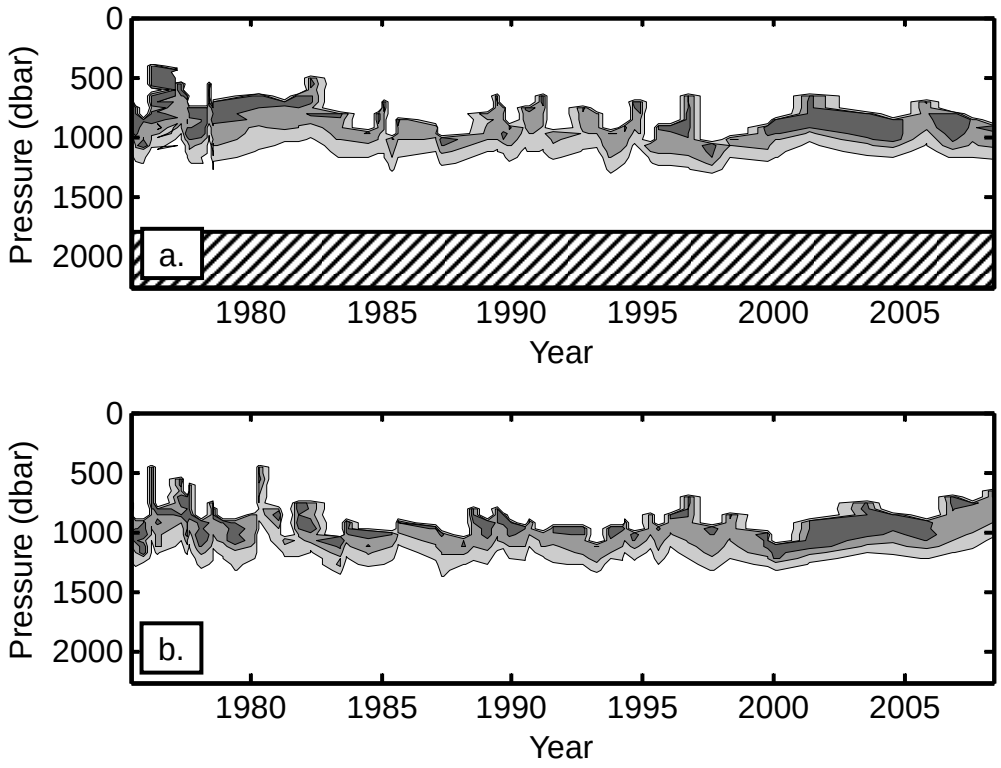

Figure 7.8. Percentage contribution of WTOW at a. station G and b. station M along the Ellett Line. Light grey: water containing between 50 and 75 % WTOW; mid grey: water containing between 75 and 95 % WTOW; dark grey: water containing greater than 95 % WTOW; hashed area: seabed.

A different method to view the data, which partly takes into account the strength of the intermediate salinity inflexion, is the percentage contribution of NSDW. Water containing greater than 5 % NSDW (all shading, Fig. 7.9) is seen between 500 and 1300 m, although as noted above in some years at station G there will be some NSDW influence below this depth not shown in the analysis. In both the eastern and western trough, a distinctive feature is the prevalence of water containing > 5 % NSDW both at the start of the record until 1978, and in the 2000s. Between 1975 and 1978 it appears that NSDW forms a larger

proportion of intermediate water at station G than at station M, whilst in the 2000s this distribution is more even between the eastern and western trough. It should be noted, that as instrumental variability decreased in 1992 when a *Sea-Bird 911+* CTD started to be used (Fig. 5.5), confidence in the accuracy of the results increases after this date. In the eastern trough (Fig. 7.9.b) water containing > 5 % NSDW is seen at intermediate depths from 1999 to 2008, and a proportion > 10 % between 2001 and 2006. At station G to the west (Fig. 7.9.a), water with a percentage contribution of NSDW > 5 % is seen between 2000 and 2008, whilst water containing > 10 % is observed between 2001 and 2005, and again in 2006. Water containing a minimum contribution of 5 % NSDW is also seen in the early and late 1980s, both east and west of the seamount, and in the late 1990s particularly at station G although this is patchier than that seen post 2000.

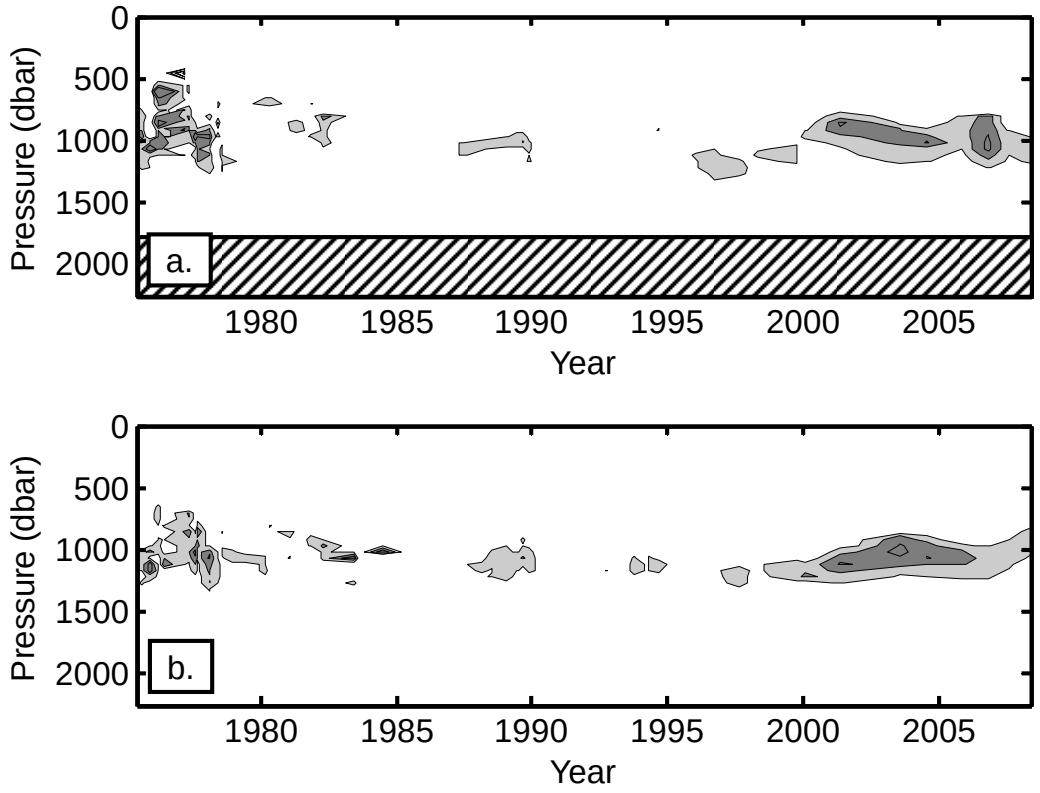

Figure 7.9. Percentage contribution of NSDW at a. station G and b. station M along the Ellett Line section. Light grey shading: water containing between 5 and 10 % NSDW; dark grey shading: water containing more than 10 % NSDW; hashed area: seabed.

The distribution of water containing greater than 5 % MOW (Fig. 7.10) shows that this water mass's influence is deeper in the water column than that of NSDW (excluding the influence of deep WTOW) being centred upon ~ 1300 m. Again a prominent feature at both station G and M is the prevalence of MOW in the later stages of the record. At station G water containing greater than 5 % MOW (all shading, Fig. 7.10.a) is observed between 1996 and 2000, and from 2001 until the end of the record in 2008. Water with an influence of more than 10 % MOW (dark grey, Fig. 7.10.a) is seen in 1996 and again between 2002 and 2007. Prior to 1996 the distribution is patchier, especially between 1983 and 1996. At station M in the eastern Rockall Trough, water with a minimum contribution of 5 % MOW (all shading, Fig. 7.10.b) forms a continual layer between 1992 and the end of the record in 2008. Water containing > 10 % MOW (dark grey, Fig. 7.10.b) is seen between 2001 and 2007 and again in 2008. Prior to 1992 water containing at least 5 % MOW was temporally irregular and between 1978 and 1987 almost absent from the record.

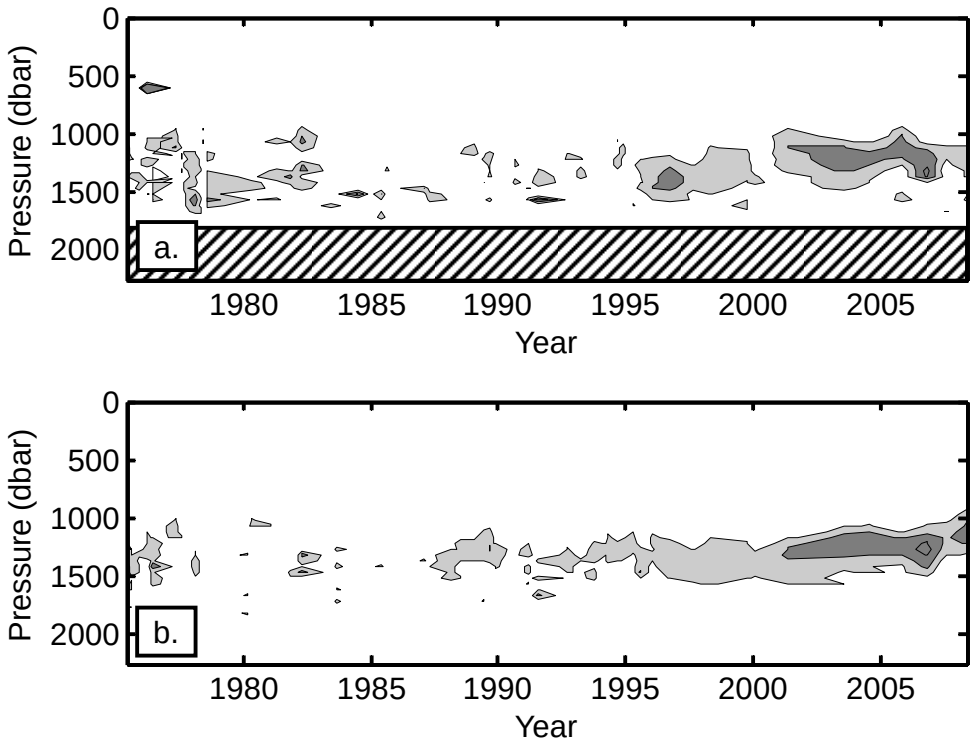

Figure 7.10. Percentage contribution of MOW at a. station G and b. station M along the Ellett Line. Light grey shading: water containing between 5 and 10 % MOW; dark grey shading: water containing greater than 10 % MOW; hashed area: seabed.

7.5. Summary

Water mass analysis has shown that WTOW is important in the northern and central Rockall Trough. At intermediate depths WTOW is present in both the eastern and western trough in a layer with weak baroclinic flow. Deep WTOW, however, is confined to the west with geostrophy indicating southward flow. Isopycnal analysis also indicates the flow of WTOW out of the Rockall Trough into the Iceland Basin. The spatial distribution of NSDW is similar to the pattern for WTOW, with the highest percentage contribution observed in the west of the Ellett Line during a particular strong overflow event. At this time, water at ~ 1700 m on the eastern flank of Rockall Bank was composed of nearly one quarter NSDW, in addition to LSW and UW. The distribution of MOW shows this water mass to lie around 250 m lower in the water column than NSDW and the associated intermediate WTOW.

Comparison of the time-series from two stations along the Ellett Line reveals the continuous influence of WTOW within intermediate waters of the Rockall Trough since 1975. However, this does not indicate that a strong intermediate salinity inflexion point was present throughout this period. A particularly prominent feature is the persistent nature of NSDW and MOW in the late 1990s and 2000s. This, and other results from both the mixing models and visual analysis of physical and chemical data, are discussed in the following chapter.

Chapter 8.
Discussion

This chapter provides an overall discussion of the results presented within this thesis. First, Al concentrations within the Rockall Trough and the applicability of Al as a water mass tracer are discussed. Next, the composition of WTOW is examined before its pathways within the basin are considered. Finally, the temporal variability of water masses along the Ellett Line are discussed and possible explanations, including variability in the Subpolar Gyre, suggested.

8.1. Aluminium in the Rockall Trough

8.1.1. Concentrations in different water masses

This work presents the first Al measurements from the Rockall Trough; hence a direct comparison with previously published data from this basin is not possible. During H44-04-12 however, Al data were collected south of the Rockall-Hatton Plateau (cyan rectangle, Fig. 4.9) in the vicinity of profiles published by Lunel (1990). A comparison between these two data sets shows an excellent agreement (Fig. 8.1) with similar magnitudes and patterns of Al concentrations observed in both surveys. This not only suggests that the data have a high accuracy, but also that Al concentrations may remain relatively constant in some water masses temporally. Several measurements of reactive Al levels have been made in upper waters of the eastern subpolar North Atlantic between 1989 and 2006 (Table 8.1). Agreement between various sources is good with all reported concentrations less than 8-10 nM despite the temporal and spatial differences in surveys. Although there is variability in the minimum values reported (1-5 nM) this is likely to be related to differences in minimum sample depth, levels of dust input, and the amount of Al removal from the surface waters. Results reported in this thesis compare well with previously published estimates (Table 8.1), again giving confidence in the quality of the data.

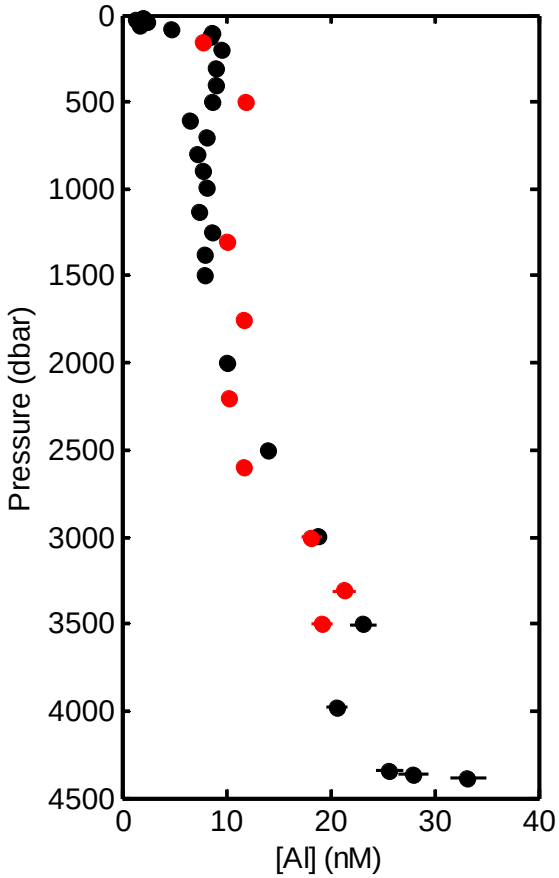

Figure 8.1. Reactive aluminium (nM) profiles from south of the Rockall Hatton Plateau. Black: Lunel (1990); red: H44-04-12. See cyan rectangle, Fig. 4.9 for station positions. Error bars, indicating total errors, are shown although for the majority of data points these are too small to be seen.

Location of samples	**[Al] (nM)**	**Reference**
Exit Faroe Bank Channel	3-7	D. Hydes (unpublished data)
Exit Faroe Bank Channel	2-7	(Hall and Measures, 1998)
Iceland Basin	5-8	D. Hydes (unpublished data)
Iceland Basin	1-8	(Hall and Measures, 1998)
Iceland Basin	3-10	(Measures et al., 2008)
Iceland Basin	2-7	(Lunel, 1990)
Iceland Basin	1-8	This study (H44-04-12)
south of Rockall Hatton Plateau	1-8	(Lunel, 1990)
south of Rockall Hatton Plateau	< 10	This study (H44-04-12)
Rockall Hatton Plateau	2-10	(Lunel, 1990)
Rockall Trough	1-8	This study (H44-04-12, CD176, D312)

Table 8.1. Reported values for reactive aluminium concentrations (nM) in upper waters within the eastern subpolar North Atlantic, with the exception of Measures et al. (2008) who report dissolved concentrations. Reactive and dissolved concentrations are very similar in upper waters in the subpolar North Atlantic (Hall and Measures, 1998).

South of the Rockall Trough, MOW is observed as a salinity (e.g. Reid, 1979; Ullgren and White, 2010) and Al (Lunel, 1990; Hall and Measures, 1998) maximum below the upper waters. Data from the southern entrance to the Rockall Trough (Fig. 5.13.b) indicate that this peak in reactive Al concentrations persists to at least 52.3 °N, as does the salinity signature. Several previous studies using θ and S have shown that MOW can be traced to 52-54 °N in the eastern North Atlantic (e.g. Holliday et al., 2000; McCartney and Mauritzen, 2001; New and Smythe-Wright, 2001) although the extent of its northward penetration may be linked to the strength of the Subpolar Gyre (Lozier and Stewart, 2008; Bozec et al., 2011). Unfortunately, as no Al samples were collected between 52.3 °N and 57.5 °N in the Rockall Trough, we are unable to comment about the degradation of the MOW Al signature. However, it seems logical to presume that as the salinity signature is eroded the Al signature undergoes a similar dilution. Indeed, a comparison between salinity and Al concentrations at the core of the MOW water mass throughout the eastern subpolar North Atlantic suggests that this is the case (Fig. 8.2). Further, mixing is linear indicating conservative behaviour of Al within this water mass.

A mid-depth Al peak of ~ 8 nM is observed in the central Rockall Trough at around 1100-1200 m (Fig. 5.15) where the WTOW and MOW-LSW mixing lines intercept. As water mass analysis reveals the core of MOW at 57.5 °N to lie 100-200 m below this maximum (Fig. 7.10), it suggests that the intermediate Al peak in the central trough cannot be fully attributed to MOW. Further, as the core of NSDW is found at around 1000-1100 m at this latitude (Fig. 7.9), slightly higher in the water column than the Al peak, it suggests that this water mass cannot entirely explain the presence of the Al maximum either. Hence, it is proposed that the mid-depth Al peak is maintained by the presence of both NSDW (and therefore WTOW) and MOW within the central Rockall Trough. The mean contributions (plus one standard deviation) of MOW and NSDW at the depth of the intermediate Al maximum during 2005 and 2006, are 7 ± 4 % and 9 ± 4 % respectively. These values, obtained from the mixing models, are similar and within the errors associated with the method. However, as MOW has a lower Al concentration than NSDW (Table 2.1), it is likely that WTOW is slightly more important to the presence of the mid-depth Al peak than MOW in the central Rockall Trough. No difference is seen between east and west of the Anton Dohrn Seamount.

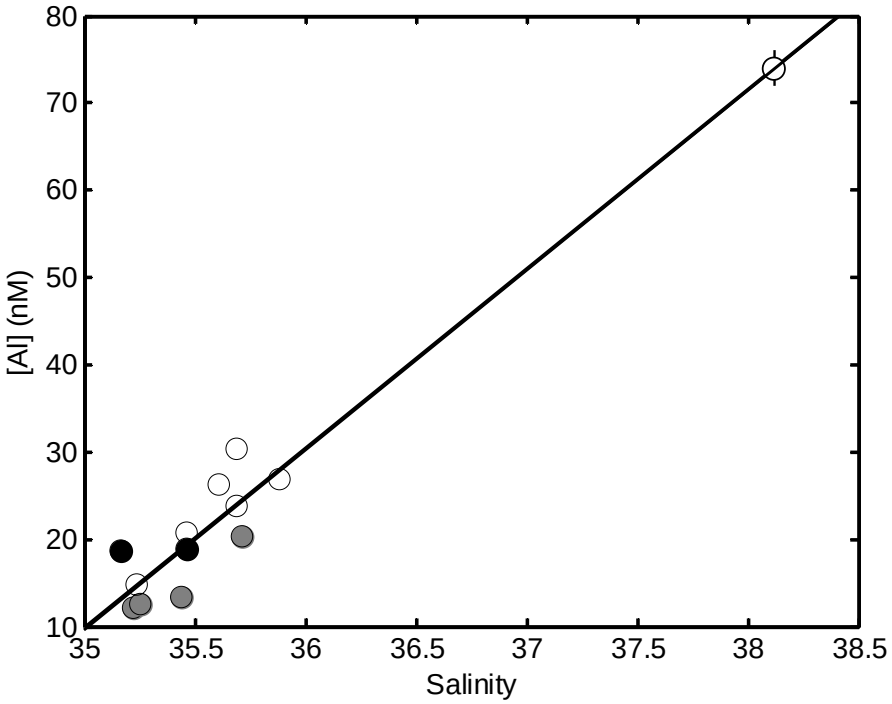

Figure 8.2. Dissolved (white) and reactive (grey) aluminium concentrations at the salinity maximum associated with MOW, against salinity (r = 0.98). Black circles show reactive data from H44-04-12. Data points come from throughout the eastern subpolar North Atlantic from de Jong et al. (2007), Hall and Measures (1998), Lunel (1990), Measures (1995) and Measures and Edmond (1988). Dissolved and reactive concentrations in MOW in the Iceland Basin are almost identical (Hall and Measures, 1998). Data from Hydes (1983) are not shown as concentrations are artificially low due to scavenging of Al onto bottle surfaces (Lunel, 1990). Error bars (indicating total errors associated with the method) are shown although for the majority of data points these are too small to be seen.

Measurements from two stations in the Iceland Basin report dissolved Al concentrations of 4.4 nM at the depth of the LSW core (Hall and Measures, 1998); at these depths reactive and dissolved values are almost identical. Low concentrations within this water mass are also described by Lunel (1990) using data from the south-eastern Iceland Basin. Data collected during H44-04-12 in the southern Iceland Basin agree extremely well with concentrations of around 5 nM at the LSW core. Further, data collected in the southern and central Rockall Trough during H44-04-12, CD176 and D312 show values of 3-7 nM within LSW. This slightly wider range may be related to the possibility that LSW enters the Rockall Trough in pulses with gradual erosion of the stagnant pool in between renewal episodes (Holliday et al., 2000; New and Smythe-Wright, 2001). As isolated LSW within

the trough mixes with water above and below (MOW and AABW), both of which have higher Al concentrations, one would expect Al levels within LSW to increase. Conversely, younger and fresher LSW is likely to have lower Al concentrations. This basic relationship however assumes that Al concentrations within LSW are relatively constant with time. Although the similarity of our measurements in the Iceland Basin to those of Hall and Measures (1998) suggests this may be the case there is insufficient evidence to prove or disprove this assumption.

No previously published Al concentrations for SAIW or AABW within the subpolar North Atlantic exist; hence, this study increases the current knowledge. Aluminium measurements within AABW in the southern Atlantic, however, report concentrations of 5-10 nM (Measures and Edmond, 1990; Measures, 1995), which are lower than our reported values from the southern Rockall Trough (10-15 nM; Table 2.1). This increase may result from mixing with overlying NADW and its associated higher Al concentrations as the AABW moves northward. This process has been observed in the South Atlantic (Measures and Edmond, 1990). Another possibility is that Al is added to AABW from the seabed, either via sediment resuspension which is thought to be important in areas of high flow rates (e.g. Lambert et al., 1984; Hall and Measures, 1998), or other diagenetic processes. Further work is required to resolve whether Al exhibits conservative behaviour or not in AABW within the North Atlantic.

Although the concentration of Al has been quantified in water exiting the Faroe Bank Channel and overflowing the Denmark Strait, this work presents the first determination of levels in WTOW. Reactive Al concentrations in DSOW are relatively low (~ 6.5 nM) whilst levels in the densest water exiting the Faroe Bank Channel are greater than 20 nM (Hall and Measures, 1998). As dissolved Al concentrations in the bottom water of the Faroe Bank Channel are much lower (13.1 nM) than reactive concentrations, it appears that sediment resuspension in the Faroese Channels is important in giving the overflow its high Al signature (Hall and Measures, 1998). Reactive Al levels are also elevated in WTOW within the Rockall Trough with the highest concentration of 14 nM measured in deep WTOW in the far west of the basin (Fig. 5.15). Unfortunately, no dissolved measurements were made; hence, we cannot say whether WTOW also has elevated reactive Al concentrations relative to dissolved levels. However, from mixing analysis it is estimated that this dense WTOW in the Rockall Trough was composed of 41 % WTOW, 18 %

MOW and 41 % LSW. Assuming MOW and LSW have reactive Al concentrations of 19 nM and 3-7 nM respectively (Table 2.1); this gives an Al level of 18-22 nM in undiluted WTOW. Silicate and dissolved Al values suggests that deep water exiting the Faroe Bank Channel originates from around 1100 m in the Norwegian Sea (Hall and Measures, 1998). Silicate data from the Wyville Thomson Ridge crest agrees with this finding, although it should be noted that this conclusion assumes that no silicate is added to the deep waters as they flow through the Faroese Channels. As reactive Al concentrations at 1100 m in the Norwegian Sea are around 13 nM (Hall and Measures, 1998), it appears that sediment resuspension is not only important to the Al signature of deep WTOW exiting the Faroe Bank Channel, but also possibly to WTOW. Further evidence for this is the observation of higher beam attenuation, which can be indicative of elevated suspended sediment levels, in the precursor to WTOW on the northern flank of the Wyville Thomson Ridge. This increased beam attenuation is coincidental with increases in reactive Al concentrations further suggesting the elevated signal is due to bottom sediment resuspension.

8.1.2. Examination of conservative behaviour

Although it is clear that Al concentrations vary between the water masses within the eastern subpolar North Atlantic, and that it may act conservatively in some water bodies, further investigation into its behaviour in the Rockall Trough is required. In order to do this, estimated Al concentrations were calculated using the same method as that used to predict CFC concentrations (equation 6.59), but with Al values of constituent water masses (Table 2.1) used as inputs instead of CFC levels. As the calculation assumes that advection and mixing are the only controls on Al distribution within the Rockall Trough, a comparison between predicted and observed values allows the conservative nature of Al to be examined. Predicted Al concentrations (Fig. 8.3.a) are lowest in the upper waters (< 5 nM) before increasing to a mid-depth peak (7-8 nM) centred on 1200 m. This maximum is coincidental with the bottom of the intermediate WTOW layer and top of the MOW-LSW layer. The layer of water containing greater than 7 nM of Al is around 250 m thick east of the Anton Dohrn Seamount but is considerably thicker in the far west of the trough (~ 500 m). Below this Al maximum concentrations in the eastern part of the trough decrease to 5-7 nM in the deep water, whilst values in the west are elevated in the layer corresponding to deep WTOW (7-9 nM). Observed concentrations (Fig. 8.3.b) are remarkably similar to

predicted concentrations, with the exception of high values in bottom samples which are probably linked to a source from the seabed. These data points were ignored during contouring to allow other general trends to be seen more easily. The magnitudes of predicted and observed concentrations match extremely well indicating that mixing and advection dominate Al distribution within the central Rockall Trough. Any other removal or input mechanisms must therefore be small, or completely balanced which seems unlikely. Hence, Al, away from the seabed, appears to behave conservatively in agreement to previous observations (Measures and Edmond, 1990; Measures and Edmond, 1992; Hall and Measures, 1998). Patterns of Al distribution also appear to agree well between the observed and predicted values, particularly the higher Al concentrations in deep water in the western trough relative to those values east of the Anton Dohrn Seamount.

8.1.3. Applicability as a water mass tracer

For a substance to be a valuable water mass tracer various conditions must be met. Perhaps most importantly, although the tracer does not have to behave conservatively distribution within the ocean must be strongly related to advection and mixing with differing concentrations between water masses. The substance must also be relatively easy to measure accurately and with a greater precision than the variability between water masses. Finally, additional information must be revealed from the tracer that is not available by less costly and easier means.

Aluminium concentrations within the eastern subpolar North Atlantic vary between water masses over one order of magnitude (2-25 nM, Table 2.1), and away from the seabed Al appears to behave conservatively. There is also the possibility that Al is non-conservative in the mixed layer of the surface ocean due to active uptake and passive scavenging on biological material. However, we have insufficient data to comment on this. Although some problems with analysis were experienced (section 4.4) comparison between our data and that previously published within the subpolar North Atlantic is very encouraging, as are the results from the interlaboratory comparison study (Table 4.2). Results from this initiative indicate a high level of accuracy, but poorer precision than the consensus values which may at least partly be explained by the less sophisticated analysis method chosen for this work. Despite this, precision values for our method (0.5-2.0 nM) are much lower than

the variability of Al concentrations between water masses. Hence, a cheap and relatively easy method exists for the analysis of Al in seawater that results in data of an acceptable quality for use as a water mass tracer in the subpolar North Atlantic.

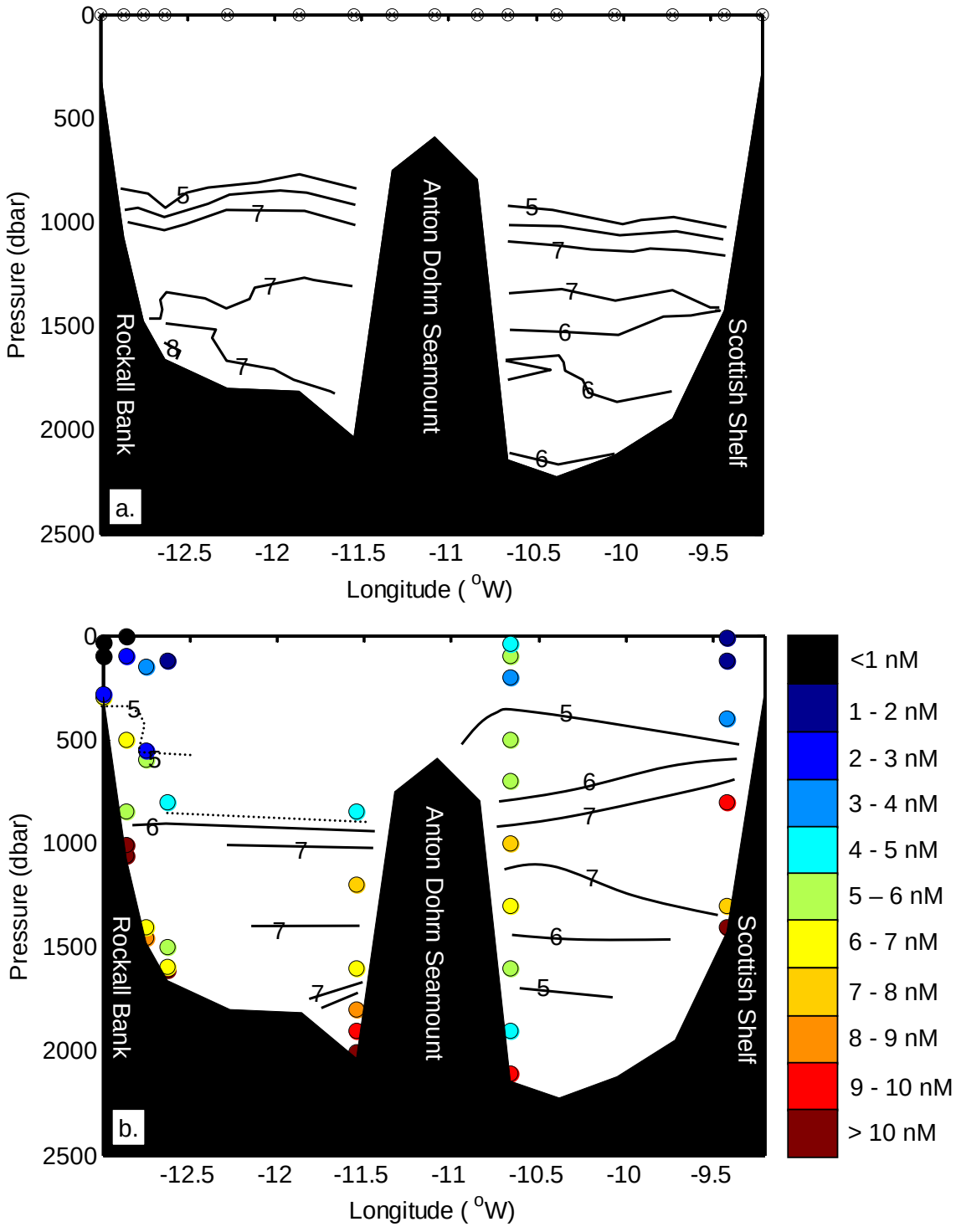

Figure 8.3. Predicted (a.) and observed (b.) aluminium distribution across the Ellett Line in 2005. Contours in b. were added by hand and ignore elevated aluminium concentrations in bottom samples. See Fig. 7.1 for section location.

Aluminium appears to be a particularly good water mass tracer of MOW and deep waters from the Faroese Channels, including WTOW, due to their elevated concentrations. The maxima associated with these water masses appear to persist for large distances and Al seems to behave conservatively. Whilst the mid-depth Al peak appears to be linked to both the presence of MOW and WTOW at that depth, deep WTOW is also clearly seen as increased Al levels in the far west of the trough (Fig. 5.15). Although no information was obtained from the Al data that was not available from other measurements, the Al data confirmed the presence of MOW and WTOW within the central Rockall Trough. As such, the value of Al as a water mass tracer, and its ability to be used in this manner, has been established. This paves the way for future work, perhaps using Al to help further identify the fate of MOW within the Rockall Trough, or its use as an additional quasi-conservative variable within water mass analysis.

8.2. Composition of WTOW

Chlorofluorocarbon data (CFC-11 and CFC-12) collected in the central Rockall Trough in 1997 and 1998 reveal that, in these years at least, NSAIW is not an important component of WTOW (section 5.8). Additionally, water properties on the northern flank of the Wyville Thomson Ridge and in the northern Rockall Trough, do not show the characteristic salinity minimum associated with MEIW (section 5.2.2). Hence, pure WTOW appears to be a mixture of upper waters and NSDW only. As NSDW is the deepest water mass within the Faroese Channels it is somewhat surprising that NSDW is the principal dense component of WTOW rather than the shallower NSAIW and / or MEIW. Surveys across the Wyville Thomson Basin to the north of the ridge, however, reveal that isopycnals at intermediate depths in the channel are pinched in the vicinity of the ridge (Mauritzen et al., 2005). The MEIW and NSAIW layers are therefore thin in the south of the basin near the Wyville Thomson Ridge and thickest towards the Faroe Islands to the north. Thus, the volume of MEIW and NSAIW available to overflow the ridge and enter the Rockall Trough are relatively small. At the same time isopycnals corresponding to the NSDW layer within the Wyville Thomson Basin are clearly seen to uplift in the vicinity of the ridge to above the crest depth (Mauritzen et al., 2005; Stashchuk et al., 2011). Hence, there is clear evidence that NSDW, rather than NSAIW or MEIW, is the

main cold northern water mass to overflow the Wyville Thomson Ridge and enter the northern Rockall Trough.

8.3. Spatial distribution and pathways of WTOW

This work comprehensively places WTOW within the Rockall Trough for the first time. It is suggested that there are two branches of WTOW: a non-specific intermediate branch which is seen in both the east and west of the trough; and a flow of denser WTOW observed only in the west.

8.3.1. Intermediate WTOW

The flow of intermediate WTOW, lying between 600-1200 m, can be inferred from the intensity of the intermediate inflexion point (section 5.6) and from isopycnal analyses (Chapter 7). In the northern Rockall Trough, to the north of Rosemary Bank, isopycnals indicate that at least some of the intermediate WTOW flows westward (arrows, Fig. 8.4). Further south in the western central trough, baroclinic flow at the depth of the intermediate WTOW appears to be weak although examination of the strength of the inflexion point suggests that net flow of the water mass is from north to south in this area. The slight erosion of the lower oxygen layer in the far west of the trough, between 800 m and 1200 m (section 5.7), implies an increased flow rate of intermediate WTOW near to Rockall Bank. Given the propensity for currents to hug topography on their right in the Northern Hemisphere (Killworth, 2001), it is highly likely that this flow is southward.

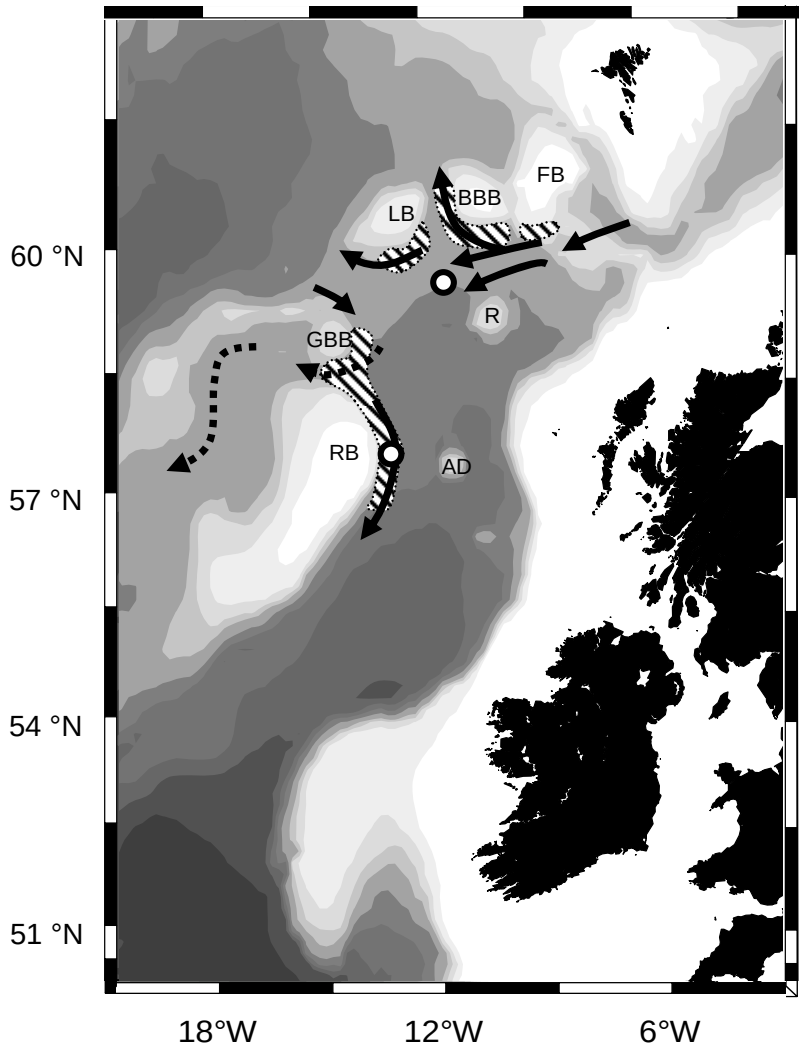

Figure 8.4. Summary of WTOW circulation within the Rockall Trough. Solid arrows: clear flow pathways; dotted arrows: less clear flow pathways. It should be noted that because of the possibility of recirculations, the arrows do not necessarily represent a net flux of WTOW. Also provided for comparison: approximate areas where bedforms indicate flow of WTOW (hatching) and approximate location of previous hydrographic observations of overflow water in the trough (white circles). See text for references. Although a clear signature of intermediate WTOW is observed in the eastern Rockall Trough (Fig. 5.9.a), circulation patterns within this area remain unclear. AD: Anton Dohrn Seamount; BBB: Bill Baileys Bank; FB: Faroe Bank; GBB: George Bligh Bank; LB: Lousy Bank; R: Rosemary Bank; RB: Rockall Bank. Contours are every 500 m from 500 m to 3000 m and at 4000 m.

Intermediate WTOW is observed in the channel between Bill Baileys Bank and Lousy Bank and is thought to be flowing towards the Iceland Basin. Although there is the possibility of anti-cyclonic recirculations of WTOW around banks to the south, a circulation of WTOW around Bill Baileys Bank is unlikely because of the shallow channel between Bill Baileys Bank and Faroe Bank to the north. At < 600 m this channel is not deep enough to enable WTOW to either exit from or re-enter the Rockall Trough. Indeed, θ-S profiles between Bill Baileys Bank and Faroe Bank only show a signature of the upper Atlantic Waters (Fig. 5.9.a). Hence, as WTOW exiting the Rockall Trough between Lousy Bank and Bill Baileys Bank is unlikely to re-enter the Rockall Trough it represents a net advection of the water mass from the Rockall Trough into the Iceland Basin to the west.

Further south, between George Bligh Bank and Lousy Bank, the distribution of WTOW (Fig. 7.5.a) and isopycnal analysis (Fig. 7.5.b) suggests westward flowing WTOW in the north of the channel with eastward flowing WTOW to the south. This may represent a cyclonic recirculation within the channel, or alternatively an anti-cyclonic recirculation around George Bligh Bank with the water in the south of the channel indicating WTOW that is re-entering the trough. Unfortunately the current dataset is unable to identify which of the two possibilities dominates. Additionally, although an anticyclonic circulation of upper waters has been observed around Rockall Bank (Dooley, 1984 in Dickson et al., 1986) and Faroe Bank (Hansen et al., 1986) no such work has been carried out around the other western banks of the Rockall Trough. Hence, it is unknown whether flow between George Bligh Bank and Lousy Bank represents a net westward flux into the Iceland Basin or not.

The question of whether an anticyclonic circulation may exist around Lousy Bank is also raised. Although interpretation of the sediments between Lousy Bank and Bill Baileys Bank clearly shows evidence of WTOW flowing northwards along the flank of Bill Baileys Bank, no reciprocal signature is observed in the west of the channel (Kuijipers et al., 1998). As this is the area where one would expect WTOW to re-enter the trough if a recirculation existed around Lousy Bank, it suggests that any recirculation around this particular bank is weak or non-existent. Certainly the sediments suggest that the flow of WTOW out of the trough between Lousy Bank and Bill Baileys Bank is stronger than any possible re-entry of the water mass in the west of the channel. This again suggests that a

net advection of WTOW from the Rockall Trough into the Iceland Basin exists between Lousy Bank and Bill Baileys Bank.

A signature of WTOW is also observed on the Rockall-Hatton Plateau. Despite the relatively horizontal isopycnals between George Bligh and Rockall Banks (Fig. 7.6), it is assumed that the water mass flows from the trough onto the plateau. This flow may possibly be intermittent or related to eddy activity; indeed a cold core eddy with WTOW at its core was observed on the Rockall-Hatton Plateau (Fig. 7.7). As the intensity of the intermediate salinity inflexion decreases from north to south on the plateau southward flow of WTOW is inferred in this area. Again the possibility of a recirculation around Rockall Bank or Hatton Bank needs to be considered. As no signature of WTOW is observed on the western flank of Rockall Bank (Fig. 5.9.a) recirculation around this feature seems unlikely. However, a weak recirculation around Hatton Bank with WTOW re-entering the Rockall-Hatton Plateau cannot be discounted.

Although there is a clear signature of intermediate WTOW in the eastern Rockall Trough (blue circles, Fig. 5.6), it is unclear how the water mass enters this area. Three possibilities are suggested: transport via a cyclonic recirculation; transport through eddies; or forcing of WTOW into the eastern trough due to blocking by an intensifying or weakening Subpolar Gyre.

A cyclonic recirculation is observed in LSW with northward flow in the eastern Rockall Trough (New and Smythe-Wright, 2001). Additionally, as the MOW-LSW layer originates from the southern trough, one would expect it to flow northwards in the eastern trough. Hence, although we have no evidence for a recirculation, indeed isopycnals suggest low baroclinic flow in the eastern trough; a cyclonic recirculation of intermediate WTOW cannot be discounted. In contrast, there have been several observations of cold core eddies in both the eastern and western Rockall Trough from float (Shoosmith et al., 2005) and recent Seaglider data (T. Sherwin, personal communication). A cold core eddy in the north-western trough was identified to have WTOW at its core with the water mass present between the bottom of the ENAW layer and the seabed (~ 1500 m) at the majority of stations (Ellett et al., 1983). An eddy comprising of WTOW was also identified on the Rockall-Hatton Plateau during this study (section 7.3.3). Further, modelling studies suggest that cold core eddies are formed in the Ymir Trough and Cirolana Deep (Stashchuk

et al., 2010; Stashchuk et al., 2011). The pathways of eddies that do not extend to the bottom of the water column are not controlled by bathymetry (Richardson et al., 2000), suggesting some eddies could enter the eastern trough. As the eddies decay the WTOW within their core may spread to fill the intermediate water column, creating a relatively stagnant layer such as that observed in the area.

The third possibility is that intermediate WTOW may be forced to flow into the eastern Rockall Trough due to blocking by an intensifying or weakening Subpolar Gyre. As the Subpolar Gyre weakens and contracts, such as in the late 1990s, the eastern limb moves westwards (Johnson and Gruber, 2007) allowing increased transport of MOW into the subpolar North Atlantic (Lozier and Stewart, 2008; Bozec et al., 2011). Conversely, as the Subpolar Gyre strengthens and expands eastwards, MOW transport northwards is reduced due to blocking by subsurface components of the Subpolar Front (Lozier and Stewart, 2008; Bozec et al., 2011). A similar mechanism is proposed for WTOW. As the Subpolar Gyre expands eastward, the waters of the western trough will be influenced prior to those further east. Similarly, as the Subpolar Gyre contracts westwards, waters in the west will be influenced by subpolar waters for longer than those to the east. As such there may be a period when the pathway of intermediate WTOW is blocked in the western trough but not to the east, forcing the water mass to flow into this part of the basin. The strength of the Subpolar Gyre decreased between 1995 and 1999 with a subsequent weakening from 2001 to 2004 (Fig. 2.5), after which the gyre strengthened (Hakkinen and Rhines, 2009). Interestingly, at the start of this period (with a 2-3 year lag), water containing > 5 % NSDW at intermediate depths is observed first at station M in the eastern trough and then 1-2 years later further west at station G (light grey shading, Fig. 7.9). This is consistent with what one might expect from a contracting Subpolar Gyre blocking WTOW in the western trough. Further links between the Subpolar Gyre and WTOW distribution in the Rockall Trough are discussed in section 8.4. Although three possible mechanisms by which intermediate WTOW enters the eastern trough have been proposed, further work is needed to confirm or discount these suggestions.

8.3.2. Deep WTOW

The flow of deep WTOW, found below 1200 m, is restricted to the western portion of the Rockall Trough (Fig. 8.4). North of Rosemary Bank, deep WTOW is seen over a broad area between Bill Baileys and Rosemary Bank with the overflow water occupying the entire water column below ENAW at stations in the north of the section (Fig. 7.2). Isopycnal analysis clearly shows this layer to be flowing southward into the northern and central Rockall Trough (arrows, Fig. 8.4). In the central trough, deep WTOW appears to be predominantly confined to the eastern flank of Rockall Bank with the water mass again occupying the whole of the intermediate and deep water column in this area (Fig. 7.3). The presence of deep WTOW in the far west of the section is confirmed by an elevated oxygen signature (Fig. 5.10), lower nitrate levels (Fig. 5.11) and higher Al concentrations (Fig. 5.15). Again, isopycnal analysis clearly shows this water to be flowing southward (section 7.2).

Deep WTOW is seen flowing westward through the channels between George Bligh and Lousy Banks, and Rockall and George Bligh Banks (arrows, Fig. 8.4). In both cases the deep WTOW is seen to hug the southern flank of the northernmost bank. Although it is thought that if a recirculation exists around Lousy Bank it is weak, and that a recirculation around Rockall Bank is unlikely, a recirculation may exist around George Bligh Bank (section 8.3.1). However, analysis in the channel between George Bligh Bank and Lousy Bank (Fig. 7.4) suggests that the denser components of WTOW whilst flowing north-westward in the north of the channel may not exhibit a south-eastward return flow on the flank of George Bligh Bank. Hence, a net flux of WTOW towards the Iceland Basin may occur. It seems likely that deep WTOW also flows through the channel between Bill Bailey and Lousy Banks although there is no direct evidence of this. As depths of the channels between the northern banks range from 1100 m to > 1200 m (except Faroe Bank to Lousy Bank at < 600 m), it is hypothesised that the densest components of deep WTOW enter the central and southern Rockall Trough. Further work is required to establish this, and to determine the southern extent of the signature of deep WTOW. Although deep WTOW is seen flowing westward between Rockall and George Bligh Banks, no evidence of the water mass is seen on the shallower Rockall Hatton Plateau.

8.3.3. Comparison with literature

The flow of intermediate and deep WTOW within the Rockall Trough agrees extremely well with the previous hydrological and geological evidence of overflow water in the basin (Fig. 8.4). In the northern trough high salinity overflow water has been observed to the west of Rosemary Bank (Ellett and Martin, 1973; Harvey and Theodorou, 1986). Interestingly WTOW was noted to be present in both the intermediate and deep water column in a cold core eddy seen in this area (Ellett et al., 1983). Further south, overflow water has been observed below 1500 m on the eastern flank of Rockall Bank (Lee and Ellett, 1965; Ellett et al., 1983; McCartney and Mauritzen, 2001). Additional corroboration of the results presented within this thesis comes from the interpretation of bottom sedimentological features. The flow of bottom water, identified as WTOW, between 800-1200 m along the southern flanks of both Faroe Bank and Bill Baileys Bank is westward (Boldreel et al., 1998; Kuijpers et al., 1998; Due et al., 2006). Southward flow of overflow water is indicated along the eastern flank of Lousy Bank, again at around 1000 m depth (Due et al., 2006), and between 500-2000 m along the eastern flanks of George Bligh Bank and Rockall Bank (Howe et al., 2001). Bedforms indicate WTOW flows westward through the channel between Bill Baileys and Lousy Bank, hugging Bill Baileys Bank to the north at about 1000 m (Kuijpers et al., 1998; Due et al., 2006). Finally, a zone of erosion similar to that seen on the eastern flank of Rockall Bank, was observed between George Bligh and Rockall Banks (Howe et al., 2001). It can therefore be confidently stated that WTOW enters the northern Rockall Trough and flows southward into the central Rockall Trough hugging the western banks as it does so. WTOW also exits the trough through the channels between Bill Baileys and Lousy Banks, and Lousy Bank and George Bligh Bank. Additionally, it appears as though WTOW flows onto the Rockall-Hatton Plateau, possibly as a result of eddies.

8.4. Temporal distribution of WTOW

This study is the first to examine, in depth, the temporal variability of WTOW within the Rockall Trough. In the intermediate water column a clear salinity inflexion, which marks the bottom of the mid-depth WTOW layer, is seen during 75 % of the Ellett Line record between 1975 and 2008 (Fig. 5.7). Similarly, water containing greater than 5 % NSDW is

seen 65 % of the time at station G in the western trough and 68 % of the time at station M in the east (Fig. 7.9). Evidence of a clear intermediate inflexion point is absent from the record between 1984-1988 and from late-1990 to mid-1994 (Fig. 5.7), when water at mid-depths either has an indistinct salinity inflexion or lies on a mixing line linking ENAW and LSW directly (Fig. 5.8). Mixing analyses also reveal the absence of water containing > 5 % NSDW between 1983/4-1986 and 1990-1994/5 (Fig. 7.9). Deep WTOW, found below 1200 m, is present around 75 % of the time between 1975 and 2008. Although the frequencies of occurrence for intermediate and deep WTOW are very similar, the periods of absence are not always coincidental. For example a signature of WTOW below 1200 m is seen in the mid-1980s and early-1990s when the clear intermediate salinity inflexion is absent (Fig. 5.7), and no water at intermediate depths contains greater than 5 % NSDW (Fig. 7.9). By contrast in 1978, when intermediate WTOW is observed, there is no evidence of deep WTOW (Fig. 5.7).

A particularly striking feature for WTOW at all depths is its persistence throughout the late 1990s and 2000s. It may be significant that during this period the Subpolar Gyre, which is thought to affect other water masses in the Rockall Trough (Hätun et al., 2005; Lozier and Stewart, 2008), was particularly weak. However, first the possibility of variability in flow over the Wyville Thomson Ridge must be considered.

8.4.1. Effect of variability in flow over the Wyville Thomson Ridge

Current meters have been deployed at the Wyville Thomson Ridge almost continuously since 2003 (Sherwin et al., 2008), however, this record is currently too short to investigate any interannual variability. Although several previous estimates of the WTOW flux exist within the literature (Table 2.2), these use different temperature definitions and methods making a comparison difficult. Additionally, there is strong evidence that the position of the measurement has an affect on the magnitude of the flux (Sherwin et al., 2008). Observations of the outflow through the Faroe Bank Channel have been made since the late-1990s, and prior to that have been modelled (e.g. Olsen et al., 2008). A positive relationship exists between the flux over the Wyville Thomson Ridge and that of Faroe Bank Channel Overflow Water (r +0.55; Davies et al., 2009). Although this link is fairly weak, it suggests that the volume of cold water exiting the Faroe Bank Channel may be

used as a partial proxy for the WTOW flux. The mean flow through the Faroe Bank Channel is particularly high between the mid-1990s until the end of the record in 2008, with a lower modelled flux in the mid-1980s and early-1990s (Fig. 8.5). These periods of reduced flow are contemporaneous with the absence of a clear signature of intermediate WTOW within the Rockall Trough, whilst the larger flux towards the end of the record is coincidental with the particularly persistent WTOW at all depths. Hence, unsurprisingly, it appears as if the temporal distribution of WTOW in the Rockall Trough may at least partly be controlled by variations in the magnitude of the flux over the Wyville Thomson Ridge. However, as there is a clear signature of deep WTOW at the Ellett Line in the mid-1980s and early-1990s, flow over the ridge during these periods cannot have ceased completely suggesting that intermediate WTOW too may still be entering the trough. As such, it is suggested that there must be an additional process at work to explain the lack of intermediate WTOW in the central Rockall Trough in the mid-1980s and early-1990s. It is proposed that increases in the strength of the Subpolar Gyre either effectively block the flow of intermediate WTOW southwards into the central trough, or enhance mixing, thereby weakening and removing the intermediate salinity inflexion. First, the effects of changes in the Subpolar Gyre on upper waters, MOW and LSW within the Rockall Trough are discussed, before the influence on NSDW is examined.

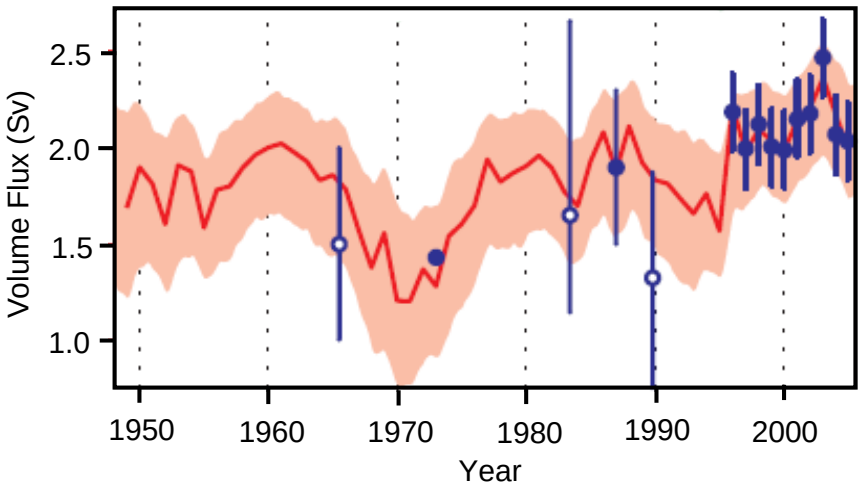

Figure 8.5. Observed and modelled deep volume flux through the Faroe Bank Channel. Red: modelled flux; red line: mean of all ensembles; red shading: two standard deviations of ensemble spread. Blue: observed fluxes with error bars; filled circles: week-month observations of transports; unfilled circles: near-synoptic estimates. From (Olsen et al., 2008).

8.4.2. Effect of variability in the strength of the Subpolar Gyre

8.4.2.1. Observed links

It is well established that the properties of upper waters in the eastern subpolar North Atlantic are affected by changes in the strength of the Subpolar Gyre (e.g. Holliday, 2003; Hätun et al., 2005; Thierry et al., 2008). When the gyre is strong, such as in the mid-1990s, upper waters in the Rockall Trough are dominated by western waters as indicated by decreasing salinities (Fig. 2.5). In contrast, during periods when the Subpolar Gyre is weak, upper waters are more saline as Subtropical Waters enter the basin from the south (Fig. 2.5).

Previous works have also raised the possibility of a link between the salinity of MOW and LSW within the Rockall Trough and the state of the NAO, and therefore position of the Subpolar Front (Lozier and Stewart, 2008; Bozec et al., 2011). It is thought that as the Subpolar Gyre strengthens and expands eastwards, the northward expansion of MOW into the Rockall Trough is blocked by subsurface components of the North Atlantic Current. Contemporaneously, the expansion of the gyre enhances flow of LSW into the eastern basins. In contrast, when the Subpolar Gyre weakens and contracts north-westwards, MOW is able to enter the Rockall Trough as indicated by elevated salinities on the isopycnal corresponding to the core of the water mass. At the same time the progress of LSW into the eastern basins is curtailed (Lozier and Stewart, 2008).

To further investigate any possible relationship between the strength of the Subpolar Gyre and water mass characteristics within the Rockall Trough three parameters were calculated. First, the maximum percentage contributions of MOW and NSDW at intermediate depths in the eastern trough (station M, Ellett Line) were calculated from output of the mixing models. An annual average was calculated for any years with multiple cruises before these percentages (p) were converted to an anomaly (a) (equation 8.1):

$$a = (p - \bar{p}) / \sigma_p \qquad (8.1)$$

where $\bar{p}$ and σ_p are the mean and standard deviations respectively of the maximum contributions between 1975 and 2008. As the mixing model sets the percentage

contribution of LSW at the core of the water mass to be 100 %, the salinity anomaly (a) at the core of LSW at station M was instead calculated (equation 8.1). In this instance p is the annually-averaged salinity at the LSW core, whilst $\overline{p}$ and σ_p are the mean and standard deviations respectively of salinities at the LSW core between 1975 and 2008.

A comparison between the observed (solid line; Fig. 8.6.a) and modelled (dotted line; Fig. 8.6.a) subpolar gyre index (see Fig. 2.5. for definition) with MOW contribution anomalies in the Rockall Trough (Fig. 8.6.c) appears to reveal a connection during some periods. When the Subpolar Gyre is weak (such as in the early-1980s and early-2000s) a larger percentage contribution of MOW is observed in the central Rockall Trough. In contrast, when the gyre is stronger (such as in the mid-1980s) MOW is a reduced component of the intermediate water column. This connection agrees with findings of Lozier and Stewart (2008). Although the relationship between the gyre index and MOW contribution anomaly is weak during the late-1980s and early-1990s, the association between the MOW salinity anomaly and NAO remains strong (Lozier and Stewart, 2008). A possible underlying longer-term trend of increasing MOW influence within the intermediate water column between 1985 and 2008 (Fig. 8.6.c) is also apparent. This, and the weaker link between the gyre index and MOW contribution anomaly during some periods, implies that processes other than the strength of the Subpolar Gyre affect the temporal distribution of MOW within the trough. Further work is required to identify these.

It appears that as the Subpolar Gyre strengthens salinity anomalies at the depth of the LSW core decrease (Fig. 8.6.d). It is thought that as the Subpolar Gyre expands, LSW is able to enter the eastern basins and renew the stagnant pool of older LSW present within the Rockall Trough (Lozier and Stewart, 2008). This manifests as sudden decreases in salinity at the depth of the LSW core (Holliday et al., 2000). The apparent relationship of a strengthening Subpolar Gyre and decreasing salinity of LSW within the Rockall Trough persists throughout the Ellett Line record. Between the start of the time-series in 1975 and 1990, the salinity anomaly at the depth of the LSW core also appears to increase as the Subpolar Gyre weakens and moves westwards. This can be explained by LSW within the trough becoming isolated as the gyre contracts (Lozier and Stewart, 2008) and the core gradually eroding as it mixes with more saline water masses above and below (Holliday et al., 2000). However, no increase in salinity at the LSW core depth is observed during the weak Subpolar Gyre in the late-1990s and early-2000s (Fig. 8.6.d). This apparent

decoupling between the weakening Subpolar Gyre and LSW characteristics within the Rockall Trough was not noted in Lozier and Stewart (2008) due to their data analysis ending in 1995. The breakdown in the relationship between the weakening gyre and LSW salinity suggests that the influence of another factor, in addition to the strength of the Subpolar Gyre is probably. A longer-term trend of decreasing salinity upon which the higher frequency trends are superimposed is also observed.

The NSDW contribution anomaly at mid-depths (Fig. 8.6.b), which indicates the presence of intermediate WTOW in the Rockall Trough, arguably appears to have the strongest relationship to the Subpolar Gyre index. When the gyre is weak, a larger percentage contribution of NSDW is seen in the central trough with a 2-3 year lag. In contrast, when the Subpolar Gyre is stronger a smaller percentage contribution of NSDW is observed, again with a 2-3 year delay. Unlike for the water masses of MOW or LSW, the relationship between the NSDW contribution anomaly and the gyre index persists throughout the whole record. Additionally, there does not appear to be any underlying longer-term trend. This raises the interesting possibility that some of the salinity changes previously attributed to MOW (Lozier and Stewart, 2008) may in fact be more strongly related to changes in the volume of intermediate WTOW, and therefore NSDW, within the trough. Indeed the σ_1 32.10 kg m^{-3} isopycnal surface (equivalent to σ_θ 27.56 kg m^{-3}) used to identify the MOW core by Lozier and Stewart (2008) lies within the intermediate WTOW layer in the Rockall Trough (e.g. Fig. 5.6).

As a strong relationship appears to exist between the Subpolar Gyre index and the maximum percentage contribution of NSDW at intermediate depths within the Rockall Trough, it is proposed that variability in the strength of the Subpolar Gyre is an important driver for the temporal persistence of this water mass (and therefore WTOW) within the Rockall Trough. Mechanisms to explain this observed link are proposed in the following section and summarised in Figure 8.7.

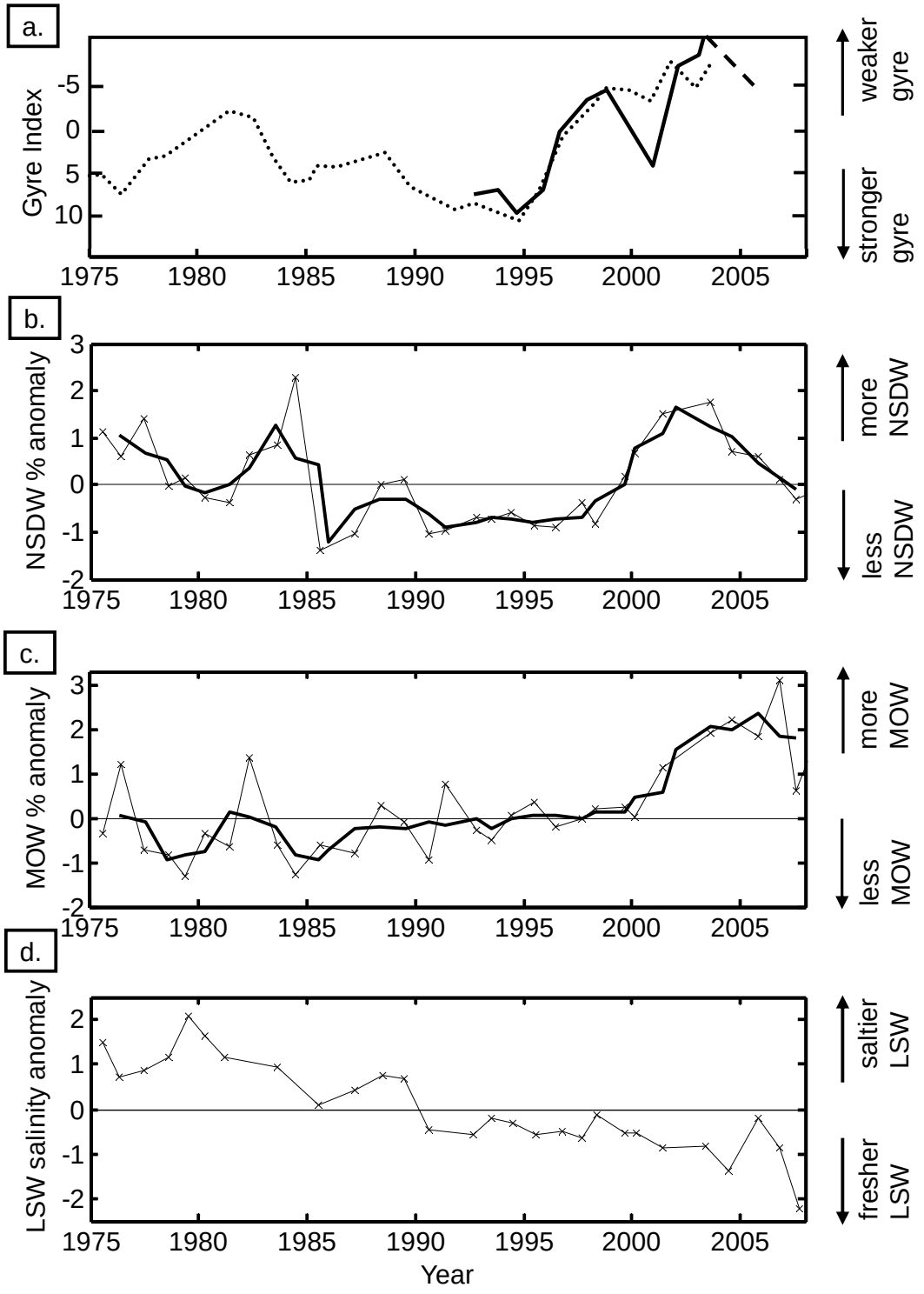

Figure 8.6. Comparison between the subpolar gyre index and water masses in the eastern Rockall Trough. a. modelled (dotted) and observed (solid) Subpolar Gyre index from Hatun et al. (2005), dashed line: approximate update from Hakkinen and Rhines (2009); b. the anomaly of the maximum NSDW contribution at intermediate depths at station M; c. the maximum percentage contribution anomaly of MOW at station M; d. salinity anomaly at the LSW core depth at station M. Thin black line in b., c. and d.: annual mean; thick black line in b. and c.: three-year running mean.

8.4.2.2. Proposed mechanism

When the Subpolar Gyre is strong it expands eastwards (Bower et al., 2002; Johnson and Gruber, 2007) enabling Subpolar Waters to influence the Rockall Trough (Fig. 8.7.a). Upper waters become cooler and fresher as western waters dominate over warmer and more saline waters from the Subtropical Gyre (Hätun et al., 2005). Subsurface components of the North Atlantic Current are thought to curtail the northward penetration of MOW (Lozier and Stewart, 2008; Bozec et al., 2011) decreasing this water mass's influence within the Rockall Trough. The eastward expansion of the Subpolar Gyre, however, enables LSW trapped westward of the gyres eastern limb to enter the Rockall Trough and renew the stagnant pool of LSW within the basin (Holliday et al., 2000; Lozier and Stewart, 2008). It is believed that as the LSW and associated intermediate waters enter the Rockall Trough they mix with intermediate WTOW eroding its signature in θ-S space. Certainly in the mid-1980s and early-1990s, when the Subpolar Gyre was strong, the properties of mid-depth waters in the central Rockall Trough indicate an increased presence of LSW (Fig. 5.8). In addition to the erosion of the signature of WTOW at intermediate depths, it is proposed that an increased volume of the LSW-upper water mixture within the trough blocks the progress of intermediate WTOW into the central basin. This is probably due to the low baroclinic flow within the intermediate WTOW layer as revealed by isopycnal analyses (sections 7.1 and 7.2). Instead, it is suggested that intermediate WTOW may pool in the northern Rockall Trough possibly with increasingly flow into the Iceland Basin or recirculation around the western banks. Further surveys during a strong Subpolar Gyre or analysis of historical data from such a period is required to prove or disprove this.

Isopycnal sections from the western trough where deep WTOW is observed reveal strong shear and southward baroclinic flow. Higher oxygen concentrations and lower nitrate values in this area also indicate that flow is relatively strong in deep WTOW compared to other intermediate and deep water masses within the trough (section 5.7). Thus, the data suggests that deep WTOW has the ability to push through the western intermediate waters associated with a stronger Subpolar Gyre when intermediate WTOW does not (Fig. 8.7.a). When the Subpolar Gyre is strong therefore, upper and intermediate waters within the Rockall Trough are dominated by those originating from the west (Subpolar Waters and LSW) rather than those from the south (MOW and Subtropical Waters) or north (NSDW

and WTOW). Despite this western dominance, deep WTOW is still an important water mass within the trough during these periods.

Conversely, as the Subpolar Gyre weakens, its eastern limb contracts north-westwards into the Iceland Basin (Bower et al., 2002; Johnson and Gruber, 2007). Hence, the cooler and fresher upper waters contained within the Subpolar Gyre are unable to enter the Rockall Trough (Fig. 8.7.b). Upper waters in the trough, therefore, become more saline as they are increasingly influenced by Subtropical Gyre waters (Hätun et al., 2005). Due to the westward movement of the North Atlantic Current, MOW is able to penetrate further northwards and increasingly influence intermediate waters within the Subpolar Gyre (Lozier and Stewart, 2008; Bozec et al., 2011). The progress of LSW eastwards into the trough, however, is inhibited by the North Atlantic Current (Lozier and Stewart, 2008). As such the LSW body within the Rockall Trough is thought to become isolated and starts to erode (Holliday et al., 2000). It is proposed that both intermediate and deep WTOW are able to enter the central and southern Rockall Trough easily due to the lack of inflowing LSW and associated western intermediate waters into the trough. Hence, upper and intermediate waters within the Rockall Trough are dominated by those originating from the south (Subtropical Waters and MOW) and north (WTOW and NSDW), rather than those from the west (LSW and Subpolar Waters). As the enhanced presences of intermediate WTOW and of MOW are co-incidental, it is speculated that the southward flow of WTOW at mid-depths may limit the northward penetration of MOW. Hence, within the Rockall Trough, the influence of MOW is only seen at densities greater than σ_θ ~27.7 kg m^{-3} (i.e. below intermediate WTOW) compared to σ_θ 27.4 - 27.75 kg m^{-3} at the southern entrance to the basin.

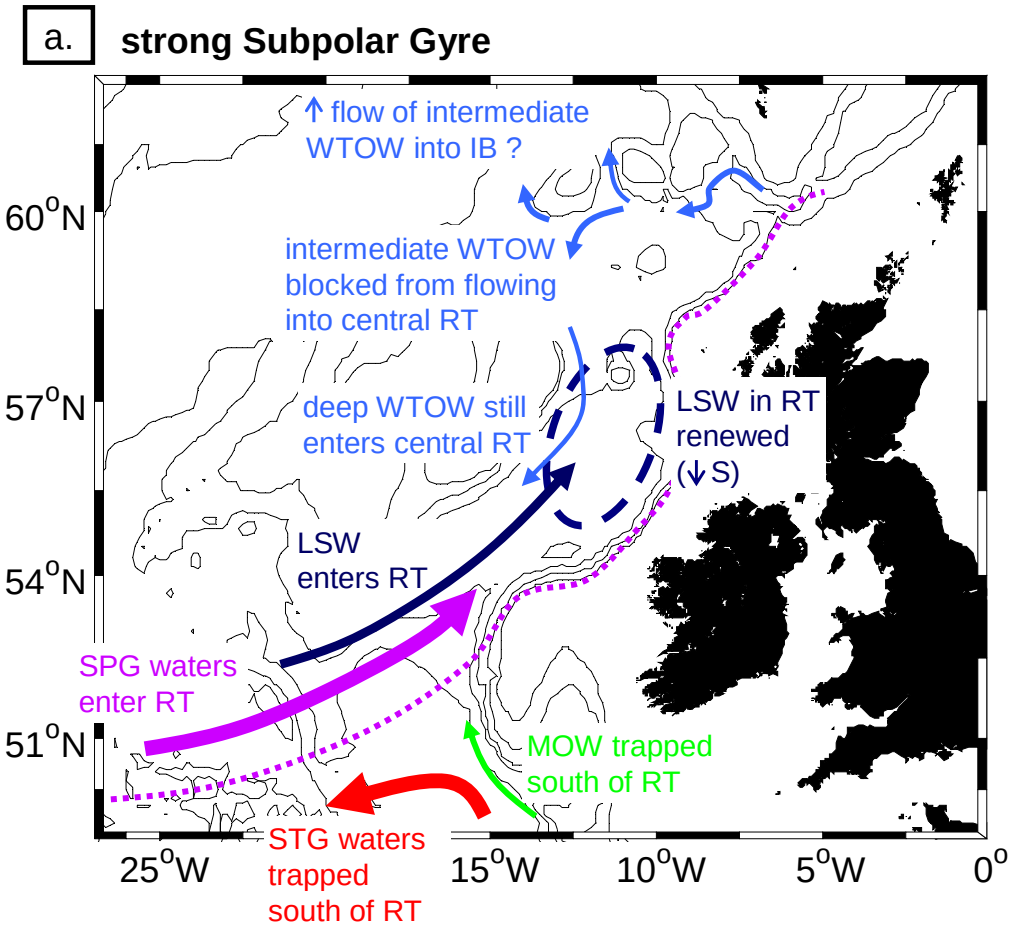
a.
strong Subpolar Gyre
↑ flow of intermediate WTOW into IB ?
intermediate WTOW blocked from flowing into central RT
deep WTOW still enters central RT
LSW in RT renewed (↓S)
LSW enters RT
SPG waters enter RT
MOW trapped south of RT
STG waters trapped south of RT
60°N
57°N
54°N
51°N
25°W
15°W
10°W
5°W
0°

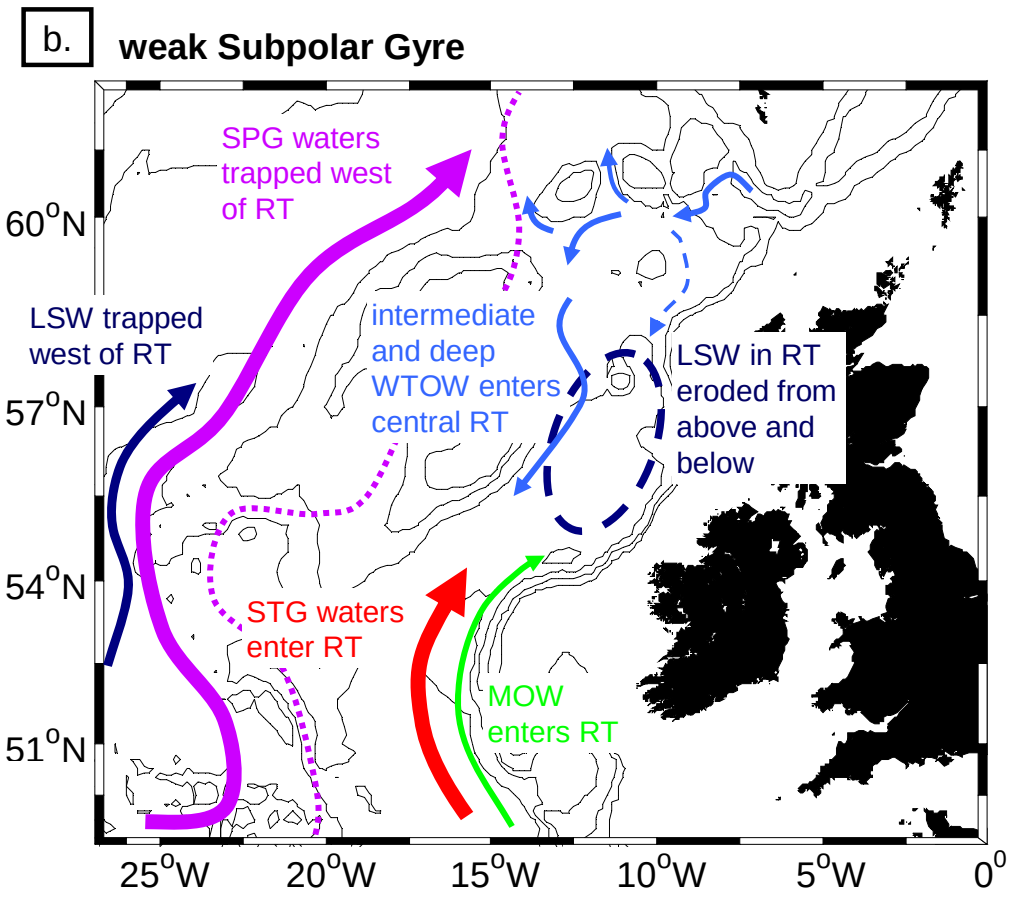
b.
weak Subpolar Gyre
SPG waters trapped west of RT
LSW trapped west of RT
intermediate and deep WTOW enters central RT
LSW in RT eroded from above and below
STG waters enter RT
MOW enters RT
60°N
57°N
54°N
51°N
25°W
20°W
15°W
10°W
5°W
0°

Figure 8.7 (previous page). Schematic of the influence of Subpolar Gyre on water masses and circulation in the Rockall Trough. a. case when Subpolar Gyre is strong and expands eastwards, b. case when Subpolar Gyre is weak and contracts westward. Purple dotted line: boundary of Subpolar Gyre; IB: Iceland Basin; RT: Rockall Trough. It should be noted that because of possible recirculations the arrows for WTOW do not necessarily represent a strong advective flux.

The temporal distribution of WTOW within the Rockall Trough raises the intriguing possibility that the water mass's presence and absence may partially explain the conflicting historical hydrological reports into its importance within the basin. Surveys conducted in the late 1970s and late 1990s, when the Subpolar Gyre was weakening, report clear evidence of WTOW within the Rockall Trough (Ellett et al., 1983; McCartney and Mauritzen, 2001; New and Smythe-Wright, 2001). Similarly, this thesis uses data collected in the late-1990s and mid-2000s when the gyre was again weak, in addition to the Ellett Line time-series which was extended to include measurements from this period. In contrast, analysis of Ellett Line data from 1975-1996 by Holliday et al. (2000) includes a significant period when the Subpolar Gyre was strong. This perhaps explains why the study concluded that WTOW is not an important water mass within the trough in contrast to findings within this thesis.

8.5. Effect of WTOW on water column stability

Water column stability in the eastern subpolar North Atlantic is thought to be heavily influenced by intermediate water masses (Wade et al., 1997). As such the presence, or absence, of intermediate WTOW in the Rockall Trough may affect the depth of winter convection within the basin and therefore heat exchange between the ocean and atmosphere. To investigate this further the Static Stability Parameter (E) throughout the water column was calculated (equation 8.2) for station M in September 1993 (CH105) and October 2006 (D312).

$$E = N^2 / g \qquad (8.2)$$

where N^2 is the squared Brunt-Väisälä Frequency (equation 8.3) determined using the *Matlab Seawater Toolbox*, and g the acceleration due to gravity.

$$N^2 \approx g\left[-(1/\rho)(\partial\sigma_t/\partial z)\right] \quad (8.3)$$

During D312 a clear signature of intermediate WTOW was observed whilst during CH105 only a very weak intermediate salinity inflexion was observed (Fig. 5.8.b). Hence, any difference between the stability of the intermediate water column between the two profiles may be attributed to the influence of WTOW and / or MOW.

The stability of the water column in 1993 (red, Fig. 8.8) and 2006 (blue, Fig. 8.8) is fairly similar except between 700 m to 1000 m. In this depth range the water column is more stable in 2006 than 1993 with values of E elevated by 0.1-0.4 x 10^{-6} m^{-1} in 2006. As this range is approximately coincidental with the depths over which intermediate WTOW is observed, this suggests that the presence of this water mass increases the stability of the mid-depth water column. Further, no change in stability between the two years is observed between 1000 m and 1400 m where a signature of MOW is observed in 2006. This suggests that the presence or absence of intermediate WTOW has a larger effect on the stability of the intermediate water column in the Rockall Trough than that of MOW. These findings suggest that when a clear signature of intermediate WTOW is observed, such as when the Subpolar Gyre is weak, the depth of winter convection in the Rockall Trough may be reduced. In contrast when intermediate WTOW is absent from the central trough and the water columns stability decreased, winter convection may reach deeper depths increasing ocean-atmosphere heat exchange. These findings will be explored further in future work.

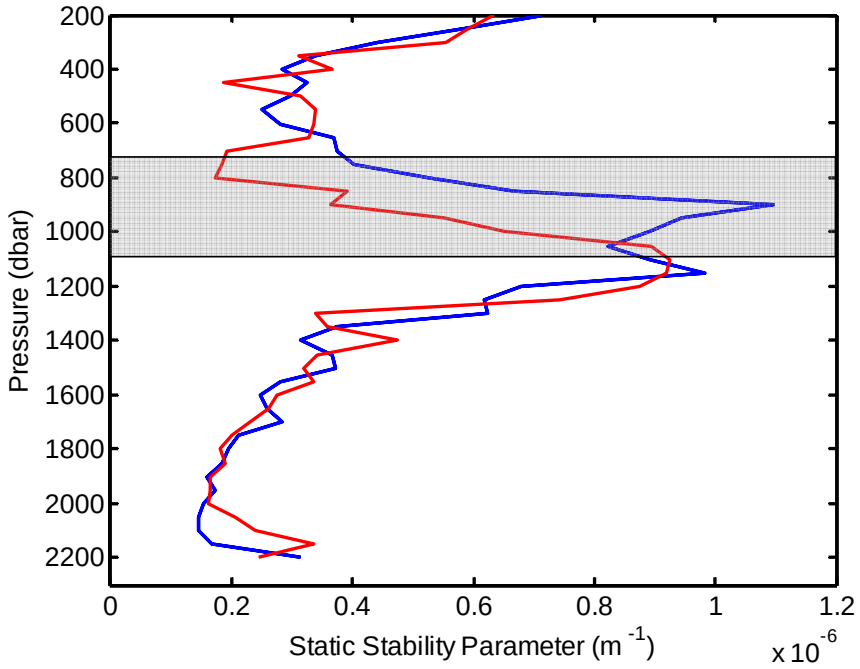

Figure 8.8. Water column stability as shown by the Static Stability Parameter (E) at station M when a clear intermediate salinity inflexion was absent (red, CH105, September 1993) and when a clear signature of intermediate WTOW was observed (blue, D312, October 2006). Grey shading shows vertical extent of intermediate WTOW in 2006. For clarity the upper 200 m is not shown.

Chapter 9.
Conclusion

This chapter provides an overall conclusion to the thesis and summarises the main findings.

9.1. Signature of WTOW

9.1.1. Temperature and salinity signature

Although WTOW cannot be readily identified in temperature or salinity plots, it has a clear signature in θ-S space. It is present as both an intermediate and deep water mass within the Rockall Trough.

Intermediate WTOW is identified as water between 600-1200 m whose properties lie close to a mixing line linking ENAW and NSDW (35.25, 8.0 °C - 34.85, 0.5 °C). As this mixing line is observed on the Wyville Thomson Ridge crest, and can clearly be seen to enter the trough via its northern boundary, it can be attributed to WTOW. The bottom of the intermediate WTOW layer is indicated by a salinity inflexion marking the transition between the WTOW mixing line and the MOW-LSW mixing line. Hence, intermediate WTOW is sandwiched between upper waters above, and a MOW-LSW mixture below, both of which enter the Rockall Trough via its southern entrance.

The occurrence of deep WTOW is identified by the presence of water that is more saline than the MOW-LSW mixing line, or LSW, at the appropriate density level. Deep WTOW is only found below the intermediate salinity inflexion at ~ 1200 m, and is shown in θ-S space by data lying between the MOW-LSW and WTOW mixing lines, and / or between the LSW water mass definition and WTOW mixing line. Unlike intermediate WTOW, deep WTOW is only found in the northernmost, north-western and western trough where it flows westward and southward along the western banks.

9.1.2. Oxygen and nutrient signature

The lower oxygen layer found at intermediate depths in large portions of the world's oceans, and its associated peak in nutrient concentrations, is also observed in the Rockall Trough between 1000-1300 m. Hence, dissolved oxygen and nutrient concentrations are difficult to use as tracers of intermediate WTOW. However, at times the lower oxygen layer is less pronounced on the eastern flank of Rockall Bank with higher oxygen concentrations and lower nitrate levels observed in this area. This is likely to be a signature of the oxygenated and fairly nitrate-low WTOW which is known to flow southward along the western boundary of the trough.

As deep WTOW is found below the lower oxygen layer, the nitrate and oxygen signature for the water mass at this depth is easier to interpret. Its presence is indicated by higher oxygen concentrations and lower nitrate levels in the far west of the trough.

Phosphate and silicate do not appear to be useful tracers of WTOW, at any depth, because concentrations in the overflow water are similar to those of other water masses found in the Rockall Trough.

9.1.3. Chlorofluorocarbon signature

Historical CFC data from the central Rockall Trough reveal that the properties of intermediate WTOW lie on a mixing line linking ENAW and NSDW in *CFC-S* space (CFC-11: 35.25, 3.0 pmol kg^1 - 34.85, 0.9 pmol kg^1; CFC-12: 35.25, 1.7 pmol kg^1 - 34.85, 0.4 pmol kg^1). As both CFC-11 and CFC-12 levels in NSAIW are much higher than in NSDW, it is clear that NSAIW is not an important constituent of WTOW at least in the late 1990s. Instead, pure WTOW is a mixture of upper waters and NSDW only. Due to the very similar temperature, salinity, oxygen and nutrient signatures of NSAIW and NSDW this distinction can only be drawn from CFC data.

Insufficient data exists to be able to comment on the CFC-11 and CFC-12 signature of deep WTOW.

9.1.4. Aluminium in the Rockall Trough

9.1.4.1. Evaluation of aluminium as a water mass tracer

Aluminium data collected during this study compare well with previously published and unpublished data collected in the subpolar North Atlantic. This, along with various method experiments, suggests that seawater samples can be collected from a regular CTD rosette and sampling bottles as long as care is taken. Additionally, if suitably clean facilities are not available at sea samples may be frozen for later shore-based analysis. However, further work is required to determine if there are any affects associated with long-term frozen storage.

Although Al is easier to measure in seawater than other trace metals, it is still more difficult to obtain high quality results compared to other more routinely measured tracers. It appears crucial that initiatives such as the interlaboratory comparison continue and that a certified reference material for Al in seawater at nanomolar levels is developed.

This thesis presents the first Al values from the Rockall Trough. Additionally, the Al signature of several water masses has been determined for the first time. As values are low in ENAW, SAIW and LSW, and elevated in NSDW and MOW, the different water masses are clearly identifiable in property-property plots.

Although Al appears to behave conservatively throughout the majority of the water column, concentrations are often elevated in bottom samples probably as a result of bottom sediment resuspension. This makes it difficult to use Al as a tracer of a bottom water mass such as AABW. It is also likely that Al behaves non-conservatively in the surface mixed layer although more work is required to determine this.

9.1.4.2. Aluminium signature of WTOW

The properties of intermediate WTOW lie on a mixing line between ENAW and NSDW in *S-Al* space (35.25, 10 nM - 34.85, 23 nM), with the bottom of this layer marked by a peak in concentrations. At stations where WTOW occupies the entirety of the water column

below ENAW, this is reflected in *S-Al* plots with data lying on the WTOW mixing line to the seabed.

Deep WTOW is identifiable as water with higher Al concentrations whose properties are intermediate to those of the MOW-LSW mixing line and ENAW-NSDW mixing line.

9.2. Pathways and circulation of WTOW

WTOW is a significant water mass in the northern Rockall Trough and the only water body to enter the basin from the north. The maximum observed contributions of NSDW to the water column in the trough, during a particularly large overflow, are 15-20 % between 600-1200 m, and 20-25 % below 1200 m.

Two branches of WTOW are identified within the basin: a slow-moving non-specific intermediate layer that fills both the eastern and western trough, and a faster-flowing deep branch that flows southward along the western boundary.

Intermediate WTOW can be traced as far south as 54-55 °N in the Rockall Trough where its signature is lost due to the strong influences of MOW and SAIW in the intermediate water column. Additionally, WTOW is seen in the channels between the western banks. It is thought that the net flow between Bill Baileys and Lousy Bank is into the Iceland Basin, however further south a recirculation of WTOW around George Bligh Bank may exist. Evidence of WTOW is also observed on the Rockall-Hatton Plateau which may be a result of eddy activity.

Although a clear signature of intermediate WTOW is observed in both the eastern and western trough, the mechanisms via which the water mass enters the eastern portion of the basin are uncertain. A cyclonic recirculation seems unlikely due to near horizontal isopycnals indicating low baroclinic flow at intermediate depths. Eddy activity and blocking by an expanding or contracting Subpolar Gyre have both been proposed, however, further work is required to confirm or discount these hypotheses.

Deep WTOW within the Rockall Trough is limited to the northernmost, north-western and western portions of the basin where it is clearly observed to flow first westward and then southward along the western banks. More work is required to determine the southern limit of the signature of deep WTOW. Components of the water mass also enter the channels between the western banks although it is uncertain if any of this recirculates and re-enters the trough.

The circulation of both intermediate and deep WTOW agrees extremely well with previous hydrological observations and sedimentological surveys.

9.3. Temporal variability of WTOW

Analysis of the Ellett Line time-series in the central Rockall Trough, reveals that intermediate WTOW is present 65-75 % of the time between 1975 and 2008 with the deep branch having a similar temporal persistence. However, evidence of a very pronounced flow of deep WTOW in the western trough, such as that observed in 2006, is only seen in a handful of years.

At all depths WTOW was particularly prevalent in the central Rockall Trough from the mid 1990s until the end of analysis in 2008. During the mid 1980s and early 1990s, a clear signature of intermediate WTOW was absent and the intermediate waters contained less than 5 % NSDW. Interestingly, at these times evidence of deep WTOW was still observed indicating that flow over the Wyville Thomson Ridge cannot have ceased. Instead, it is proposed that changes in the strength of the Subpolar Gyre affect the temporal variability of intermediate WTOW in the Rockall Trough. When the gyre is weak, such as in the late 1990s and early 2000s, the Subpolar Front and associated western waters lie to the west of the trough. Hence, intermediate waters within the basin are influenced predominantly by the southern and northern water masses of MOW and WTOW respectively. When the gyre strengthens, such as in the mid 1980s and early 1990s, its eastern boundary moves eastward into the Rockall Trough. Intermediate waters within the basin are therefore more heavily influenced by those from the west, including LSW, and the southward flow of intermediate WTOW into the central trough is inhibited. Further work is required to investigate this hypothesis.

9.4. Summary

Within this thesis we have conclusively shown, for the first time, that WTOW is an important water mass within the Rockall Trough and is temporally persistent, particularly in the last two decades. Although further work is required to fully resolve the pathways of intermediate WTOW within the eastern trough, in the west of the basin WTOW clearly flows southward along the eastern flanks of the banks separating the Rockall Trough from the Iceland Basin. Additionally, WTOW is thought to enter the Iceland Basin to the west at least via the channel between Bill Baileys and Lousy Bank. However, a recirculation may exist around George Bligh Bank. The physical and chemical definitions, and identifying features of WTOW, within the Rockall Trough have been described allowing easy identification of this water mass in future studies (e.g. McGrath et al., 2012). The work presented within this thesis represents an increase in current knowledge of both the circulation and water mass distribution within the eastern subpolar North Atlantic. As such, it has a valuable contribution to future modelling studies, analysis of the Ellett Line time-series, and investigation into the presence of biological species within the Rockall Trough.

Appendix A.

Calibrations of the conductivity (salinity) sensor

A.i. 0804S

A.ii. H44-04-12

A.iii. CD176

A.i. Sc0804

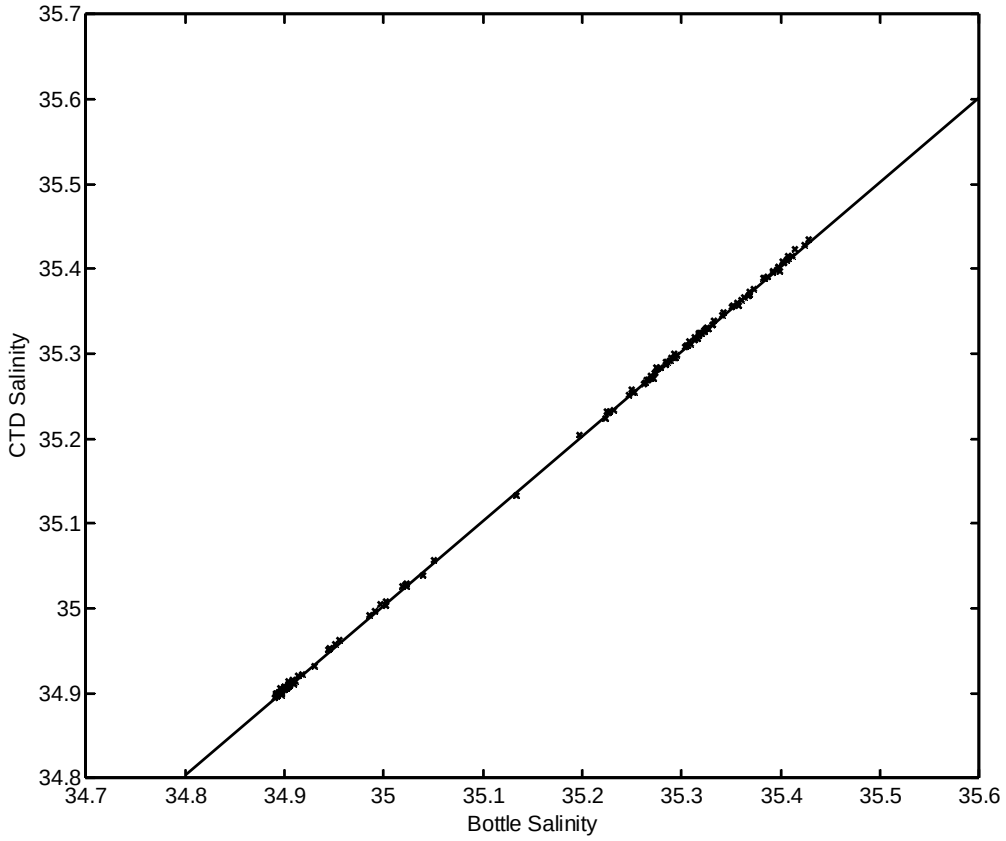

Figure A.1. Averaged bottle salinity against sensor salinity for 0804S.
sensor salinity = 0.998 x bottle salinity + 0.091
r = 1.000

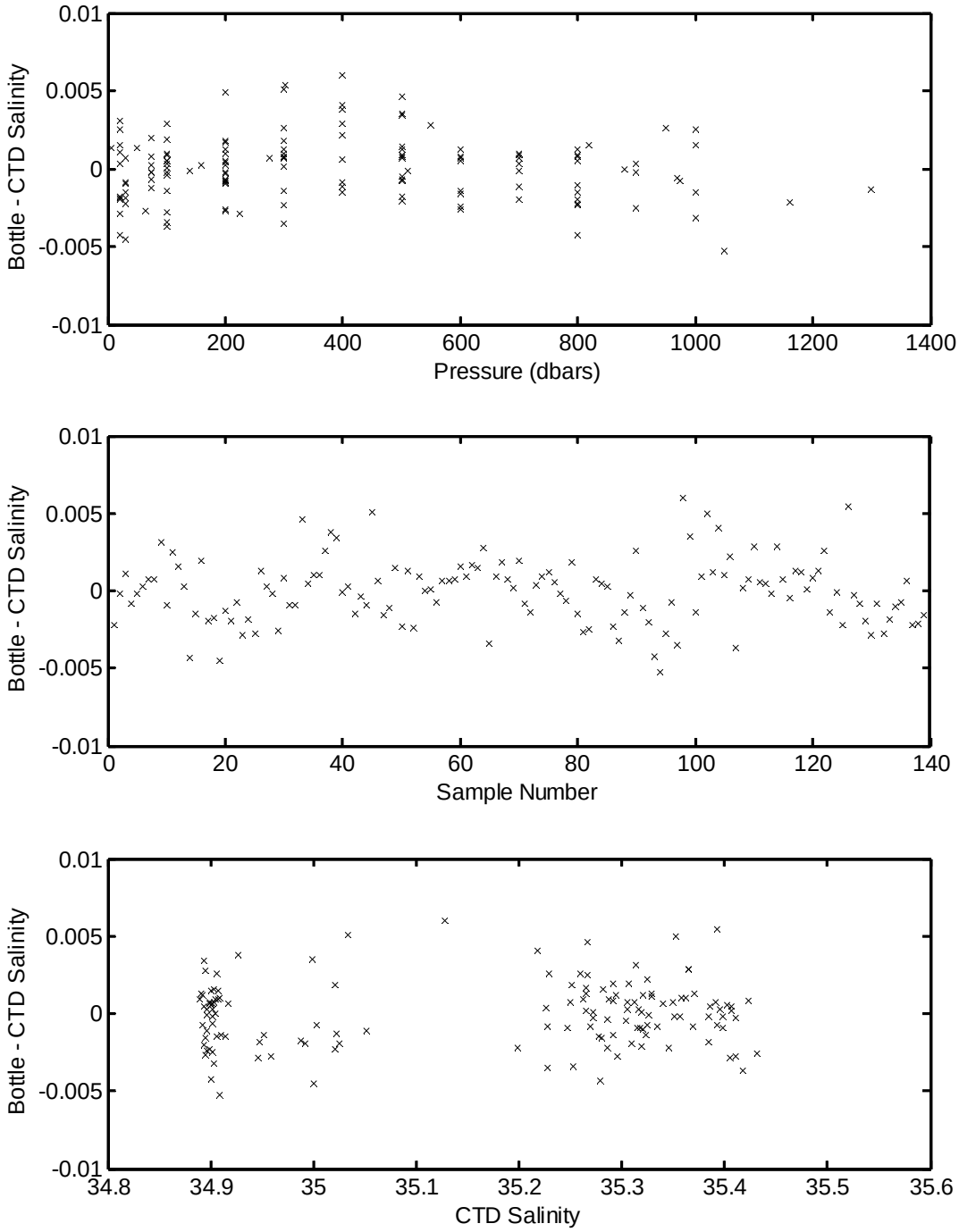

Figure A.2. Residual (bottle – corrected sensor salinity) plots for 0804S.
a. Pressure (dbar) against residual
b. Sample number against residual
c. Sensor salinity against residual

A.ii. H44-04-12

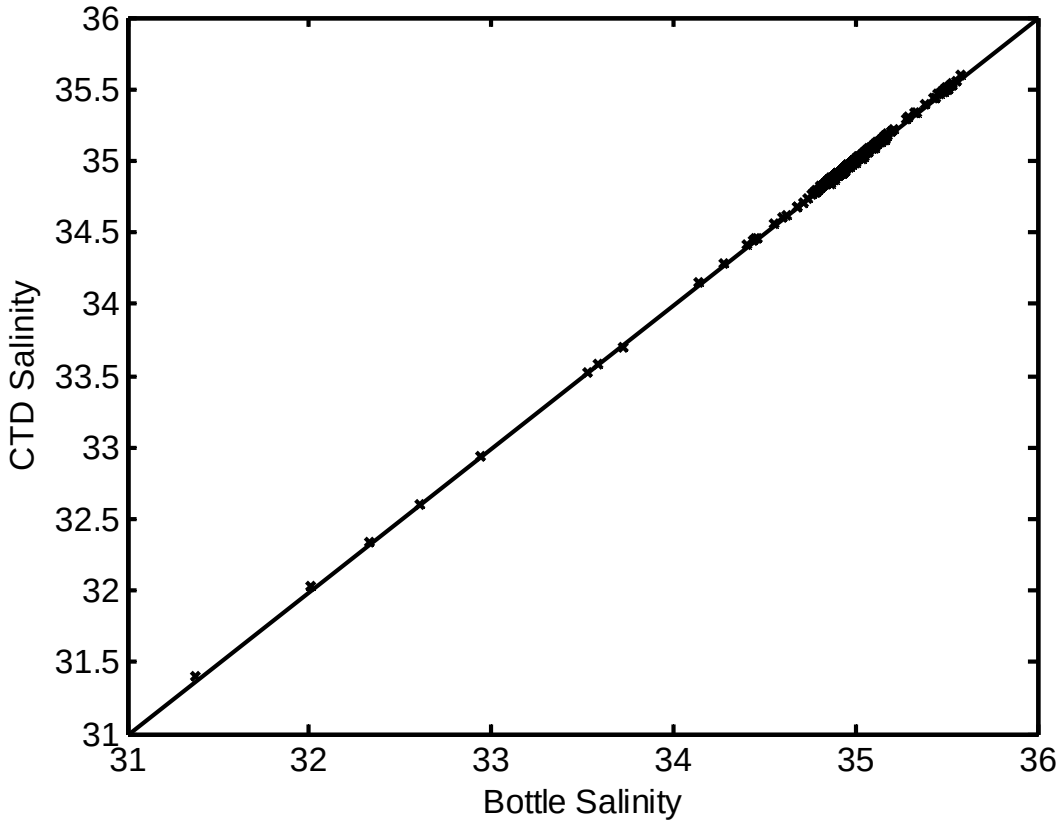

Figure A.3. Bottle salinity against sensor salinity for H44-04-12.
sensor salinity = 1.000 bottle salinity + 0.012
r = 1.000

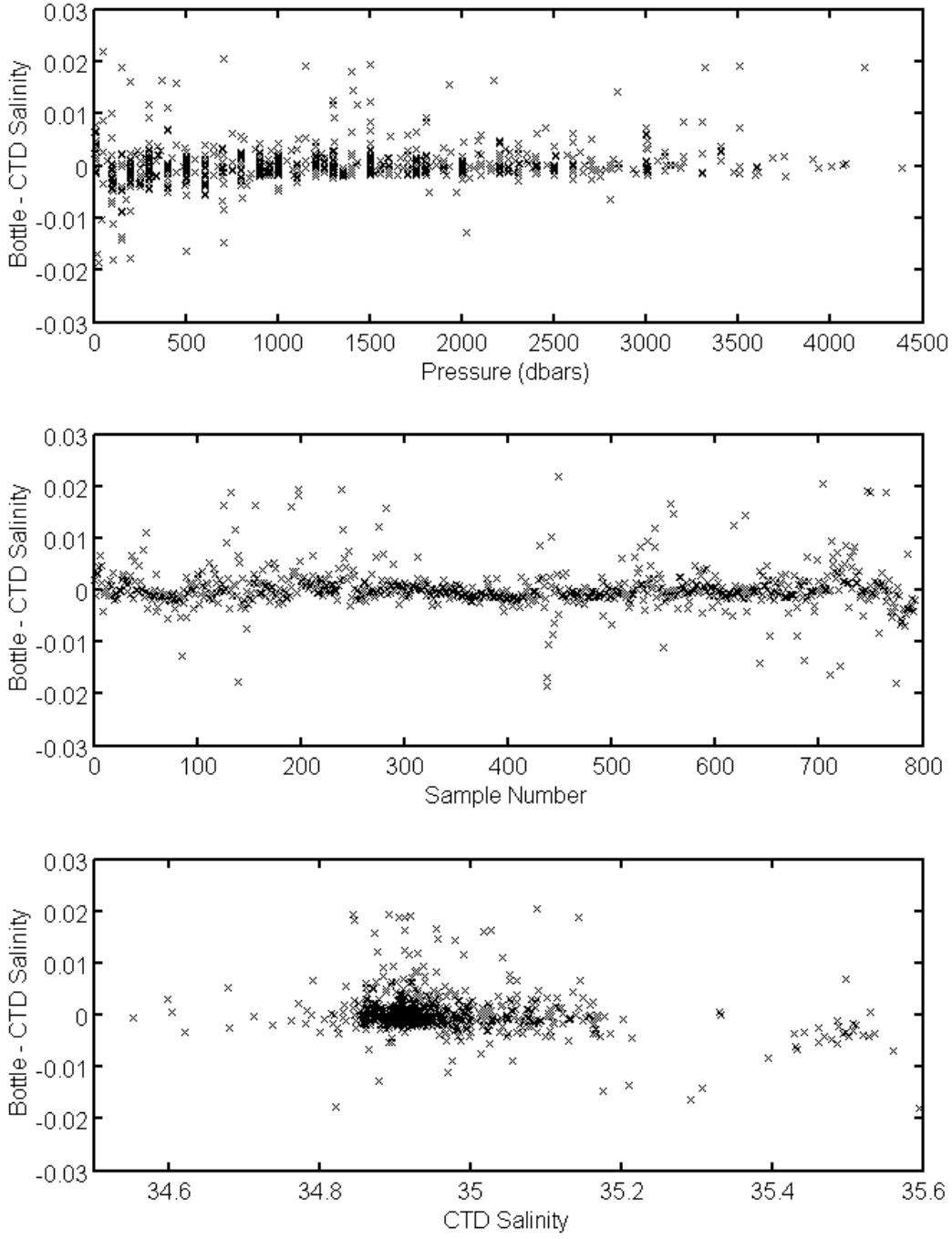

Figure A.4. Residual (bottle – corrected sensor salinity) plots for H44-04-12.
a. Pressure (dbar) against residual
b. Sample number against residual
c. Sensor salinity against residual

A.iii. CD176

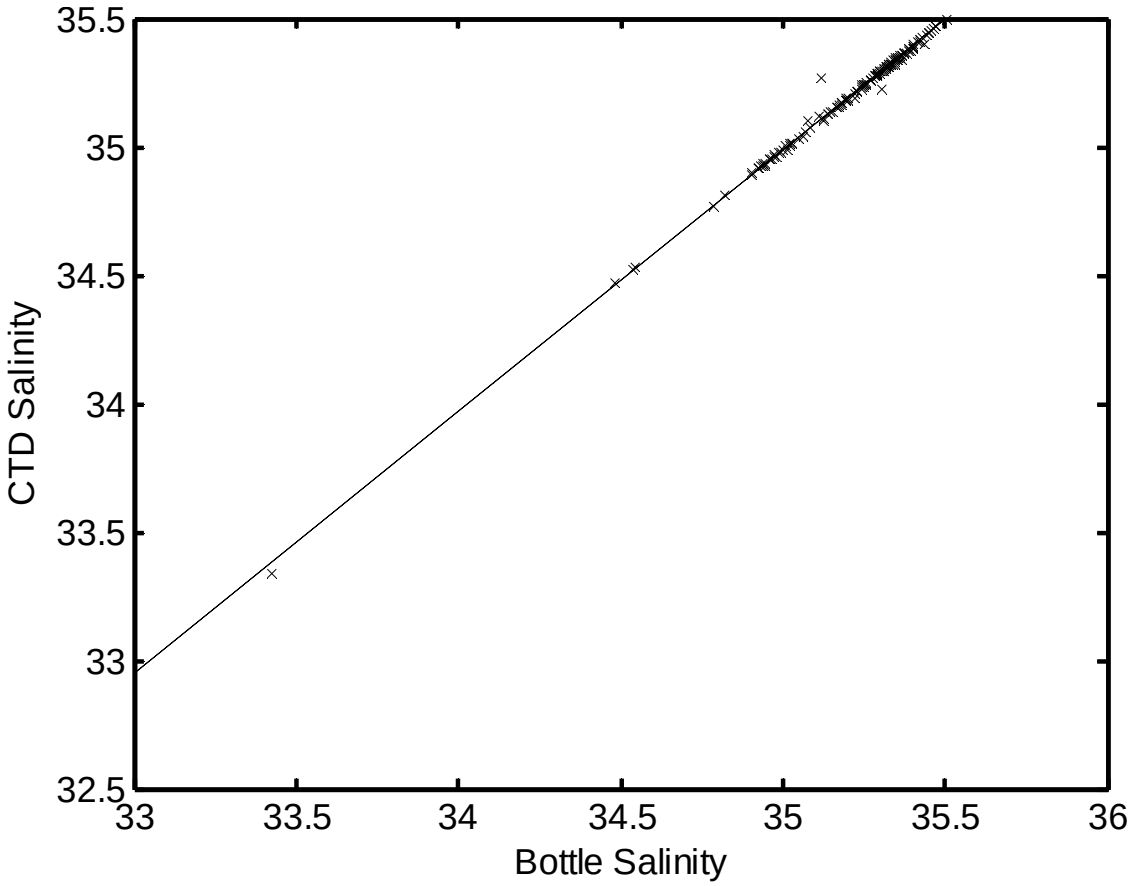

Figure A.5. Bottle salinity against sensor salinity for CD176.
sensor salinity = 1.016 x bottle salinity – 0.558
r = 0.998

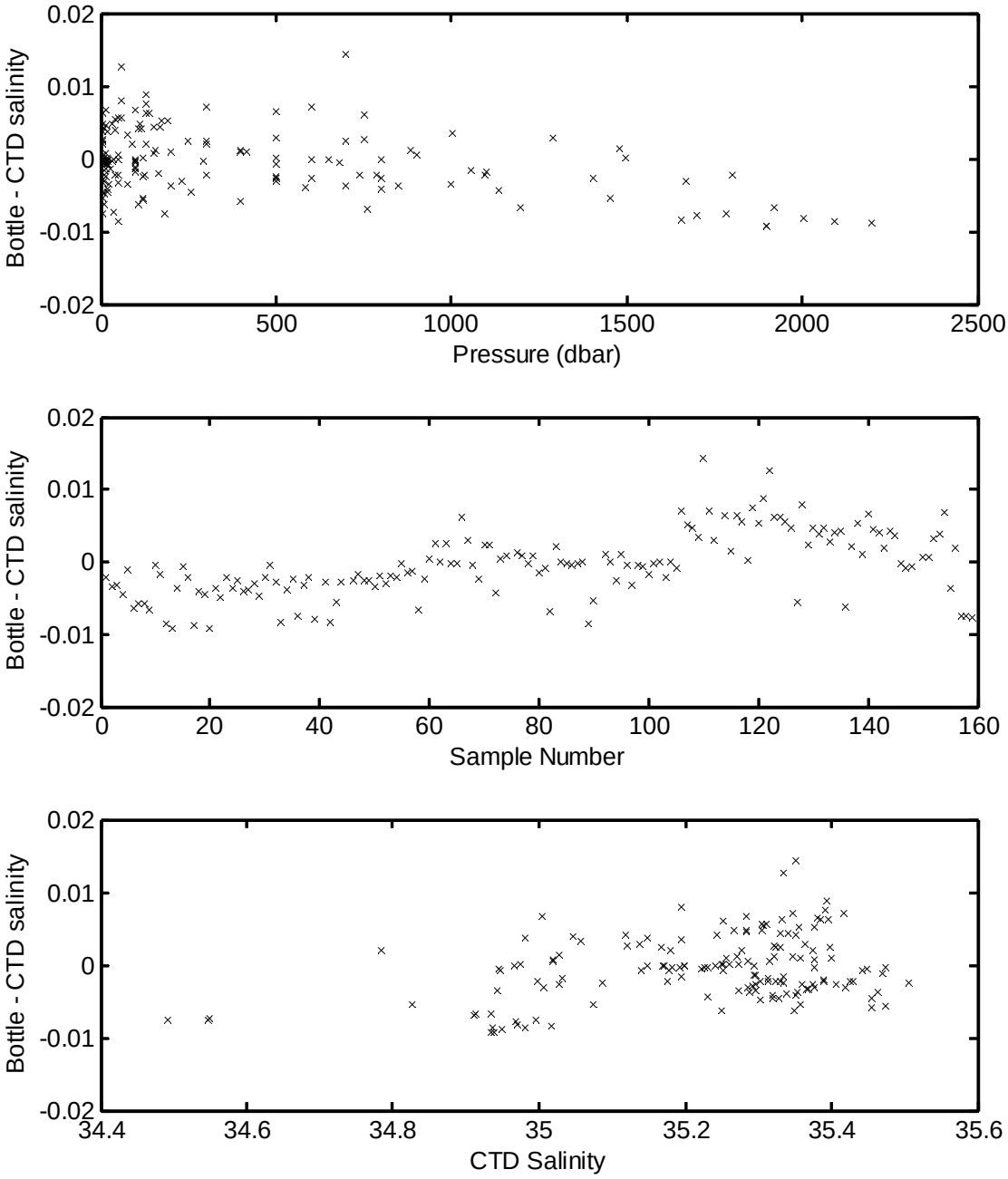

Figure A.6. Residual (bottle – corrected sensor salinity) plots for CD176.
a. Pressure (dbar) against residual
b. Sample number against residual
c. Sensor salinity against residual

Appendix B.

Calibrations of the dissolved oxygen sensor

B.i. 0804S

B.ii. CD176

B.i. Sc0704

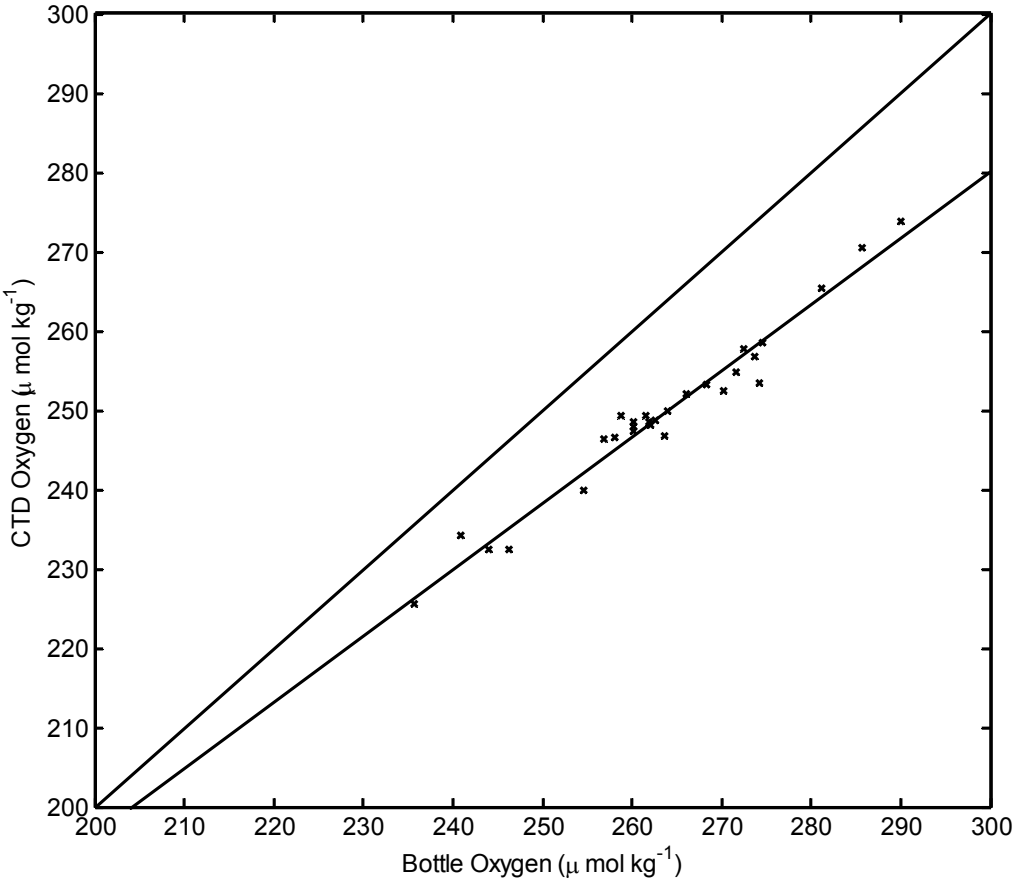

Figure B.1. Bottle oxygen (μmol kg^{-1}) against sensor oxygen (μmol kg^{-1}) for 0804S.
sensor oxygen (μmol kg^{-1}) = 0.836 x bottle oxygen (μmol kg^{-1}) + 29.402
r = 0.980

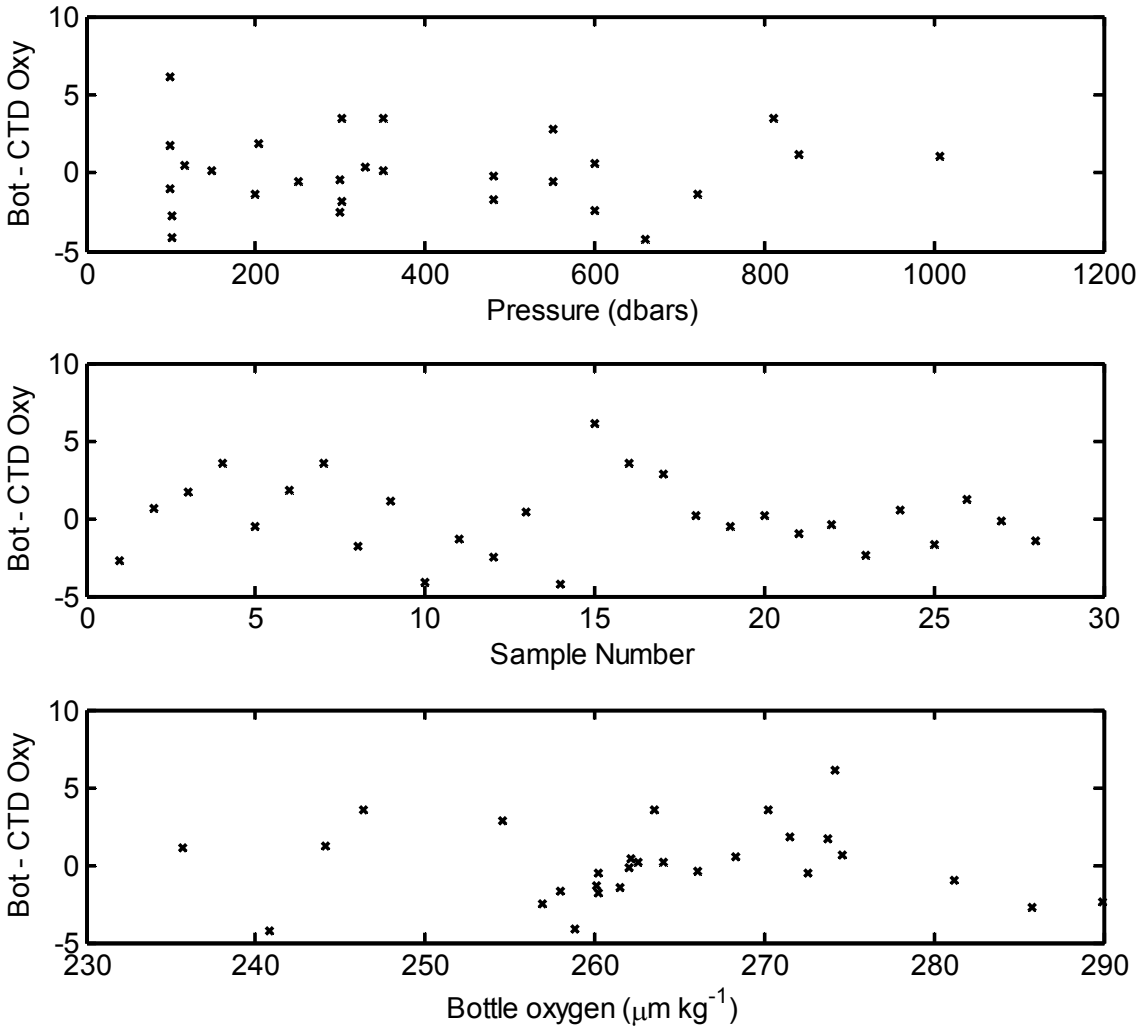

Figure B.2. Residual (bottle – corrected sensor oxygen) plots for 0804S.
a. Pressure (dbar) against residual
b. Sample number against residual
c. Bottle oxygen (μmol kg $^{-1}$) against residual

B.ii. CD176

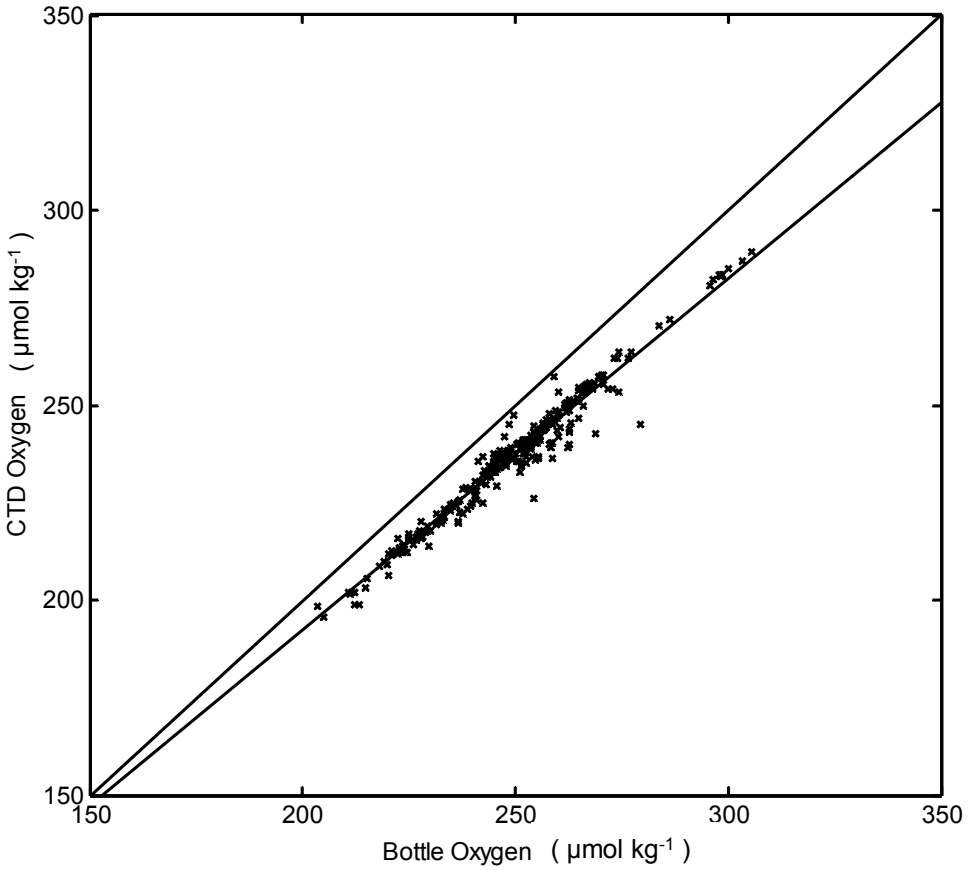

Figure B.3. Bottle oxygen (µmol kg^{-1}) against sensor oxygen (µmol kg^{-1}) for CD176.
sensor oxygen (µmol kg^{-1}) = 0.902 x bottle oxygen (µmol kg^{-1}) + 12.071
r = 0.977

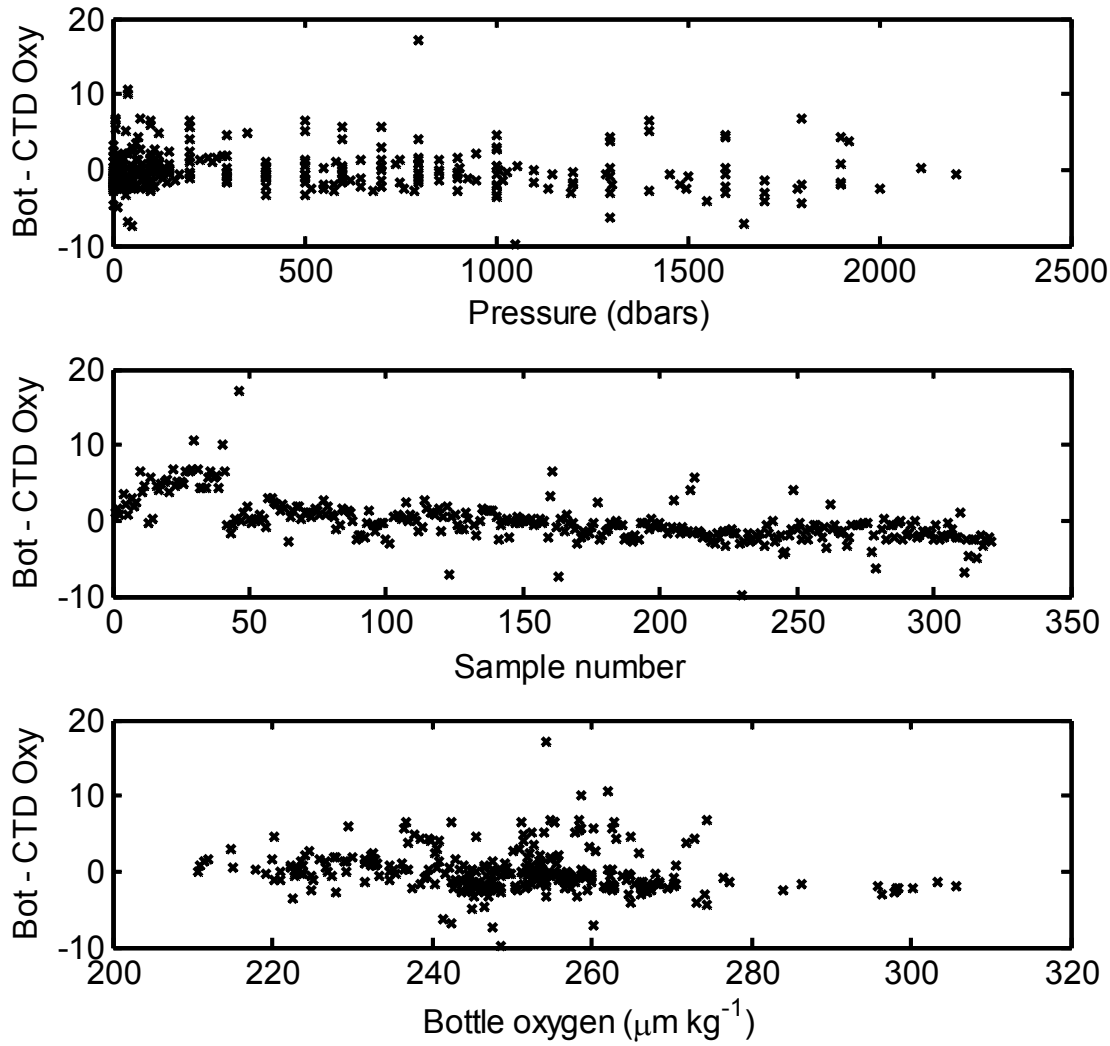

Figure B.4. Residual (bottle – corrected sensor oxygen) plots for CD176.
a. Pressure (dbars) against residual
b. Sample number against residual
c. Bottle oxygen (μmol kg^{-1}) against residual

Appendix C.

Ellett Line timeseries

C.i. standard station list

C.ii. occupations between 1975 and 2008

C.i. Ellett Line stations in the Rockall Trough

Station Name	Latitude (°N)	Longitude (°W)	Depth (m)
A	57.583	13.633	130
B	57.567	13.333	210
C	57.550	13.000	330
D	57.542	12.867	1000
E	57.533	12.633	1658
F	57.508	12.250	1817
G	57.492	11.850	1812
H	57.483	11.533	2020
I	27.467	11.317	750
J	57.450	11.083	550
K	57.400	10.867	850
L	57.367	10.667	2076
M	57.300	10.383	2340
N	57.233	10.050	2100
O	57.150	9.700	1900
P	57.100	9.417	1050
Q	57.050	9.217	350
R	57.000	9.000	135

Table C.1. List of Ellett Line stations within the Rockall Trough.

From: http://www.noc.soton.ac.uk/obe/PROJECTS/EEL/stationlist.php

C.ii. Ellett Line sections across the Rockall Trough between 1975 and 2008.

Year	Month	Cruise
(1975	Mar.	C3_75)
1975	May	C7_75
1975	Jul.	C10_75
(1975	Aug. / Sep.	C12_75)
1975	Nov.	C14_75
1976	Mar. / Apr.	C5a_76
1976	May / Jun.	C8_76
(1976	Aug. / Sep.	C12_76)
(1976	Oct.	C15_76)
(1976	Dec.	C17_76)
1977	Feb. / Mar.	C4_77
1977	Apr.	C6_77
1977	Jul.	C10_77
1977	Jul.	C11_77
1977	Aug. / Sep.	C13_77
1978	Jan. / Feb.	C2_78
1978	Apr.	C6_78
1978	May / Jun.	C9_78
1978	Jul	C11B_78
1978	Sep.	C11D_78
1978	Nov.	C14_78
1979	May	C7_79
1979	Jun. / Jul.	C7_79
1979	Sep.	C13_79
1979	Oct. / Nov.	C16_79
(1980	Feb. / Mar.	C4_80)
1980	Apr. / May	C7_80
1980	Jun.	C9B_80
(1980	Sep.	C13_80)
(1980	Sep.	C14_80)
1980	Oct.	C15_80

Year	Month	Cruise
1981	Jan. / Feb.	C2_81
1981	Apr.	C6_81
1981	Jul.	C10_81
1981	Oct.	C15_81
1982	Jan. / Feb.	C2_82
(1982	Apr. / May	C7_82)
(1982	Aug.	C12_82)
1982	Oct.	C15_82
1983	Feb.	C3_83
1983	May / Jun.	C7_83
1983	Aug. / Sep.	C11_83
(1984	Jun. /Jul.	C2_84)
1984	Nov. / Dec.	C10_84
1985	Jan. / Feb.	C1_85
1985	May	C4_85
1985	Aug.	C8_85
1987	Jan.	C9_87
1987	Apr. / May	C14_87
1987	Nov. / Dec.	C22_87
(1988	Feb. / Mar.	C25_88)
1988	Jun.	C30_88
1989	Jan. / Feb.	D180_89
1989	May	LF1_89
1989	Aug.	LF2_89
1989	Nov. / Dec.	CD44_89
1990	Mar.	C63_90
1990	Jun. / Jul.	C67_90
1990	Aug. / Sep.	C71_90
1991	Feb. / Mar.	C75_91
(1991	Jul.	C81_91)
1992	Sep. / Oct.	C97_92

Year	Month	Cruise
1993	Mar.	C101_93
1993	May	C103_93
1993	Sep.	C105_93
1994	Mar.	C110_94
1994	Apr. / May	C112_94
1994	Aug.	C114_94
1994	Nov.	C116_94
1995	Apr. / May	CD92_95
1995	Jul.	C120_95
1996	Jan.	C124_96
1996	Sep. / Nov.	D223_96
1997	Aug. / Sep.	D230_97
1998	Apr. / Jun.	D233_98
1999	Sep. / Oct.	D242_99
2000	Jan. / Feb.	D245_00
2000	May	SC07_00
2001	May / Jun.	D253_01
2003	Apr.	SC07_03
2003	Jul.	P300_2_03
2004	Jul.	P314_04
2005	Oct.	CD176_05
2006	Oct.	D312_06
2007	Jul.	D321_07
2008	May	SC05_08

Table C.2. Metadata for all cruises occupying the Ellett Line CTD stations in the Rockall Trough between 1975 and 2008.
Prefixes indicate ship: C - RRS Challenger, CD - RRS Charles Darwin, D - RRS Discovery, LF - RV Lough Foyle, P - FSS Poseidon and SC - FRV Scotia.
Brackets indicate cruises that are not used within this thesis because only one or two stations were occupied because of bad weather or instrumental problems, data quality is lower or because data are not available.

References

Abdullah, M., 1985, Trace metals as oceanic tracers, their interaction and residence, *Rit Fiskideildar*, **9**, 60-69.

Ahran, M., 1990, The North Atlantic current and subarctic intermediate water, *Journal of Marine Research*, **48**, 109-144.

Ammerman, J., 2001, Determination of orthophosphate by flow injection analysis. *Lachat Instruments*, 17 pp.

Anderson, L. and J. Sarmiento, 1995, Global ocean phosphate and oxygen simulations, *Global Biogeochemical Cycles*, **9**, 621-636.

Anon, 2009, Thermoscientific Nalgene Plastics Technical Guide 2009, *http://www.nalgenelabware.com/pdf/NalgenePlasticsTechGuide0209.pdf*, 64 pp.

Asher, W. and R. Wanninkhof, 1998, Transient tracers and air-sea gas transfer, *Journal of Geophysical Research*, **103**, 15939-15958.

Bacon, S., 1998, RRS Discovery cruise 230, 7th - 17th September 1997. Two hydrographic sections across the boundaries of the subpolar gyre. *Southampton Oceanography Centre*, 85 pp.

Beal, L. and H. Bryden, 1997, Observations of an Agulhas Undercurrent, *Deep Sea Research I*, **44**, 1715-1724.

Bearman, G., 2001, *Ocean chemistry and deep-sea sediments*, Butterworth-Heinemann, 128 pp.

Bersch, M., 2002, North Atlantic Oscillation-induced changes of the upper-layer circulation in the northern North Atlantic, *Journal of Geophysical Research*, **107**, doi:10.1029/2001JC000901.

Bersch, M., J. Meincke, and A. Sy, 1999, Interannual thermocline changes in the northern North Atlantic, *Deep Sea Research I*, **46**, 55-75.

Biscaye, P. and S. Ettreim, 1977, Suspended particulate loads and transports in the nepheloid layer of the abyssal Atlantic Ocean, *Marine Geology*, **23**, 155-172.

Blindheim, J. and F. Rey, 2004, Water-mass formation and distribution in the Nordic Seas during the 1990s, *ICES Journal of Marine Science*, **61**, 846-863.

Boldreel, L., M. Anderson, and A. Kuijpers, 1998, Neogene seismic facies and deep-water gateways in the Faeroe Bank area, NE Atlantic, *Marine Geology*, **152**, 129-140.

Booth, D. , 1988, Eddies in the Rockall Trough, *Oceanologica Acta*, **11**, 213-219.

Borenas, K. and P. Lundberg, 1988, On the deep-water flow through the Faroe Bank Channel, *Journal of Geophysical Research,* **93**, 1281-1292.

Borenäs, K. and P. Lundberg, 2004, The Faroe-Bank Channel deep-water overflow, *Deep Sea Research II*, **51**, 335-350.

Boswell, S. and D. Smythe-Wright, 1996, Dual-detector system for the shipboard analysis of halocarbons in sea-water and air for oceanographic tracer studies, *The Analyst*, **121**, 505-509.

Bower, A., B. Le Cann, T. Rossby, W. Zenk, J. Gould, K. Speer, P. Richardson, M. Prater, and H. Zhang, 2002, Directly measured mid-depth circulation in the northeastern North Atlantic Ocean, *Nature*, **419**, 603-607.

Bowie, A., D. Whitworth, E. Achterberg, R. Mantoura, and P. Worsfold, 2002, Biogeochemistry of Fe and other trace elements (Al, Co, Ni) in the upper Atlantic Ocean, *Deep-Sea Research I*, **49**, 605-636.

Bozec, A., S. Lozier, E. Chassignet, and G. Halliwell, 2011, On the variability of the Mediterranean Overflow Water in the North Atlantic from 1948 to 2006, *Journal of Geophysical Research*, **117**, doi:10.1029/2011JC007191.

Brewer, P., D. Spencer, P. Biscaye, A. Hanley, P. Sachs, C. Smith, S. Kadar, and J. Fredericks, 1976, The distribution of particualte matter in the Atlantic Ocean, *Earth and Planetary Science Letters*, **32**, 393-402.

Brierley, A., 2003, RRS Discovery 264 Cruise Report. Biophysical studies of zooplankton dynamics in the northern North Atlantic: summer, 25 July - 28 August 2002. *National Environmental Research Council, 98 pp.*

Broecker, W., 1974, "NO", a conservative water-mass tracer, *Earth and Planetary Science Letters*, **23**, 100-107.

Broecker, W. and T. Takahashi, 1981, Hydrography of the central Atlantic - IV. Intermediate waters of Antarctic origin, *Deep Sea Research A*, **28**, 177-193.

Brown, M. and K. Bruland, 2008, An improved flow-injection analysis method for the determination of dissolved aluminium in seawater, *Limnology and Oceanography: Methods*, **6**, 87-95.

Bruland, K., R. Franks, G. Knauer, and J. Martin, 1979, Sampling and analytical methods for the determination of copper, cadmium, zinc and nickel at the nanogram per litre level in seawater, *Analytica Chimica Acta*, **105**, 223-245.

Bryden, H., J. Candela, and T. Kinder, 1994, Exchange through the Strait of Gibraltar, *Progress in Oceanography*, **33**, 201-248.

Buat-Menard, P. and R. Chesselet, 1979, Variable influence of the atmospheric flux on the trace metal chemistry of oceanic suspended matter, *Earth and Planetary Science Letters*, **42**, 399-411.

Bullister, J. and T. Tanhua, 2010, Sampling and measurement of chlorofluorocarbons and sulfur hexafluoride in seawater. *ICPO Publication Series No. 134*, 11 pp.

Bullister, J., 1989, Chlorofluorcarbons as time-dependent tracers in the ocean, *Oceanography*, **2**, 12-17.

Bullister, J. and R. Weiss, 1988, Determination of CCl3F and CCl2F2 in seawater and air, *Deep Sea Research A*, **35**, 839-853.

Bullister, J. and B. Lee, 1995, Chlorofluorocarbon-11 Removal in Anoxic Marine Waters, *Geophysical Research Letters*, **22**, 1893-1896.

Burrows, M. and S. Thorpe, 1999, Drifter observations of the Hebrides slope current and nearby circulation patters, *Annales Geophysicae*, **17**, 280-302.

Burton, J. and P. Statham, 1988, Trace metals as tracers in the ocean, *Philosophical transactions of the Royal Society of London A*, **325**, 127-145.

Caschetto, S. and R. Wollast, 1979, Vertical distribution of dissolved aluminium in the Mediterranean Sea, *Marine Chemistry*, **7**, 141-155.

Castro, C., F. Perez, S. Holley, and A. Rios, 1998, Chemical characterisation and modelling of water masses in the Northeast Atlantic, *Progress in Oceanography*, **41**, 249-279.

Chester, R., 2000, *Marine Geochemistry*, 2 ed., Unwin Hyman, London, 520 pp.

Chou, L. and R. Wollast, 1997, Biogeochemical behaviour and mass balance of dissolved aluminium in the western Mediterranean Sea, *Deep Sea Research II*, **44**, 741-768.

Coale, K. , R. Gordon, and X. Wang, 2005, The distribution and behavior of dissolved and particulate iron and zinc in the Ross Sea and Antarctic circumpolar current along 170°W, *Deep sea Research I*, **52**, 295-318.

Davies, P., A. Cuthbertson, V. Vlasenko, N. Stashchuk, T. Sherwin, and B. Hansen, 2009: Modelling the variability of the Wyville Thomson Ridge Overflow. *Oceans 2025 Annual Science Meeting*, Poster.

de Boer, C., 1998, Water mass distribution in the Iceland Basin calculated with an Optimal Parameter Analysis, *ICES Co-operative Research Report*, **225**, 228-246.

de Brauwere, A., S. Jacquet, F. de Ridder, F. Dehairs, R. Pintelon, J. Schoukens, and W. Baeyens, 2007, Water mass distributions in the Southern Ocean derived from a parametric analysis of mixing water masses, *Journal of Geophysical Research*, **112**, doi: 10.1029/2006JC003742.

de Jong, J., M. Boye, M. Gelado-Caballero, K. Timmermans, M. Veldhuis, R. Nolting, C. van de Berg, and H. de Baar, 2007, Inputs of iron, manganese and aluminium to surface waters of the Northeast Atlantic Ocean and the European continental shelf, *Marine Chemistry*, **107**, 1290142.

Diamond, D., 2001a, Determination of silicate in brackish or seawater by flow injection analysis. Lachat Instruments, 13 pp.

Diamond, D., 2001b, Determination of nitrate/nitrite in brackish or seawater by flow injection analysis. Lachat Instruments, 14 pp.

Dickson, R., W. Gould, C. Griffiths, K. Medler, E. Gmitrowicz, 1986, Seasonality in currents of the Rockall Channel, *Proceedings of the Royal Society of Edinburgh*, **88B**, 103-125.

Dickson, R. and R. Kidd, 1987: 36. Deep circulation in the southern Rockall Trough - the oceanic setting of site 610. *Initial reports of the deep sea drilling project.*, W. F. Ruddimann, R. B. Kidd, E. Thomas, and E. AL., Eds., U.S. Government printing office, 1061-1074, doi:10.2973/dsdp.proc.94.136.1987.

Dickson, R. R. and J. Brown, 1994, The production of North Atlantic Deep Water, sources, rates and pathways, *Journal of Geophysical Research*, **99**, 12319-12341.

Dooley, H. and E. Henderson, 1980, Low frequency currents north of Rockall Bank, *ICES C.M. 1980,* **C25**, 11 pp.

Dooley, H. and J. Meincke, 1981, Circulation and water masses in the Faroese Channels during Overflow-73, *Deutsche Hydrographische Zeitschrift*, **34**, 41-55.

Due, L., H. van Aken, L. Boldreel, and A. Kuijpers, 2006, Seismic and oceanograhic evidence of present-day bottom-water dynamics in Lousy Bank-Hatton Bank area, NE Atlantic, *Deep-Sea Research I*, **53**, 1729-1741.

Ellett, D., 1979, Hydrographic conditions in the Rockall Channel, January-March 1977, *Conseil International pour l'exploration de la mer, annales biologiques*, **34**, 56-59.

Ellett, D., 1993a, The north-east Atlantic: A fan-assisted storage heater? *Weather*, **48**, 118-126.

Ellett, D., 1993b, Transit times to the NE Atlantic of Labrador Sea Water signals, *ICES C.M. 1993*, **C25**, 1-12.

Ellett, D. and K. Martin, 1973, The physical and chemical oceanography of the Rockall Channel, *Deep Sea Research and Oceanographical Abstracts*, **20**, 585-625.

Ellett, D. and D. Roberts, 1973, The overflow of Norwegian Sea Deep Water across the Wyville-Thomson Ridge, *Deep Sea Research and Oceanographical Abstracts*, **20**, 819-835.

Ellett, D. and A. Edwards, 1978, A volume transport estimate for Norwegian Sea overflow water across the Wyville-Thomson Ridge, *ICES Co-operative Research Report*, **C19**, 12 pp.

Ellett, D., P. Kruseman, G. Prangsma, R. Pollard, H. van Aken, A. Edwards, H. Dooley, and W. Gould, 1983, Water masses and mesoscale circulation of north Rockall Trough waters during JASIN 1978, *Philosophical transactions of the Royal Society of London A*, **308**, 250-252.

Ellett, D., A. Edwards, and R. Bowers, 1986, The hydrography of the Rockall Channel - an overview, *Proceedings of the Royal Society of Edinburgh,* **88B**, 61-81.

Escriche, J. and F. Hernandez, 1985, Fluorimetric determination of aluminium with morin after extraction with isobutyl methyl ketone. Part II. Extraction-fluorimetric determination of aluminium in natural and waste waters, *The Analyst*, **110**, 287-290.

Fine, R., 2011, Observations of CFCs and SF6 as Ocean Tracers, *Annual Review of Marine Science,* **3**, 173-195.

Flegal, A. and C. Patterson, 1983, Vertical concentration profiles of lead in the central Pacific at 15°N, 20°S., *Earth and Planetary Science Letters*, **64**, 19-32.

Fogelqvist, E., J. Blindheim, T. Tanhua, S. Østerhus, E. Buch, and F. Rey, 2003, Greenland-Scotland overflow studied by hydro-chemical multivariate analysis, *Deep Sea Research I,* **50**, 73-102.

Fuglister, F., 1960, Atlantic Ocean Atlas of temperature and salinity profiles and data from the International Geophysical Year of 1957-1958., *The Woods Hole Oceanographic Institution Atlas Series*, **1**, 209 pp.

Gammon, R. and D. Wisegarver, 1981, Chlorofluoromethanes in the northeast Pacific: measured vertical distributions and application as transient tracers of upper ocean mixing, *Journal of Geophysical Research*, **87**, 9441-9454.

Grasshoff, K., K. Kremling, and M. Ehrhardt, 1999, *Methods of seawater analysis*, 3 ed., Wiley-VCH, 632 pp.

Gronvall, H. and J. Launiainen, 1997, R/V Aranda 12/1998. VEINS - Nordic WOCE: Studies of the overflow across the Greenland-Scotland Ridge and the formation of the Denmark Strait overflow water. *Finnish Institute of Marine Research*, 24 pp.

Hakkinen, S. and P. Rhines, 2004, Decline of Subpolar North Atlantic circulation during the 1990s, *Science*, **304**, 555-559.

Hakkinen, S. and P. Rhines, 2009, Shifting surface currents in the northern North Atlantic Ocean, *Journal of Geophysical Research*, **114**, doi:10.1029/2008JC004883.

Häkkinen, R., P. Rhines, and D. Worthen, 2011a, Atmospheric blocking and Atlantic multidecadal ocean variability, *Science*, **334**, 655-659.

Häkkinen, R., P. Rhines, and D. Worthen, 2011b, Warm and saline events embedded in the meridional circulation of the northern North Atlantic, *Journal of Geophysical Research*, **116**, doi:10.1029/2010JC006275.

Hall, G., 1998, Relative contamination levels observed in different types of bottles used to collect water samples, *Explore*, **101**, 1-7.

Hall, I. and C. Measures, 1998, The distribution of Al in IOC stations of the North Atlantic and Norwegian Sea between 52° and 65°N, *Marine Chemistry*, **61**, 69-85.

Hansen, B., D. Ellett, and D. Meldrum, 1986, Evidence for an anticyclonic circulation on Faroe Bank, *ICES C.M. 1986*, **C:15**, 1-15.

Hansen, B. and S. Østerhus, 2000, North Atlantic-Nordic Seas exchanges, *Progress in Oceanography*, **45**, 109-208.

Hansen, B., S. Østerhus, W. J. Gould, and L. J. Rickards, 2000, North Atlantic-Norwegian Sea Exchanges: the ICES NANSEN Project, *ICES Cooperative Research Report*, **225**, 79 pp.

Harvey, J., 1982, θ-S relationships and water masses in the eastern North Atlantic, *Deep Sea Research A*, **29**, 1021-1033.

Harvey, J. and A. Theodorou, 1986, The circulation of Norwegian Sea overflow water in the eastern North Atlantic, *Oceanologica Acta*, **4**, 393-402.

Hätun, H., A. Sandø, H. Drange, B. Hansen, and H. Valdimarsson, 2005, Influence of the Atlantic Subpolar Gyre on the Thermohaline Circulation, *Science*, **309**, 1841-1844.

Hill, A. and E. Mitchelson-Jacob, 1993, Observations of a poleward-flowing saline core on the continental slope of Scotland, *Deep Sea Research I*, **40**, 1521-1527.

Hinrichsen, H. and M. Tomczak, 1993, Optimum multiparameter analysis of the water structure in the Western North Atlantic Ocean, *Journal of Geophysical Research*, **98**, 10155-10169.

Holliday, N., 2002: The interannual variability of the circulation and ventilation of the North Atlantic Subpolar Gyre, University of Liverpool, 236 pp.

Holliday, N., 2003, Air-sea interaction and circulation changes in the northeast Atlantic, *Journal of Geophysical Research-Oceans*, **108**, doi:10.1029/2002JC001344.

Holliday, N., R. Pollard, J. Read, and H. Leach, 2000, Water mass properties and fluxes in the Rockall Trough, 1975-1998, *Deep Sea Research I*, **47**, 1303-1332.

Holliday, N., S. Hughes, S. Bacon, A. Beszczynska-Möller, B. Hansen, A. Lavín, H. Loeng, K. Mork, S. Østerhus, T. Sherwin, and W. Walczowski, 2008, Reversal of the 1960s to 1990s freshening trend in the northeast North Atlantic and Nordic Seas, *Geophysical Research Letters*, **35**, doi:10.1029/2007/GL032675.

Howard, A., A. Coxhead, I. Potter, and A. Watt, 1986, Determination of dissolved aluminium by the micelle-enhanced fluorescence of its lumogallion complex, *The Analyst*, **111**, 1379-1382.

Howe, J., M. Stoker, and K. Woolfe, 2001, Deep-marine seabed erosion and gravel lags in the north-western Rockall Trough, North Atlantic Ocean, *Journal of the Geological Society, London*, **158**, 427-438.

Huhn, O., W. Roether, P. Beining, and H. Rose, 2001, Validity limits of carbon tetrachloride as an ocean tracer, *Deep-Sea Research Part I*, **48**, 2025-2049.

Huhn, O., H. Hellmer, M. Rhein, C. Rodehacke, W. Roether, M. Schodlok, and M. Schröder, 2008, Evidence of deep- and bottom-water formation in the western Weddell Sea, *Deep Sea Research II*, **55**, 1098-1116.

Hurrell, J., 1995, Decadal trends in the North Atlantic Oscillation: Regional temperatures and precipitation, *Science*, **269**, 676-679.

Hydes, D., 1977, Dissolved aluminium concentration in sea water, *Nature*, **268**, 136-137.

Hydes, D., 1979, Aluminium in seawater: control by inorganic processes, *Science*, **205**, 1260-1262.

Hydes, D., 1983, Distribution of aluminium in waters of the North East Atlantic 25°N to 35°N, *Geochimica et Cosmochimica Acta*, **47**, 967-973.

Hydes, D., 1989, Seasonal variation in dissolved aluminium concentrations in coastal waters and biological limitation of the export of riverine input of aluminium to the deep sea, *Continental Shelf Research*, **9**, 919-929.

Hydes, D. and P. Liss, 1976, Fluorimetric method for the determination of low concentrations of dissolved aluminium in natural waters, *The Analyst*, **10**1, 922-931.

Hydes, D. and P. Liss, 1977, The behaviour of dissolved aluminium in estuarine and coastal waters, *Estuarine and Coastal Marine Science*, **5**, 755-769.

Hydes, D., G. De Lange, and H. De Baar, 1988, Dissolved aluminium in the Mediterranean, *Geochimica et Cosmochimica Acta*, **52**, 2107-2114.

Johnson, C., T. Sherwin, D. Smythe-Wright, T. Shimmield, and W. Turrell, 2010, Wyville Thomson Ridge Overflow Water: Spatial and temporal distribution in the Rockall Trough, *Deep Sea Research I*, **57**, 1153-1162.

Johnson, G. and E. Schneider, 1969, Depositional ridges in the North Atlantic, *Earth and Planetary Science Letters*, **6**, 416-422.

Johnson, G. and N. Gruber, 2007, Decadel water mass variations along 20°W in the Northeastern Atlantic Ocean, *Progress in Oceanography*, **73**, 277-295.

Jones, B. and R. Laslett, 1994, Methods for analysis of trace metals in marine and other samples., *Aquatic Environment Protection: Analytical Methods*. Ministry of Agriculture, Fisheries and Food, Lowestoft., **11**, 9-18.

Karstensen, J. and M. Tomczak, 1998, Age determination of mixed water masses using CFC and oxygen data, *Journal of Geophysical Research*, **103**, 18599-18609.

Kase, R., A. Biastoch, and D. Stammer, 2001, On the mid-depth circulation in the Labrador and Irminger Seas, *Geophysical Research Letters*, **28**, 3433-3436.

Kawase, M. and J. Sarmiento, 1986, Circulation and nutrients in mid-depth Atlantic waters, *Journal of Geophysical Research*, **91**, 9749-9770.

Killworth, P., 2001, On the rate of descent of overflows, *Journal of Geophysical Research*, **106**, 22267-22275.

Kramer, J., P. Laan, G. Sarthou, K. Timmermans, and H. De Baar, 2004, Distribution of aluminium in the high atmospheric input region of the subtropical waters of the North Atlantic Ocean, *Marine Chemistry*, **88**, 85-101.

Kremling, K. and D. Hydes, 1988, Summer distribution of dissolved Al, Cd, Cu, Mn and Ni in the north-east Atlantic surface waters, *Continental Shelf Research*, **8**, 89-105.

Kuijpers, A., M. Anderson, N. Kenyon, H. Kunzendorf, and T. van Weering, 1998, Quaternary sedimentation and Norwegian Sea overflow pathways around Bill Bailey Bank, northeastern Atlantic, *Marine Geology*, **152**, 101-127.

Lambert, C., J. Bishop, P. Biscaye, and R. Chesselet, 1984, Particulate aluminium, iron, and manganese chemistry at the deep Atlantic boundary layer, *Earth and Planetary Science Letters*, **70**, 237-248.

Lavender, K., R. Davis, and W. Owens, 2000, Mid-depth recirculation observed in the interior Labrador and Irminger Seas by direct velocity measurements, *Nature*, **407**, 66-68.

LeBel, D., W. Smethie, M. Rhein, D. Kieke, R. Fine, J. Bullister, D. Min, W. Roether, R. Weiss, C. Andrie, D. Smythe-Wright, and E. Jones, 2008, The formation rate of North Atlantic Deep Water and Eighteen Degree Water calculated from CFC-11 inventories observed during WOCE, *Deep Sea Research I*, **55**, 891-910.

Lee, A. and D. Ellett, 1965, On the contribution of overflow water from the Norwegian sea to the hydrographic structure of the North Atlantic Ocean, *Deep Sea Research and Oceanographical Abstracts*, **12**, 129-142.

Libes, S., 1992, *An introduction to Marine Biogeochemistry*, Wiley, New York, 752 pp.

Loose, B., P. Schlosser, W. Smethie, and S. Jacobs, 2009, An optimised estimate of glacial melt from the Ross Ice Shelf using noble gases, stable isotopes, and CFC transient tracers, *Journal of Geophysical Research*, **114**, doi: 10.1029/2008/JC005048.

Lozier, M. and N. Stewart, 2008, On the temporally-varying northward penetration of Mediterranean Overflow Waters, *Journal of Physical Oceanography*, **38**, 2097-2103.

Lunel, T., 1990: Trace metal concentrations and isotopes as tracers of oceanic processes, Earth Sciences, University of Cambridge, 169 pp.

Lunel, T., M. Rudnicki, H. Elderfield, and D. Hydes, 1990, Aluminium as a depth-sensitive tracer of entrainment in submarine hydrothermal plumes, *Nature*, **344**, 137-139.

Mackas, D., K. Denman, and A. Bennett, 1987, Least squares multiple tracer analysis of water mass composition, *Journal of Geophysical Research*, **92**, 2907-2918.

Mackin, J. and R. Aller, 1984, Processes affecting the behaviour of dissolved aluminium in estuarine waters, *Marine Chemistry*, **14**, 213-232.

Mamayev, O., 1975, *Temperature - salinity analysis of world ocean waters, Vol. 11, Elsevier Oceanography Series*, Elsevier Scientific Publishing Company, 374 pp.

Mann, C., A. Coote, and D. Garner, 1973, The meridional distribution of silicate in the western Atlantic Ocean, *Deep Sea Research and Oceanographical Abstracts*, **20**, 791-801.

Maring, H. and R. Duce, 1987, The impact of atmospheric aerosols on trace metal chemistry in open ocean surface seawater, 1, Aluminium, *Earth and Planetary Science Letters*, **84**, 381-392.

Mauritzen, C., J. Price, T. Sanford, and D. Torres, 2005, Circulation and mixing in the Faroese Channels, *Deep Sea Research I*, **52**, 883-913.

McCartney, M., 1992, Recirculating components to the deep boundary current of the northern North Atlantic, *Progress in Oceanography*, **29**, 283-383.

McCartney, M. and C. Mauritzen, 2001, On the origin of the warm inflow to the Nordic Seas, *Progress in Oceanography*, **51**, 125-214.

McGrath, T., G. Nolan, and E. McGovern, 2012, Chemical characteristics of water masses in the Rockall Trough, *Deep Sea Research I*, **61**, 57-73.

Measures, C. I., 1995, The distribution of Al in the IOC stations of the eastern North Atlantic between 30°S and 34°N, *Marine Chemistry*, **49**, 267-281.

Measures, C., 1999, The role of entrained sediments in sea ice in the distribution of aluminium and iron in the surface waters of the Arctic Ocean, *Marine Chemistry*, **68**, 59-70.

Measures, C., B. Grant, M. Khadem, D. Lee, and J. Edmond, 1984, Distribution of beryllium, aluminium, selenium and bismuth in the surface waters of the western North Atlantic and Caribbean, *Earth and Planetary Science Letters*, **71**, 1-12.

Measures, C., J. Edmond, and T. Jickells, 1986, Aluminium in the northwest Atlantic, *Geochimica et Cosmochimica Acta*, **50**, 1423-1429.

Measures, C. and J. Edmond, 1988, Aluminium as a tracer of the deep outflow from the Mediterranean, *Journal of Geophysical Research*, **93**, 591-595.

Measures, C. and J. Edmond, 1989, Shipboard determination of aluminium in seawater at the nanomolar level by electron capture detection gas chromatography, *Analytical Chemistry*, **61**, 544-547.

Measures, C. and J. Edmond, 1990, Aluminium in the South Atlantic: Steady-state distribution of a short residence time element, *Journal of Geophysical Research*, **95**, 5331-5240.

Measures, C. and J. Edmond, 1992, The distribution of aluminium in the Greenland Sea and its relationship to ventilation processes, *Journal of Geophysical Research*, **97**, 17787-17800.

Measures, C., W. Landing, M. Brown, and C. Buck, 2008, High-resolution Al and Fe data from the Atlantic Ocean CLIVAR-CO2 Repeat Hydrography A16N transect: Extensive linkages between atmospheric dust and upper ocean geochemistry, *Global Biogeochemical Cycles*, **22**, doi:10.1029/2007GB003042.

Mecking, S. and M. J. Warner, 1999, Ventilation of Red Sea Water with respect to chlorofluorocarbons, *Journal of Geophysical Research*, **104**, 11087-11097.

Meincke, J., 1978, On the distribution of low salinity intermediate waters around the Faroes, *Deutsche Hydrographische Zeitschrift*, **31**, 50-64.

Middag, R., C. van Slooten, H. De Baar, and P. Laan, 2011, Dissolved aluminium in the Southern Ocean, *Deep Sea Research II*, **58**, 2647-2660.

Miller, A., 1950, A study of mixing processes over the edge of the continental slope, *Journal of Marine Research*, **9**, 145-160.

Miller, J. and J. Miller, 1989, *Statistics for Analytical Chemistry*, Ellis Horwood Limited, 233 pp.

Minakawa, M. and Y. Watanabe, 1998, Aluminium in the East China Sea and Okinawa Trough, marginal sea areas of the western North Pacific, *Journal of Oceanography*, **54**, 629-640.

Moody, J. and R. Lindstrom, 1977, Selection and cleaning of plastic containers for storage of trace element samples, *Analytical Chemistry*, **49**, 2264-2267.

Moore, R., 1981, Oceanographic distributions of zinc, cadmium, copper and aluminium in the waters of the central Arctic, *Geochimica et Cosmochimica Acta*, **45**, 2475-2482.

Moore, R. and G. Millward, 1984, Dissolved-particulate interactions of aluminium in ocean waters, *Geochimica et Cosmochimica Acta*, **48**, 235-241.

Moran, S. and R. Moore, 1991, The potential source of dissolved aluminium from resuspended sediments to the North Atlantic Deep Water, *Geochimica et Cosmochimica Acta*, **55**, 2745-2751.

Moran, S., R. Moore, and S. Westerlund, 1992, Dissolved aluminium in the Weddell Sea, *Deep Sea Research A*, **39**, 537-547.

Morris, A., R. Howland, and A. Bale, 1986, Dissolved aluminium in the Tamar Estuary, southwest England, *Geochimica et Cosmochimica Acta*, **50**, 189-197.

Murray, S. and W. Johns, 1997, Direct observations of seasonal exchange through the Bab el Mandab Strait, *Geophysical Research Letters*, **24**, 2667-2560.

Needler, G. and R. Heath, 1975, Diffusion coefficients calculated from the Mediterranean salinity anomaly in the North Atlantic Ocean, *Journal of Physical Oceanography*, **5**, 173-182.

New, A. and D. Smythe-Wright, 2001, Aspects of the circulation in the Rockall Trough, *Continental Shelf Research*, **21**, 777-810.

New, A., S. Barnard, P. Herrmann, and J. Molines, 2001, On the origin and pathway of the saline inflow to the Nordic Seas: insights from models, *Progress in Oceanography*, **48**, 255-287.

Nishikawa, Y., K. Hiraki, A. Morishige, A. Tsuchiyama, and T. Shigematsu, 1967, Fluorophotometric determination of aluminium and gallium with lumogallion, *Japan Analyst (Bunseki Kagaku)*, **16**, 692-697.

Nolting, R., H. de Baar, K. Timmermans, and K. Bakker, 1999, Chemical fractionation of zinc versus cadmium among other metals nickel, copper and lead in the northern North Sea, *Marine Chemistry*, **67**, 267-287.

Obata, H., N. Yoshiyuki, A. Dia Sotto, and Y. Yoshiyuki, 2004, Dissolved Al, In, and Ce in the eastern Indian Ocean and the southeast Asian Seas in comparison with the radionuclides 210Pb and 210Po, *Geochimica et Cosmochimica Acta*, **68**, 1035-1048.

Obata, H., D. Alibo, and Y. Nozaki, 2007, Dissolved aluminium, indium and cerium in the Sea of Japan and the Sea of Okhotsk: Comparison to the marginal seas of the western North Pacific, *Journal of Geophysical Research*, **112**, doi:10.1029/2006/JC003944.

Olsen, S., B. Hansen, D. Quadfasel, and S. Østerhus, 2008, Observed and modelled stability of overflow across the Greenland-Scotland Ridge, *Nature*, **455**, doi:10.1038/nature07302.

Olsson, K., E. Jeansson, T. Tanhua, and J. Gascard, 2005, The East Greenland Current studied with CFCs and released sulphur hexafluoride, *Journal of Marine Systems*, **55**, 77-95.

Open-University, 2001, *Ocean Circulation*, 2 ed., Butterworth-Heinemann, 286 pp.

Orians, K. and K. Bruland, 1985, Dissolved aluminium in the central North Pacific, *Nature*, **316**, 427-429.

Orians, K. and K. Bruland, 1986, The biogeochemistry of aluminium in the Pacific Ocean, *Earth and Planetary Science Letters*, **78**, 397-410.

Østerhus, S., W. Turrell, B. Hansen, P. Lundberg, and E. Buch, 2001, Observed transport estimates between the North Atlantic and the Arctic Mediterranean in the Iceland-Scotland region, *Polar Research*, **20**, 169-175.

Perez, F., C. Mouriño, F. Fraga, and A. Rios, 1993, Displacement of water masses and remineralisation rates off the Iberian Peninsula by nutrient anomalies, *Journal of Marine Research*, **51**, 869-892.

Perez, F., A. Rios, C. Castro, and F. Fraga, 1998, Mixing analysis of nutrients, oxygen and dissolved inorganic carbon in the upper and middle North Atlantic ocean east of the Azores, *Journal of Marine Systems*, **16**, 219-233.

Pollard, R., M. Griffiths, S. Cunningham, J. Read, F. Perez, and A. Rios, 1996, Vivaldi 1991 - a study of the formation, circulation and ventilation of Eastern North Atlantic Central Water, *Progress in Oceanography*, **37**, 167-192.

Pollard, R., J. Read, N. Holliday, and H. Leach, 2004, Water masses and circulation pathways through the Iceland Basin during Vivaldi 1996, *Journal of Geophysical Research*, **109**, doi:10.1029/2003JC002067.

Poole, R. and M. Tomczak, 1999, Optimum multiparameter analysis of the water mass structure in the Atlantic Ocean thermocline, *Deep Sea Research I*, **46**, 1895-1921.

Read, J., 2001, CONVEX-91: water masses and circulation of the Northeast Atlantic subpolar gyre, *Progress in Oceanography*, **48**, 461-510.

Read, J. and R. Pollard, 1992, Water masses in the region of the Iceland-Faroes Front, *Journal of Physical Oceanography*, **22**, 1365-1378.

Reid, J., 1979, On the contribution of the Mediterranean Sea outflow to the Norwegian-Greenland Sea, *Deep Sea Research A*, **26**, 1199-1223.

Reimann, C., U. Siewers, H. Skarphagen, and D. Banks, 1999, Does bottle type and acid-washing influence trace metal analyses by ICP-MS on water samples? A test covering 62 elements and four bottle types: high density polyethene (HDPE), polypropene (PP), fluorinated ethene propene copolymer (FEP) and perfluoroalkoxy polymer (PFA), The *Science of the Total Environment*, **239**, 111-130.

Ren, J., J. Zhang, J. Q. Luo, X. Pei, and Z. Jiang, 2001, Improved fluorometric determination of dissolved aluminium by micelle-enhanced lumogallion complex in natural waters, *The Analyst*, **126**, 698-702.

Resing, J. and C. Measures, 1994, Fluorometric determination of Al in seawater by flow injection analysis with in-line preconcentration, *Analytical Chemistry*, **66**, 4105-4111.

Rhein, M., J. Fischer, W. Smethie, D. Smythe-Wright, R. Weiss, C. Mertens, D. Min, U. Fleischmann, and A. Putzka, 2002, Labrador Sea Water: Pathways, CFC inventory, and formation rates, *Journal of Physical Oceanography*, **32**, 648-665.

Richardson, P. , A. Bower, and W. Zenk, 2000, A census of Meddies tracked by floats, *Progress in Oceanography*, **45**, 209-250.

Roether, W., B. Klein, and K. Bulsiewicz, 2001, Apparent loss of CFC-113 in the upper ocean, *Journal of Geophysical Research*, **106**, 2679-2688.

Saager, P., H. deBaar, J. deJong, R. Nolting, and J. Schijf, 1997, Hydrography and local sources of dissolved trace metals Mn, Ni, Cu, and Cd in the northeast Atlantic Ocean, *Marine Chemistry*, **57**, 195-216.

Saunders, P., 1990, Cold outflow from the Faroe Bank Channel, *Journal of Physical Oceanography*, **20**, 28-43.

Schott, F., K. Koltermann, L. Stramma, A. Sy, R. Zahn, and W. Zenk, 1999, Cruise Report: Meteor, North Atlantic, 1997, Cruise Number 39, 18th April - 14th September 1997. *Institut für Meerskunder der Universität Hamburg,* 203 pp.

Shapiro, S., P. Schlosser, and W. Smethie, 1997, The use of 3H and tritiogenic 3He to determine CFC degradation and vertical mixing rates in Framvaren Fjord, Norway, *Marine Chemistry*, **59**, 141-157.

Sherwin, T. and W. Turrell, 2005, Mixing and advection of a cold water cascade over the Wyville Thomson Ridge, *Deep Sea Research I*, **52**, 1392-1413.

Sherwin, T. , C. Griffiths, M. Inall, and W. Turrell, 2008, Quantifying the overflow across the Wyville Thomson Ridge into the Rockall Trough, *Deep Sea Research I*, **55**, 396-404

Sherwin, T., J. Read, N. Holliday, and C. Johnson, In Press, The impact of changes in North Atlantic Gyre distribution on water mass characteristics in the Rockall Trough, *ICES Journal of Marine Science*.

Shigematsu, T., Y. Nishikawa, K. Hiraki, and N. Nagano, 1970, Fluorimetric determination of trace amount of aluminium in natural water by lumgallion method; masking of ferric iron with o-phenanthroline, *Japan Analyst (Bunseki Kagaku)*, **19**, 551-554.

Shoosmith, D., P. Richardson, A. Bower, and H. Rossby, 2005, Discrete eddies in the northern North Atlantic as observed by looping RAFOS floats, *Deep-Sea Research II*, **52**, 627-650.

Silva, N., N. Rojas, and A. Fedele, 2009, Water masses in the Humboldt Current System: Properties, distribution, and the nitrate deficit as a chemical tracer for Equatorial Subsurface Water off Chile, *Deep Sea Research II*, **56**, 1004-1020.

Skelly, E. and F. DiStefano, 1988, Clean room and microwave digestion techniques: Improvement in detection limits for aluminium determination by GF-AAS, *Applied Spectroscopy*, **42,** 1302-1306.

Smethie, W., R. Fine, A. Putzka, and E. Jones, 2000, Tracing the flow of North Atlantic Deep Water using chlorofluorocarbons, *Journal of Geophysical Research*, **105**, 14297-14323.

Smythe-Wright, D., 1999, RRS Discovery Cruise 233, 23 April - 01 June 1998. A Chemical and Hydrographic Atlantic Ocean Survey. *Southampton Oceanography Centre*, No. 86, 78 pp.

Stashchuk, N., V. Vlasenko, and T. Sherwin, 2010, Insights into the structure of the Wyville Thomson Ridge overflow current from a fine-scale numerical model, *Deep Sea Research I*, **57**, 1192-1205.

Stashchuk, N., V. Vlasenko, and T. Sherwin, 2011, Numerical investigation of deep water circulation in the Faroese Channels, *Deep Sea Research I*, **58**, 787-799.

Stinchcombe, M., 2007, RRS Discovery Cruise D312, 11th-31st October 2006. The extended Ellett Line 2006. *National Oceanography Centre, Southampton*, 146 pp.

Stoll, M., H. van Aken, H. deBaar, and M. Kraak, 1996, Carbon dioxide characteristics of water masses in the northern North Atlantic Ocean, *Marine Chemistry*, **55**, 217-232.

Sutheimer, S. and S. Cabaniss, 1995, Determination of trace aluminum in natural waters by flow-injection analysis with fluorescent detection of the lumogallion complex, *Analytica Chimica Acta*, **303**, 211-221.

Sy, A., M. Rhein, J. Lazier, K. Koltermann, J. Meincke, A. Putzka, and M. Bersch, 1997, Suprizingly rapid spreading of newly formed intermediate waters across the North Atlantic Ocean, *Nature*, **286**, 675-679.

Takayanagi, K. and C. Gobeil, 2000, Dissolved aluminium in the upper St. Lawrence Estuary, *Journal of Oceanography*, **56**, 517-525.

Talley, L. and M. McCartney, 1982, Distribution and circulation of Labrador Sea Water, *Journal of Physical Oceanography*, **12**, 1189-1205.

Tanhua, T., K. Olsson, and E. Jeansson, 2008: Tracer evidence of the origin and variability of Denmark Strait Overflow Water. *Arctic-Subarctic Ocean Fluxes: Defining the role of the Northern Seas in climate*, B. Dickson, J. Meincke, and P. Rhines, Eds., Springer, 475-503.

Thierry, V., E. de Boisséson, and H. Mercier, 2008, Interannual variability of the subpolar mode water properties over the Reykjanes Ridge during 1990-2006, *Journal of Geophysical Research*, **113**, doi:10.1029/2007JC004443.

Tomczak, J., 1981, A multi-parameter extension of temperature/salinity diagram for the analysis of non-isopycnal mixing, *Progress in Oceanography*, **10**, 147-171.

Tomczak, M., 1999, Some historical, theoretical and applied aspects of quantitative water mass analysis, *Journal of Marine Research*, **57**, 275-303.

Tria, J., C. Butler, P. Haddad, and A. Bowie, 2007, Determination of aluminium in natural water samples, *Analytica Chimica Acta*, **558**, 153-165.

Tsuchiya, M., 1989, Circulation of the Antarctic Intermediate Water in the North Atlantic Ocean, *Journal of Marine Research*, **47**, 747-755.

Tsuchiya, M., L. Talley, and M. McCartney, 1992, An eastern Atlantic section from Iceland southward across the equator, *Deep Sea Research A*, **39**, 1885-1917.

Tulloch, D. and J. Tait, 1959, Hydrography of the north-western approaches to the British Isles, *Marine Research*, **1**, 1-32.

Turrell, W., G. Slesser, R. Adams, R. Payne, and P. Gillibrand, 1999, Decadal variability in the composition of Faroe Shetland Channel bottom water, *Deep Sea Research I*, **46**, 1-25.

Turrell, W. and T. Sherwin, 2003, A re-examination of the Wyville-Thomson Ridge overflow, and its relevance to fluxes west of Britain, *ICES C.M. 2003*, **T08**, 25 pp.

Ullgren, J. and M. White, 2010, Water mass interaction at intermediate depths in the southern Rockall Trough, northeastern North Atlantic, *Deep Sea Research I*, **57**, 248-257.

Upadhyay, S. and R. Gupta, 1994, Aluminium in the north-western Indian Ocean (Arabian Sea), *Marine Chemistry*, **47**, 203-214.

Upadhyay, S. and R. Sen Gupta, 1995, The behaviour of aluminium in waters of the Mandovi estuary, west coast of India, *Marine Chemistry*, **51**, 261-276.

van Aken, H. and C. de Boer, 1995, On the synoptic hydrography of intermediate and deep water masses in the Iceland Basin, *Deep Sea Research I*, **42**, 165-189.

van Aken, H. and G. Becker, 1996, Hydrography and through-flow in the north-eastern North Atlantic Ocean: the NANSEN project, *Progress in Oceanography*, **38**, 297-346.

Wade, I., D. Ellett, and K. Heywood, 1997, The influence of intermediate waters on the stability of the eastern North Atlantic, *Deep Sea Research I*, **44**, 1405-1426.

Walker, S., R. Weiss, and P. Salameh, 2000, Reconstructed histories of the annual mean atmospheric mole fractions for the halocarbons CFC-11, CFC-12, CFC-13, and carbon tetrachloride, *Journal of Geophysical Research*, **105**, 14285-14296.

Waugh, D., T. Haine, and T. Hall, 2004, Transport times and anthropogenic carbon in the subpolar North Atlantic Ocean, *Deep Sea Research I*, **51**, 1475-1491.

Webster, L., 2004a, *Determination of silicate in seawater using the Bran and Luebbe AA3 in a containerised laboratory*. Fisheries Research Services, 11 pp.

Webster, L., 2004b, *Determination of phosphate in seawater using a Bran and Luebbe AA3 in a containerised laboratory*. Fisheries Research Services, 11 pp.

Webster, L., 2005, *Determination of ToxN in seawater using the Bran and Luebbe AA3 in a containerised laboratory*. Fisheries Research Services, 11 pp.

Will, F., 1961, Fluorimetric determination of aluminium in the part-per-billion range., *Analytical Chemistry*, **33**, 1360-1362.

Wyrtki, K., 1962, The oxygen minima in relation to ocean circulation, *Deep Sea Research and Oceanographical Abstracts*, **9**, 11-23.

Yashayaev, I., 2007, Hydrographic changes in the Labrador Sea, 1960-2005, *Progress in Oceanography*, **73**, 242-276.

Yashayaev, I., H. van Aken, N. Holliday, and M. Bersch, 2007, Transformation of the Labrador sea water in the subpolar North Atlantic, *Geophysical Research Letters*, **34**, doi:10.1029/2007GL031812.

Yeats, P., S. Westerlund, and A. Flegal, 1995, Cadmium, copper and nickel distributions at four stations in the eastern central and south Atlantic, *Marine Chemistry*, **49**, 283-293.

You, Y., 2002, Quantitative estimate of Antarctic Intermediate Water contributions from the Drake Passage and the southwest Indian Ocean to the South Atlantic, *Journal of Geophysical Research*, **107**, doi.10.1029/2001JC000880.

You, Y., R. Lutjeharms, O. Boebel, and W. de Ruijter, 2003, Quantification of the interocean exchange of intermediate water masses around southern Africa, *Deep Sea Research II*, **50**, 187-228.

Zar, J., 1984, *Biostatistical Analysis*, 2 ed., Prentice Hall, New Jersey, 718 pp.

Zhang, J., H. Xu, and J. Ren, 2000, Fluorimetric determination of dissolved aluminium in natural waters after liquid-liquid extraction into n-hexanol, *Analytica Chimica Acta*, **405**, 31-42.